Primary characterisation of a novel mouse model of tauopathy

Zelah Joel

UCL

Thesis submitted for the degree of Doctor of Philosophy

August 2015

Declaration

I declare that the work presented herein is my own, except where indicated.

Acknowledgements

Firstly I would like to thank my supervisor, Dr Frances Edwards, for welcoming me into her lab as an undergraduate, and for then helping and encouraging me to undertake my PhD. Mostly, however, I would like to thank you for being so friendly and supportive and for creating such a nice atmosphere within the lab.

Thank you to the post docs, Dr Damian Cummings, Dr Dervis Salih and Dr Marina Yasvoina without whom we would all be lost! In particular, Damian, I really couldn't have done it without you. Thank you for answering my endless questions and making it all seem easy.

I also want to thank Rivka and my fellow PhD students, Ashley, Angelo, Tiffanie, Josh, Wenfei and Tom, as well as all of the BSc and MSc students who have come and gone- you really did make my PhD. I can't say I have had many low points, but nevertheless thank you for holding my hand throughout this process!

Finally, thank you to my friends and family for your support, but most of all thank you Fletcher, for putting up with me being a student for the last 10 years!

Abstract

The protein tau has gained notoriety due its role in many neurodegenerative disorders including the most prevalent form of dementia, Alzheimer's disease, as well as the hereditary frontotemporal dementia with parkinsonism linked to chromosome 17 (FTDP-17). The development of novel systems for investigating tau-mediated dysfunction and possible ways in which this may be reversed or even prevented are therefore essential.

The present study provides primary characterisation of a novel transgenic mouse model of tauopathy, known as TauD35. This model harbours transgenic human tau containing the FTDP-17 mutation, P301L, under the control of the CaMKIIα promoter. As demonstrated in Alzheimer's disease, hippocampal neurones are particularly vulnerable to tau dysfunction, fuelling the decision to choose the hippocampus as the site of this initial characterisation. Molecular biology, immunohistochemistry, behavioural and electrophysiological techniques were employed at 4, 13 and 24 months of age in order to investigate pathology development over time.

Investigations revealed two sublines within the TauD35 model, with one line harbouring approximately double the number of transgene copies ($_{HIGH}$TAU) compared to the other ($_{LOW}$TAU). Both transgenic lines developed intraneuronal inclusions formed from pathological tau species relevant to human tauopathies in an age- and dose-dependent manner, as tested with specific antibodies. At 4-months, prior to tau aggregation, an increase in paired-pulse ratio was detected at entorhinal cortex to dentate gyrus synapses. At 13-months, the two lines exhibited large disparity in NFT load, with $_{HIGH}$TAU animals displaying behavioural changes consistent with the symptoms of FTDP-17 patients. Neuronal loss was evident in the CA1 region of $_{HIGH}$TAU mice by 17.5 months of age, coinciding with the development of a pathological phenotype. These data show that both TauD35 models mimic cardinal features of human tauopathies, and thus provide valuable tools in which to study tau dysfunction as well as assess possible therapeutics.

Table of Contents

List of figures

Chapter 1: Introduction

Chapter 2: Methods

Chapter 3: Results, Molecular biology

Chapter 4: Results, Histology

Chapter 5: Results, Behaviour

Chapter 7: Discussion

List of tables

Chapter 2: Methods

Chapter 6: Results, Electrophysiology

Chapter 7: Discussion

Abbreviations

(d)ACSF	(dissection) Artificial cerebrospinal fluid
(f)AD	(familial) Alzheimer's disease
AMPA-R	α-Amino-3-hydroxy-5-methyl-4-isoxazolepropionic acid Receptor
Amyloid-β	Amyloid-beta protein
AP5	2-amino-5-phosphonopentanoic acid
ATP	Adenosine triphosphate
CA1	Cornu Ammonis region 1
CA3	Cornu Ammonis region 3
Ca^{2+}	Calcium ion
CaMKIIα	Calcium/calmodulin-dependent kinase II-α isoform
CNQX	6-cyano-7-nitroquinoxaline-2,3-dione
CNS	Central nervous system
DG	Dentate Gyrus
DMSO	Dimethyl sulfoxide
EC(II)	Entorhinal cortex (layer 2)
eEPSC	Evoked excitatory postsynaptic current
fEPSP	Field excitatory postsynaptic potential
FTDP-17	Frontotemporal dementia with parkinsonism linked to chromosome 17
FTLD	Frontotemporal lobar degeneration
RT-qPCR	Reverse transcriptase quantitative real-time polymerase chain reaction
LTD	Long-term depression
LTP	Long-term potentiation

MAPT	Microtubule-associated protein tau gene
mEPSC	Miniature excitatory postsynaptic current
MF	Mossy fibre pathway
Mg^{2+}	Magnesium ion
mPP	Medial perforant path
MT	Microtubule
MTBR	Microtubule binding repeat
n	Number of release sites
Na^{2+}	Sodium ion
NFT	Neurofibrillary tangle
NMDA-R	N-methyl-D-aspartate Receptor
PCR	Polymerase chain reaction
PD	Parkinson's disease
PP	Perforant path
PPD	Paired-pulse depression
PPF	Paired-pulse facilitation
PPR	Paired-pulse ratio
Pr	Release probability
PrP^{c}	Cellular prion protein
PSD (95)	Postsynaptic density (protein 95)
PTP	Post-tetanic potentiation
q	Quantal size
qPCR	Quantitative real-time polymerase chain reaction
SC	Schaffer collateral-commissural pathway

SDS-PAGE	Sodium dodecyl sulfate-polyacrylamide gel electrophoresis
sEPSC	Spontaneous excitatory postsynaptic current
STP	Short-term potentiation
$tau^{-/-}$	Tau knock-out mouse model
TBS	Tris-buffered saline
TTX	Tetrodotoxin
VGCC	Voltage gated calcium channel
WT	Wild-type mice (littermates)

IMPORTANT PREFACE

Data presented herein describes the initial hippocampal characterisation of a novel mouse model of tauopathy, TauD35, which overexpresses human tau containing the P301L mutation under the CaMKIIα promoter. The mouse model was developed at GlaxoSmithKline (GSK) in order to study the effects of tau dysfunction and the development of tau pathology within the mouse brain, as a model of frontotemporal dementia with parkinsonism linked to chromosome-17 (FTDP-17) and other neurodegenerative tauopathies.

Primary investigations concentrated on analysis of synaptic transmission within the TauD35 line, at a comparable age (4-months) to other transgenic mouse models (in particular the APP_{SWE} x $PS1_{M146V}$ model of rising amyloid-β) used within the lab. This would allow for the identification of the earliest possible common alterations in synaptic transmission resulting from changes in either tau or amyloid-β.

Over the following year and half, mice were aged at UCL for behavioural and further electrophysiological testing. During this time, it became apparent that a proportion of the TauD35 transgenic mice within the colony developed a moribund phenotype at approximately 17-20 months of age. Of the 28 transgenic mice maintained until this age, only 8 were seen to develop this pathological phenotype. This observation initiated questions as to why this phenotype was seen only in a small proportion of transgenic animals. Later communication with GSK Neurosciences Therapeutic Area (Shanghai, China) highlighted additional inconsistences within the TauD35 line that they had observed during histological experimentations.

I was therefore prompted to further examine the transgene properties of this novel mouse line. I sought advice and technical assistance from Stuart Martin (Head of the Molecular Biology Unit at UCL), and together we were able to design a qPCR experiment using uniquely designed TaqMan® primers/probe for the CaMKIIα promoter sequence in order to investigate the transgene copy number.

With only one year of my PhD remaining, I discovered that indeed two transgenic lines existed within the TauD35 mouse line, with one line harbouring approximately double the number of transgene copies as the other. *The two transgenic models were appointed*

$_{HIGH}$TAU and $_{LOW}$TAU respectively. These differences in transgene copy number, as determined using qPCR (see below), may be the result of genetic recombination or two independent integration events. Following this important discovery, I confirmed these findings using Western blot and histological techniques.

Separating electrophysiological and behavioural data collected previously from transgenic mice has resulted in low/inconsistent sample numbers for some experiments. Without prior knowledge of differences in transgene copy number, and thus measures to selectively breed both lines, the $_{HIGH}$TAU line has been seen to decline in numbers. This has unfortunately resulted in difficulty in attempts to increase sample numbers, in particular for aged animals.

Separate breeding colonies have now been established within the lab, however, additional experiments cannot now be completed within the time frame of my PhD, as these mice will not have reached a sufficient age.

CHAPTER 1

An introduction to the present study

The present study concentrates on tau, a protein that has gained notoriety due its role in many neurodegenerative disorders known collectively as *tauopathies*. This heterogenous group of diseases includes the most prevalent form of dementia, Alzheimer's disease (AD), making the development of novel systems in which to investigate tau dysfunction, and possible ways in which this may be reversed or even prevented, essential.

The novel mouse model presented harbours human cDNA containing the frontotemporal dementia with parkinsonism linked to chromosome 17 (FTDP-17) missense mutation, P301L, and is known as *TauD35*. The transgene lies under the control of the Ca2+/calmodulin-dependent protein kinase (CaMKIIα) promoter, and is thus strongly expressed within the hippocampus (www.mouse.brain-map.org (Lein et al., 2007)). With the obvious vulnerability of the hippocampus to tau pathology development and neurone loss (discussed below), one may expect early, substantial changes within the hippocampus in such a model. Therefore initial work concentrates within this brain structure. A description of hippocampal neuroanatomy is thus provided, with literature linking tau dysfunction and the hippocampus discussed.

As a new transgenic line, with no current publications detailing its characterisation, my PhD project aims to employ current techniques to provide an initial description of this mouse model, so that this may provide a reference source for future work. The present study confirms functionality of the line through the use of molecular biology and histological techniques, as well as providing initial insight into the functional consequences of tau dysfunction, using behavioural and electrophysiological testing. A short introduction into the use of these functional experiments within the hippocampus is given at the end of this chapter.

An introduction to tau

As the average life expectancy of man continues to increase, it leads us towards a dramatic increase in the incidence of dementia. The term 'dementia' does not describe a single disease, but rather a set of symptoms often described under a blanket term as cognitive decline; that principally include memory loss, personality and behavioural changes, as well as problems with language, attention and problem solving. The most prevalent form of dementia is by far Alzheimer's disease (AD), which accounts for approximately 50-60% of all dementia cases (Blennow et al., 2006). Apart from the huge economic burden caused by the ever-increasing cases of dementia, the enormous emotional distress caused by this set of diseases means we must intensify our search for a preventative therapy.

In 1986 it was identified that the neurofibrillary tangles (NFTs) first described by Alois Alzheimer 80 years prior, were in fact aggregates of abnormally hyperphosphorylated protein tau (Grundke-Iqbal et al., 1986a, Grundke-Iqbal et al., 1986b, Ihara et al., 1986, Kosik et al., 1986). From this discovery sprung much interest in this protein tau, with large amounts of work over the next few years concentrating on its isolation and characterisation.

The physiological role of tau

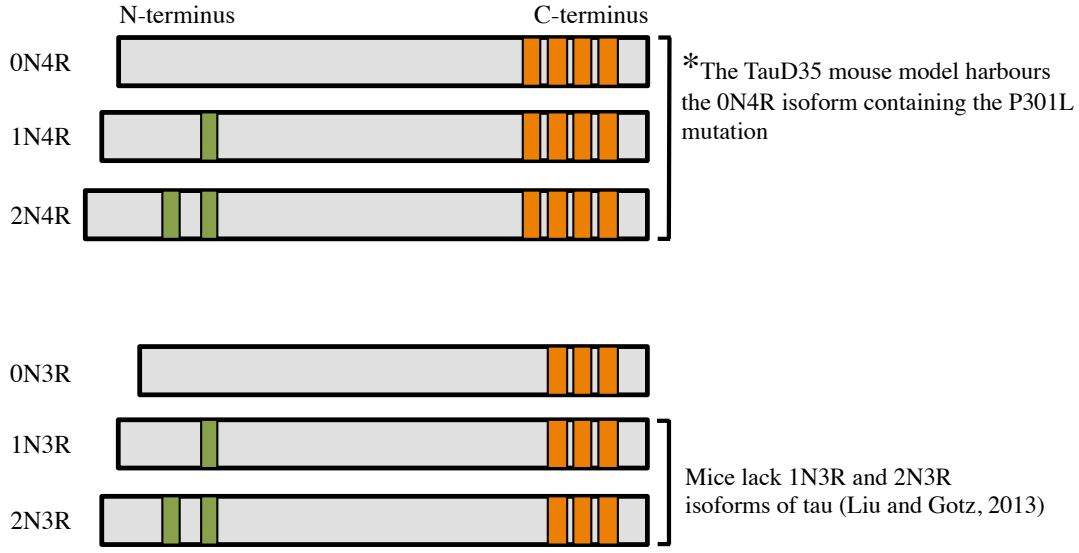

Figure. 1.1. The 6 isoforms of tau present within the human central nervous system. Alternative splicing of the *MAPT* gene produces 6 isoforms of tau in the human central nervous system. Isoforms are split into 2 groups containing either three or four microtubule binding repeats (3R or 4R) in the carboxyl terminal of the protein (shown in orange). The isoforms also differ in the presence of either: zero, one or two inserts (0N, 1N or 2N) in the amino terminal of the protein (shown in green).

The principle function of tau protein is to promote the assembly of microtubules (MTs) (Weingarten et al., 1975). MTs play a crucial role in many cellular functions, including: maintaining the structure of cells as part of the cytoskeleton, allowing the transport of intracellular cargoes, and in spindle formation during mitosis. Physiologically, the majority of tau is primarily located in the axons of mature neurones (Binder et al., 1985, Li et al., 2011) and (in different isoforms (Avila et al., 2004)) is found in both the central (CNS) and peripheral nervous systems. There are six known isoforms of tau in the human CNS, resulting from the alternative splicing of exons 2, 3 and 10 of the microtubule associated protein tau (*MAPT*) gene (Ballatore et al., 2007) (Figure 1.1). The isoforms differ from each other in the number of MT binding repeats (MTBRs) they contain (either 3 (3R) or 4 (4R)) (Goedert et al., 1989b), as well as the presence of either zero (0N), one (1N) or two (2N) 29-amino acid long inserts in the amino (projection) terminal of the protein (Goedert et al., 1989a). In contrast to human tau, murine tau only ever exists in four isoforms, with only three isoforms (0N4R, 1N4R and 2N4R) present in adult mice (Liu and Gotz, 2013). The precise physiological roles of these different isoforms remain unknown. While they are likely to be broadly functionally similar, it has been shown that 4R tau isoforms display a greater potency in promoting tubulin assembly than do 3R isoforms (Goedert and Jakes, 1990), whereas 3R isoforms bind with a far greater affinity to the Src family tyrosine kinase, Fyn (Bhaskar et al., 2005). In the human adult brain 3R and 4R tau are expressed in a 1 to 1 ratio, with changes to this ratio towards an increase 4R tau indicative of neurodegenerative tauopathies (Goedert and Jakes, 2005). Recent work has also uncovered the differential cellular location of murine tau isoforms containing different numbers of amino terminal inserts, indicating functional differences exist between these different isoforms (Liu and Gotz, 2013).

Through its close association with MTs, it is probable tau takes on a key role in regulating axonal transport. Physiologically, tau is in an equilibrium, bound to, and detached from MTs (Ballatore et al., 2007), and it is likely this plays some function in transport along MTs. Studies by Dixit et al., (2008) showed that tau may regulate the motor proteins dynein and kinesin differently, implying the critical role of its spatial location on cellular transport.

In 1977 it was determined that tau is a phosphoprotein (Cleveland et al., 1977). Tau contains approximately 85 phosphorylation sites, of which only a handful are phosphorylated under physiological conditions

[http://cnr.iop.kcl.ac.uk/hangerlab/tautable (Hanger et al., 2009)]. This relatively dephosphorylated state is believed to increase the ability of tau to promote MT formation (Lindwall and Cole, 1984), thus implying that the phosphorylation status of tau plays a regulatory role in its function, including axonal transport (Ballatore et al., 2007). More recently it has become clear that under pathological circumstances, including various dementias, an atypical phosphorylation of tau occurs leading tau to become 'hyperphosphorylated'. Some evidence indicated that this pathological addition of phosphate groups may occur in a temporal cascade (Kimura et al., 1996, Bertrand et al., 2010a), performed by proline-directed kinases, such as glycogen synthase kinase-3 (GSK-3), cyclin-dependent kinase 5 (cdk5), mitogen-activated protein kinase (MAPK) and c-Jun N-terminal kinases (JNKs) (Mandelkow and Mandelkow, 2012).

Hyperphosphorylation is not, however, an absolute indicator of disease, with higher levels of phosphorylation also present in the foetal brain (Brion et al., 1993) and in hibernating animals (Arendt et al., 2003, Arendt and Bullmann, 2013). Other conditions resulting in a reduction in body temperature and stress on the body, have also been shown to cause the hyperphosphorylation of tau, such as starvation, cold water stress and anaesthesia (Yanagisawa et al., 1999, Okawa et al., 2003, Planel et al., 2007, Petry et al., 2014), possibly due to effects on the balance of kinase/phosphatase activity (Planel et al., 2007).

Along with stabilizing and promoting MT assembly, tau also engages with a whole host of other proteins and structures, including: presenilin-1 (part of the catalytic core of the ϒ-secretase enzyme, one of the enzymes responsible for the cleavage of the amyloid precursor protein) (Takashima et al., 1998), the protein actin (which forms microfilaments, one of the major components of the cytoskeleton), the plasma membrane (Brandt et al., 1995), adenosine triphosphate (ATP) (Farid et al., 2013) and SH3 domains of the Src family of tyrosine kinases (Src, Lck and Fyn) (Lee et al., 1998), to name just a few (a full table of the binding partners of tau is given in Mandelkow and Mandelkow 2012), with these interactions also likely influenced by the phosphorylation state of tau. While research over the last decade or so has focused on tau's relationship with MTs, it is likely that these various other interactions may indeed be important in the function of tau and its role in disease, with the relationship between tau and Fyn (along with additional, related interactions) presently the topic of intense research (Ittner et al., 2010, Mondragon-Rodriguez et al., 2012, Boehm, 2013).

While the accumulation of hyperphosphorylated tau in the pathological state is the most prominent modification, it is noteworthy that tau has also been found to undergo various additional post-translational modifications in the brains of patients affected by various dementias. These include: nitration, ubiquitination, glycation, glycosylation and truncation (Pevalova et al., 2006).

The role of tau in dementia

In the years following the discovery that tau protein was the major constituent of NFTs, it was learnt that familial forms of AD (fAD) were caused by mutations in the genes that play a role in the production of amyloid-β (Goate et al., 1991). This work, coupled with earlier observations linking Down's syndrome with AD (Glenner and Wong, 1984), soon prompted the complete Amyloid Hypothesis of AD (Hardy and Higgins, 1992), and studies into the role of tau in neurodegeneration began to decline. However, it seemed that, although the evidence was pointing towards amyloid-β being the main causative factor of AD, the characteristic amyloid-β plaques did not correlate to the severity of disease. Instead, NFTs composed of tau protein, along with neuronal and synaptic loss, correlated far better with the degree of cognitive decline and memory impairment in AD (Terry et al., 1991, Arriagada et al., 1992, Gomez-Isla et al., 1996, Gomez-Isla et al., 1997, Giannakopoulos et al., 2003).

In 1994, an autosomal dominant inherited form of frontotemporal dementia with parkinsonism (FTDP) was linked to chromosome 17 (FTDP-17) (Wilhelmsen et al., 1994), in particular the specific region within chromosome 17 in which the tau gene lies (17q21.31). By 1998, it had been shown that genetic mutations within the tau gene resulted in FTDP-17 (Hutton et al., 1998).

FTDP-17 is a rare form of dementia, which displays a highly heterogeneous phenotype even between members of the same family. However, there are three fundamental features including behavioural changes, cognitive decline and parkinsonism, of which patients usually display at least two once the disease is fully developed (Wszolek et al., 2006). Currently, approximately 100 families harbouring 38 different mutations in the *MAPT* gene have been identified (*ibid*). These mutations can be split broadly into 2 groups: 1) those that affect the alternative splicing of the *MAPT* gene, with the majority increasing levels of 4R tau and 2) those that have their effect at the protein level, by disrupting MT binding (although several mutations do effect both) (*ibid*). It has been shown that 4 of the most studied missense mutations (G272V,

V337M, R406W and P301L) make tau a more susceptible substrate for hyperphosphorylation (Alonso Adel et al., 2004) and it is therefore possibly via this modification that these mutations disrupt MT binding. The majority of FTDP-17 cases present an early onset, typically around 40-60 years of age, an age similar to cases of fAD (Selkoe and Podlisny, 2002). While mutations in the *MAPT* gene account for the vast majority of cases of FTDP-17, it is of note that the remaining instances that are not found to result from *MAPT* mutations directly, still see a genetic link to the same region of chromosome 17q21 (Wszolek et al., 2006).

FTDP-17 is not, however, the only disease to exhibit tau pathology exclusively. Instead, it is just one of a heterogeneous group of diseases all displaying abundant tau deposition and neuronal degeneration, including: progressive supranuclear palsy, Pick's disease, argyrophilic grain disease and corticobasal degeneration (Cairns et al., 2007). Collectively, these disorders (as well as AD) are known as *tauopathies*.

Along with Pick's disease, FTDP-17 also falls under the umbrella term of frontotemporal lobar degeneration (FTLD), due to the predominant loss of the frontal and temporal lobes in this group of diseases (*ibid*). In addition to these tauopathy disorders, other forms of FTLD exist, in which tau pathology is not noted. These forms of FTLD present different pathological inclusions, such as those positive for ubiquitin, possibly comprised of TAR DNA-binding protein 43 (TDP-43) (*ibid*). It is typical for FTLD patients to present with the clinical syndrome of frontotemporal dementia (FTD), which presents as a change in behaviour, such as increased disinhibition or impulsivity. Others regularly exhibit the syndromes of semantic dementia or primary progressive non-fluent aphasia, observed as dysfunctions in language. Parkinsonism also manifests in a proportion of FTLD patients, as well as a clinical diagnosis of amyotrophic lateral sclerosis in certain individuals (*ibid*).

Interestingly tau has also been shown to have links to Parkinson's disease (PD) (reviewed in (Wray and Lewis, 2010). PD is primarily thought of as a movement disorder caused by neuronal loss in the substantia nigra and is associated with protein aggregates of α-synuclein, known as Lewy bodies. However, the research field now recognises PD as a more complex entity. Most patients display some level of cognitive decline, with a proportion developing clinically diagnosed dementia. Of these patients, 50% see the occurrence of senile plaques and NFTs, resulting in a secondary diagnosis of AD (Irwin et al., 2013). As well as these human cases, it has been observed that a

mouse model of PD harbouring the E46K α-synuclein mutation develops abundant neuronal tau inclusions, with the origin of these tau aggregates attributed to both a direct and indirect action of the mutated α-synuclein protein (Emmer et al., 2011). Genome-wide association studies have also revealed that mutations in *MAPT* provide a genetic risk factor for the development of PD (Simon-Sanchez et al., 2009). Together, these distinct studies reveal an important relationship between tau and PD. Presently the most active area of research into links between PD and tau concentrate on the interesting possibilities of synergistic effects between α-synuclein and tau in causing fibrillisation of each other (Giasson et al., 2003, Guo et al., 2013a), as is discussed below.

Tau risk factors for dementia

Despite the discovery that specific mutations in the *MAPT* gene can directly result in familial tauopathy disorders, the causes of sporadic nonhereditary tauopathies, including the vast majority of AD cases, remain unidentified. For patients presenting with a sporadic form of a disease, it may be that while they are not harbouring a direct genetic cause, they may possess certain genetic risk factors that contribute to disease development. With regards to the development of tauopathy disorders, an enhanced risk has been associated with the inheritance of a particular haplotype from chromosome 17.

The *MAPT* gene lies within a ~900kb region of DNA on chromosome 17 that can be inherited in 2 forms, created as a consequence of an ancient inversion of this section of DNA, known as haplotype 1 and 2 (H1 and H2) (Stefansson et al., 2005). Inheritance of H1 (or particular subtypes of H1 such as H1c) has been shown to increase the risk of developing certain neurodegenerative tauopathies, including progressive supranuclear palsy, corticobasal degeneration and AD, as well as possibly PD (reviewed by Pittman et al., (2006)). The consequences of this inversion are unknown, but it likely gives rise to changes in *MAPT* transcription levels or splicing through haplotype specific single-nucleotide or insertion-deletion polymorphisms (Myers et al., 2007).

It is clear that changes in tau protein can play an important part in the development of various neurodegenerative disorders, as is evidenced by its role in a variety of different neurodegenerative tauopathy disorders. Moreover, tau dysfunction alone is proved to be sufficient to cause such disorders, as is seen with the observation that mutations in *MAPT* result in FTDP-17. With a large social and economic burden being presented by such diseases, it is critical to determine the exact effects of such dysfunction, their time course and if and where intervention would be most effective.

What makes tau 'toxic'?

The defining feature of all tauopathies is the presence of NFTs. For many years it was assumed that since NFTs were detectable, they must mediate the observed toxicity culminating as neurodegeneration. However, within the last decade or so, both for tau and other amyloidogenic proteins, such as amyloid-β, it has been suggested that this is not the case (review for tau: Spires-Jones et al., 2011, Kopeikina et al., 2012; for amyloid-β: Klein et al., 2001, Haass and Selkoe, 2007, Klein, 2013), possibly with the formation of such insoluble aggregates even acting as a protective mechanism (Alonso Adel et al., 2006, Gotz et al., 2008, Treusch et al., 2009) as has been described for huntingtin (Arrasate et al., 2004).

It is now widely agreed that the major (or at least initial) harmful species of amyloid-β comes in the form of diffusible, soluble amyloid-β oligomers (Walsh and Selkoe, 2007) (although elucidating the exact toxic species of amyloid-β has not been easy (Lesne, 2013)). The idea that tau toxicity is induced in a similar way, by undefined soluble species, began based on the observation that some patients with FTDP-17 display high tau phosphorylation, along with a large amount of neurodegeneration, while only showing mild NFT formation (Bird et al., 1999); conversely young cognitively healthy individuals had been found to display interneuronal tau lesions while appearing cognitively normal (Braak and Braak, 1997). More recently, SantaCruz et al., (2005) used a regulatable transgenic mouse model carrying a FTDP-17 related mutation (P301L) under the CaMKII promoter, to show that suppression of the transgene even for a brief period of 6-8 weeks, resulted in the recovery of memory deficits and the cessation of neuronal death; with longer suppression (4-4.5 months) even resulting in an increased brain weight. However, the most striking result was that despite this reversal of transgene effects, and independently of transgene expression, NFTs continued to accumulate, arguing that NFTs cannot be the toxic species of tau. In 2011, Fox et al., showed that NFT-bearing neurones are just as likely as non-NFT-bearing neurones to express the intermediate-early gene, *Arc,* following exposure to an enriched environment. This result implies that the presence of a pathological tau aggregate does not impair the ability of individual hippocampal neurones to respond to physiologically relevant stimuli. Reinforcing the results of SantaCruz et al., (2005), they then showed that following suppression of the transgene for 6 weeks, *Arc* expression in transgenic brains equalled that of control brains despite the continuous presence of NFTs. Further

work on this mouse model has also identified early multimeric tau species, which were found to correlate far better with memory loss than NFTs (Berger et al., 2007). In line with this work, Rocher et al., (2010) showed through electrophysiological techniques that, while the expression of mutated tau caused significant structural and functional changes in cortical neurones, this was independent of whether or not the neurones contained NFTs.

Along with the research discussed above, many more studies have linked soluble, rather than fibrillar forms of tau to toxic effects (Jaworski et al., 2009, Lasagna-Reeves et al., 2011, Patterson et al., 2011); an idea also supported by work in a drosophila model of human tauopathy (Feuillette et al., 2010). Taken all together, it is highly likely that the toxic species of tau is an unspecified intermediate of single tau monomers and large aggregated fibrils.

As well as being small low-order aggregates, the toxic species of tau is also likely to be hyperphosphorylated (Feuillette et al., 2010, Hoover et al., 2010, Zempel et al., 2010; discussed by Iqbal et al., 2009). As mentioned, hyperphosphorylation is not an indicator of a disease state *per se*, but rather hyperphosphorylation may contribute to tau toxicity through either: 1) initiating the missorting of tau from its physiological axonal location through reducing MT binding (Zempel et al., 2010), or allowing tau to by-pass a diffusion barrier (Li et al., 2011). This would disrupt the physiological functions of tau within the axon, as well result in further possibly deleterious effects, such as increasing the targeting of Fyn to the postsynaptic site, which may contribute to raising neuronal excitotoxicity (discussed below). 2) Facilitating tau misfolding (Jeganathan et al., 2008), perhaps enabling the formation of an aggregation nucleus, which may work to form soluble oligomeric species, disrupting naïve tau in addition to facilitating pathology propagation (also discussed below).

Indeed, therapeutics in which tau toxicity is targeted through the development of kinase inhibitors or restoration of phosphatase activity are in development, and present potentially viable treatment options for the future (Iqbal et al., 2014).

There may also be a role for truncated forms of tau in neurodegenerative disease. Tau contains many cleavage sites available to a host of proteases, including, calpain, puromycin-sensitive aminopeptidase and caspases (Mandelkow and Mandelkow, 2012). Of these many possible cleavage sites, one of the most studied is the caspase-mediated cleavage of tau at aspartic acid 421 (D421) (Gamblin et al., 2003). While it has been

shown that this truncated form of tau does not generally increase cell death (as was once thought) (de Calignon et al., 2010), it may play a role in increased cell death when cells are subjected to stressors (Matthews-Roberson et al., 2008), as well as promoting aggregation through the prevention of tau adopting its preferred 'paperclip' formation (Jeganathan et al., 2006). Other tau fragments have also been reported to have pro-aggregation properties (Frost et al., 2009a, McMillan et al., 2011), with an apparent importance placed on the MTBRs in fibril formation, a property likely due to the β-structure of the second and third MTBRs (Mandelkow and Mandelkow, 2012).

The findings outlined above support the view that 'toxic tau' is not yet in the form of large aggregated NFTs, but instead exists in a yet unspecified, soluble state. They also, however, highlight the unknown with regards to this soluble toxic tau, be it hyperphosphorylated, truncated, conformationally changed, oligomeric or all of the above. Amplifying these uncertainties is the large variety of tauopathy disorders. How does one explain the heterogeneity of these disorders if a single toxic entity of tau is the same for all? Interestingly, recent investigations have worked to answer this question. These data suggest, that specific oligomeric conformations may exist that produce distinctive toxicity in different tauopathy disorders (Sanders et al., 2014), perhaps targeting specific brain areas or neuronal types. This idea of 'strains' of toxic tau may go some way to explaining the variability of this group of diseases.

Assuming the toxicity of small soluble oligomers of amyloid-β or diffusible hyperphosphorylated tau, rather than large insoluble aggregates, allows one to imagine how early 'undetectable' toxicity might occur, and also how this toxicity may even be able to propagate, allowing for the progression of the disease (discussed below). It is, however, conceivable that the long-term presence of NFTs within neurones will result in deleterious effects, even if just by presenting a physical obstruction within the neurone and thus contributing to dysfunction later in the disease.

Alzheimer's disease: The most prevalent tauopathy

Due to the prevalence and long history of investigation, a significant amount of research into the role of tau dysfunction in disease has concentrated on its role in AD. In understanding the part that tau plays in the development of this widespread dementia, clues may be provided that are found to be applicable to other tauopathies.

While for years theories on the aetiology of AD had omitted tau, the importance of tau in AD now seems to be well established. This was highlighted by several studies that indicated tau is a vital component on the pathway to amyloid-β toxicity. An early report by Rapoport et al., (2002) demonstrated that neurones cultured from tau knockout ($tau^{-/-}$) mice were resistant to amyloid-β induced degeneration. Despite the use of a high concentration of amyloid-β in this experiment (20μM), this led to further work on the role of tau in facilitating amyloid-β toxicity. Roberson and colleagues (2007) blocked amyloid-β induced neuronal dysfunction via a reduction in tau expression, through the use of transgenic mouse models. Importantly, these results were later supported by similar experiments (Ittner et al., 2010, Jin et al., 2011). It has even been shown that the robust result of amyloid-β-induced impairment of long-term potentiation (LTP) in the hippocampus is dependent on the presence of tau (Shipton et al., 2011). Along with preventing dendritic toxicity induced by amyloid-β, a reduction in tau has also been shown to prevent amyloid-β defects in axonal transport in cultured neurones (Vossel et al., 2010).

While it has been shown that tau is essential in mediating the effects amyloid-β, several lines of evidence support the notion that the primary dysfunction occurring in AD involves amyloid-β. The first piece of evidence for this is the fact that familial forms of AD (fAD) are the result of genetic mutations in either amyloid precursor protein (APP) (Goate et al., 1991) or the presenilins (1 or 2) (Schellenberg et al., 1992, Levy-Lahad et al., 1995). Each of these mutations results in increased levels of extracellular amyloid-β_{1-42} (Scheuner et al., 1996), therefore leading to the hypothesis that mutations causing fAD may initiate development of the disease through increases in amyloid-β levels. Mutations in *MAPT* can cause FTDP-17, a tauopathy that does not display amyloid-β pathology; however, these mutations do not result in the development of AD. Similarly, mice expressing a tau transgene do not develop any amyloid-β pathology, whereas amyloid transgenic mice can display hyperphosphorylated tau, although full NFTs are not observed (Duyckaerts et al., 2008). More recently however, Umeda et al., (2014) have worked with the hypothesis that the lack of full NFT formation in amyloid-β transgenic models is due to the low propensity of murine tau to aggregate *in vivo*. They therefore introduced a low level (10% of endogenous) of WT human tau into a model expressing mutant amyloid precursor protein (APP) at near endogenous levels and saw an acceleration of pathology, with NFT development by 18 months of age.

Further work has also shown that tau pathology is aggravated by intracranial injection of synthetic amyloid-β (Gotz et al., 2001b), as well as amyloid-β containing brain extract (Bolmont et al., 2007). This is also the case in APP and tau double transgenic mice, where tau pathology is exacerbated but there is no effect on amyloid-β pathology compared to single transgenic counterparts (Lewis et al., 2001, Bolmont et al., 2007, Terwel et al., 2008, Hurtado et al., 2010). In addition, it has been shown that in a triple transgenic mouse model (APPxPS1xTau), intraneuronal amyloid-β immunoreactivity is one of the first detectable pathological signs (Oddo et al., 2003b). One must be careful, however, of claims that, because amyloid-β deposition precedes tau deposition, this is evidence that amyloid-β acts upstream of tau (Oddo et al., 2003a). Indeed we see that there is certainly some controversy over which protein first appears as insoluble deposits (Schonheit et al., 2004, Braak and Del Tredici, 2011b, Braak et al., 2011).

The nature of the fundamental interaction between amyloid-β and tau has yet to be elucidated. If the cascade of events in AD begins with amyloid-β, what occurs downstream of this, involving a crucial role for tau, and ending in widespread aggregate deposition and neuronal loss?

Dysfunction at the synapse

As mentioned, it has long been known that physiologically, tau is enriched within axons (Binder et al., 1985) where it plays a role in the stabilization of MTs, possibly through providing protection from severing proteins (Jean and Baas, 2013). Considering this location and function, it is reasonable that pathological tau, which has become hyperphosphorylated and detached from MTs, may contribute to presynaptic dysfunction through disrupting axonal transport (reviewed by Millecamps and Julien, 2013). More recent data has, however, placed tau more specifically at the synapse, with evidence from humans suggesting that low levels of unphosphorylated monomeric tau are present in both pre- and postsynaptic terminals under physiological conditions (Tai et al., 2012). This presynaptic localisation may be further enhanced under pathological circumstances, with data collected using a mouse model in which human tau carrying the P301L mutation was overexpressed within the entorhinal cortex (EC), indicating that pathologically phosphorylated tau accumulates within presynaptic boutons of the perforant path (PP). This accumulation was associated with enlarged presynaptic terminals and ultrastructural abnormalities including, enlarged synaptic vesicles, fewer

small synaptic vesicles, as well as the presence of vesicular-tubular structures (Harris et al., 2012).

In addition to potentially deleterious presynaptic functions, intriguing data has also placed tau at the postsynaptic site. Despite the long held recognition of an association between tau and the Src family tyrosine kinase, Fyn (Lee et al., 1998), it wasn't until 2010, that work by Ittner et al., uncovered that the nature of this interaction was the tau-dependent targeting of Fyn to the postsynaptic site, revealing a novel dendritic function for tau, as well as exposing an association of tau with the postsynaptic density protein 95 (PSD-95). This finding was later corroborated by Mondragon-Rodriguez et al., (2012), who placed tau at the postsynaptic site under physiological conditions in rat hippocampal cultures, where it was found to interact with a complex containing PSD-95, Fyn and the N-methyl-D-aspartate glutamate receptor (NMDA-R). These studies led to the suggestion that tau is present in dendrites under normal conditions at very low levels, with its presence becoming particularly significant in disease. The discovery of even low levels of tau in the dendrites of neurones under physiological conditions provided an interesting link in solving the puzzle of the cellular mechanisms involved in AD, spurring a considerable amount of research into tau and its interactions at the postsynaptic site.

Even without a physiological role for postsynaptic tau, it is possible that pathologically, tau may be present postsynaptically. It is well established that a rather early occurrence in tau pathology is its mislocalisation from the axon to the somatodendritic compartment, with this thought to largely result from hyperphosphorylation (Avila et al., 2004). One established function of tau phosphorylation (at least the phosphorylation of the KXGS motifs in the MTBR domains (Zempel et al., 2010)) is to negatively regulate its binding to MTs (Lindwall and Cole, 1984). It is therefore possible that detachment from tubulin caused by hyperphosphorylation may simply lead to unbound tau diffusing down its concentration gradient into the somatodendritic compartment, and possibly into dendritic spines (Hoover et al., 2010). It is also possible that the phosphorylation of particular sites, but not others, promotes missorting of tau into dendritic compartments (Zempel et al., 2010). Indeed, pathologically phosphorylated tau has been associated with the postsynaptic terminal using a variety of techniques in a variety of models, including: array tomography in a transgenic mouse model (Kopeikina et al., 2013), green fluorescent protein-tagged tau transfection in dissociated rat hippocampal primary neurone cultures

(Hoover et al., 2010) and immunostaining of synaptic terminals from human AD patients (Tai et al., 2012).

Unlike tau, the endogenous function of amyloid-β remained controversial for many years despite great interest in the protein with regards to its role in disease. Relatively recent research, however, has suggested that physiologically amyloid-β is involved in synaptic transmission, a finding that holds particular interest when looking at the pathological involvement of amyloid-β in AD. Abramov et al., (2009) showed, through use of a competitive inhibitor to the amyloid-β degrading enzyme neprilysin, that endogenous amyloid-β peptides positively regulate the release probability (Pr) of neurotransmitter, reporting no observed effect on postsynaptic function. Consistent with the idea that amyloid-β plays a role in regulating Pr, Cummings et al., (2015) demonstrated that an increase in Pr is one of the earliest changes detected in transgenic mice with raised amyloid-β. Puzzo et al., (2011) also found that depleting endogenous amyloid-β prevented the induction of LTP, possibly via reducing post-tetanic potentiation (PTP). Amyloid-β reduction also impaired learning and memory in behavioural tasks. Taken together, these results suggest a presynaptic role for endogenous amyloid-β in regulating transmitter release, a crucial function for both basal synaptic operation and learning and memory.

A synaptic function for both amyloid-β and tau is fitting, considering that the synapse provides the site for some of the earliest changes in AD (Oddo et al., 2003b, Scheff et al., 2006), and that it is well established that synaptic loss provides one of the best correlates of cognitive decline in AD (DeKosky and Scheff, 1990, Terry et al., 1991). In keeping with this, current opinion has gone on to suggest that the toxic interaction between amyloid-β and tau may occur at the synapse, as will be discussed below (reviewed by Ittner and Gotz, 2011 and Spires-Jones and Hyman, 2014).

Toxic effects of tau at the synapse with links to amyloid-β

For the synaptic localisation of tau and amyloid-β to be relevant to the field of AD, more than just their presence is required. They must also be shown to exert toxicity, resulting in either synaptic dysfunction, or the synapse loss that correlates so well with characteristic cognitive decline of patients (DeKosky and Scheff, 1990, Terry et al., 1991). In the case of tau, such effects have been demonstrated by multiple studies over recent years through the use of transgenic mouse models of tauopathy, including spine

loss (Rocher et al., 2010, Crimins et al., 2012, Xu et al., 2014), or more subtle (often earlier) changes in synaptic function (Yoshiyama et al., 2007, Hoover et al., 2010, Dalby et al., 2014). The specific mechanisms by which such alterations occur, however, remain controversial.

One of the primary synaptotoxic actions of pathological tau is thought to centre on its role in disruptions to MT-dependent axonal transport. In particular, disruption of anterograde transport via interactions with kinesin (Dubey et al., 2008, Ittner et al., 2009, Kanaan et al., 2011), with one of the most important cargoes in terms of toxicity thought to be mitochondria (discussed by Eckert et al., 2014). Due to their large elongated shape and high-energy demands, neurones are particularly dependent on the efficient transport of mitochondria throughout the cell. As well as providing vital ATP, synaptic mitochondria are involved in the regulation of intracellular Ca^{2+} concentration; functions essential for synaptic vesicle release and thus effective synaptic transmission (Vos et al., 2010).

In addition to being implicated in disruptions to mitochondrial transport, tau has also been associated with impairing mitochondrial function directly. Expression of P301L mutated tau in both neuroblastoma cell cultures (Schulz et al., 2012) and transgenic mice (David et al., 2005, Rhein et al., 2009) has been shown to specifically inhibit the activity of complex I of the electron transfer chain, with increasing age and pathology development in mice resulting in a significant reduction in ATP production. A large reduction in ATP production was also noted in the neuroblastoma cells, along with a reduction of mitochondrial membrane potential and increased susceptibility to oxidative stress. The mechanism by which this occurs, however, is still not understood and may indeed represent an indirect effect of tau dysfunction (Eckert et al., 2014). Amyloid-β oligomers have also been found to cause a range of alterations in the function of synaptic mitochondria (as is discussed by Pagani and Eckert, 2011). One of the most highlighted effects is the reduction in complex IV activity induced by amyloid-β, observed in both isolated mitochondria from cultured neuroblastoma cells and in transgenic animal models of amyloid-β dysfunction (Rhein et al., 2009, Lim et al., 2010). Interestingly, the distinct actions of tau and amyloid-β on mitochondrial function were shown to have synergistic effects in a triple transgenic mouse model, resulting in an accelerated reduction in mitochondrial membrane potential and increased reactive oxygen species production with age (Rhein et al., 2009).

Mitochondria are dynamic organelles, undergoing continual fragmentation and elongation through processes known as fission and fusion, respectively. This flexibility allows for renewal and redistribution, and is key for healthy mitochondria and thus cell survival (Chan, 2006). Both tau and amyloid-β have been reported to have affects on mitochondrial dynamics, however, possibly resulting in opposing results. It seems that overall, amyloid-β induces mitochondrial fragmentation possibly through reducing levels of the mitochondrial fusion protein, OPA1 (Wang et al., 2009). Results for tau are somewhat less clear, yet recent evidence suggests that tau causes mitochondrial elongation (DuBoff et al., 2012), resulting in possible consequences on the elimination of damaged mitochondria.

In addition to the combined effects on mitochondrial transport and function, pathological tau and amyloid-β have also been linked to synaptotoxicity through interactions with synaptic receptors. In terms of amyloid-β, numerous binding partners have been identified at the synapse, with the issue of which may be functionally important in AD still the matter of hot debate. Central, however, appears to be the direct and indirect actions of amyloid-β on postsynaptic glutamate receptors, with both the activation of processes involved in excitotoxicity and neuronal death, and the initiation of mechanisms involved in long-term depression (LTD) and synapse loss, being reported (Spires-Jones and Hyman, 2014). A simplified overview of some of the significant and most highlighted interactions of amyloid-β at the synapse is given in Figure 1.2.

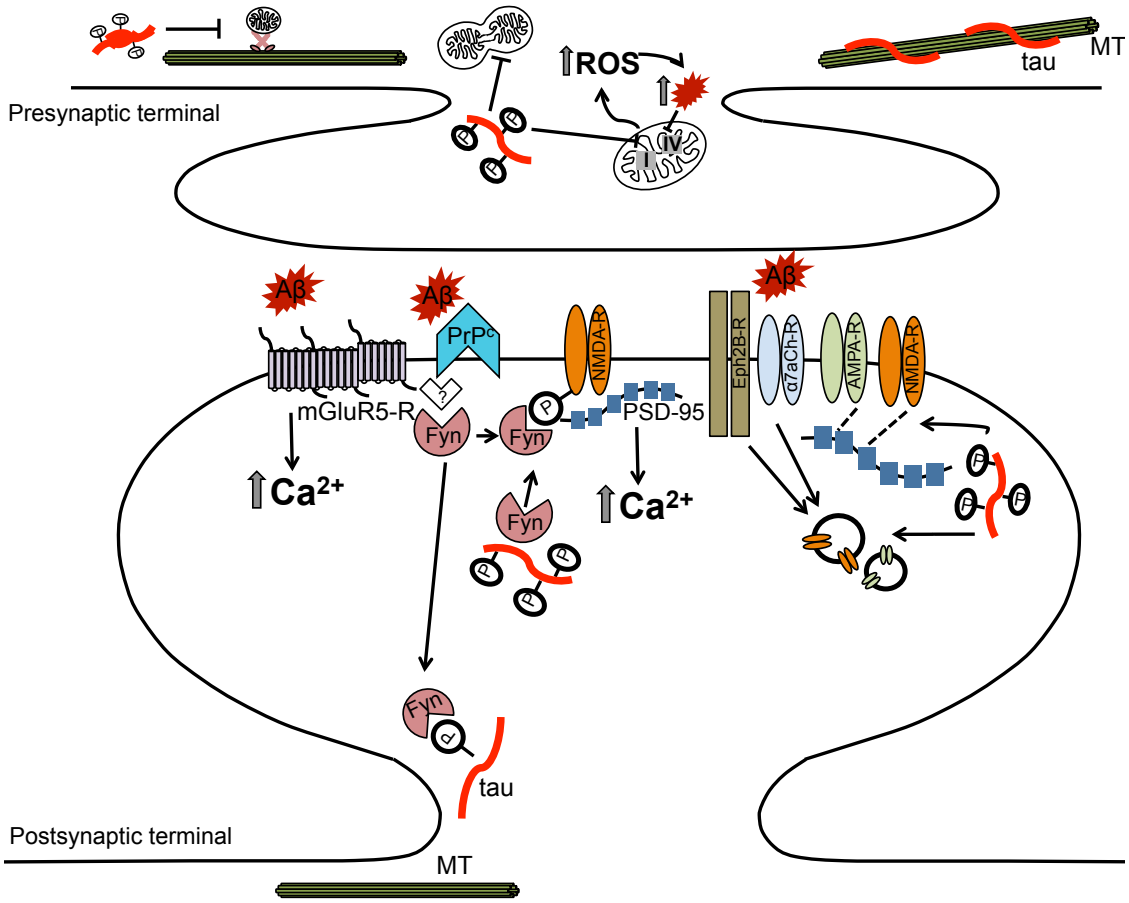

Figure 1.2. Simplified schematic of some of the cooperative actions of amyloid-β and tau at the synapse. Hyperphosphorylation and mislocation of tau to the somatodendritic compartment may affect axonal transport of essential cargoes, including mitochondria, to the presynaptic terminal (Dubey et al., 2008, Ittner et al., 2009, Kanaan et al., 2011). Both amyloid-β and tau have been shown to inflict deleterious effects on mitochondrial function (depicted here in the presynaptic terminal), including a role for tau in reducing activity of complex I (Rhein et al., 2009, Schulz et al., 2012), and amyloid-β in reducing complex IV activity (Rhein et al., 2009, Lim et al., 2010).

The actions of tau in targeting Fyn to the postsynaptic site are depicted (Ittner et al., 2010). Here Fyn works to phosphorylate NMDA-Rs, thus facilitating their interaction with PSD-95, stabilizing them within the synapse and thus increasing Ca^{2+} influx (Ittner et al., 2010). Tau has also been proposed to disrupt NMDA-R and AMPA-R trafficking and anchoring (Hoover et al., 2010).

Key amyloid-β-binding partners relating to glutamate receptor alterations are shown. While there is no evidence for the direct binding of amyloid-β to NMDA-Rs, many studies have demonstrated binding in close proximity, with the suggestion that the effects of amyloid-β are NMDA-R-dependent (De Felice et al., 2007, Decker et al., 2010). Amyloid-β has also been shown to alter synaptic NMDA-R expression via an interaction with α7-nicotinic acetylcholine receptors (α7aCh-Rs) (Snyder et al., 2005) and the NMDA-R regulatory receptor, Eph2B (Cisse et al., 2011). PrP^c has been shown interact directly with amyloid-β (Lauren et al., 2009), activating Fyn via an as yet unknown intermediary (Um and Strittmatter, 2013), which in turn phosphorylates tau, as well as NMDA-Rs (Larson et al., 2012, Um et al., 2012). In addition to interactions with ionotropic glutamate receptors, the metabotropic glutamate receptor 5 (mGluR5-R) has also been implicated in facilitating amyloid-β synaptotoxicity. Renner et al. (2010) showed that amyloid-β caused clustering of mGluR5-Rs by inhibiting lateral diffusion, increasing Ca^{2+} influx and neurotoxicity.

One interesting suggestion as to how tau brings about changes in synaptic functioning was alluded to above, revolving around the role of tau in mediating the targeting of Fyn to the postsynaptic compartment (Ittner et al., 2010). This interaction provides another viable route to link tau dysfunction with amyloid-β, making theories regarding this relationship appealing. Within the postsynaptic terminal, Fyn works to phosphorylate the GluN2B subunit of the NMDA-R, stabilizing it through facilitating the interaction of the receptor with PSD-95. As disruption of this interaction prevents excitotoxic damage, it seems that it is via its interaction with PSD-95, that these NMDA-Rs are linked to excitotoxic signalling. Ittner et al., (2010) showed that in tau knock-out ($tau^{-/-}$) mice, as well as in mice harbouring a truncated form of tau (Δtau), there was reduced postsynaptic Fyn localization, resulting in lower NMDA-R phosphorylation, destabilized NMDA-R/PSD-95 interaction and therefore protection from amyloid-β-induced excitotoxicity. Intriguingly, in 2012, it was demonstrated that cellular prion protein (PrP^{c}), which was already known to bind amyloid-β (Lauren et al., 2009), formed a complex with amyloid-β and Fyn (Larson et al., 2012, Um et al., 2012). This resulted in Fyn activation and thus the phosphorylation and stabilization of the NMDA-R at the postsynaptic site. This work provided a mechanism by which amyloid-β oligomers could result in increased NMDA-R mediated excitotoxicity. Roberson and co-workers (2011) supported these findings by showing that a reduction in tau was protective against the detrimental synergistic actions of amyloid-β and Fyn on synaptic transmission and network activity. These data strengthen the idea of cooperation between amyloid-β, Fyn and tau, possibly through tau-dependent targeting of Fyn to the postsynaptic site (Ittner et al., 2010). Interestingly, it has been reported that mutations in *MAPT,* as well as the phosphorylation of tau, increase its interaction with Fyn (Bhaskar et al., 2005). This increased association could in theory increase dendritic targeting of Fyn by tau, further perpetuating amyloid-β toxicity.

Of note, it has been demonstrated that the NMDA-R open channel blocker, 3,5-dimethyladamantan-1-amine (memantine), preferentially blocks activation of GluN2B containing NMDA-Rs (Grimwood et al., 1996), and thus it is perhaps through inhibiting toxicity created via Fyn activation, that the drug provides beneficial effects both experimentally (De Felice et al., 2007) and as a symptomatic treatment for AD patients (Zadori et al., 2014).

As depicted in Figure 1.2., the process of amyloid-β toxicity at the synapse is complicated, with many interrelated and seemingly conflicting mechanisms of action

reported. Through tau-dependent interactions with Fyn, amyloid-β is linked to increased excitatory activity and neuronal excitotoxicity (Roberson et al., 2011, Boehm, 2013). This mechanism of toxicity appears distinct from the synaptic depression and spine loss so often reported as a consequence of amyloid-β (as discussed by Koffie et al., 2011). In this vein, amyloid-β has even been linked to the activation of the striatal-enriched phosphatase (STEP) (Snyder et al., 2005), which actually works to inactivate Fyn. It is, however, feasible that these conflicting actions operate in a temporal manner, with Fyn activation occurring rapidly and STEP working with a delay of a few minutes (Boehm, 2013).

Pathological species of tau have also been linked to changes in glutamate receptor densities and functioning through the work of Hoover et al., (2010). This study suggested that one of the earliest consequences of tau hyperphosphorylation and mislocation from the axonal compartment is its entry into dendritic spines. They demonstrated that this pathological tau was able to disrupt glutamatergic synaptic transmission through reducing synaptic expression of NMDA and AMPA receptors, likely via the impairment of receptor trafficking or anchoring to the PSD.

Overall, the picture of toxicity at the synapse is extremely complicated. Current evidence for the role of pathological tau in synaptotoxicity has focused on disruption to axonal transport, as well as deleterious effects on mitochondrial and glutamate receptor functioning; however, with the physiological role of tau at the postsynapse now exposed, understanding of the part played by tau in synapse dysfunction and loss is set to increase.

Tau staging in AD

The initial observations by Braak & Braak (1991) that tau pathology in AD patients follows a defined course of progression set the groundwork for some very interesting work investigating tau propagation in AD. They set out six 'Braak stages' of tau pathology progression, which are still widely used today. Each stage sees involvement of a new brain region, along with a worsening of pathology in areas already affected. Stage 1 sees involvement of the transentorhinal cortex, particularly the Pre-α projection neurones; in stage 2, pathology is evident in the hippocampus, in particular the Cornu Ammonis area 1 (CA1) and subiculum; stage 3 sees involvement from the entorhinal region proper. In most cases at this point there are also some mild changes in parts of the limbic system. Stage 4 features a far stronger involvement of the limbic regions with mild involvement of the isocortex. The main feature of stage 5 is that the isocortex is

severely affected, with a more pronounced alteration of the subcortical nuclei. Lastly, in stage 6, all prior areas mentioned now display severe alterations, including considerable cell loss and ghost tangles. All isocortical and subcortical nuclei are now severely affected.

Since this original staging, Heiko Braak has revised these ideas to possibly include an earlier 'stage 0', in which intraneuronal pretangle material can be seen in the lower brainstem, namely the noradrenergic neurones of the locus coeruleus, even before the age of 30 and with no involvement of the cerebral cortex (Braak and Del Tredici, 2011b, a). It is, however, of note here, that in order draw the conclusion that the locus coeruleus presents the initial site of tau dysfunction based on data collected from pre-symptomatic individuals, one must assume that pathologically related alterations in tau (such as the phosphorylation of S202 and T205, as recognised by the AT8 antibody used by Braak and Del Tredici) do not regress. One may argue, however, that examples of transient tau phosphorylation (at sites including the AT8 epitope) during hibernation (Arendt et al., 2003), or even anaesthesia (Planel et al., 2007), provide us with a basis to challenge this assumption. Also noteworthy, is that a proportion of the 38 cases displaying tau positive neurites and cell bodies within the locus coeruleus had suffered acute head trauma or viral infections prior to death. As is the case of head trauma in chronic traumatic encephalopathy (Ling et al., 2015), it is not impossible that these insults have driven the tau pathology noted, rather than the pathology representing the first stage of AD development.

A staging scheme for the development of NFTs has also been created in a transgenic mouse model of tau and amyloid-β pathology. Within this model, the spatiotemporal pattern of NFT development appeared relatively similar to that seen in sporadic AD patients despite the obvious differences in the form of tau expressed, levels of expression and use of a non-physiological promoter. This highlights the vulnerability of specific cell groups, in particular the authors emphasise parallels in EC and hippocampal pathology (Hurtado et al., 2010).

Specific vulnerability

It is from this work by Braak and Braak (1991) that the pattern of tau pathology development through synaptically connected areas in AD was made obvious. This observation initiated the idea that tau pathology might spread through anatomically connected areas by transferring its pathological structure, in a way not dissimilar to prion

proteins (discussed further below). However, despite the apparent synaptic spread, the question of what instigates pathology/neurodegeneration in the primary cells, and why some neurones along the synaptic path appear more susceptible, remained. In answer to these questions, the differential vulnerability of neurones is often offered as an explanation. However, what it is that makes certain neurone types more vulnerable is still an area of debate.

As we have seen, pretangle material has been detected in subcortical nuclei of very young (<30 year-old) individuals (Braak and Del Tredici, 2011b). The authors propose that neurones of the locus coeruleus may more easily revert to an undifferentiated state due to their extremely long, unmyelinated axons. They suggest this may be facilitated by the relative instability of unmyelinated axons compared to those displaying a high degree of myelination, with axonal sprouting possibly acting as a trigger for tau phosphorylation.

This theory is in keeping with the more general view on what causes neuronal vulnerability in a variety of neurodegenerative disorders. Commonly, it is the size of neurones, along with the myelination and length of axons that is assumed to be responsible for their susceptibility (reviewed in Morrison et al., 1998 and Mattson and Magnus, 2006), a reasonable hypothesis due to the high-energy demands and critical dependence on axonal transport of these large neurones. Myelination is also known to reduce the amount of energy used by the neurone, as well as possibly providing trophic support (Nave, 2010). A lack of myelin may therefore result in a higher energy turnover and possible increased risk of oxidative stress, thus causing these neurones to be more susceptible to dysfunction and death. However, size and myelination does not account for all neuronal vulnerability, and thus additional factors must contribute. These may include: increased risk of excitotoxicity due to high numbers of AMPA and NMDA glutamate receptors, or low levels of calcium-binding proteins such as calbindin; compromised neurotrophic factor signalling; high concentrations of somatodendritic neurofilament; or lowered ability to deal with misfolded proteins based on proteasomal degradation ability (Morrison et al., 1998, Mattson and Magnus, 2006).

In fact, the true reason for such specialised susceptibility in all neurodegenerative disorders remains only speculative, and likely relies on a combination of factors including: morphology, neurochemical and functional characteristics and location within neuronal networks, including the properties of surrounding cells such as glia.

Propagating tau

The highly conserved pattern of NFT formation in AD led to the theory that tau may in some way be able propagate through the brain in a similar way to prion proteins. Ideas about the prion-like properties of tau have flourished within the last 5 years, and it is currently one of the most 'fashionable' ideas within the world of AD and tauopathy research. What is possibly most exciting is that these ideas are not solely applicable to tau, but reach into other neurodegenerative disorders, including α-synuclein in PD, which also displays a stereotypical pattern of propagation in the brain (Goedert et al., 2010).

One very interesting case report published in 1997 provides some strong and invaluable evidence that tau pathology is capable of spreading through the brain via anatomically connected areas. Duyckaerts et al., describe the unusual case of a woman with AD, who 27 years prior had suffered the disconnection of a region of cortex from adjoining cortical areas and basocortical afferents following surgery to remove a tumour. Upon post-mortem examination this disconnected area showed almost no tau pathology, despite adjacent cortical areas, as well as the contralateral cortex, displaying many NFTs. The disconnected area, however, did exhibit amyloid-β pathology.

For tau to be able to propagate in a way similar to prion proteins, it must be able to confer a pathological state. Some of the first evidence for this was provided by Clavaguera et al., (2009), when they showed that injection of brain extract from transgenic mice harbouring the P301S mutation into the brains of mice transgenic for wild-type human tau, induced the assembly of the wild-type human tau, not only at the site of injection, but also at distant anatomically connected areas. In an almost simultaneous publication, Frost et al., (2009a) demonstrated that extracellular tau aggregates, made up of truncated tau (containing only MTBRs), but not monomers, were taken up into C17.2 cultured cells where they induced the fibrillisation of intracellular full-length tau. These intracellular tau fibrils were found to be capable of promoting further aggregation. This work has since been supported by many studies, using both exogenous application of tau fibrils to cultured cells (Guo and Lee, 2011, Sanders et al., 2014), as well as intracerebral injection of synthetic tau fibrils into transgenic tau mice (Iba et al., 2013, Peeraer et al., 2015) to demonstrate the ability of tau fibrils to seed further tau aggregation. Further to this, exogenous tau has been found to prompt the co-

aggregation of endogenous tau, showing that its pathological properties are capable of being transmitted to the host protein (Mocanu et al., 2008, de Calignon et al., 2010).

Getting from cell to cell

It is possible that the process of how a pathological form of a protein propagates through the cellular network is different for the various amyloidogenic proteins involved in different diseases, giving rise to diverse patterns of distribution. In the case of tau, it seems that spread occurs synaptically to anatomically connected areas. A recent publication by de Calignon et al., (2012) used a novel mouse model, expressing mutated (P301L) human tau selectively in layer II of the entorhinal cortex (ECII), to examine the progression of tau pathology up to 24 months. Tau misfolding was detected in the axons of entorhinal cortical neurones at 3 months of age; and by 6-months, misfolded tau was present in the soma of these neurones. From here, these neurones displayed a progression towards the later stages of tau pathology with the development of aggregates by 12-months. As predicted, tau pathology was next identified in the dentate gyrus (DG) of the hippocampus (the terminus of the PP, the main output of the ECII/III to the hippocampus), with tau aggregates present in granule cell soma by 18 months of age. CA1 and CA3 also showed aggregation of tau in the soma of cells by 21-months. This sequential development of pathology in areas that (largely) do not express the transgene, does indeed suggest that tau pathology spreads to downstream neurones. These data were corroborated by a similar study in which Lui et al., (2012) generated a comparable mouse model, expressing P301L mutated tau confined to the EC. Again, tau pathology was seen to spread from the EC to anatomically connected neurones over the lifetime of the mouse.

It is perhaps conceivable that as tau is physiologically an axonal protein, and is linked to axonal transport, that it might use these systems to spread through the brain. However, the mechanisms underlying how this may be achieved remain unknown. Aguzzi & Rajendran (2009) provide an interesting review on the subject of transcellular spread, in which they examine how aggregates may be released from cells and then taken up into others. Among the most commonly suggested mechanisms for protein aggregate release are: that it could be part of the normal synaptic physiology; it may occur during degradation of the neurone, axon or synapse, or perhaps it is part of an exocytotic process as a means of clearance, in an attempt to avoid toxicity (Simon et al., 2012).

The picture is similarly speculative with regards to the uptake of tau following its release (discussed in detail by Gerson and Kayed, 2013). Currently, the strongest evidence indicates that tau oligomers/small aggregates gain entry to neurones through an endocytotic process, evidenced by the observed co-localisation of internalised tau with the glycan, dextran (Frost et al., 2009a, Wu et al., 2013). Wu et al., extended this through the observations that tau internalisation was inhibited by the dynamyin inhibitor, Dynasore, and that tau was then observed to co-localise with the early endosomal and lysosomal markers, Rab5 and Lamp1, respectively. This suggests that tau is transported through the endosomal pathway to lysosomes where it is destined to be degraded; however, only a small amount would need to escape this degradation and gain access to the cytosol in order to work as a seeding nucleus for naïve tau aggregation.

Based on existing literature, it seems feasible that small intracellular tau aggregates are released by cells (in exosomes) as a means of eliminating excess protein, or indeed upon the degradation of the neurone or axon. These low weight aggregates could then be taken up via pinocytosis by synaptically connected cells (as the synapse is where the cells are in closest contact) and transported either anterogradely or retrogradely within the cell (Wu et al., 2013), where they could cause naïve tau misfolding, as is discussed below.

What makes tau likely to misfold and aggregate?

Tau is a naturally disordered and unfolded protein, containing only a low amount of secondary structures throughout its length (Mandelkow and Mandelkow, 2012). It is also highly soluble and heat stable due to its hydrophilic nature (*ibid*), causing its aggregation to perhaps seem unlikely. However, as is evidenced from the multiple tauopathies discussed above, tau certainly holds the ability to aggregate, creating the NFTs characteristic of many neurodegenerative disorders.

The key factor that may lie at the heart of tau's tendency for aggregation, is the occurrence of 2 groups of 6 specific amino acids, present at the beginning of the second and third MTBRs (R2 and R3) (Mandelkow and Mandelkow, 2012). These domains exhibit a high propensity to form β-structures and therefore provide tau with the ability to form highly ordered cross β-sheets (Berriman et al., 2003), a property shared by many other amyloidogenic proteins (reviewed by Soto, 2003).

With the amino- and carboxy-domains of tau cleaved, the MTBR region aggregates readily *in vitro* to form filaments comparable to those observed in AD (Wille et al., 1992, Frost et al., 2009a). In fact it has since been shown, that the truncation of tau at only D421 is sufficient to allow the initiation of aggregation *in vivo* (de Calignon et al., 2010), suggesting that even alterations (without full removal) of the possibly 'protective' terminal domains can be enough to permit fibril formation. This spontaneous aggregation, however, cannot be achieved with full-length tau without the addition of further reagents or modifications of the protein (Frost et al., 2009a).

Aggregate inducing reagents commonly used *in vitro* include polyanions, such as heparin, as well as free fatty acids, such as arachidonic acid. Although the exact mechanism by which such reagents work is incompletely understood, their action is believed to be based in their ability to compensate the positive charge in the middle section of the tau protein, thus reducing the repulsion between tau molecules, and facilitating aggregation (Chirita et al., 2003, Mukrasch et al., 2007). Due to their low concentration within the brain, it is unlikely these reagents work *in vivo*, although similar acidic co-factors within neurones are possible.

Even though tau is a disordered protein, recombinant tau has been shown to have an affinity for an overall suprastructure when in solution, in which the ends of the tau protein fold inwards towards the centre, creating a paperclip-like structure (Jeganathan et al., 2006). A hypothesis proposed by Iqbal et al., (2009), suggests that the amino- and carboxy-domains act to protect tau from self-aggregating. When they become phosphorylated however, they unfold, exposing the β-structures of R2 and R3, allowing aggregation. There is, however, evidence to contradict this mechanism. Jeganathan et al., (2008) demonstrated that rather than opening the 'paperclip' structure, *in vitro* pseudo-phosphorylation (specifically of the AD-associated AT8, AT100 and PHF-1 epitopes) worked to further compact this configuration. The contraction was associated with an increase in MC1 reactivity, an antibody recognising a 'pathological conformation' of tau occurring early on in disease development (Weaver et al., 2000). Consequently, it may be through the compaction and stabilization of tau's folded global structure that hyperphosphorylation promotes aggregation, possibly through exposing the β-structure motifs, although exactly how this may occur is unknown.

The inclusion of FTDP-17 mutations increases the susceptibility of tau to become hyperphosphorylated (Alonso Adel et al., 2004), and this may in turn be the path by which mutations such as P301L increase the tendency of tau to form β-sheets and consequently aggregate. Certain FTDP-17 mutations also act to increase the ratio of

4R:3R tau (Goedert and Jakes, 2005), thus possibly increasing the propensity to aggregate by simply increasing the amount of susceptible β-structure regions present in the tau molecule. It is also possible, that the physical effect of a mutation such as P301L directly facilitates the ability of tau to form a β-sheet structure (von Bergen et al., 2001).

Despite aggregation-enabling modifications of tau, nucleation still requires a high enough local concentration of the exposed R2 and R3 domains to overcome the entropy opposing the formation of ordered fibres (Eisenberg and Jucker, 2012). A large increase in tau concentration has been noted in AD brains previously (Khatoon et al., 1992), as well as possibly providing a major contributing factor in many animal models of tauopathy, where exogenous tau is highly overexpressed (Lewis et al., 2000, SantaCruz et al., 2005).

Misfolded tau can 'seed' the misfolding of naïve tau

All of these elements help tau to overcome the nucleation barrier and form an aggregation nucleus. This may then be used to 'seed' further aggregation of naïve intracellular soluble tau, and as described above, propagate this from cell to cell.

The ability of tau to seed further tau aggregation is certainly well established, demonstrated through a variety of experiments using both cell systems (Frost et al., 2009a, Guo and Lee, 2011, Kfoury et al., 2012, Sanders et al., 2014) and animal models (Clavaguera et al., 2009, de Calignon et al., 2012, Liu et al., 2012, Iba et al., 2013, Peeraer et al., 2015). How exactly this seeding is achieved is another question, which has begun to be addressed by the Diamond laboratory through a series of key experiments.

Initially, the group demonstrated that a distinct fibril conformation formed using recombinant tau protein harbouring FTDP-17 related mutations, was able to be transmitted to WT tau protein. This conformation was different to that adopted by WT protein when induced to aggregate through incubation with arachidonic acid alone (Frost et al., 2009b). This study suggested that the conformational change in the protein that leads to aggregation is transmitted via templating. In order to confirm a direct protein-protein interaction between the aggregate seed and unfolded protein, Kfoury et al., (2012) then used Fluorescence Resonance Energy Transfer (FRET) to reveal that the tau protein of the donor cells and corresponding tau of recipient cells were indeed in direct contact. More recently, Sanders et al., (2014) have extended the idea of tau aggregates existing and propagating as distinct strains. They established 2 individual tau aggregate

species based on multiple tests including morphological, biochemical and toxicity analysis. These strains were also found to harbour different seeding efficiencies, and using both non-neuronal cell and *in vivo* models the group were able to demonstrate robust inheritance of each species. This study corroborated the earlier work presented, providing further evidence that tau aggregates work to seed fibrillisation via a template induction mechanism which works through direct protein-protein interaction.

With regards to seeding, however, is it only tau that is able to induce tau aggregation (homotypic seeding), or are other amyloidogenic proteins containing similar amyloid-forming segments also able to promote the aggregation of tau (heterotypic seeding)?

Seeding by other amyloidogenic proteins

The seeding of tau pathology by other amyloidogenic proteins is a very interesting concept. While some studies suggest that heterotypic seeding does not occur (Frost et al., 2009a, Sanders et al., 2014), others have provided evidence that under certain circumstances, other proteins are indeed able to instigate the aggregation of tau.

The most compelling evidence has been demonstrated using α-synuclein to seed tau aggregation. In 2013, Guo et al., showed that a particular α-synuclein fibril strain was able to promote tau aggregation both *in vitro* and *in vivo*. The fibrillar aggregates of α-synuclein and tau were found to be closely associated with one another intracellularly, supportive of the mechanism of physical templating described above. *In vivo*, the injection of these α-synuclein preformed fibrils resulted not only in tau pathology at the site of injection, but also in distant, anatomically connected areas, indicating that these heterotypic seeded tau aggregates were able to propagate.

This study provided conformation of earlier work performed *in vitro*, in which α-synuclein preformed fibrils were seen to promote the aggregation of tau in non-neuronal cells (Waxman and Giasson, 2011), as well as a study that demonstrated synergistic fibril promotion between α-synuclein and tau (Giasson et al., 2003).

While α-synuclein aggregates do occur alongside tau and amyloid-β pathology in a proportion of AD cases, as well as NFTs and plaques commonly existing in PD (reviewed in Galpern and Lang, 2006), the co-occurrence of these pathologies is not assured. Of course, in AD however, plaques and tangles always occur in parallel. Following the 'amyloid hypothesis' as well as evidence presented above, it does indeed

seem that in AD amyloid-β initiates disease progression. One may therefore consider the tempting theory that small amyloid-β aggregates may seed the fibrillisation of tau.

Amyloid-β has been shown to exacerbate tau pathology using a variety of protocols, from intracranial injection of amyloid-β (Gotz et al., 2001b, Bolmont et al., 2007), to cross breeding of amyloid-β and tau transgenic mice (Lewis et al., 2001, Bolmont et al., 2007, Terwel et al., 2008, Hurtado et al., 2010). While these studies confirm a role for amyloid-β in intensifying or even initiating tau pathology, they do not establish amyloid-β as capable of seeding tau fibrillisation. In fact, on the contrary, evidence has suggested that amyloid-β is not capable of directly seeding tau aggregation (Giasson et al., 2003, Sanders et al., 2014). The reason why some proteins such as α-synuclein appear to be capable of seeding tau, while others such as amyloid-β are not, however, remains unclear.

Existing mouse models of tauopathy

Much of the research discussed within this introduction was dependent on the development and use of transgenic animal models. In particular transgenic mice, which since their development during the early 1980s, have provided an invaluable tool for research into the aetiology, mechanisms and possible therapy of countless human diseases. The success of mice as disease models is a result of the relative ease with which they can be genetically modified, their sufficient genetic and neuroanatomical similarity to humans, as well as their size and short life-span, which makes them relatively inexpensive and time efficient with regards to pathology development and breeding.

The development of tauopathy mouse models began in 1995, with a transgenic model expressing the longest isoform of human tau protein, under the human Thy-1 promoter (Gotz et al., 1995). This transgenic tau was seen to mislocate to the somatodendritic compartment of neurones, as well as show phosphorylation at AD relevant sites, although it did not form NFTs. Following this study, further mouse models were developed, each overexpressing different WT isoforms of tau under a variety of promoters, with differing pathological results (a table of transgenic tau strains is given in Gotz and Ittner, 2008).

It was only after the identification of the first FTDP-17 genetic mutations (Hutton et al., 1998), however, that transgenic models of tauopathy surged. In 2000,

Lewis et al., published the first transgenic mouse model presenting prompt NFT formation, using a tau transgene harbouring the P301L mutation. Subsequently many more lines have been established, carrying different FTDP-17 mutations under several promoters (Gotz and Ittner, 2008). Of particular interest is the more recent development of a line expressing human tau carrying the P301L mutation, which can be supressed following doxycycline administration due to the inclusion of a Tet-Off system within the transgene (rTg4510) (SantaCruz et al., 2005). This model has enabled many key findings since its creation, including the observation reported within the original description: that following transgene suppression and the reversal of memory deficits and cell loss cessation, NFTs continued to accumulate. This finding provided one of the first indications that NFTs are not sufficient to cause cognitive decline or neuronal degeneration.

In 2012, the progressive nature of research using transgenic animals was demonstrated when two groups simultaneously developed mouse lines expressing transgenic P301L tau confined within the EC (primarily layer II of the medial EC). This was achieved through crossbreeding rTg4510 mice with a line expressing a tetracycline transactivator under the control of the neuropsin promoter (de Calignon et al., 2012, Liu et al., 2012). Advanced transgenic models such as these provide a novel way in which to answer more specific questions related to the mechanism of a disease; in this case, resolving questions on the propagation of tau.

In contrast to animals engineered to overexpress particular tau constructs, $tau^{-/-}$ models have also provided insight into the role of tau in disease. The first $tau^{-/-}$ mouse was created by Harada et al., (1994) by inserting a neomycin resistance cassette into exon 1 of the tau gene. Surprisingly, these mice displayed a relatively mild phenotype, with the role of tau seemingly compensated by another MT-associated protein within large calibre axons. Some smaller calibre axons however, did show disruption to MT organisation and stability, with a later study revealing some muscle weakness and behavioural changes (Ikegami et al., 2000). This seeming lack of overt pathology argued that tau was not in fact essential to axon development nor did it seem to critically effect normal neuronal functioning. Subsequent to this, two further $tau^{-/-}$ models were developed using similar methods (Dawson et al., 2001, Tucker et al., 2001), which have been utilised in critical experiments for AD, exposing the dependence of amyloid-β effects on tau (Rapoport et al., 2002, Roberson et al., 2007, Shipton et al., 2011).

Another significant line of experiments arising from the creation of tau$^{-/-}$ models, was the role that endogenous murine tau plays in the development of pathology resulting from the insertion of human tau transgenes. This line of study was initiated by the work of Andorfer et al., (2003), who discovered that the removal of endogenous tau facilitated the development of pathology produced by the overexpression of WT human tau. The pathology development in the absence of murine tau appeared to be the consequence of an altered tau isoform ratio, with 3R tau expressed at a higher-level then 4R tau in these animals. This situation is abnormal in mice, which physiologically express only 4R isoforms during adulthood (Liu and Gotz, 2013), and thus it seemed that altering the isoform ratio in mice was sufficient to result in pathology, as is the case in certain tauopathies (Goedert and Jakes, 2005). A lack of isoform ratio alteration may then be used to explain the absence of pathology in a model expressing only the longest 4R2N human tau isoform on a murine tau null background (Terwel et al., 2005). In contrast, this reasoning does not clarify the apparent exacerbating effect of endogenous tau removal in mice overexpressing the 4R1N human isoform carrying the G272V and P301S mutations (Ando et al., 2011). It is hypothesised by Ando et al., that the aggravated pathology in this line may be due to a lack of interference from WT murine tau. Human and murine tau are heterogeneous at their amino-terminals, possibly causing murine tau to harbour a lower tendency to aggregate due to it being less prone to phosphorylation, less negatively charged or less likely to adopt a pathological conformation. This finding is an important consideration for the study of tau pathology initiation in models still expressing endogenous murine tau.

The disadvantages of mouse models of tauopathy

As we have seen, the variety of mouse models available for tauopathy research is already sizable, and has given us the ability to make great advances in understanding of the role of tau in disease. The potential for more sophisticated models is even greater, providing the opportunity to answer specific questions, such as the mechanisms of tau propagation, in a way previously impossible. However, critical to our progression, is a better understanding of exactly what questions can be asked of a mouse model, a point which will be discussed further following consideration of the drawbacks of mouse models of tauopathy.

The first criticism often offered revolves around the fact that the majority of tau models are based on genetic mutations that cause the relatively rare familial FTDP-17, when

many tauopathies (including all AD cases) are not the result of mutations in the *MAPT* gene. Of course, disease development requires an initiating factor and as has been touched upon, certain mouse models have indeed attempted to instigate the disease process simply through the overexpression of a single human WT 4R isoform (Gotz and Ittner, 2008) in the hope of modelling certain tauopathies that see a shift towards 4R tau (Goedert and Jakes, 2005). More recently an interesting mouse model has been established, which carries AD-related genetic mutations at endogenous levels, in the presence of all human tau isoforms on a murine tau null background (Guo et al., 2013b). This model provides a more physiologically relevant line for the study of AD, where amyloid-β can provide the initiating element for tau dysfunction. Disappointingly, however, such models show a relative lack of tau pathology, with no NFTs observed, likely due either to the amount of time needed to develop pathology, or to inherent differences between mice and humans.

Neurodegenerative diseases develop over decades in humans, while mice provide only a 2-2.5 year window in which to replicate the full disease. We know that NFTs can form extremely quickly within mice (<24 hours) (de Calignon et al., 2010), and thus rather than the actual formation of aggregates, it is the slow initiation of this process which may take time beyond the bounds of the life span of a mouse. This unavoidable issue may provide one explanation as to why tau pathology is difficult to obtain without the high overexpression of mutated human tau accelerating the process. The other possibility is that factors critical to pathology development are different in mice, such as differences in misfolded protein degradation or even variations in the immune response. These aspects may modify the processes leading to disease, in effect making mice more resistant to disease development through the more common, 'physiologically-relevant' routes.

Inherent differences between mice and humans may be further exaggerated by the frequent use of inbred background strains, such as the C57Bl/6 line. While these genetically uniform strains do provide significant benefits in facilitating reproducibility, use of such inbred lines does mean that we are looking for pathological changes in a homogeneous population that aim to be relevant in the highly heterogeneous group of human patients. To overcome this problem, robust pathological changes should be identified in multiple animal models in order to increase reliability. For this we need a variety of models, which is why the development of different animal models is still important. In the tauopathy field, the rTg4510 mouse line has dominated research since

its development. The mouse I present in this thesis provides a complementary model to accompany the rTg4510. It harbours the same mutation under the same promoter, but is on a different background line, expressing a different level of tau compared to endogenous protein. To test a therapeutic treatment (such as tau immunotherapy) in both of these models would provide a better grounding for further clinical work than the use of only one of these models.

What should we aim to gain from mouse models?

Transgenic mouse models have been undeniably useful thus far in furthering our understanding of many diseases, however, it is also important to recognise their drawbacks and design experiments moulded to their benefits. In terms of tau, two main questions must be answered: 1) what is the defining moment of pathological tau generation? Here, models in which pathology develops slowly (such as that created by Andorfer et al., (2003), which expresses WT human tau on a murine tau null background) provide a larger window, and possibly more physiological relevance for functional studies into the consequences of tau phosphorylation, mislocation and oligomer formation; 2) how does pathological tau cause neurodegeneration? For this question, a later stage model is required, and thus overexpressing models that show significant neurodegeneration are suitable. Also important for AD is dissection of the interaction between amyloid-β and tau. While the model created by Guo et al., (2013b) did not show NFT pathology or neurodegeneration, it still provides a useful model for early interactions between the 2 proteins. Electrophysiological experiments may be suited here, in an attempt to uncover subtle changes in synaptic transmission, with comparisons drawn between the tau expressing and $tau^{-/-}$ models.

The hippocampus

The hippocampal formation (or hippocampus) describes a unique neuronal network consisting of various subregions, found relatively conserved within mammals. It includes the EC, DG, hippocampus proper (CA1, CA2 and CA3), subiculum, presubiculum and parasubiculum, and is found in humans sitting deep within the medial temporal lobe of the brain. From here it forms widespread connections to other brain regions via outputs through the EC and fimbria. Within the hippocampus lies the famous excitatory trisynaptic loop, a relatively simple, largely unidirectional circuitry that connects the subregions of the formation. This, along with the organised distribution of

many of its inputs has made the hippocampus the most common site for studies into synaptic plasticity.

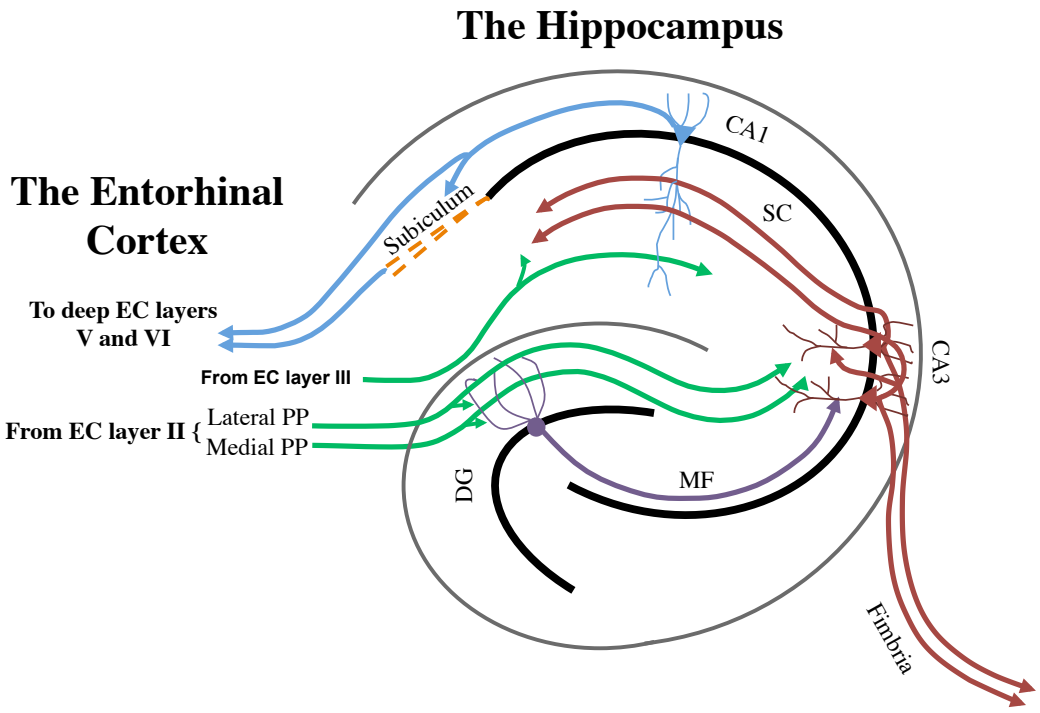

Figure 1.3. Simplified schematic of the hippocampal network. The network is principally unidirectional. Input from the entorhinal cortex connects to the dentate gyrus and CA3 regions via the medial and lateral perforant paths (mPP and lPP, respectively). CA3 cells receive input from the dentate gyrus via mossy fibres (MF). CA3 then connects to CA1 via the Schaffer collateral-commisural (SC) pathway, as well as forming collateral connections with other CA3 neurones. CA1 also receives direct input via the perforant path from layer III of the entorhinal cortex. CA1 neurones provide input to the subiculum, which in turn forms the main output of the hippocampus to the deep layers of the entorhinal cortex.

A schematic of the intrinsic hippocampal connections is seen in Figure 1.3. This somewhat simplified view serves to show the unique organisation of the hippocampus, as well as providing some basis for later reference. The circuit begins in the EC, where, from cortical layer II, the medial (mPP) and lateral (lPP) perforant paths project to the DG and CA3 regions (van Groen et al., 2003). A direct connection is also made between layer III of the EC and the CA1 and CA3 regions (*ibid*). The principle cells of the DG, known as granule cells, project to the large pyramidal cells of CA3 through what are termed mossy fibres (MF). Two branches of axons then extend from the CA3 region; one leaves the hippocampus via the fimbria, while the other is sent through CA2 to the pyramidal cells of CA1, as the Schaffer collateral (SC) pathway. These fibres are correctly termed the Schaffer commissural-collateral pathway as they include commissural projections from the contralateral CA3 region, however, for the purpose of

the present study we shall simply refer to the SC pathway. CA3 neurones are also highly connected to each other, by way of CA3-CA3 collateral connections. Finally, the CA1 region projects to an area known as the subiculum, with both the CA1 and subiculum projecting back to the EC (deep layers) forming the main output of the hippocampus.

The hippocampus and neurodegenerative tauopathies

As we have seen, NFT pathology follows a highly conserved topographical and hierarchical pattern of development in AD, with the hippocampus providing one of earliest brain regions to be affected (Braak and Braak, 1991). This characteristic pattern of tau pathology advancement is paralleled by (and often exceeded by (Gomez-Isla et al., 1996, Gomez-Isla et al., 1997)) neuronal loss. Not only does the hippocampus suffer a considerable loss of neurones (particularly the CA1 region (West et al., 1994)), but it is also one of first and most quickly progressing areas of degeneration early in the disease (Scahill et al., 2002), with reductions in volume likely reflecting not only the loss of neurones, but also neuropil, including synapses. The selective distribution of NFT pathology and neuronal loss is compatible with the temporal development of cognitive symptoms in AD. The hippocampus is believed to play a major role in the consolidation and retrieval of new declarative memories, in particular episodic memories (that is memories of experienced events), an idea first prompted by the discovery that lesions to the hippocampus in human patients severely impaired memories formed following the lesion (Scoville and Milner, 1957). It is defects in this type of memory that is so characteristic of the initial symptoms of AD, and it is likely due to isolation and degeneration of medial temporal lobe structures including the hippocampus.

For FTDP-17, the pattern of NFT development and neurone loss is less well defined due to the rarity of cases and large heterogeneity of clinical and neuropathological features. Typical to the disease is substantial atrophy of the frontal and temporal lobes; however, tau pathology within the hippocampus has been described, including from cases possessing the P301L mutation (Spillantini et al., 1998, Mirra et al., 1999).

In addition to human tauopathies, the rTg4510 murine model harbouring human tau carrying the P301L mutation under the CaMKII promoter displays particular vulnerability of hippocampal neurones (Spires et al., 2006). Combined, these demonstrations of vulnerability led us to select hippocampus as the site of the initial characterisation presented within this thesis.

Studying the function of the hippocampus

The hippocampus and behaviour

The role of the hippocampus in learning and memory was largely determined through observing behavioural deficits caused by selective lesions to this brain region. Through the use of this technique, numerous studies in various species have confirmed the importance of the hippocampus, and adjacent EC, in the memory and processing of spatial information (for example, a review of these data in rats is given by Jarrard, 1993). This function relies on the work of specialised neurones residing in the hippocampus and surrounding regions, which have been identified over the years using electrophysiological techniques. These cell types include: the place cells of the hippocampus and medial EC (O'Keefe and Dostrovsky, 1971, O'Keefe, 1979); head direction cells of the dorsal presubiculum (and other brain regions) (Taube et al., 1990, Taube, 2007); grid cells of the medial EC, pre- and parasubiculum (Hafting et al., 2005, Boccara et al., 2010); as well as the boarder cells of the medial EC (Solstad et al., 2008). Together, these neurones work to encode a representation of external space and the animals' position within it.

In addition to the processing of spatial information, damage to the hippocampus and surrounding regions has also been observed to cause deficits in declarative memory, as was demonstrated by the well-known case of patient H.M. following surgery to correct for severe epilepsy (Scoville and Milner, 1957). Recently, Buzsaki and Moser (2013) have put forward an interesting theory linking the hippocampal/EC-dependent coding of spatial information, with both semantic and episodic memory in humans. They suggest that the more sophisticated mechanisms of memory in humans have evolved from navigations systems, with both based on the same fundamental network. The authors propose that the roots of semantic memory (memory of general facts independent of temporal context) lie in allocentric navigation (navigation of space using distal cues), while the origins of episodic memory (memory of autobiographical events that occurred at a particular time and place) lie in egocentric navigation (navigation using internally-generated cues).

In order to test hippocampal function in rodents, various different tests incorporating spatial memory assessment have been developed. These include a variety of different mazes in which the animal must remember a particular location (such as the location of the platform in the Morris water maze (Morris, 1981)), as well as mazes in which the

animal must remember which location it has previously visited and alter its response accordingly (such as the T-maze or Y-maze).

Due to the sensitivity of the T-maze forced alternation task to hippocampal dysfunction (Dudchenko, 2001), this test was chosen to examine the function of the hippocampus within the present study. This 'working memory' version of the T-maze has also been reported to show high sensitivity to the phenotype of a mouse model of amyloid-β dysfunction (Tg2576) (Stewart et al., 2011) despite its relative simplicity, further fuelling our decision to use this protocol to assess the effects of tau transgene expression within the hippocampus

The hippocampus and electrophysiology

The unique structure of the hippocampus lends itself particularly to electrophysiological study, due to its largely unidirectional circuitry and densely packed cell layers. As is described in Appendix 1, the tight lamina structure of the cell layers facilitates extracellular field recording due to the simultaneous synaptic stimulation of the postsynaptic neurones creating a current 'sink' large enough to be recorded. This current sink is recorded as the postsynaptic response, and can be stably recorded for long periods of time in various different tissue preparations. This ability to record for a long time from a population of cells led to the discovery of LTP (Bliss and Gardner-Medwin, 1973, Bliss and Lømo, 1973), a phenomenon currently considered the best cellular model of learning and memory.

LTP recordings within the hippocampus are now commonly used to assess the capacity for learning and memory in models of dementia, performed both *in vivo* and *in vitro*. From these studies using a variety of different preparations it has often been reported that amyloid-β oligomers inhibit LTP (Haass and Selkoe, 2007). In terms of LTP and tau dysfunction, the majority of studies have focused on the SC-CA1 synapse, where a reduction in LTP has been reported in 'pro-aggregant' tau transgenic mice (Sydow et al., 2011), in P301S transgenic mice recorded *in vivo* (Yoshiyama et al., 2007), in rTg4510 transgenic mice harbouring the P301L mutation (Hoover et al., 2010), as well as under certain induction conditions in aged mice expressing human WT tau (Polydoro et al., 2009).

In addition to extracellular field recordings, electrophysiology allows the identification of more subtle changes in synaptic transmission through the use of patch clamp experiments of single neurones within a network. Overall, few studies have employed patch clamp techniques to examine the effect of tau dysfunction on single

neuronal properties, basal synaptic transmission and evoked activity, however, those studies performed have concentrated within the hippocampus and cortex (Hoover et al., 2010, Crimins et al., 2012).

Conclusion

The role of tau in neurodegenerative disease is well established, with it seeing involvement in rare forms of dementia including, FTDP-17, progressive supranuclear palsy, Pick's disease, and corticobasal degeneration; as well as the most prevalent dementia, AD. Dissection of the aetiology of these diseases continues to rely heavily on the use of mouse models, which provide a way to model aspects of these disorders in a mammalian system. However, in order to further our understanding and test novel treatments for tauopathy disorders, additional complementary models are required to provide the variation necessary to establish effective therapies for the heterogeneous human population.

Herein I describe the first characterisation of a novel mouse model of tauopathy. Using molecular biology techniques, I provide characterisation at the genetic and protein level in TauD35 mice, providing confirmation of the functionality of the transgene. This work is complemented by histological techniques, which allow investigation of age-dependent development of tau pathology and neuronal loss within these mice.

Considerable evidence has so far pointed towards the synapse being the site of the initial dysfunction occurring in AD (Oddo et al., 2003b; Scheff et al., 2006). It therefore follows that I undertake electrophysiological characterisation of synaptic transmission in these mice at ages corresponding to histological data. Behavioural tests were also used to provide some insight into hippocampal-dependent memory as well as locomotor activity and anxiety.

CHAPTER 2

Materials and Methods

All experiments were conducted according to UK Home office regulations under the Animals (Scientific Procedures) Act 1986 and in agreement with the GlaxoSmithKline statement on the use of animals, as well as UCL local ethical guidelines.

Mouse Model

Transgenic TauD35 mice were generated by GlaxoSmithKline (Harlow, UK) on the background mouse line C57Bl/6J (Charles River, UK) via pronuclear injection. The mice harbour human tau cDNA for the 0N4R isoform carrying the P301L mutation under the alpha isoform of the Ca^{2+}/ calmodulin dependent protein kinase II (CaMKIIα) promoter. The present study represents the first characterisation of this novel mouse model. Non-transgenic littermates were used as wild-type (WT) controls. All mice used in the present study were male. Following weaning at 21 days of age, environmental enrichment of the mice began. Mice were group-housed at GSK in cages (20x35x45cm) with a maximum of 8 mice, with 12h light /12h dark cycle and *ad libitum* access to food and water. Environmental enrichment consisted of the placement of novel objects within the cage, including running wheels and plastic tubes, along with different forms of housing and bedding, which were changed once a week. Food location was also regularly changed. At approximately 3 months of age the mice were transported to University College London Biological Services Unit, where their enrichment was continued. Tails samples from all mice were collected post-mortem for re-genotyping using standard PCR protocols, as well as transgene copy number determination using TaqMan® qPCR.

Molecular Biology

Conventional PCR

Genotype confirmation was performed at UCL by Rivka Steinberg, using conventional PCR methods

Briefly, genomic DNA was extracted using the 'HotSHOT' lysis method. Alkaline lysis reagent (25 mM NaOH, 0.2 mM EDTA, pH 12) was added to tissue samples prior to heating to 95°C for 30 minutes. The sample was then cooled to 4°C before the addition of neutralisation buffer (40 mM Tris-HCl, pH 5). The PCR reaction was performed through addition of MyTaq™ DNA Polymerase (Bioline) reaction buffer and primer pair: 5'-AAGACCAAGAGGGTGACACGG-3', 5'-CCCGTCTTTGCTTTTACTGACC-3', using the cycling parameters: 94°C (2 mins), 58°C (30 secs), 72°C (4 mins) and 30 second extension time, for 30 cycles.

TaqMan® qPCR

Copy number confirmation was performed by Stuart Martin, Head of Molecular Biology Unit, UCL

Genomic DNA was extracted using the 'HotSHOT' lysis method described above. Unique TaqMan® primer and probe sequences were generated using Applied Biosystems custom design sequence using the published sequence for the CaMKIIα promoter sequence (Accession# AJ222796). The qPCR assay was run with 4µl of genomic DNA per well, with each sample run in triplicate to reduce error, using the published protocol: Applied Biosystems TaqMan® copy number assays protocol, p21-25.

Brain tissue extraction

Brains were collected from WT, $_{LOW}$TAU and $_{HIGH}$TAU (where available) mice, at 4, 13 and 24 months old. Brains were extracted on ice, hemisected, and dissected into cerebellum, cortex and hippocampus (<5 minutes) before being snap frozen on dry ice and stored at -80°C.

Protein extraction

Mouse hippocampal samples were sonicated (Branson Sonifier, 450) for 30 seconds at 9-12W in RIPA buffer (1% [v/v] Triton X-100, 1% [w/v] sodium deoxycholate, 0.1% [w/v] SDS, 0.15M NaCl, 20mM Tris-HCl (pH 7.4), 2mM EDTA (pH 8.0), 50mM NaF, 40mM β-glycerophosphate, 1mM EGTA (pH 8.0), 2mM sodium orthovanadate, protease inhibitor tablet (Roche), aprotinin and phosphatase inhibitor cocktail 1 and 2 (1:100; Sigma), 1mM PMSF: approximately 1ml for 100mg tissue).

For *total* extract protein, homogenates were spun at 17,950g for 10 minutes at 4°C and the supernatant collected. Sample buffer (312.5mM Tris (pH 6.8), 10% [w/v] SDS, 250mM DTT, 50% [v/v] glycerol, 0.025% [w/v] bromophenol blue) was added prior to boiling the samples at 95°C for 10 minutes and storing at -20°C.

Sarkosyl-insoluble tau extracts were obtained as described previously (SantaCruz et al., 2005) (Figure 2.1.) 90µl of homogenate was ultracentrifuged at 150,000g for 15 minutes at 4°C. The supernatant (*S1*) was removed for storage and the pellet re-homogenised in 4 volumes of 10mM Tris (pH 7.4), 0.8M NaCl, 1mM EGTA, 10% sucrose, 1mM PMSF and ultracentrifuged as above. The resulting pellet was discarded and the supernatant incubated with 1% sarkosyl (30% sarkosyl NL30, BDH) for 1hr at 37°C, prior to ultracentrifugation at 150,000g for 30 minutes at 4°C. The supernatant was again collected for storage (*S2*) and the pellet re-suspended in 20µl 10mM Tris (pH 8) and 1mM EDTA and labelled *P3:* sarkosyl insoluble tau. Sample buffer (312.5mM Tris (pH 6.8), 10% [w/v] SDS, 250mM DTT, 50% [v/v] glycerol, 0.025% [w/v] bromophenol blue) was added to all fractions prior to boiling the samples at 95°C for 10 minutes and storing at -20°C.

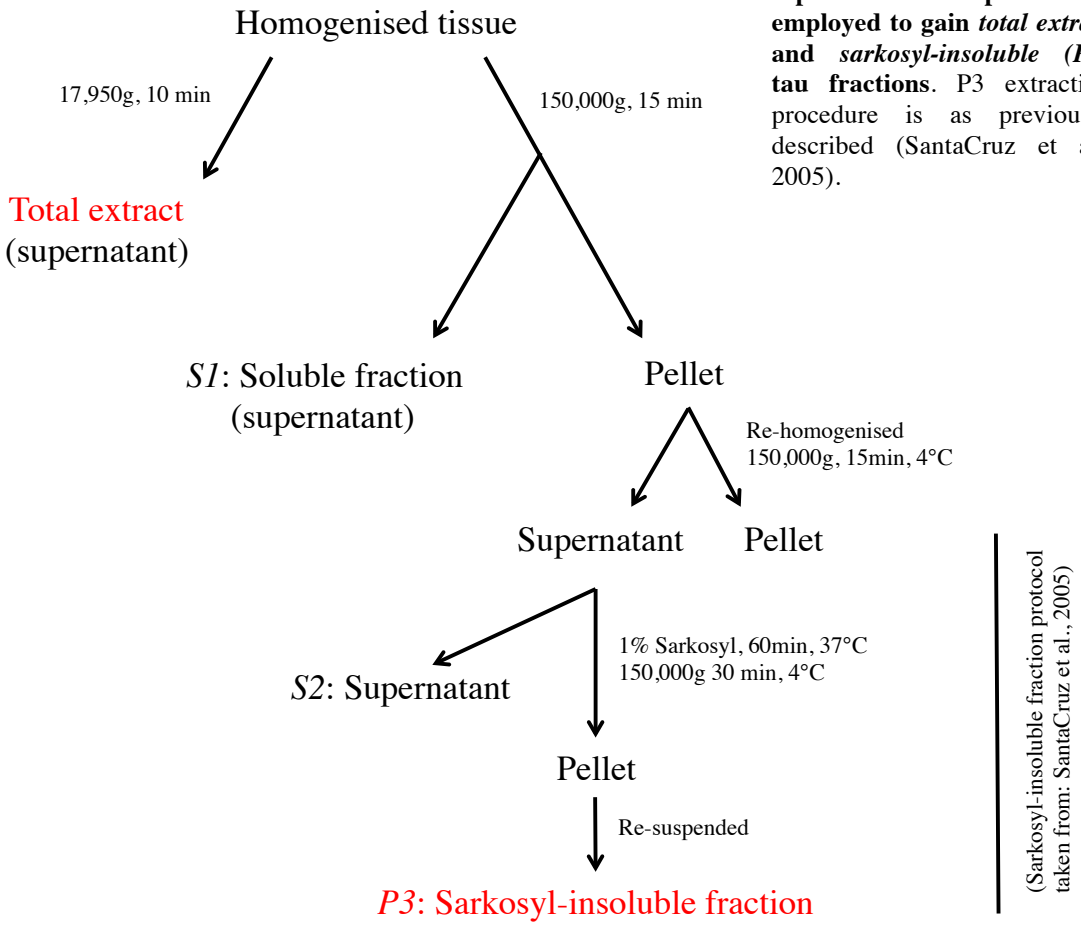

Figure 2.1. Schematic representation of procedures employed to gain *total extract* and *sarkosyl-insoluble (P3)* tau fractions. P3 extraction procedure is as previously described (SantaCruz et al., 2005).

Western blot analysis

Protein corrected (Bradford assay) samples were resolved by sodium dodecyl sulfate-polyacrylamide gel electrophoresis (SDS-PAGE) using 8-10% polyacrylamide gels. Molecular weights were verified using a molecular weight standard (BioRad, #161-0374). Proteins were transferred to a nitrocellulose membrane (0.45µm, BioRad) using electroblotting (30V, overnight). Following transfer, membranes were washed in Tris-buffered saline (TBS), prior to blocking against non-specific antibody binding in 5% milk/TSB for 1 hour at room temperature. Membranes were incubated in primary antibody (at the appropriate concentration, see below) in 5% milk/TBS overnight at 4°C. Following overnight incubation, membranes were washed in 0.05% Tween-20/TBS for five changes of 7 minutes each at room temperature, and then for 10 minutes in 5% milk/TSB. Horseradish peroxidase-conjugated goat anti-mouse (1:10,000; Jackson ImmunoResearch, #115-035-146) incubation was performed in 5% milk/TSB for 1 hour at room temperature. Membranes were washed again for five changes of 7 minutes in

0.05% Tween-20/TBS at room temperature, before a final wash of 5 minutes in TBS. Peroxidase activity was revealed using an enhanced chemiluminescence detection kit (ECL, Amersham). Image acquisition and densitometric analysis was performed using ImageLab (v4.1, BioRad) as described (Taylor et al., 2013).

Density values for bands of interest were normalized against heat shock protein 9 (HspA9, GRP75 (N52A/42) Cambridge Biosciences, #MMS-5164-100), or for sarkosyl-insoluble extract, total protein per lane was detected using Amido Black (Sigma Aldrich).

Antibodies

Table 2.1. Primary tau antibodies used for Western blot analysis:

Antibody (mouse monoclonal)		*Dilution*	*Supplier (Catalogue #)*
HT7	Tau 159-163, human tau	1:5000	Pierce Antibodies (MN1000)
DA9	Tau 102-140, total tau	1:5000	Gift from Peter Davies
CP13	pS202	1:1000	Gift from Peter Davies
PHF1	pS396/pS404	1:1000	Gift from Peter Davies

Histology

Mice

Three primary ages of mice were used for histological study (age in months (average age in months±SEM, sample number)): 4 (4.2±0.1, n=8), 13 (13.0±0, n=7) and 24 (23.9±0.3, n=7). For cell counts an additional time point was included at 17.5-months-old (17.7 ± 0.37, n=4).

Transcardial Perfusion

All mice used for histological study were transcardially perfused unless otherwise stated.

Animals were deeply anaesthetised via intraperitoneal injection of pentobarbital with local anaesthetic (1:10 Euthatal:Intra-Epicaine, National Veterinary Supplies). Once a surgical plane of anaesthesia was reached (established via toe pinch) the mice were transcardially perfused with Phosphate Buffer Saline (PBS) (0.1M, pH 7.2-7.4) followed by 10% Buffered Formal Saline (Pioneer Research Chemicals Ltd). The brains were removed and post-fixed in 10% buffered formal saline for ~24hrs, before being transferred to PBS/sodium azide (0.03%) for storage at 4°C.

Slicing

Prior to sectioning, brains were cryoprotected in sucrose solution (30% sucrose, 0.03% sodium azide, PBS 0.1M, pH 7.2-7.4) for ~24hrs. Transverse hippocampal sections were cut at 30μm from the left hemisphere using a frozen sledge microtome (SM 2000 R, Leica). In order to study NFT formation throughout the whole hippocampus, each hemisphere was sliced entirely and collected into a 24-well plate containing PBS/sodium azide (0.03%) for storage at 4°C. Of a total of ~6 transverse sections per well, 3-4 were found to contain complete and usable hippocampal sections. This provided sufficient separation of each hippocampal section (740μm), removing the risk of double counts.

Antibodies

Table 2.2 Primary antibodies used for immunohistochemistry:

Antibody (mouse monoclonal). Colour indicates the emission wavelength of the fluorophore-conjugated secondary antibody used to visualise each primary antibody listed.		*Dilution*	*Supplier (Catalogue #)*
HT7	Tau 159-163, human tau	1:500	Pierce Antibodies (MN1000)
AT8	pS202/pT205 *Early* indicator of pathological tau (Su et al., 1994)	1:300	Pierce Antibodies (MN1020)
CP13	pS202 *Early* indicator of pathological tau (Su et al., 1994)	1:200	Gift from Peter Davies
MC1	Tau 7-9 and 326-330, conformational change. *Early* indicator of pathological tau (Weaver et al., 2000)	1:200	Gift from Peter Davies
PHF1	pS396/pS404 *Late* indicator of pathological tau (Su et al., 1994)	1:200	Gift from Peter Davies
Iba1	C-terminus of Iba1 Iba1 is a calcium-binding protein specific to microglia (Imai et al., 1996)	1:500	Wako (019-19741)

Immunohistochemistry (IHC)

Standard IHC techniques were employed: sections were washed in PBS followed by PBS-Triton (0.3% Triton X-100 in PBS) before application of blocking solution (8% horse serum, PBS-Triton) for 1h. Incubation with primary antibody in blocking solution was performed overnight at 4°C. Sections were again washed with PBS-Triton. The appropriate secondary antibody (1:500 streptividin-AlexaFlour488 (Molecular Probes) or 1:500 goat anti-mouse-AlexaFlour594 (Invitrogen)) was added to blocking solution for 2h incubation at room temperature in the dark. Following PBS wash, DAPI (1:10,000) was applied to all sections for 5 minutes. Sections were washed for a final time in PBS before mounting. Age-matched sections from WT controls were stained in

parallel for all ages. Sections were mounted in anatomical order onto SuperFrost® Plus glass slides (VWR International) by floating on PBS/water. Fluoromount G (SouthernBiotech) mounting medium was added before applying the coverslip.

Nissl Stain

Sections were mounted as above and left to dry overnight prior to staining. For staining, sections were dipped in dH_20 before being submerged in 1% w/v cresyl violet (Alfa Aesar, Massachusetts) for ~ 2 minutes and blotted to remove excess. Sections were de-stained in 70% ethanol containing 1% glacial acetic acid for <1 minute. Sections were dried by submersion in 100% ethanol for ~ 2 minutes, prior to submersion in xylene (~3 minutes) to remove H_20 completely. DPX mounting medium (Sigma) was added before applying the coverslip.

Imaging and data analysis

Sections were imaged for quantification using an EVOS® FL Auto Cell Imaging System (Life technologies). For immunohistochemistry and Nissl staining, tile images were taken of the whole (transverse) hippocampus using a 20X objective. For immunohistochemistry and cell counts an area of 400μm x 240μm was defined in the CA1, CA3 and the inner blade of the DG. Due to high density Nissl staining in the DG, cell counts could not be reliably obtained for this area. Cell counts were preformed using Adobe Photoshop CS6. For NFT counts within the DG, only cells within the DG granule cell layer were included. NFT counts for double labelled sections (AT8/HT7) included only cells positive for both antibodies. Cell counts using Nissl staining included all principle cells within the defined area, with cells identified by their morphology. Where NFTs/cells could not be individually distinguished, but stain was present, a count of 1 was awarded. NFT and cell counts are therefore an underestimate of true number. Sample sizes (n) given for immunohistochemistry and cell counts indicate the number of animals used to calculate means. A minimum of 3 sections were used to create a mean for each animal. All statistical analyses were performed using Microsoft Excel and PRISM v6 (Graphpad Software, Inc). Representative confocal images were taken using a laser scanning confocal microscope (Zeiss LSM 510) with a 60X Plan-Apochromat oil immersion objective (1.4 numerical aperture).

Behaviour

Housing

Prior to beginning behavioural testing, mice were single housed (in cages 30 x 19 x 17cm) to allow for food consumption to be monitored during diet restriction. Mice were kept on a 12h light /12h dark cycle, with *ad libitum* access to water. A level of environmental enrichment was maintained, with the placement of one form of housing and a toy (for example, a plastic tube or wooden block) in each cage. Housing, bedding and toys were changed weekly. Free feeding weight was recorded for each mouse for 5 days. The target weight for each mouse was set as 90% of the average of their free feeding weight. During this free feeding time mice were introduced to the food reward (Nestlé Carnation condensed milk) and handled each day to reduce anxiety during testing. Mice on a restricted diet were weighed, monitored and fed daily.

For all behavioural tests, mice were transferred to the test room within their home cage. Transfer between the home cage and test apparatus was achieved using a single cardboard tube to which the mice were accustomed.

T-Maze forced alternation task

The protocol used for testing within the T-maze was adapted from that previously reported for use on mice (Cacucci et al., 2008). The maze was constructed from 3 clear Perspex arms (50 x 8 x 10cm), with the 2 goal arms positioned at 90° angles from the start arm, with a black floor. Black wooden blocks were used to block start and goal arms. A food reward (Nestlé Carnation condensed milk) was placed in a small cup at the end of each goal arm. The maze was placed on a table in a room displaying distal visual cues. Lighting in the test room was kept dimmed. The maze was cleaned with 70% ethanol between each run and each mouse to reduce odour cues.

All mice were habituated to the maze for 4 days, during which time they were placed in the maze for 5 minutes, with all arms open for exploration. During the first 2 days drops of food reward were placed on the floor as well as the food cups to promote exploration. During the last 2 days of habituation, food was restricted to the food wells at the end of each arm.

The mice were then trained at the task for a total of 3 weeks (5 days a week). For the first 2 weeks training was performed once a day. During this time each mouse ran 6 trials a day, consisting of one sample and one choice run. For the third week, training was performed twice a day. For the sample run, the mouse was held in the 'start' arm with a wooden block preventing entry into one of the goal arms. The start block was then raised and the mouse was free to enter the unblocked goal arm to receive its food reward. After consuming the reward (20s maximum consumption time), the mouse was then placed back into the start arm. Now both goal arms were unblocked. When the start block was raised again, the mouse was free to choose which arm to enter. On this choice run, only the arm which had been previously blocked contained the food reward. The choice made by the mouse was considered correct if the arm not previously visited was chosen. Response times were recorded for all runs. The mouse was then placed back into its home cage until its next trial.

The goal arms were pseudoramdomly altered, as to which was open on the sample run. Each was presented three times out of the 6 trials for each mouse, with no more than 2 consecutive trials with the same sample location. If the incorrect arm was chosen during the choice run, the mouse was confined to that arm for 20 seconds and then returned to its home cage. During this training period the choice run immediately followed the sample run, with a maximum delay of 30 seconds for cleaning and resetting the maze.

Following this training period, delays were introduced between the sample and choice runs. Delay times of 1, 3, 6 and 10 minutes were chosen, during which time the mouse was placed back in its home cage. During the fourth week delays of 1, 3 and 6 minutes were performed, with delays of 1 and 10 minutes performed the following week. The first day of each week began with a day of trials with no delays. Delays of 1, 3 and 6 minutes were performed over 4 days, with each mouse receiving 2 trials of each delay pseudorandomly alternated per day. Delays of 1 and 10 minutes were performed over a 2-day period. 10-minute delays were pseudoranomly interspersed with 1-minute delays to reduce the possibility of the mice becoming unmotivated to perform the task.

Data were averaged across 2-day blocks. Response times for sample and choice runs were plotted for all mice. Statistical analyses were performed using Microsoft Excel and PRISM v6 (Graphpad Software, Inc).

Locomotor and anxiety testing: Open Field

The open field consisted of a circular arena (diameter: 47.5cm), with a white floor and walls (36cm high). Lighting in the test room was kept dimmed. Behaviour in the open field was recorded using a camera (dacQUSB, Axona, St. Albans, UK) at a sample rate of 4 frame/sec, positioned directly above the arena. Mice were placed in the centre of the arena and allowed to freely explore for the test time of 15 minutes. The arena was cleaned using 70% ethanol after each test.

Mice were tracked within a defined area of interest (optical division of equal areas consisting of the central circle vs. peripheral ring) using Image Pro (v7.0). Analysis of data was completed using custom functions created using R statistical programming (v2.14.1). Data are presented in 5-minute time bins to allow for the evaluation of the change in behaviour over time. Statistical analyses were performed using Microsoft Excel and PRISM v6 (Graphpad Software, Inc).

Light/Dark Box

The test apparatus consisted of a smaller dark 'safe' compartment (20 x 20 x 30cm), and a larger light 'aversive' compartment (30 x 30 x 30cm). Lighting in the test room was bright. Behaviour in the test box was viewed by way of a camera, positioned directly above the test box, linked to a computer screen, which was viewed from a position not visible to the mice. The test lasted 6 minutes. Mice were placed in the light compartment and the parameters of interest recorded in real time. The test box was cleaned with 70% ethanol after each test. Statistical analyses were performed using Microsoft Excel and PRISM v6 (Graphpad Software, Inc).

Electrophysiology

Acute brain slice preparation

Mice were killed by decapitation. The brain was quickly removed (<1 minute) while being submerged in ice-cold '*dissection'* artificial cerebrospinal fluid (dACSF) containing: 125mM NaCl, 2.5mM KCl, 1.25mM NaH_2PO_4, 26mM $NaHCO_3$, 25mM glucose, 0.5mM $CaCl_2$ and 3mM $MgCl_2$, 310-320mOsm/kg, pH 7.4. Following this rapid removal, the brain was placed into a beaker containing ice-cold dACSF for approximately 2 minutes before being dissected. Dissection first involved the removal of the cerebellum; following this the brain was hemisected and a dorsal segment removed from the brain at an angle of approximately 105° from the midline surface (Edwards et al., 1989). The two hemispheres were glued (Henkel Loctite Adhesives, Ltd) onto a slicing stage containing ice-cold dACSF. Transverse hippocampal slices of 400μm were cut using an Integra-slice 7550 vibratome (Campden Instruments Ltd, Leicestershire UK) fitted with a ceramic blade, and placed into an incubation chamber containing dACSF for approximately 5 minutes. Slices were heated to 37°C and then transferred through 2 incubation chambers (37°C) containing ACSF as above, except with increasing $CaCl_2$ and decreasing $MgCl_2$ concentration (0.5mM/1mM, 1mM/1mM respectively) for approximately 5 minutes each. The final incubation chamber contained standard ACSF (as above except with 2mM $CaCl_2$ and 1mM $MgCl_2$). This final incubation chamber was initially heated to 37°C, once all slices had been placed into the chamber it was left to cool to room temperature (22-25°C). Slices were left to recover in this final chamber for at least 40 minutes before use. The reduction in temperature aimed to slow deterioration of the health of the cells. The incubation ACSF was continuously bubbled with 95% O_2/ 5% CO_2 (Carbogen, BOC Medical).

Whole-cell patch clamping and data acquisition

For recording, slices were placed into a submersion-style recording chamber at room temperature (22-25°C) where they were perfused continuously with oxygenated standard ACSF. Micropipettes were pulled from borosilicate glass: 1.5mm outer diameter, 0.86mm inner diameter (Harvard Apparatus, Kent UK) to a resistance of 4-6MΩ. Pipettes were filled with a CsCl-based internal solution composed of: 140mM CsCl, 2mM $CaCl_2$, 5mM HEPES, 10mM EGTA, and 2mM Mg-ATP, pH 7.2-7.3, 280-

290mOsm/kg. Principle cells were identified by their location and distinctive soma. Whole-cell patch clamp recordings were carried out using an Axopatch 1D patch clamp amplifier (Molecular Devices Inc, Berkshire UK); holding potential -70mV; x10 gain.

Access resistance (<50MΩ) was assessed repeatedly throughout the recording through injection of a voltage test-pulse (+5mV, duration 40ms), no difference was observed between WT and TauD35 mice (data not shown). All signals were filtered at 10kHz (low pass Bessel filter; Axopatch 1D patch-clamp amplifier; Molecular Devices Inc, Berkshire UK) and subsequently at 2kHz (low pass Bessel filter; Brownlee Precision 440) prior to digitization (10kHz, Digidata 1322A; Molecular Devices, Inc). Spontaneous and miniature synaptic currents were acquired using Strathclyde Electrophysiology Data Recorder (WinEDR v3.2.6), while evoked postsynaptic currents were acquired using Strathclyde Whole Cell Analysis Program (WinWCP v4.3.2) (University of Strathclyde, Electrophysiology Software).

Spontaneous and miniature excitatory postsynaptic currents

In order to isolate excitatory currents, cells were voltage clamped at -70mV in the presence of SR95531 (6μM, GABAzine, Abcam; a gamma-aminobutyric acid type A ($GABA_A$) receptor antagonist). To isolate miniature excitatory currents, tetrodotoxin (1μM, TTX, Abcam; a voltage-gated sodium channel blocker), was applied in addition to SR95531. Appropriate concentration stock solutions were prepared in distilled water and stored in aliquots at -20°C. Final concentrations were prepared in ACSF as needed and were washed into the chamber for a period of 5 minutes prior to recording. Length of the recording time varied between 20 and 50 minutes depending on the frequency of events (a minimum of 30 excitatory events were recorded).

Evoked excitatory postsynaptic currents

Evoked (e) EPSCs were recorded in the presence of 6μM SR95531, from both the dentate gyrus (DG), via stimulation to the medial perforant path (mPP), and from CA1 via stimulation to the Schaffer collateral (SC) pathway.

DG granule cells or CA1 pyramidal cells were patched using the whole-cell configuration described above. A glass microelectrode filled with ACSF was placed in either the mPP or the SC pathway to evoke presynaptic action potentials using a square pulse constant-voltage stimulator (Digitimer Ltd. Constant voltage isolated stimulator.

Model DS2A - Mk.II). The stimulus intensity used was determined via visual assessment of the size of response when deemed large enough for accurate analysis. Intensities ranged from 0.1 to 25V (pulse duration 100μs). For paired-pulse ratios two stimuli were applied at 25, 50, 100, 200, 400, 800 and 1500ms intervals. Each pair of stimuli constituted one sweep. 10 sweeps were recorded for each inter-pulse interval. Paired-pulse ratios were calculated as the amplitude eEPSC2/eEPSC1.

For AMPA-R desensitization experiments, cyclothiazide (CTZ) (Tocris) was used at a concentration of 100μM. Evoked EPSCs were recorded as above, however, only inter-pulse intervals of 25 and 50ms were applied. A 20-minute washout period was used for washout experiments.

Extracellular field recordings

Recordings were made using an AxoClamp-2B amplifier and acquired using an ITC-16 digitizer, Instrutech (NY, USA) and WinWCP v4.3.2. Both recording and stimulating microelectrodes (1-2MΩ) were filled with ACSF, and placed in the stratum radiatum of CA1. Schaffer collaterals were stimulated using a Grass SD9 stimulator (RI, USA), with a stimulus duration of 100μs. For several recordings, the fibre volley could not be analysed as it was indiscernible from the stimulus artefact. For these experiments, the AMPA-R antagonist, 6-cyano-7-nitroquinoxaline-2,3-dione (CNQX, 20μM), was applied following experiment completion in order to confirm the response quantified was indeed synaptic. The stimulation strength was set to that which evoked 30-50% of the maximal field excitatory postsynaptic potential (fEPSP), as determined through use of input-output recording. The maximum response was defined as the initiation of a population spike or plateau in fEPSP amplitude. Paired-pulse profile recordings were then made using inter-pulse intervals of 25, 50, 100, 200 and 400ms. Prior to LTP induction, fEPSP slopes were monitored for a minimum of 15 minutes to ensure stable synaptic transmission. Two high-frequency stimulus train protocols were used to elicit LTP in different experiments. The first, described as 'weak tetanus' consisted of 20 pulses at 100Hz, repeated 3 times at 1.5s intervals. The second, 'strong tetanus' consisted of 100 pulses at 100Hz, repeated 5 times at 1.5s intervals. Following application of the tetanus, fEPSPs were recorded for a further 60 minutes. All fEPSP data were obtained using paired stimuli with an inter-pulse interval of 50ms (excluding

paired-pulse profile recordings during which the inter-pulse interval was varied) and with a 10 sec delay between each sweep.

D-AP5 (Abcam) was used at a concentration of 25μM. Following input-output and paired-pulse profile recordings, a 10-minute period of stable fEPSP slopes was established. D-AP5 was then infused for a period of 10 minutes. As before, fEPSP slopes were monitored to ensure stability for a minimum of 15 minutes before LTP induction. D-AP5 washout began 15 minutes after high frequency stimulation.

In order to confirm a synaptic response, for a subset of experiments the AMPA-R antagonist, 6-cyano-7-nitroquinoxaline-2,3-dione (CNQX) (Abcam), was applied at a concentration of 20μM following experiment completion.

Data analyses

All data analyses were performed by the experimenter blinded to genotype. Spontaneous and miniature synaptic currents were analysed using WinEDR v3.2.6 and WinWCP v4.3.2. The detection thresholds were set such that the recorded signal had to remain above 3 pA for 2 ms in order to be detected as a current. In all conditions, dead time was set at 20 ms and running mean period at 10 ms. All signals were inspected by eye with the criterion that the rise time must be less than the decay time. Rise times were measured 20 to 80% of the maximum amplitude and decay times were fitted with a single exponential curve to generate the time constant tau (τ) (time to reach 1-1/e of the asymptote). To obtain an average amplitude and decay time constant value per recording, the number of averaged digitized points was set at 10.

Evoked currents were analysed using WinWCP v4.3.2. A minimum of 10 sweeps were recorded for all inter-pulse intervals. Sweeps were then averaged to create an average trace for each interval and the amplitude (taken as the mean of 10 digitized points) of each response was measured. eEPSC2/eEPSC1 was used to determine the paired-pulse ratio for each inter-pulse interval.

Field potentials were also analysed using WinWCP v4.5. Sweeps were averaged in blocks of 6, giving an averaged field potential for 1 minute of recording time. For input-output and paired-pulse recordings, 6 sweeps were recorded and averaged for each stimulus intensity or inter-pulse interval, respectively. Averaged field potential slopes

were analysed using a linear fit to the initial portion (10-50%) of the slope (Figure 2.2.). Sweeps recorded for 15 minutes prior to LTP induction were taken as the baseline, with all following records taken as a percentage of the mean of these baseline recordings.

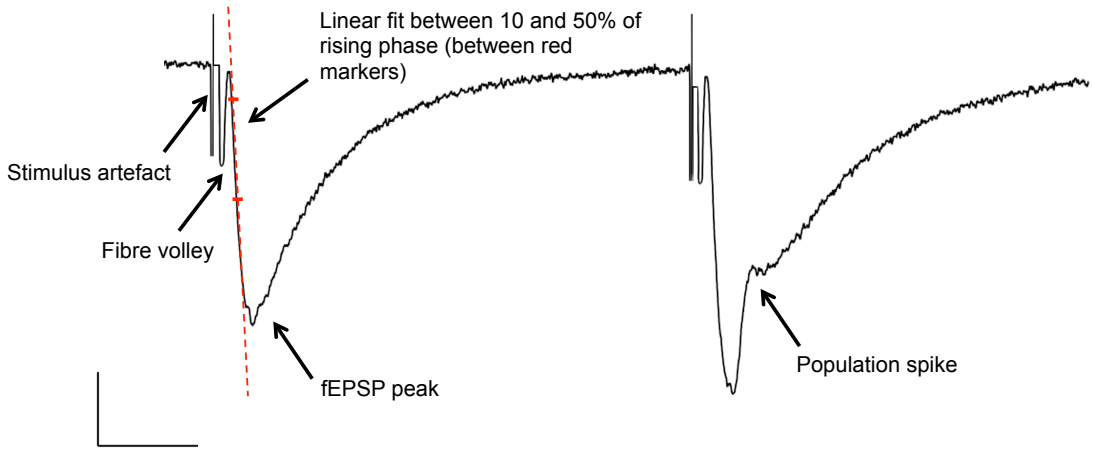

Figure 2.2. Representative averaged fEPSP traces indicating the stimulus artefact, fibre volley, synaptic fEPSP and population spike. A linear slope was fitted to the initial (10-50%) portion of the slope as a measure proportional to response amplitude as indicated (dashed red line). Scale: 0.2mV, 10ms.

Statistics

Results are expressed as means ± S.E.M. If a data point differed more than two standard deviations from the mean for any one of the measured parameters, all parameters for that cell were excluded from statistical analysis. In the case of amplitude distributions, the data would not be expected to fit a Gaussian curve. Therefore the median amplitude was taken for all data sets. As the medians would be expected to be normally distributed across animals within each condition, the means of the median amplitude were then used for parametric analysis. The sample sizes (n) given throughout the text refer to the number of animals used to calculate means; the total number of cells is indicated in parentheses. No more than one cell was ever recorded from the same slice. Differences between group means were assessed with unpaired two-tailed *t*-tests (assuming equal variances). Analysis of variance (ANOVA) was used to compare multiple parameters. Differences were considered significant if $p<0.05$. All statistical analyses were performed using Microsoft Excel, PRISM v6 (Graphpad Software, Inc).

CHAPTER 3

Introduction: Molecular biology

One of the key factors believed to contribute to the development of pathological tau species present in neurodegenerative tauopathies, is the extensive addition of phosphate groups to the protein, known as hyperphosphorylation (reviewed in Iqbal et al., 2009). This is thought to be one of the key factors in instigating a cascade of events, initially leading to the formation of small soluble tau oligomers and culminating in the emergence of NFTs and cell death (*ibid*.). Thus, the detection of these features is imperative for a model of tauopathy.

For the novel TauD35 mouse model to be usable, insertion of the human tau transgene containing the P301L mutation must be functional, in that it retains the ability to be transcribed and translated into protein. In order for this protein then to provide a fundamental characteristic of neurodegenerative tauopathies, it must undergo hyperphosphorylation, which in time renders it insoluble, resulting in the presence of aggregated forms of tau protein. These elements were primarily tested using molecular biology techniques, with the characterisation presented within this chapter forming the basis for further work with this mouse model. In understanding the genetics and protein expression levels, we are able to provide grounding for further investigation and a basis for explaining any differences observed compared to WT mice. It also allows the model to be placed in the context of published literature on existing transgenic mouse lines.

Through the use of qPCR and Western blot techniques, this chapter provides insight into transgene concentration, its consequence on protein expression, and the development of phosphorylated and aggregated tau species across 4-, 13- and 24-month-old mice.

Development of the TauD35 mouse model at GlaxoSmithKline

The TauD35 mouse line was developed at the Platform Technology Sciences unit, GSK (Stevenage, UK) in order to study the effects of the overexpression of human tau containing the P301L mutation. This proline to leucine missense mutation at position 301 lies within exon 10 (2^{nd} MTBR) of the tau gene, and is one of the most common mutations resulting in FTDP-17 (Wszolek et al., 2006).

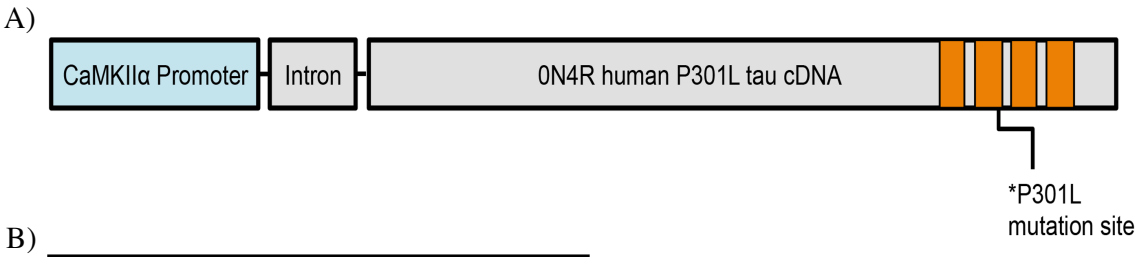

Figure 3.1. The CaMKIIα promoter restricts transgene expression to the forebrain. A) Schematic representation of the transgene construct harboured by the TauD35 mice line. The 0N4R isoform of tau, containing the P301L mutation within exon 10 lies downstream of the CaMKIIα promoter. MTBRs are represented in orange. B) Transverse section from a 24-month-old $_{LOW}$TAU transgenic mouse stained using the human specific antibody, HT7. Note the presence of pathological human tau in forebrain regions. Scale: 1000μm

The model was created on the C57Bl/6J background line, via conventional pronuclear injection techniques. The transgene construct contains the 0N4R isoform of tau encompassing the P301L mutation, under the CaMKIIα promoter (Figure 3.1.A)). CaMKIIα is expressed postnatally in mice, with expression beginning at birth (Parsley et al., 2007). Dramatic increases are evident by day 8, by which time expression within all hippocampal subregions (as well as the rest of the brain) appears comparable to that observed in adult mice (*ibid*). Such expression removes transgene effects on embryo development. CaMKIIα is also largely 'forebrain-specific' (Figure 3.1.B)), and thus use of its promoter avoids motor deficits caused by transgenic tau expression within the spinal cord, as is seen in other tauopathy models (Lewis et al., 2000, Terwel et al., 2005).

All mice were genotyped using conventional PCR methods on ear tissue samples prior to shipping to the Biological Services Unit, UCL, at 3 months of age. Tail samples were collected from all mice post-mortem for re-genotyping and TaqMan® qPCR analysis.

Pathological phenotype present in a subset of transgenic mice between 17 and 20 months of age

While at UCL, it became apparent that a proportion of the TauD35 transgenic mice within the colony developed a moribund phenotype between 17-20 months of age. Of the 28 transgenic mice maintained until this age, 8 were seen to develop this pathological phenotype. This manifested in piloerection, sunken eyes, hunched posture, decreased grooming and difficulties in movement initiation (akinesia) with reduced ambulation.

Mice approaching this age were therefore put under close observation and used prior to any discomfort or euthanized following veterinary advice.

Similar pathological phenotypes have previously been described for mice harbouring transgenic tau containing the P301L mutation. For mice expressing transgenic tau under the control of the murine prion protein promoter, motor dysfunction has been attributed to spinal cord pathology (Lewis et al., 2000). However, some impairment has been noted in mice where expression is under the control of the CaMKIIα promoter, excluding expression from the cerebellum, brain stem and spinal cord (Ramsden et al., 2005). Here dysfunction including decreased ambulation, hunched posture and hind-limb dysfunction were attributed to a loss of higher motor input, supported by observations of pathological changes in the dorsal corticospinal tracts.

With transgenic tau expression also confined to the forebrain in TauD35 mice, it is possible common dysfunctions such as the hunched posture and reduced ambulation are due to degeneration of populations of cortical neurones, resulting in a loss of higher motor input. Indeed, gross neurodegeneration and an enlargement of ventricles was observed in the TauD35 mice presenting with this moribund phenotype (Figure 4.1., Chapter 4 and Figure 7.2., Chapter 7), however, degeneration of neuronal populations outside of the hippocampus were not quantified in the present study. Investigations into possible spinal and/or muscular pathology, and conformation of degeneration in descending motor pathways would be required to comment further.

Genetic characterisation

Primary validation of the TauD35 mouse line at the Platform Technology Sciences unit, GSK (Stevenage, UK) consisted of conventional PCR, and protein expression analysis in the form of Western blotting and immunohistochemistry. These techniques provide information on the stability of the transgene (in detecting possible 'drop-out') and the levels of protein expressed (indicating possible transgene silencing or copy number differences), respectively.

Production of a transgenic mouse model via classical pronuclear injections techniques continues to be favoured method since its development in the early 1980s (Ittner and Gotz, 2007). However, the nature of the technique means that the transgene is inserted randomly into the genome. Expression is therefore subject to the position of integration,

as well as the unpredictability of the number of transgene copies inserted, due to DNA integrating as concatemers. In some cases, the transgene can insert into more than one site within the genome, an event that cannot be detected using conventional PCR methods. During subsequent breeding, it is possible for these integration sites to segregate, creating variation in the transgene copy number harboured by offspring. Genetic recombination events during meiosis may also result in alterations to the transgene copy number inherited by offspring.

Following inconsistences observed during pilot studies conducted at the GSK Neurosciences Therapeutic Area (Shanghai, China), along with the observation that only a proportion of TauD35 mice developed a pathological phenotype in old age, I was prompted to further examine the transgene properties of this novel mouse line. In collaboration with Stuart Martin, we were able to design a qPCR experiment using uniquely designed TaqMan® primers/probe for the CaMKIIα promoter sequence in order to investigate the transgene copy number. Transgene copy number was determined using crude DNA extracts from ear clip tissue samples, or tail tissue samples collected post-mortem.

Protein characterisation

In order to understand the level of tau protein expression in the TauD35 mice across a range of ages, I employed the use of the Western blotting. Developed by Towbin et al., (1979), Western blotting has become a common technique for the detection and quantification of proteins within a complex sample. The technique works by separating proteins based on molecular weight using gel electrophoresis, the proteins can then be transferred to a membrane for detection using appropriate antibodies.

Monomeric human tau protein separated using Western blot is characteristically observed as a 'smeared' triplet of bands, migrating between ~55 and 75kDa. The six different isoforms of tau migrate with slightly different molecular weights due to the inclusion or omission of exons 2, 3 and 10. Heterogeneous phosphorylation of each of these isoforms results in small increases in molecular weight due to the addition of phosphate groups, and these factors combine to create the characteristic smear (Buee et al., 2000). Upon de-phosphorylation, these isoforms are seen to migrate with reduced molecular weights of between ~45 and 65kDa. In this state, the isoforms can be

distinguished and correspond to recombinant tau weights (Goedert et al., 1992, Hanger et al., 2002).

Adult mice express only three of the six isoforms of tau found in humans (Liu and Gotz, 2013). These include only the 4R isoforms, migrating with de-phosphorylated weights of: ~50kDa (0N4R), ~58kDa (1N4R) and ~65kDa (2N4R) (Buee et al., 2000). The transgene construct harboured by the TauD35 mice consists of only the 0N4R isoform, and thus this is additive to the murine isoform present. Large variations in the degree of phosphorylation of the overexpressed mutant human isoform, possibly due to it providing a more amenable substrate for kinases (Alonso Adel et al., 2004), is thought to result in its smeared appearance, spanning 50-60kDa, as has often been observed with mouse models harbouring the same human isoform (Sahara et al., 2002, SantaCruz et al., 2005, Berger et al., 2007, Sahara et al., 2013, Petry et al., 2014).

Results: Molecular Biology

TauD35 transgene copy number

Identification of two separate TauD35 transgenic lines determined using TaqMan® qPCR

In order to ascertain the number of transgene copies harboured by TauD35 animals, qPCR techniques were employed. Due to the insufficient length of conserved human and murine tau sequence, transgene copy number could be determined solely through the development of a probe to the CaMKIIα promoter. Assuming murine homozygosity of CaMKIIα (and therefore an endogenous gene copy number of two), results gathered from transgenic animals were analysed relative to WT copy numbers. Initial results revealed that the copy number of the tau transgene in TauD35 mice was high (with an estimated minimum of 5 copies), but more importantly, there were two clear groups within the transgenic line, one displaying almost double the number of transgene copies of the other. *The 2 lines present were appointed $_{HIGH}$TAU and $_{LOW}$TAU respectively.*

Analysis of this kind only allowed us an idea of transgene copy number, relative to WT controls run alongside each set of samples; however, the indication of 2 transgenic groups prompted more in-depth research.

Transgene copy number is not necessarily correlated to mRNA or protein expression in conventional transgenesis, and therefore determining mRNA or protein expression levels

provides the only definitive answer as to whether differences in gene copy numbers result in an expression effect. In this case, where only copy number of the promoter had been determined, conformation of the functionality of the extra gene dose proved even more important. In order to investigate whether transgene copy number differences were translated to differences in human tau protein levels between $_{HIGH}$TAU and $_{LOW}$TAU mice, Western blot techniques were employed.

$_{HIGH}$TAU mice develop pathological phenotype by 17-20 months of age

In order to determine why only a proportion of TauD35 mice develop the pathological phenotype described previously, mice displaying this characteristic phenotype were investigated with regards to transgene copy number. All tissue samples available from these mice were tested. The results showed that all mice belonging to this group were of the high copy number mouse line ($_{HIGH}$TAU). Due to this, $_{HIGH}$TAU mice were not available above 20 months of age for experimentation.

Western Blot Validation

Western blot analysis was performed using total extract hippocampal homogenate, except where indicated. All tau antibodies used detected their anticipated tau species, migrating between 50 and 70kDa, in WT, $_{LOW}$TAU and $_{HIGH}$TAU mice. The smeared appearance of the tau species between 50 and 60kDa in transgenic mice is in keeping with previous literature, in which a 0N4R tau construct containing the P301L mutation is harboured by different mouse models (Sahara et al., 2002, SantaCruz et al., 2005, Berger et al., 2007, Sahara et al., 2013, Petry et al., 2014).

Confirming the existence of two transgenic lines:
Different levels of human tau protein in the hippocampus of $_{LOW}$TAU vs. $_{HIGH}$TAU mice

The human-specific antibody, HT7, was used to assess whether tau protein levels reflect the differences in transgene copy number between $_{LOW}$TAU and $_{HIGH}$TAU mice. HT7 displays high specificity for human tau, with no non-specific binding observed in WT mice. Hippocampal tissue from 4-month-old mice was used as this age is prior to observable aggregate formation in both lines (Chapter 4). Human tau levels were increased significantly by 170% from $_{LOW}$TAU to $_{HIGH}$TAU mice ($p=0.0126$).

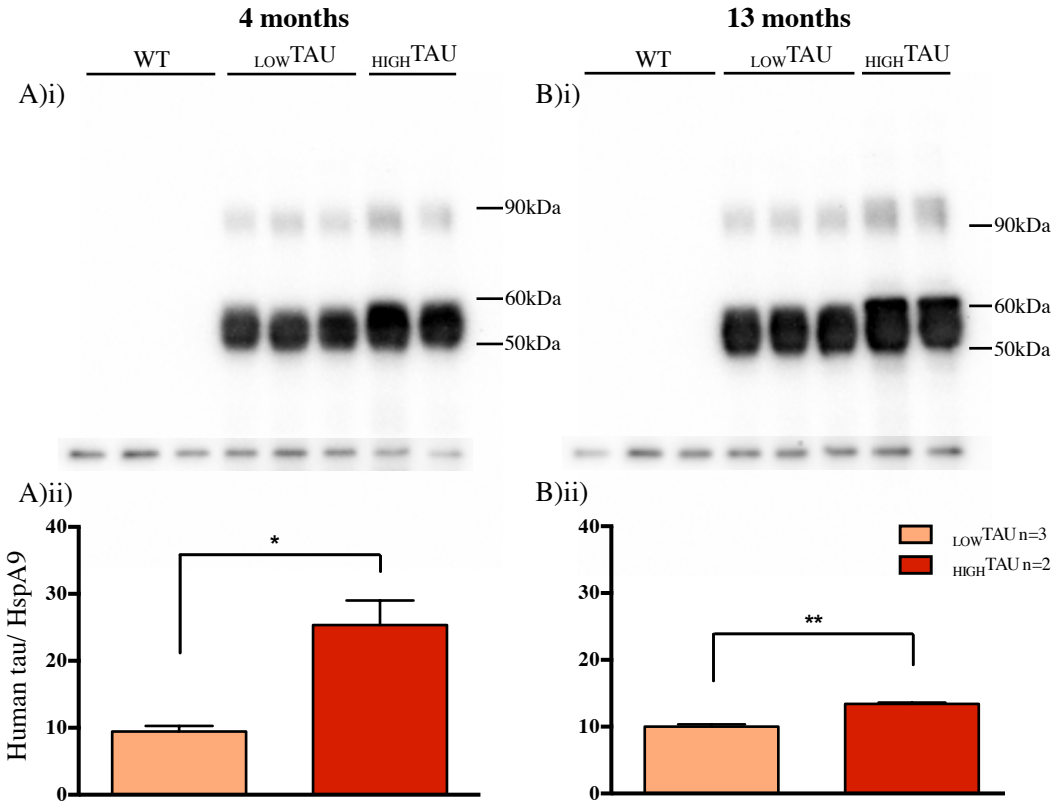

Figure 3.2. $_{HIGH}$TAU mice express significantly more human tau protein within the hippocampus compared to $_{LOW}$TAU animals at 4 (A) and 13 (B) months of age. A)i) *and* B)i) Western blot of total extract, using the human-specific antibody, **HT7**. No human tau protein is observed in WT mice at either age. A)ii) *and* B)ii)Density values for human tau normalised to HspA9 loading control are expressed as mean ± SEM. Significance evaluated using 2-tailed Students *t*-test; $p<0.05$*, $p<0.01$**

To test whether the differences observed in human tau levels between the two transgenic lines were maintained with increasing age, and to provide confirmation to previous results gained, tissue from 13-month-old mice was also tested. The level of human tau protein present in $_{LOW}$TAU mice was similar to mice of 4 months of age. While still highly significant ($p=0.0043$), the percentage increase of 34% recorded in $_{HIGH}$TAU mice at 13-months was decreased from that seen at the younger age of 4-months. This result is likely due to the existence of tau aggregates in 13-month-old $_{HIGH}$TAU mice (Chapter 4), with tau that is incorporated into tangle-like inclusions lost during initial low speed centrifugation in the preparation of total extract homogenate (Berger et al., 2007). In addition to the large band present between 50 and 60kDa, all transgenic mice also exhibit higher molecular weight species (~90kDa), which are discussed further below.

These results provide validation to the transgene copy number differences seen using TaqMan® qPCR. Further validation using Western blot techniques came while performing characterisation experiments (see below).

Western Blot Characterisation of $_{LOW}$TAU and $_{HIGH}$TAU mice

Both $_{LOW}$TAU and $_{HIGH}$TAU mice display relatively low levels of mutated human tau

In order to determine the relative levels of tau in $_{LOW}$TAU and $_{HIGH}$TAU hippocampus compared to endogenous WT murine tau, the pan-tau antibody DA9 was used to assess tissue from 4-month-old mice. This age is prior to observable aggregate deposition in both lines (Chapter 4).

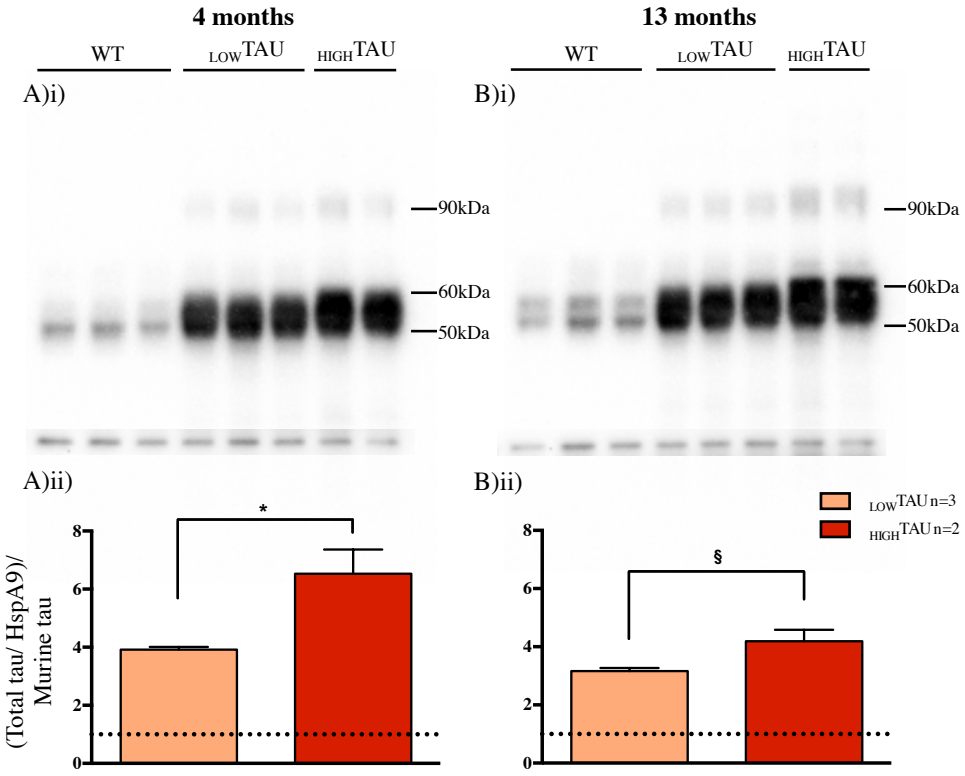

Figure 3.3. Comparison of total tau expression in WT, $_{LOW}$TAU and $_{HIGH}$TAU mice at 4 (A) and 13 (B) months of age. A)i) *and* B)i) Western blot of total extract, using the pan-tau antibody, **DA9**. A)ii) *and* B)ii) All density values normalised to HspA9 loading control. Total tau in transgenic mice normalised to WT, represented by line at 1. Plotted values are expressed as mean ± SEM. Significance evaluated using a 2-tailed Students t-test; $p<0.05$*, $p=0.051^{\S}$

WT mice display bands migrating at ~50kDa, ~58kDa and ~67kDa (*seen only with high overexposure*) corresponding to the 3 endogenous monomeric isoforms of tau expressed in adult mice (Buee et al., 2000, Adams et al., 2009, Liu and Gotz, 2013), with small increases in molecular weight due to endogenous phosphorylation, when compared to de-phosphorylated/ recombinant tau (Hanger et al., 2002). At this age, the ~50kDa band (representing the 0N4R isoform) constitutes the more prominent species of the three, with the 2N4R (~67kDa) isoform constituting the least prevalent isoform, as is consistent with previous data using hippocampal samples from young adult mice (Liu and Gotz, 2013).

A large increase in the prominent 50-60kDa tau species is observed in both transgenic lines when compared to WT mice. In contrast to WT, only one diffuse band spanning 50-60kDa is apparent, due to the abundant expression of the 0N4R isoform and indicting higher varieties of phosphorylated tau species. Levels of tau in $_{LOW}$TAU mice at 4 months of age were found to be approximately 4 times the level of WT murine tau. Tau expression in the $_{HIGH}$TAU line was significantly increased, with these mice displaying a 6.5 times increase.

In order to provide validation of this finding, 13-month samples were also evaluated for total tau. An apparent increase in the 1N4R (~58kDa) isoform was detected in WT mice at this age compared to 4-month-old mice. Despite this increase in murine tau, $_{LOW}$TAU mice presented >3 times the level of tau protein, similar to relative levels detected at 4 months. The level of tau relative to endogenous tau at 13 months in $_{HIGH}$TAU mice was decreased when compared to younger samples. As stated earlier, this decrease is likely due to the incorporation of tau into large aggregates at 13 months (Chapter 4), and their loss during initial low speed centrifugation.

Transgenic mice also display higher molecular weight tau species (discussed further below) in addition to the prominent 50-60kDa band. Smaller species are assumed to be degradation products of tau, or possibly truncated forms of tau as has been suggested previously (Tai et al., 2012).

The relatively small increase in tau protein levels in TauD35 mice, makes both the $_{HIGH}$TAU and $_{LOW}$TAU lines relatively mild transgenic models, compared to other similar lines such as the rTg4510 mouse model, in which tau is expressed 13-fold (SantaCruz et al., 2005).

Age-dependent changes in tau phosphorylation

Two phosphorylation dependent antibodies: CP13, which recognises tau phosphorylation at S202 and PHF-1, which recognises the phosphorylation sites, S396 and S404, were employed to investigate the cardinal feature of pathological tau, hyperphosphorylation. Both CP13 and PHF-1 display high specificity when compared to other tau phosphorylation dependent antibodies (Petry et al., 2014). Samples from 4, 13 and 24 month old mice were analysed in order to investigate the age-dependent aspect of tau phosphorylation.

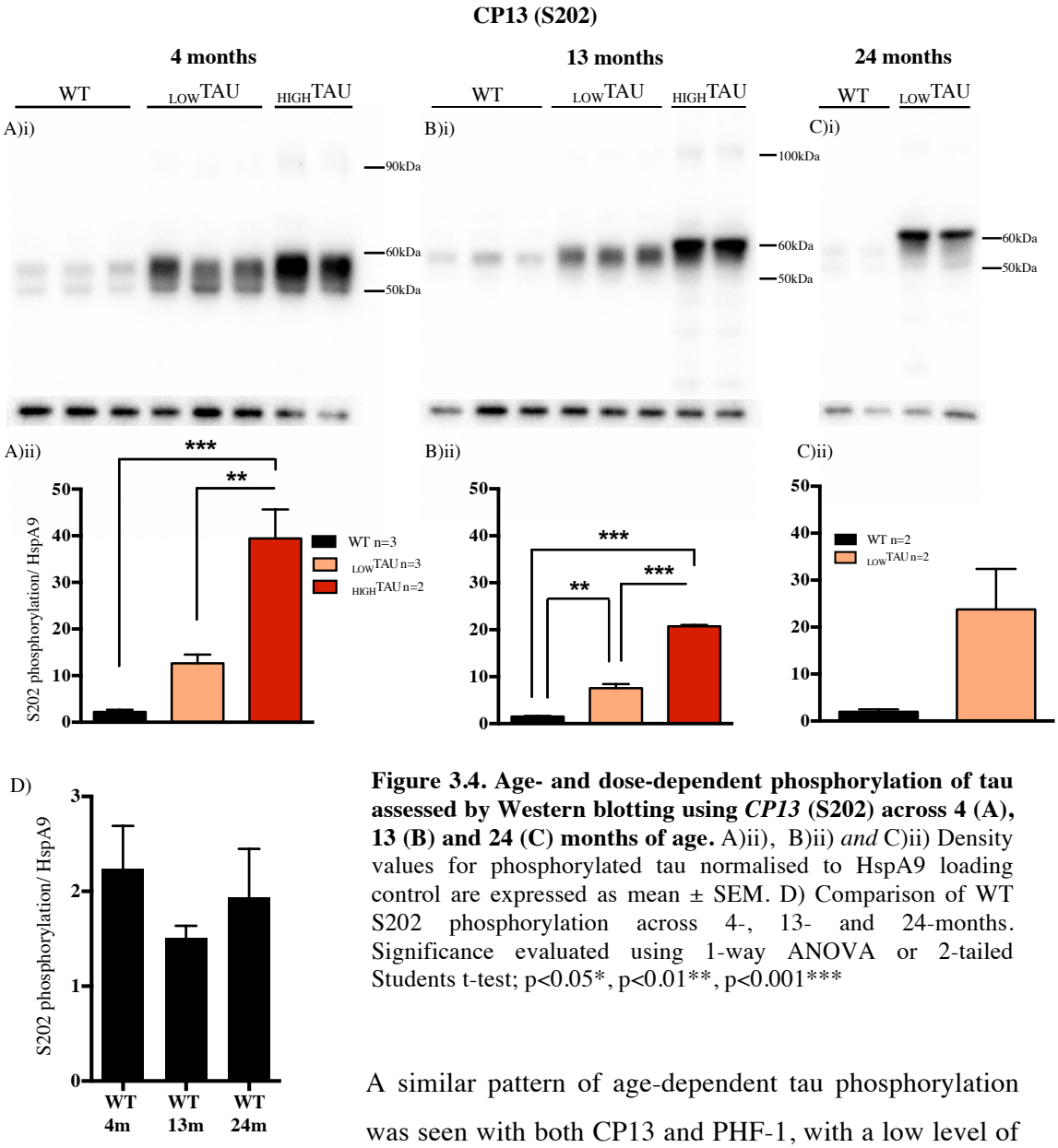

Figure 3.4. Age- and dose-dependent phosphorylation of tau assessed by Western blotting using *CP13* (S202) across 4 (A), 13 (B) and 24 (C) months of age. A)ii), B)ii) *and* C)ii) Density values for phosphorylated tau normalised to HspA9 loading control are expressed as mean ± SEM. D) Comparison of WT S202 phosphorylation across 4-, 13- and 24-months. Significance evaluated using 1-way ANOVA or 2-tailed Students t-test; $p<0.05$*, $p<0.01$**, $p<0.001$***

A similar pattern of age-dependent tau phosphorylation was seen with both CP13 and PHF-1, with a low level of phosphorylation present in WT mice at all ages observed with both antibodies. Using CP13, 4-month-old WT mice display two distinct bands migrating at ~50 and ~58kDa, representing S202 phosphorylation of both the 0N4R and 1N4R endogenous isoforms respectively. Taken together, overall S202 phosphorylation of endogenous murine tau isoforms is not seen to change from 4 – 24 months of age (Figure 3.4.D)). In contrast to CP13, the degree of S396/S404 (PHF-1) phosphorylation in WT mice was observed to alter with age (Figure 3.5.D)). At 4-months, the 0N4R tau isoform shows as having a higher degree of S396 and S404 phosphorylation (Figure 3.5.A)i)). By 13 months, phosphorylation of the 0N4R (~50kDa) and 1N4R (~58kDa) isoforms appears equal (Figure 3.5.B)i)), resulting in an increase in overall murine tau phosphorylation at S396 and S404 sites. A significant reduction in overall WT PHF-1 reactivity is seen between 13 and 24 months ($p=0.021$)(Figure 3.5.C)i) and D)).

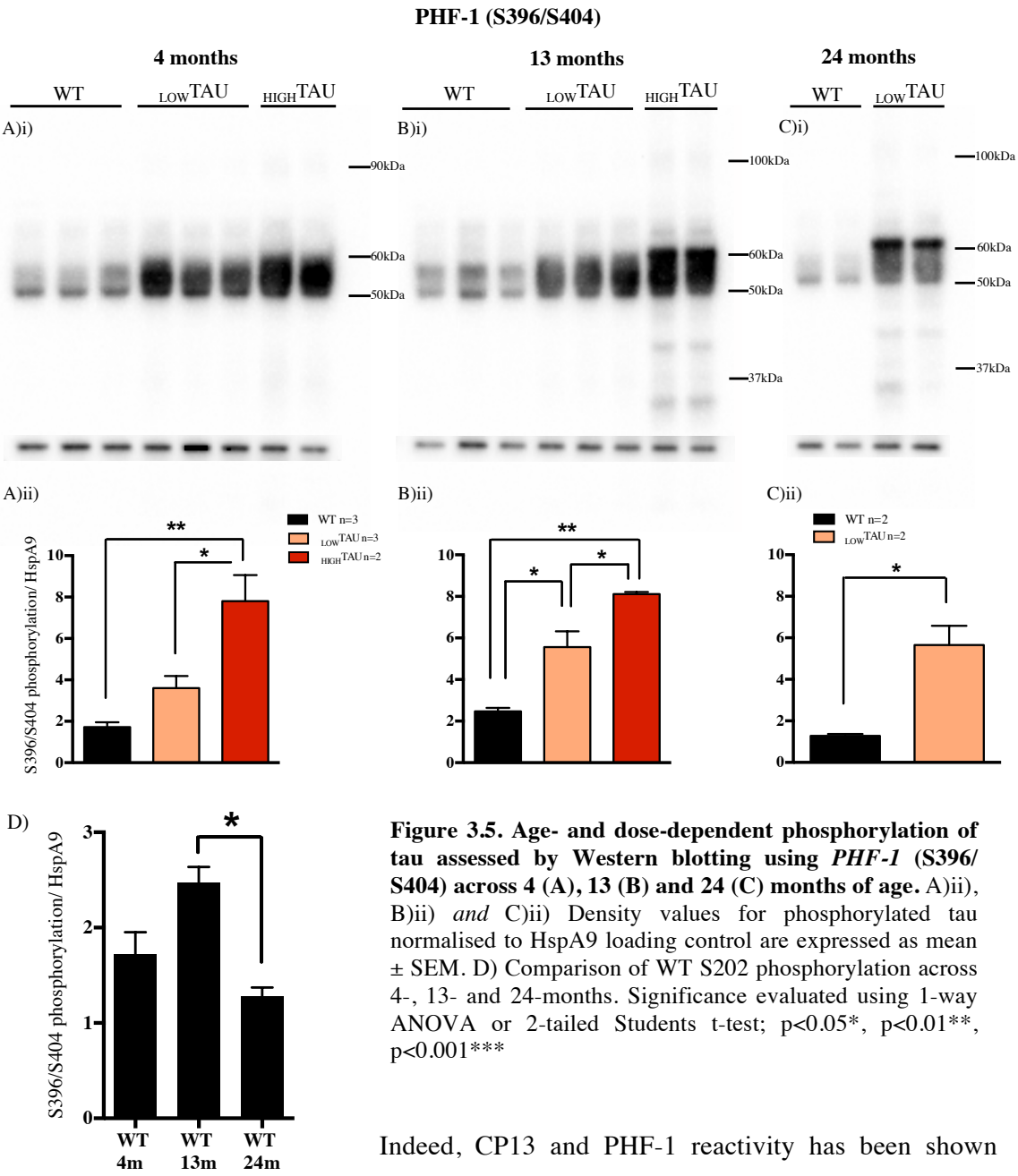

Figure 3.5. Age- and dose-dependent phosphorylation of tau assessed by Western blotting using *PHF-1* (S396/ S404) across 4 (A), 13 (B) and 24 (C) months of age. A)ii), B)ii) *and* C)ii) Density values for phosphorylated tau normalised to HspA9 loading control are expressed as mean ± SEM. D) Comparison of WT S202 phosphorylation across 4-, 13- and 24-months. Significance evaluated using 1-way ANOVA or 2-tailed Students t-test; $p<0.05$*, $p<0.01$**, $p<0.001$***

Indeed, CP13 and PHF-1 reactivity has been shown previously in non-transgenic control mice (Adams et al., 2009, Petry et al., 2014). A degree of phosphorylation is expected physiologically, due to its role in the regulation of tau binding to MTs and the consequential regulation of axonal transport (Ballatore et al., 2007).

Transgenic mice display a large amount of both S202 (CP13) and S396/S404 (PHF-1) phosphorylation when compared to WT at all ages. In contrast to WT controls, phosphorylated species from transgenic mice are more diffuse, particularly those species phosphorylated at the PHF-1 epitope, reflecting a more heterogenous degree of overall phosphorylation of the human 0N4R isoform, which creates species of slightly altered molecular weight.

In 4 and 13 month old mice, we also observe clear increases in phosphorylation in $_{HIGH}$TAU compared to $_{LOW}$TAU mice. These increases are most dramatic at 4 months, where S202 phosphorylation is increased by 211% from $_{LOW}$TAU to $_{HIGH}$TAU mice (Figure 3.4.A)), with S396/S404 phosphorylation increased by 117% (Figure 3.5.A)).

Interestingly, as well as increases in the amount of tau phosphorylated, the size of phosphorylated tau species was also seen to change in an age- and dose-dependent manner, observed with both CP13 and PHF-1. At 4 months, transgenic mice present phosphorylated tau species between 50 and 60kDa (Figure 3.4.A)i) and (Figure 3.5.A)i)). With age, the phosphorylated tau species displayed a higher molecular weight. By 24 months, the majority of tau migrated with an apparent molecular weight of 64kDa (Figure 3.4.C)i) and (Figure 3.5.C)i)). This age-dependent 'shift' from 50-60 to 64kDa is characteristic of pathological tau, and is caused by the hyperphosphorylation of tau in disease (SantaCruz et al., 2005, Berger et al., 2007, Sahara et al., 2013). Using a protein fraction similar to that used in the present study, Sahara et al., (2013) observe an almost identical age-dependent phosphorylation of S396 and S404, relative to the different (and more pathologically aggressive) mouse model used.

Smaller species of tau migrating below 50kDa in 13 month old $_{HIGH}$TAU and 24 month old $_{LOW}$TAU are speculated to be degradation products of tau or may possibly represent truncated forms of tau as has been suggested previously (Tai et al., 2012)

Sarkosyl-insoluble tau: Western blot analysis of P3 fraction

As we see from Figure 3.2. A)i) and B)i) the detection of human tau from total hippocampal homogenate, in both $_{LOW}$TAU and $_{HIGH}$TAU mice, results in a large 'smeared' band, from which individual tau species cannot be resolved. This is due to the variety of phosphorylation states of normal soluble tau species (Sahara et al., 2002, SantaCruz et al., 2005, Berger et al., 2007). It is known that the type of 0N4R isoform found in the paired helical filaments of AD migrate with an apparent weight of 64kDa due to hyperphosphorylation (Goedert et al., 1992, Buee et al., 2000, Lewis et al., 2000). This form of tau is insoluble when incubated with the detergent sarkosyl. Sarkosyl incubation is thus often used to remove other non-aggregated/soluble forms of tau, allowing for the detection of filamentous forms only. NFTs themselves are also lost during initial centrifugation (Greenberg and Davies, 1990, Berger et al., 2007), resulting

in the sarkosyl-insoluble (P3) fraction containing only dispersed paired helical filaments which, following denaturing, can be run on an SDS-PAGE gel (Greenberg and Davies, 1990). These filaments are derived from less aggregated populations of paired helical filaments, such as neuropil threads or filaments dissociated from NFTs and are considered indicative of the severity of aggregated tau pathology (SantaCruz et al., 2005).

The relative levels of sarkosyl-insoluble tau in $_{LOW}$TAU and $_{HIGH}$TAU mice of increasing age were compared. In both 4 and 13 month old $_{LOW}$TAU mice, insoluble tau migrating at ~54kDa was observed. The amount of tau of this weight was increased in $_{HIGH}$TAU mice at 4 months. By 13 months of age however, $_{HIGH}$TAU mice displayed the greater, 64kDa tau along with continued expression of ~54kDa tau. This apparent dose-dependency aspect of insoluble tau formation has been noted previously (Sahara et al., 2002). With increasing age, ~54kDa tau is reduced, with the 64kDa band becoming the more prominent of the two bands by 24 months. These observations are in keeping with previous data from a similar mouse model (SantaCruz et al., 2005), in which the development of insoluble tau migrating at 64kDa coincides with the development of large numbers of NFTs (see Chapter 4).

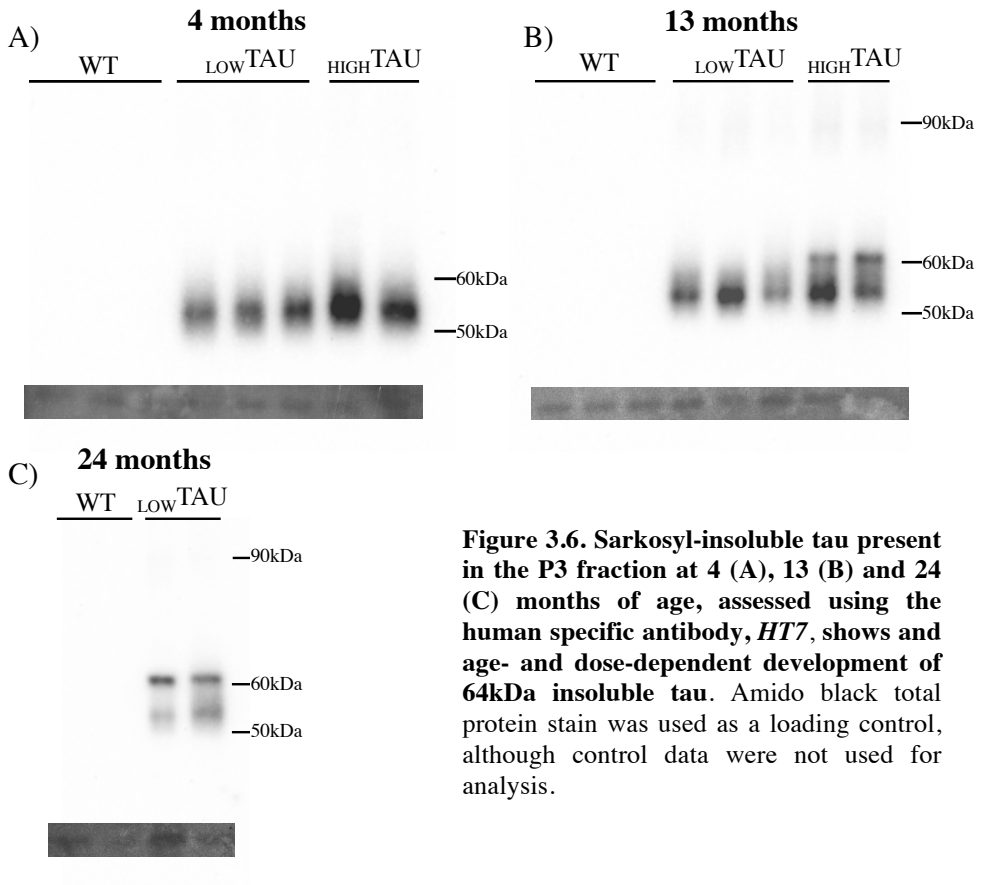

Figure 3.6. Sarkosyl-insoluble tau present in the P3 fraction at 4 (A), 13 (B) and 24 (C) months of age, assessed using the human specific antibody, *HT7*, shows and age- and dose-dependent development of 64kDa insoluble tau. Amido black total protein stain was used as a loading control, although control data were not used for analysis.

Due to the fractionation procedure employed, classical loading controls for the sarkosyl-insoluble fractions cannot be used, often resulting in a lack of loading control (SantaCruz et al., 2005, Berger et al., 2007). The total protein stain, Amido Black, provided a loading control for the present study, although the quality of stain was not sufficient for quantification. Sarkosyl-insoluble tau was thus not quantified; images (Figure 3.6) are therefore for qualitative purposes only.

High molecular weight bands detected in transgenic mice of all ages

Along with the prominent band migrating at 50-60kDa, another, higher molecular weight band, ~85-100kDa, was found to be present in all transgenic mice, identified with both DA9 and HT7 antibodies at 4 and 13 months of age. Phosphorylation dependent antibodies CP13 and PHF-1 also detected a higher molecular weight band migrating at ~90-100kDa, observed in $_{LOW}$TAU mice only when overexposed (*not shown in Figure 3.4.A)i) and B)i) and Figure 3.5.A)i) and B)i)*). It is possible these bands represent oligomeric species of tau, as has been suggested for higher molecular weight species previously (Berger et al., 2007, Tai et al., 2012). Slight variations in molecular weight creating a 'smeared' appearance are assumed to represent differences in phosphorylation status. While the apparent molecular weights are not quite sufficient to suggest multimeric structures (two or more tau molecules) of full-length tau, it is possible these species are made up of oligomeric hyperphosphorylated truncated forms of tau.

These higher molecular weight species are also observed in the sarkosyl-insoluble fraction of all transgenic mice at 13 months. A small amount of these higher weight species are also detected at 24 months and can be seen by overexposure (*not shown in Figure 3.6*.). Unlike the disperse filaments of this fraction that are disassociated by boiling with SDS and DTT, these species likely represent higher order aggregates that are at least partially resistant to this denaturation process.

Summary and Discussion: Molecular Biology

Transgene copy number determined using TaqMan® qPCR led to the discovery that in fact, the TauD35 mouse model exists as two transgenic lines, with one line harbouring approximately double the number of transgene copies than the other, resulting from either changes to copy number via recombination events, or two separate transgene integration events that became separated during breeding. These lines were appointed $_{HIGH}$TAU and $_{LOW}$TAU, respectively, and are referred to as such throughout. Differences in transgene dose between the two transgenic lines are reflected in the amount of human tau protein expressed, indicating that the additional copies of the human cDNA harboured by $_{HIGH}$TAU mice are indeed functional. This is confirmed through observed increases in the phosphorylation of tau between $_{LOW}$TAU and $_{HIGH}$TAU mice.

Between 17 and 20 months of age, $_{HIGH}$TAU mice develop a pathological phenotype comparable to that described previously in aged mice harbouring a similar transgene (Ramsden et al., 2005). Due to this moribund phenotype, $_{HIGH}$TAU mice over 20 months of age were not available for experimentation.

Characterising $_{LOW}$TAU and $_{HIGH}$TAU transgenic mice

The characteristic 'shift' of the 0N4R isoform of human tau from ~54kDa to 64kDa is often used to indicate the development of insoluble tau pathology and thus NFTs. The 64kDa weight is caused by the hyperphosphorylation of 0N4R tau (Goedert et al., 1992), and is a species found in AD and FTDP-17 patients (Buee et al., 2000). The development of this species (in both $_{LOW}$TAU and $_{HIGH}$TAU mice) is therefore supportive of the use of TauD35 mice as a tool to study the development of pathological tau relevant in disease.

Sarkosyl-insoluble tau migrating at the lower weight of ~54kDa has been observed previously (Sahara et al., 2002, SantaCruz et al., 2005), in particular at younger ages. This may represent a form of tau which displays less phosphorylation (as de-phosphorylated/recombinant tau migrates at 52kDa (Buee et al., 2000)), but which is included into tau filaments, possibly as a result of other modifications such as ubiquitination and glycation (Buee et al., 2000). By investigating these smaller species using electron microscopy, Sahara et al., (2002) show that they are indeed filamentous,

albeit with a shorter fibre length than those forms of tau detected in older animals. It is therefore possible that insoluble tau migrating at ~54kDa represents a species with a low level of phosphorylation in a filamentous form, which may act as a filament precursor/ nucleation site for additional aggregation into mature NFTs. Due to the difficulty of working with such a small volume of original homogenate (as is provided by a single hippocampus), the ~54kDa band may also include a small amount of contamination from the sarkosyl-soluble fraction (S2).

The dispersed filaments under study when looking at sarkosyl-insoluble tau may represent an intermediate step (or steps) in the development of mature NFTs (Goedert et al., 1992), and thus the apparent decrease at 24 months may be due to the more complete development of NFTs and their loss during initial centrifugation. The apparent higher presence of overall insoluble tau at 13 months in $_{HIGH}$TAU mice, compared to $_{LOW}$TAU 24 month mice, may reflect their increased capacity for NFT development. Decreases in the amount of ~54kDa tau with age/ dose are accompanied by increases in 64kDa species. This may reflect the hyperphosphorylation of tau on its way to becoming integrated into more mature aggregates/ NFTs.

In addition to hyperphosphorylated 64kDa tau accumulation, higher molecular weight (~85-100kDa) human tau species were observed in both $_{LOW}$TAU and $_{HIGH}$TAU mice from as young as 4 months. Thought to be oligomers of tau (Berger et al., 2007, Tai et al., 2012), these species were found to be partly sarkosyl-insoluble and SDS resistant, and contain a proportion of tau phosphorylated at S202 and/or S396/S404 in $_{HIGH}$TAU mice. The apparent reduction in the sarkosyl-insoluble forms of these higher molecular weight species at 24 months, compared to 13 months, could possibly be due to the more complete development of NFTs at 24 months and their loss during centrifugation.

Overall, both $_{LOW}$TAU and $_{HIGH}$TAU mice were found to express relatively low amounts of human tau (4 and 6.5 times respectively) in comparison to endogenous murine tau. This finding makes both models relatively mild transgenic lines in contrast to similar mouse models of tauopathy (SantaCruz et al., 2005). Interestingly, the relatively small difference in protein level between $_{LOW}$TAU and $_{HIGH}$TAU mice is seen to result in large differences in the amount of tau that is hyperphosphorylated and insoluble in sarkosyl, indicative of large differences in tau pathology.

CHAPTER 4

Introduction: Histology

The presence of aggregated tau protein within the brain is a fundamental feature of all neurodegenerative tauopathies (including AD and FTDP-17). In AD, the development of NFTs follows a stereotypical pattern, beginning in the medial temporal lobe (EC and hippocampus) before spreading through limbic structures and finally reaching isocortical and associative areas (Braak and Braak, 1991). Indeed, the extent of such pathology has been shown to correlate to the severity of cognitive decline in AD patients (Arriagada et al., 1992, Giannakopoulos et al., 2003, Guillozet et al., 2003), making the presentation of this cardinal feature paramount for a new model of tauopathy. Neuronal loss represents another key feature of neurodegenerative tauopathies, and has been shown to possess a topographical and hierarchical pattern paralleling that of NFT development. However, within the same brain region neuronal loss can exceed the NFT burden (Gomez-Isla et al., 1996, Gomez-Isla et al., 1997), making it a superior correlate of cognitive decline.

We therefore investigated the age- and dose-dependent development of both NFT pathology and neurone loss within TauD35 mice. As the transgene harboured by the TauD35 models is expressed under the CaMKIIα promoter, and is thus strongly expressed within the hippocampus (www.mouse.brain-map.org (Lein et al., 2007), Figure 3.1.B)), and with the obvious vulnerability of the hippocampus to NFT development and neurone loss (as displayed in AD), one may expect primary NFT pathology and neuronal loss within the hippocampus of TauD35 mice.

Performing pathological tau and cell count analysis also allows these novel transgenic lines to be placed in context with existing literature using other transgenic lines harbouring the same mutation (Lewis et al., 2000, Ramsden et al., 2005, Terwel et al., 2005) and makes the interpretation of future results possible. Here, histological characterisation also provided further validation of differences in transgene copy number.

Identification of pathological tau

Western blot data presented in the previous chapter revealed that tau is forming insoluble paired helical filaments in both $_{LOW}$TAU and $_{HIGH}$TAU mice from 4 months of age. However, the nature of the tissue preparation protocol for these Western blot experiments means the origins of these filaments are not mature NFTs. At this age, these filaments were also not found to be hyperphosphorylated. Thus, while being indicative that a process of tau aggregation has begun, histological analysis is essential to determine whether mice exhibit full NFT pathology and thus model a key characteristic of tauopathies. As well as confirming that NFTs are indeed formed in these models, use of a range of ages from both lines means that we are able to characterise pathology in an age- and dose-dependent manner.

In order to perform this primary validation and characterisation, good antibody selection was vital. Antibodies needed to be specific for tau, recognise common pathological epitopes found in both human patients as well as other mouse models, and also cover a wide range of pathological species. To this end, a range of both commercial and non-commercial (kindly provided by Peter Davies, Albert Einstein College of Medicine, USA) antibodies were chosen, including: HT7 (human tau), MC1 (misfolded human tau), as well as CP13, AT8 and PHF-1 (tau phosphorylated at a variety of serine and threonine residues),

The AT8 epitope (tau phosphorylated at S202/T205) is believed to play a role in regulating further phosphorylation of tau at other disease-associated sites (Bertrand et al., 2010a), and is therefore likely an epitope phosphorylated early in the cascade of tau phosphorylation (Kimura et al., 1996). The antibody CP13 recognises tau phosphorylated at S202. As this is one of the sites included in the AT8 epitope it is likely CP13 recognises one of the earliest tau sites to be phosphorylated (Su et al., 1994). The MC1 epitope is created from the folding of tau into a distinct pathological conformation (Jicha et al., 1997), a process also believed to occur early in the development of pathological tau (Weaver et al., 2000). Sites thought to constitute those phosphorylated later in the disease process include the epitope of PHF-1 (S396/S404) (Su et al., 1994). By using the human specific antibody HT7 and co-staining with AT8, we were able to identify whether the tau protein forming pathological species was of human origin and therefore due to the translation of the transgene.

Neuronal cell counts: Cresyl Violet Nissl Stain

As with the development of NFTs, neuronal loss has also been shown to occur prior to the presentation of symptoms in AD patients. It has been demonstrated that even in mild AD, prior to any significant cognitive decline, substantial reductions in volume are visible within the hippocampus (Lehericy et al., 1994, Jack et al., 1997) and EC (Gomez-Isla et al., 1996) of patients relative to cognitively normal age-matched controls. Indeed, the topographical, hierarchical pattern of neuronal loss in AD has been shown to parallel the development of NFTs (Gomez-Isla et al., 1996, Gomez-Isla et al., 1997), despite neurone loss in some brain areas greatly exceeding NFT burden (Gomez-Isla et al., 1997). Some have even suggested NFT formation is the principle event associated with neuronal loss in the EC and CA1 areas (Giannakopoulos et al., 2003). As well as correlating with each other, both NFT load and neuronal loss correlate well with duration and severity of illness (Gomez-Isla et al., 1996, Gomez-Isla et al., 1997, Giannakopoulos et al., 2003). Due to these data, and the fact that brain atrophy caused by neuronal loss is a major feature of many forms of dementia and thus provides further validation of these novel lines as models of dementia, neuronal loss within both $_{LOW}$TAU and $_{HIGH}$TAU mice was also investigated using a Nissl stain.

It is now 120 years ago that work by Franz Nissl first exposed the ability of cationic dyes (such as cresyl violet) to label small granules within neuronal (and some glial) cell bodies. The method is based on the interaction of such dyes with the DNA and RNA within these cells. It is the RNA that creates the so-called granular 'Nissl bodies', due to its high concentration in the rough endoplasmic reticulum and ribosomes within the cytoplasm. The preferable staining of neurones is due to their high concentration of rough endoplasmic reticulum, required to meet their need for a high degree of protein synthesis. Staining in this way provides a clear depiction of the neuronal cell soma and can therefore be used to identify and count the number of principle neuronal cells within a given area.

Significant neuronal cell loss in the CA1 region of $_{HIGH}$TAU mice at 17.5 months of age

Neuronal loss is a characteristic feature of neurodegenerative tauopathies, and for this reason represents one of the desirable traits of a tauopathy model. As the number of neurones within a defined area may impact conclusions drawn about the number of tau aggregates, initial groundwork consisted of assessing neuronal loss within the hippocampus of both $_{HIGH}$TAU and $_{LOW}$TAU mice compared to WT controls. Principle cells were identified and counted using a Nissl stain. Pyramidal cells of the CA1 and CA3 cell layers were investigated in mice ranging from 4 to 24 months. Due to high density of cells in the DG, cell numbers could not be reliably obtained for this area and therefore have not been quantified.

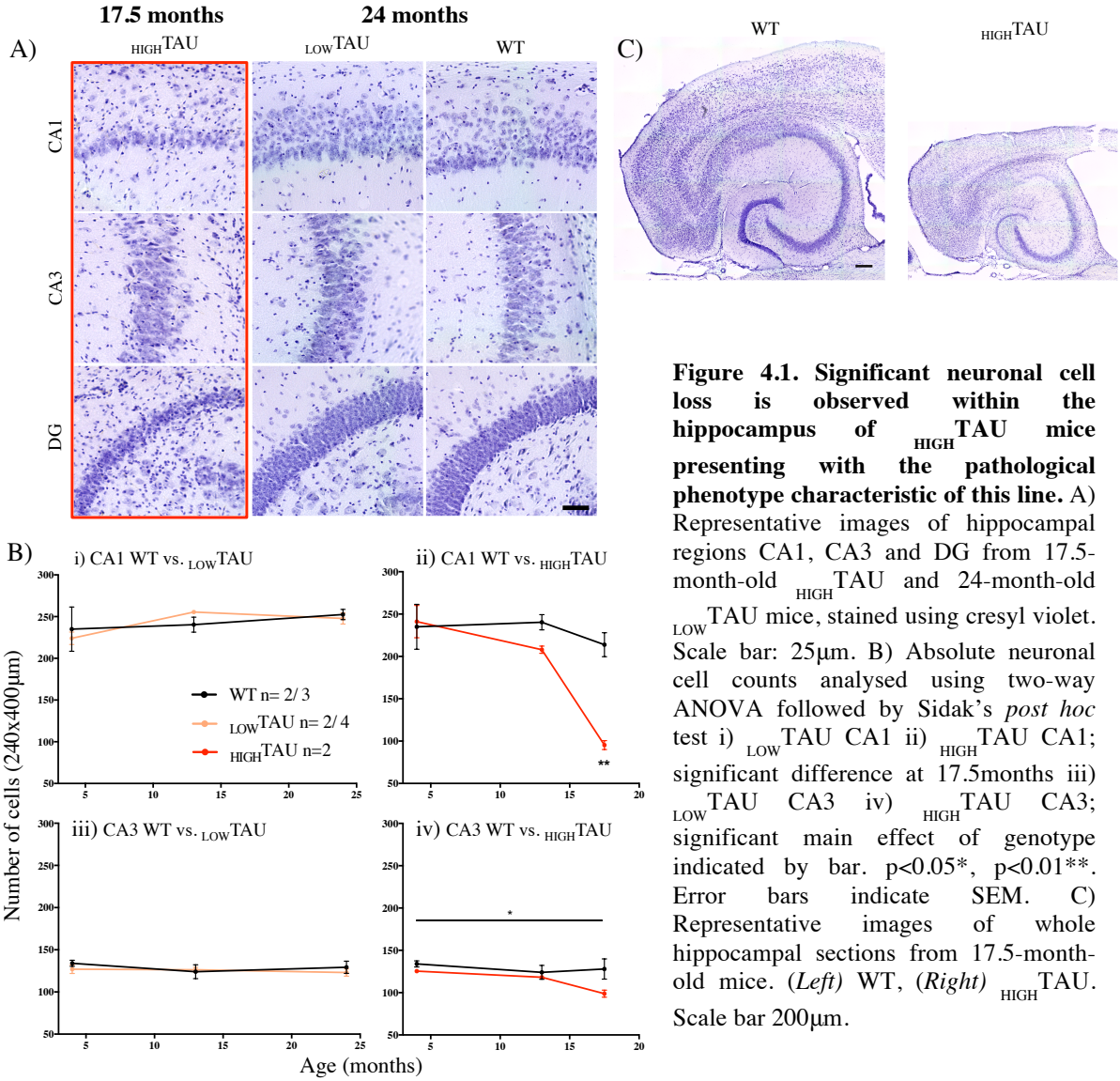

Figure 4.1. Significant neuronal cell loss is observed within the hippocampus of $_{HIGH}$TAU mice presenting with the pathological phenotype characteristic of this line. A) Representative images of hippocampal regions CA1, CA3 and DG from 17.5-month-old $_{HIGH}$TAU and 24-month-old $_{LOW}$TAU mice, stained using cresyl violet. Scale bar: 25µm. B) Absolute neuronal cell counts analysed using two-way ANOVA followed by Sidak's *post hoc* test i) $_{LOW}$TAU CA1 ii) $_{HIGH}$TAU CA1; significant difference at 17.5months iii) $_{LOW}$TAU CA3 iv) $_{HIGH}$TAU CA3; significant main effect of genotype indicated by bar. $p<0.05$*, $p<0.01$**. Error bars indicate SEM. C) Representative images of whole hippocampal sections from 17.5-month-old mice. *(Left)* WT, *(Right)* $_{HIGH}$TAU. Scale bar 200µm.

Neuronal cell counts from WT controls were not found to differ across the 20-month age range studied, assessed using a one-way ANOVA (WT CA1: 4m 235.0 ± 26.6; 13m 240.3 ± 9.0; 17.5m 213.8 ± 14.2; 24m 252.6 ± 6.2, p=0.53. WT CA3: 4m 134.0 ± 3.6; 13m 124.0 ± 8.2; 17.5m 128.0 ± 12.0; 24m 129.2 ± 7.3, p=0.8). This finding indicates neuronal loss in the CA1 or CA3 areas does not occur with normal ageing in mice within this time frame. This is analogous to data collected previously from control C57Bl6/J mice (Calhoun et al., 1998) as well as healthy human patients (West et al., 1994), which indicates there is no neuronal loss with age within the hippocampus, along with other brain regions (Gomez-Isla et al., 1996, Gomez-Isla et al., 1997).

No significant differences were found in the number of neurones between WT and $_{LOW}$TAU mice at 24 months of age in either the CA1 or CA3 cell layers (Figure 4.1.B)i) and B)ii)). This finding reveals that up until this time, while extensive tau pathology is evident, $_{LOW}$TAU mice do not exhibit neuronal loss within the hippocampus, and thus do not display a fundamental characteristic of neurodegenerative tauopathies.

As no $_{HIGH}$TAU mice survived until 24 months of age, neuronal loss was assessed in the oldest $_{HIGH}$TAU mice available (17.5-months) using age-matched controls. The mice used here already presented with the pathological phenotype typical of $_{HIGH}$TAU mice of this age (piloerection, hunched spine and akinesia) and were culled for ethical reasons. Significant cell loss was observed in the CA1 cell layer, with a decrease of 55% from WT to $_{HIGH}$TAU mice (Sidak *post-hoc* test, p=0.0074, Figure 4.1.B)ii)). Within the CA3 region, a main effect of genotype was detected (genotype: $F_{(1, 8)} = 7.015$, $p = 0.0293$) with cell numbers reduced by 23% in $_{HIGH}$TAU mice at 17.5 months (Figure 4.1.B)iv)). An overview of the hippocampus shows the reduction in hippocampal volume along with an enlargement of the lateral ventricle in $_{HIGH}$TAU mice when compared to WT animals (Figure 4.1.C)). The large cell loss observed in the CA1 region in the $_{HIGH}$TAU mice bears a resemblance to the degeneration seen in the rTg4510 mouse model, where significant neuronal loss (~60%) is apparent in the CA1 region (SantaCruz et al., 2005). Indeed, comparable findings have also been reported in human AD cases, where the largest and most significant neuronal loss within the hippocampus is found in the CA1 area (West et al., 1994).

In order to investigate when cell loss begins in $_{HIGH}$TAU animals, we then compared cell numbers in 4- and 13-month $_{LOW}$TAU and $_{HIGH}$TAU mice to WT controls. As expected

from the results observed at 24-months, $_{LOW}$TAU mice showed no neuronal cell loss in either the CA1 or CA3 cell layers (Figure 4.1.B)i) and iii)). Moreover, no significant cell loss was detected at these younger ages in the CA1 or CA3 regions of $_{HIGH}$TAU mice compared to WT controls (Figure 4.1.B)ii) and iv)).

These data highlight the more pathologically aggressive nature of the $_{HIGH}$TAU line of TauD35 mice. It may be hypothesised that the characteristic pathological phenotype and premature mortality seen in this line is the result of substantial neuronal cell loss throughout the brain (Figure 4.2.C), see also Figure 7.2., Chapter 7).

Identification of tau pathology with $_{LOW}$TAU and $_{HIGH}$TAU mice

In order to validate the novel TauD35 mouse lines as models of tauopathy, it was of course imperative to determine whether they do indeed develop the cardinal feature of these neurodegenerative diseases: the NFT. The CA1, CA3 and DG regions of the hippocampus were examined for the presence and cellular location of pathological tau, using a wide range of antibodies including: HT7 (human tau), MC1 (misfolded human tau), as well as CP13, AT8 and PHF-1 (tau phosphorylated at a variety of serine and threonine residues). This array of antibodies allowed us to determine whether tau present in TauD35 mice forms common pathological species detected in human tauopathy cases. Employing these antibodies against different forms of tau across 4-, 13- and 24-month-old mice also allowed us some understanding of the age-dependent development of pathological tau. In addition we hypothesised that the presence of higher levels of mutated human tau protein in $_{HIGH}$TAU mice would contribute an earlier onset and more severe degree of tau pathology within these mice compared to the $_{LOW}$TAU mouse line, and thus by examining both lines simultaneously we were able to gain insight into the dose-dependency of pathological tau accumulation.

Sections from age-matched WT mice were stained in parallel with each of the antibodies against pathological tau. No labelling was observed in any WT sections (Figures 4.5., 4.6., 4.7. and 4.8.).

Both $_{LOW}$TAU and $_{HIGH}$TAU mice develop characteristic NFTs

For the present study, the specific tau antibodies described were chosen for the detection of mature NFTs. Antibody labelling of NFTs provides superior specificity over alternative approaches such as Thioflavin-S or Gallyas silver stains. Such detection methods do not identify tau exclusively, but rather rely on the presence of β-pleated sheets (LeVine, 1999) or affinity for silver ions (Uchihara, 2007) respectively, to expose tau aggregates. With small, optimally handled samples, immunohistochemistry provided us with the most reliable detection method available for NFT identification. In combining primary antibodies with fluorescently conjugated secondary antibodies and imaging with an epifluorescent microscope, we are able to visualise pathological tau in detail. Further to this, higher resolution confocal imaging (Figure 4.2.B)) allowed us to determine that aggregates exhibited the condensed, twisted morphology characteristic of mature NFTs (Bancher et al., 1989, Augustinack et al., 2002), and they are thus referred to as such throughout. In addition, the morphology of NFTs observed within the present study is comparable to both mouse models and human patients harbouring the same, P301L, mutation (Figure 4.9.)(Spires et al., 2006).

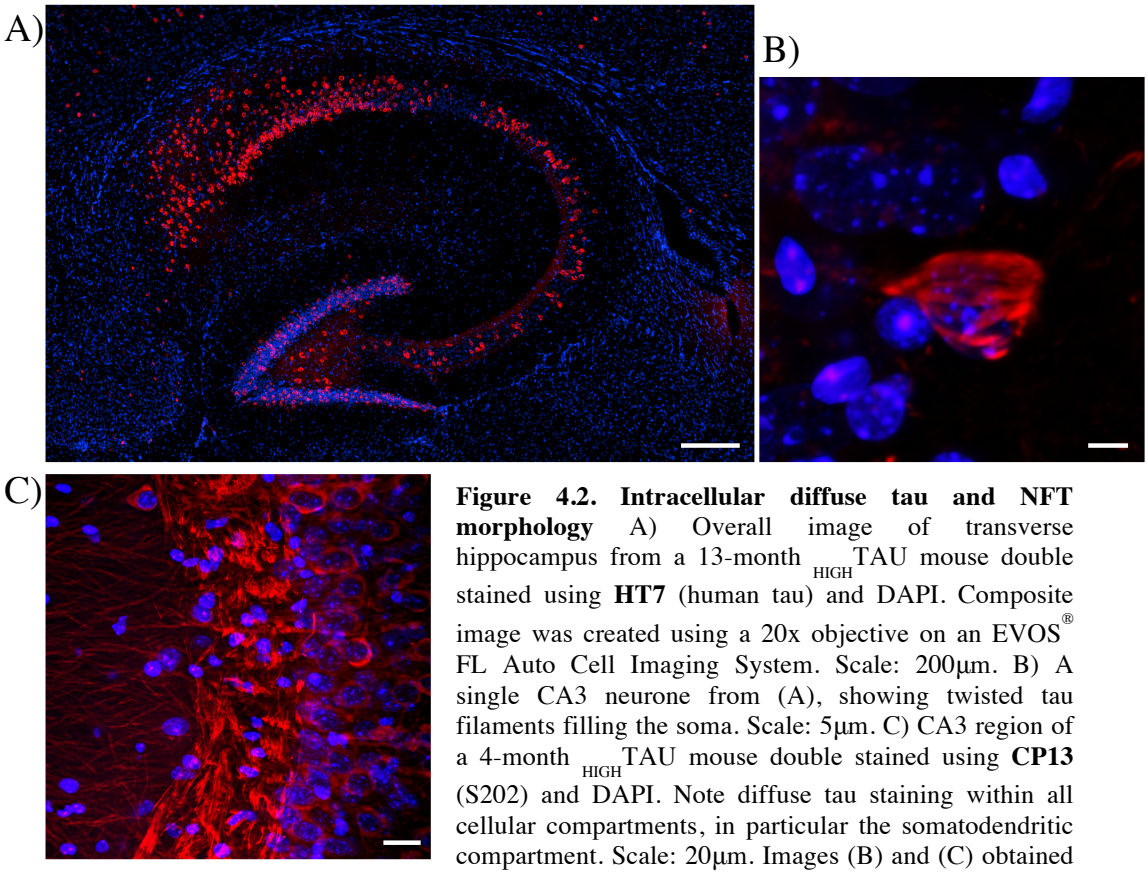

Figure 4.2. Intracellular diffuse tau and NFT morphology A) Overall image of transverse hippocampus from a 13-month $_{HIGH}$TAU mouse double stained using **HT7** (human tau) and DAPI. Composite image was created using a 20x objective on an EVOS® FL Auto Cell Imaging System. Scale: 200µm. B) A single CA3 neurone from (A), showing twisted tau filaments filling the soma. Scale: 5µm. C) CA3 region of a 4-month $_{HIGH}$TAU mouse double stained using **CP13** (S202) and DAPI. Note diffuse tau staining within all cellular compartments, in particular the somatodendritic compartment. Scale: 20µm. Images (B) and (C) obtained using a Zeiss LSM 510 confocal microscope with 60x oil immersion objective.

We observe no aggregate pathology throughout the hippocampus in either $_{LOW}$TAU or $_{HIGH}$TAU mice at 4 months of age. However, some diffuse staining with CP13 is observed in the soma and dendrites of cells across the hippocampus of both lines (Figure 4.2.C) and Figure 4.6.). This pattern of CP13 reactivity within neuronal processes has been observed previously in the young mice of other tauopathy mouse models (Ramsden et al., 2005, Adams et al., 2009), and may represent tau in a pre-tangle state (Kimura et al., 1996, Augustinack et al., 2002). All other antibodies produced no staining except in mossy fibres (discussed below). The presence of CP13 reactivity in the absence of other phosphorylation-dependent antibody stain at this young age supports the opinion that S202 is phosphorylated early in pathological tau development.

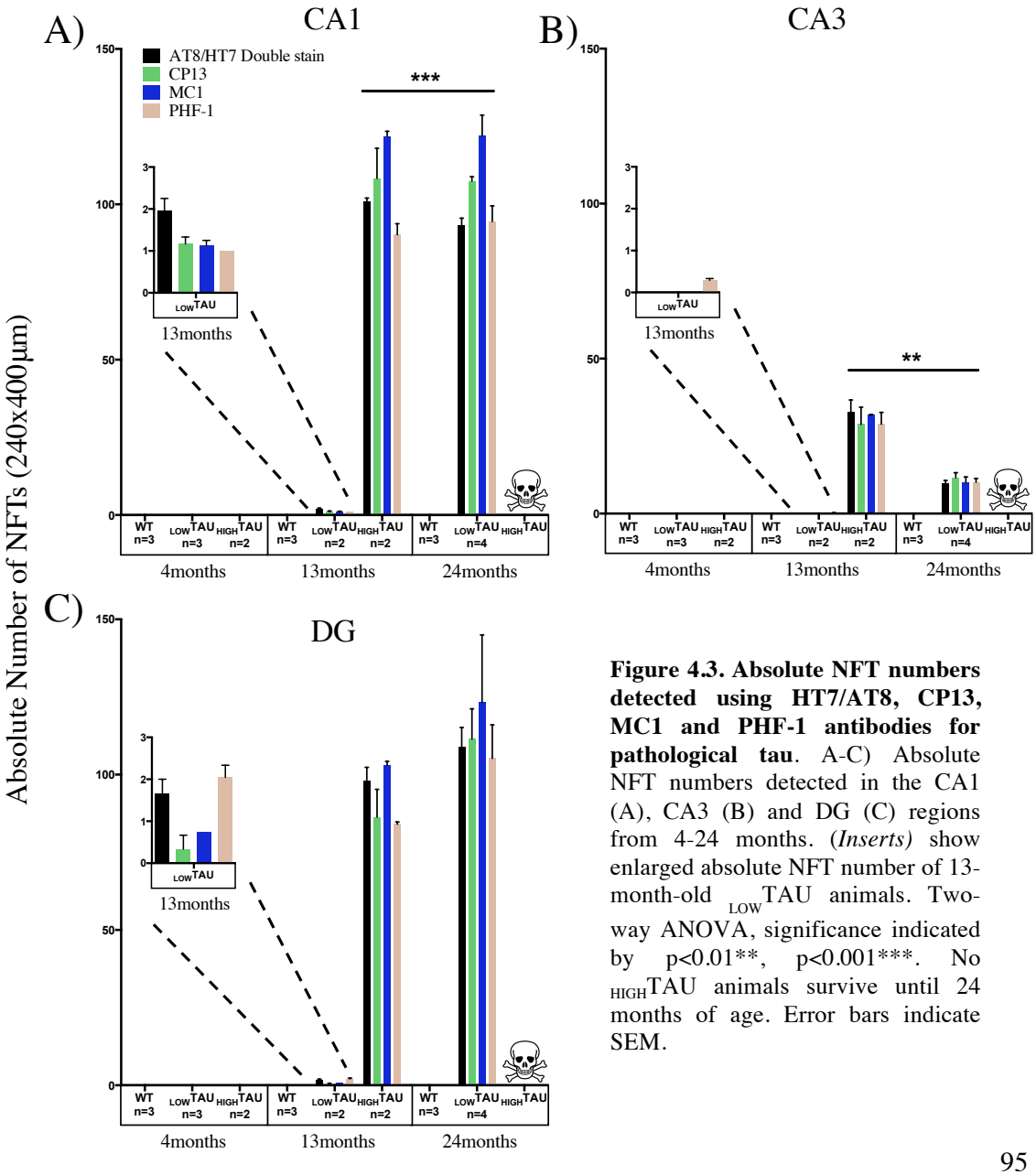

Figure 4.3. Absolute NFT numbers detected using HT7/AT8, CP13, MC1 and PHF-1 antibodies for pathological tau. A-C) Absolute NFT numbers detected in the CA1 (A), CA3 (B) and DG (C) regions from 4-24 months. (*Inserts)* show enlarged absolute NFT number of 13-month-old $_{LOW}$TAU animals. Two-way ANOVA, significance indicated by p<0.01**, p<0.001***. No $_{HIGH}$TAU animals survive until 24 months of age. Error bars indicate SEM.

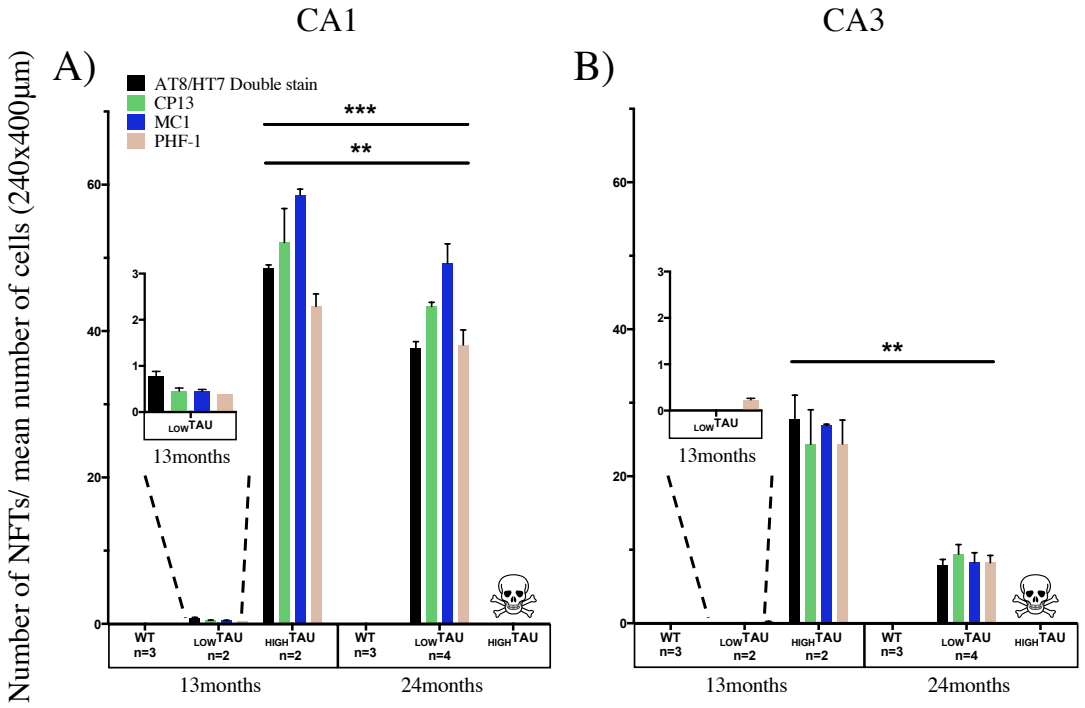

Figure 4.4. The ratio of NFTs detected using HT7/AT8, CP13, MC1 and PHF-1 antibodies for pathological tau to the average number of cells per animal. Calculated ratios of the number of NFTs to the average number of cells per animal counted in the CA1 (A) and CA3 (B) regions in 13- and 24-month-old mice. (*Inserts)* show enlarged NFT ratios of 13-month-old $_{LOW}$TAU animals. Two-way ANOVA, significance indicated by p<0.01**, p<0.001***. No $_{HIGH}$TAU animals survive until 24 months of age. Error bars indicate SEM.

A substantial difference in tau pathology is observed between the two transgenic lines by 13 months of age. Here $_{LOW}$TAU mice present few/ sparse NFTs, whereas $_{HIGH}$TAU mice show severe aggregate numbers in each region of the hippocampus, detected with all AT8/HT7, CP13, MC1 and PHF-1 (Figure 4.3.A), B) and C)).

Absolute NFT numbers for $_{HIGH}$TAU mice at 13-months were compared to $_{LOW}$TAU mice at 24 months of age by way of a two-way ANOVA, providing a comparison between the two transgenic lines at ages when each displayed severe NFT pathology. This allowed an assessment of whether differences in transgene dose results in the same eventual pattern of tau pathology, simply on a different timescale.

No difference was observed in NFT numbers between 13-month $_{HIGH}$TAU and 24-month $_{LOW}$TAU mice within the DG (Figure 4.3.C)). Within the CA1 region, a main effect of antibody was detected, indicating differences in the number of aggregates detected with each of the four antibodies used in this region in both transgenic lines (antibody: $F_{(3, 12)} = 14.71$, p=0.0003, Figure 4.3.A)). The highest number of NFTs in both $_{HIGH}$TAU 13-month and $_{LOW}$TAU 24-month-old mice were detected using MC1.

Compared to the antibody that recognised the second highest number of inclusions (CP13), MC1 identified 12.5% more tangles in the CA1 region of 13-month-old $_{HIGH}$TAU mice. In 24-month-old $_{LOW}$TAU mice, MC1 identified 13.6% more NFTs than CP13 in the CA1 region. This result supports data collected from AD patients, where the conformational change in tau recognised by the MC1 antibody is one of earliest detected pathological alterations to the protein (Weaver et al., 2000). The detection of higher numbers of NFTs by MC1 may also be contributed to by the nature of NFT maturation, such as epitope truncation, obstruction or dephosphorylation (Uchihara, 2007). As MC1 recognises a conformational change in tau, rather than a specific phosphorylation site, it may be that its epitope is preserved throughout the development of a NFT. For both 13-month $_{HIGH}$TAU and 24-month $_{LOW}$TAU mice, PHF-1 detected the lowest number of NFTs compared to all other antibodies. This result is in keeping with phosphorylation patterns observed in human patients showing S396 is one of later sites of tau to be phosphorylated (Kimura et al., 1996), as well as data from similar mouse models (Ramsden et al., 2005).

Fewer NFTs were detected within the CA3 area compared to other hippocampal regions studied, in both 13-month $_{HIGH}$TAU and 24-month $_{LOW}$TAU mice. By comparing absolute aggregate numbers in this area, significantly fewer NFTs were detected in 24-month $_{LOW}$TAU animals, with a main effect of genotype detected between this group and 13-month $_{HIGH}$TAU animals (genotype: $F_{(1, 4)} = 49.22$, $p=0.0022$, Figure 4.3.B)). As no neuronal loss is recorded within the CA3 region of 24-month $_{LOW}$TAU mice, one must conclude that the lower transgene copy number of these mice results in the production of fewer NFTs in this region.

In order to account for any neuronal cell loss in $_{HIGH}$TAU 13-month-old mice, where cell counts were available for CA1 and CA3, the ratio of NFT numbers to the average number of cells in that area per animal were compared. Comparison of the ratio of NFT numbers in the CA1 region between 13-month $_{HIGH}$TAU and 24-month $_{LOW}$TAU mice revealed fewer NFTs in $_{LOW}$TAU mice, a feature previously masked by a low level of cell loss in this area at 13 months of age. In addition to a main effect of antibody established using absolute numbers, a main effect of genotype between the two lines at the different ages became apparent (antibody: $F_{(3, 12)} = 16.77$, $p=0.0001$, genotype: $F_{(1, 4)} = 22.15$, $p=0.0093$, Figure 4.4.A)). Compared NFT ratio calculations for the CA3 region

showed comparable reductions in $_{LOW}$TAU 24-month-old mice as were seen with absolute NFT counts (genotype: $F_{(1, 4)} = 53.27$, p=0.0019, Figure 4.4.B)).

All inclusions reactive with AT8, and thus phosphorylated at S202/T205, were also found to be reactive for the human-specific antibody HT7, at all ages, irrespective of tau dose. This finding suggests that no NFTs are formed from purely murine tau phosphorylated at S202/T205. This does not, however, exclude the possibility that murine tau is incorporated into inclusions along with transgenic human tau.

Thus, the hippocampus of TauD35 mice shows an age- and dose-dependent neuronal accumulation of misfolded and abnormally phosphorylated tau associated with AD.

Mossy fibre staining

Tau is modified in axons prior to mislocation

A degree of mossy fibre staining was seen across all ages (4-, 13- and 24-months) with each of the antibodies: HT7/ AT8 (Figure 4.5.), CP13 (Figure 4.6.), MC1 (Figure 4.7.) and PHF-1 (Figure 4.8.) in all transgenic mice. Staining showed a heterogeneous pattern, even within the same age group with each antibody. These variations in mossy fibre staining between mice may be expected, due to individual variations and minor differences in slicing angle. No staining was observed in age-matched WT controls.

Both transgenic lines displayed a level of mossy fibre reactivity with all tau antibodies at 4 months of age, prior to the detection of tau aggregates. Mossy fibre reactivity with antibodies CP13, MC1 and PHF-1 has been observed previously in young tauopathy mice (Harris et al., 2012). Within both the 13- and 24-month groups, a decrease in mossy fibre staining was consistently associated with the development of NFTs, possibly due to the mislocation of tau into the somatodentritic region decreasing axonal levels.

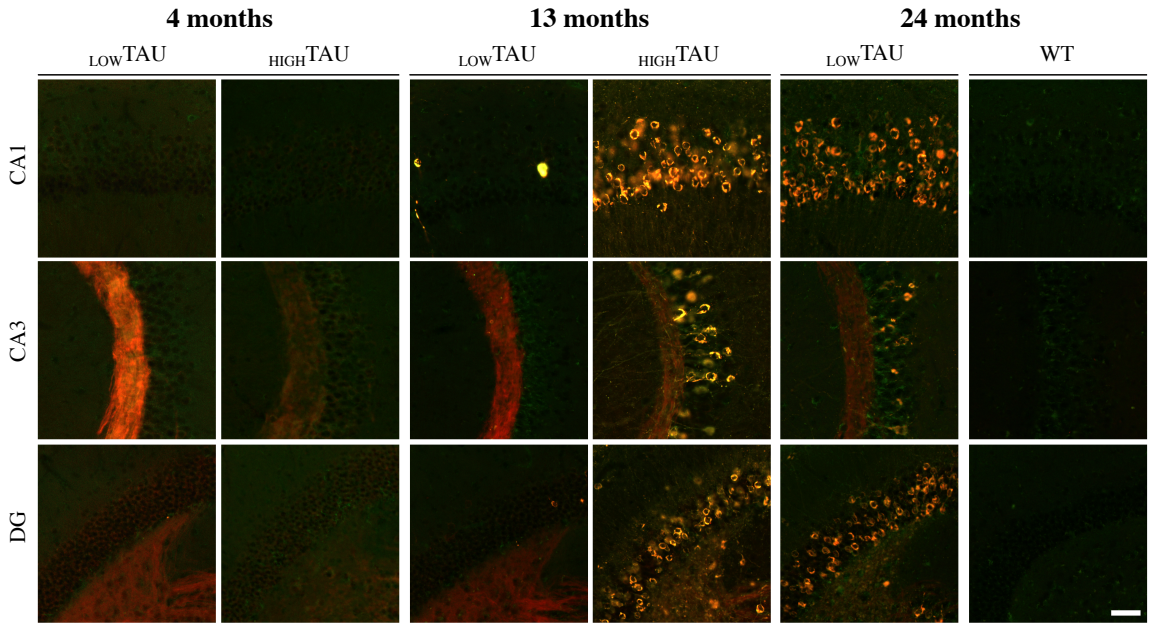

Figure 4.5. Representative images of the CA1, CA3 and DG regions of the hippocampus from $_{LOW}$TAU and $_{HIGH}$TAU mice at 4, 13 and 24 months of age double stained using AT8 and HT7. WT sections from 24-month-old mice are included. Sections were double stained HT7 (human tau, *red*) and AT8 (S202/ T205, *green*). Mossy fibre staining is evident from 4 months of age in both $_{LOW}$TAU and $_{HIGH}$TAU animals. At 13-months, a large discrepancy is observed in the number of NFTs between $_{LOW}$TAU and $_{HIGH}$TAU mice. Scale: 25µm.

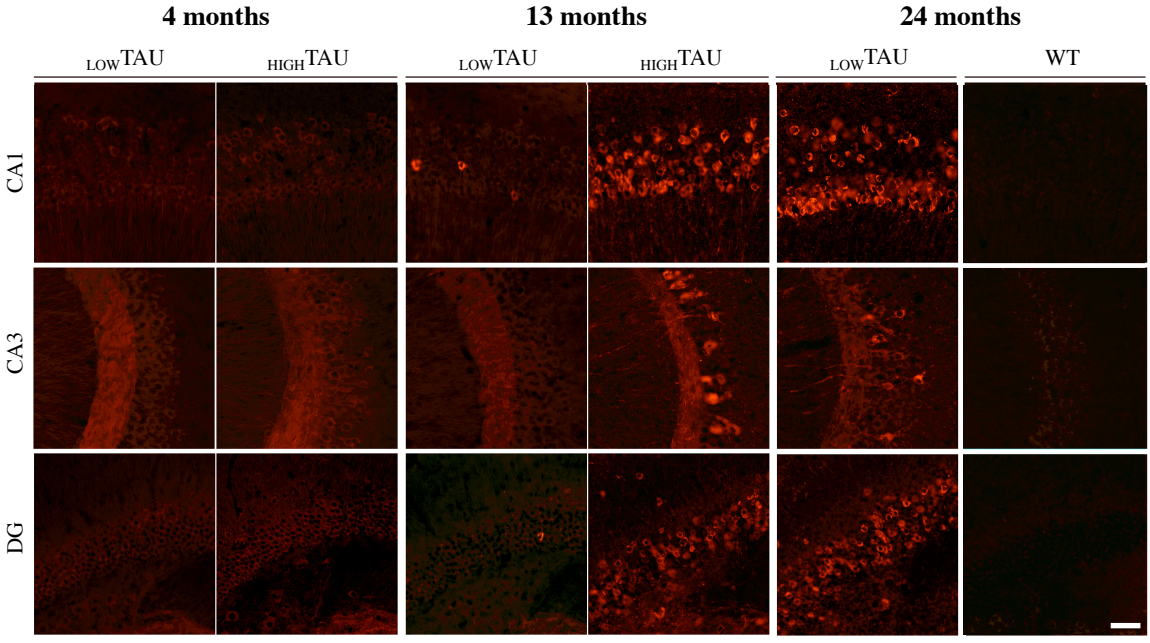

Figure 4.6. Representative images of the CA1, CA3 and DG regions of the hippocampus from $_{LOW}$TAU and $_{HIGH}$TAU mice at 4, 13 and 24 months of age stained using CP13. WT sections from 24-month-old mice are included. Sections were stained using CP13 (S202). Mossy fibre staining is observed from 4-months. Diffuse tau is also evident within the somatodendritic compartment from 4 months of age in both $_{LOW}$TAU and $_{HIGH}$TAU animals. At 13-months, a large discrepancy is observed in the number of NFTs between $_{LOW}$TAU and $_{HIGH}$TAU mice. Scale: 25µm.

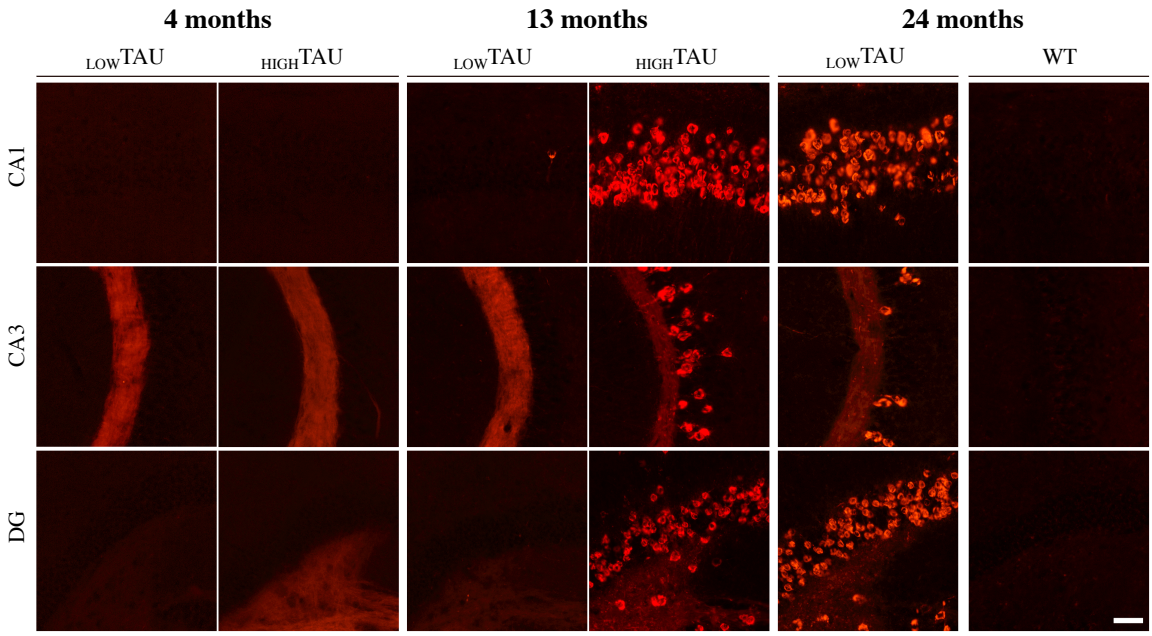

Figure 4.7. Representative images of the CA1, CA3 and DG regions of the hippocampus from $_{LOW}$TAU and $_{HIGH}$TAU mice at 4, 13 and 24 months of age stained using MC1. WT sections from 24-month-old mice are included. Sections were stained using MC1 (misfolded tau). Mossy fibre staining is observed from 4 months of age. At 13-months, a large discrepancy is observed in the number of NFTs between $_{LOW}$TAU and $_{HIGH}$TAU mice. Scale: 25µm.

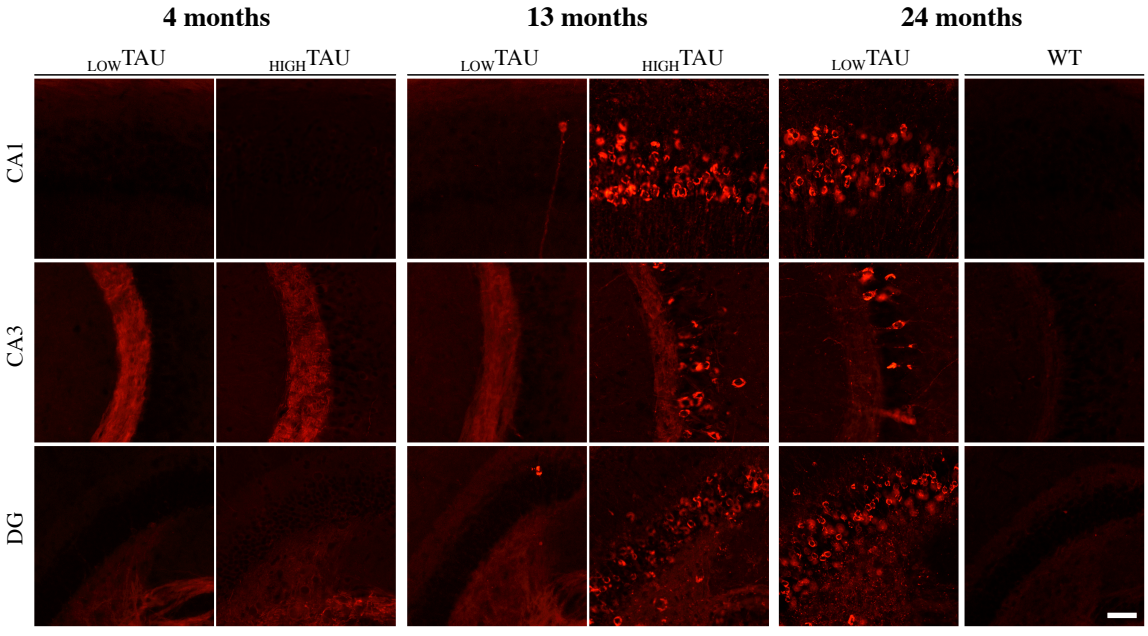

Figure 4.8. Representative images of the CA1, CA3 and DG regions of the hippocampus from $_{LOW}$TAU and $_{HIGH}$TAU mice at 4, 13 and 24 months of age stained using PHF-1. WT sections from 24-month-old mice are included. Sections were stained using PHF1 (S396/ S404). Mossy fibre staining is observed from 4 months of age. At 13-months, a large discrepancy is observed in the number of NFTs between $_{LOW}$TAU and $_{HIGH}$TAU mice. Scale: 25µm.

Summary and Discussion: Histology

Principle cell numbers were evaluated in the CA1 and CA3 regions of the hippocampus in both $_{LOW}$TAU and $_{HIGH}$TAU mice compared to age-matched WT littermates. No cell loss was observed up to 24-months of age in $_{LOW}$TAU mice, even though extensive pathology was evident. In $_{HIGH}$TAU mice of 17.5-months of age, already presenting with the characteristic pathological phenotype associated with this line, significant cell loss in the CA1 area had become apparent. The large (>50%) reductions in neuronal cell numbers seen in this region are in agreement with similar mouse models (SantaCruz et al., 2005) and even human AD cases (West et al., 1994), highlighting the vulnerability of the CA1 pyramidal cells to tau dysfunction. The large reduction in hippocampal volume (Figure 4.1.C)), while contributed to by the loss of neurones, also likely includes the loss of neuropil including synapses. The presentation of one of the cardinal features of neurodegenerative tauopathies within their lifespan, brands the $_{HIGH}$TAU mice line a more favourable model compared to $_{LOW}$TAU mice in this respect. The $_{LOW}$TAU model does, however, provide an increased opportunity to investigate the very earliest effects of tau dysfunction, through prolonging the initiation phase of pathology development. The ability to study dose-dependent effects of tau through the use of both lines also provides a valuable opportunity.

Immunohistochemistry provided a way to investigate the presence and location of pathological tau. Using a common antibody (CP13) for the detection of phosphorylated tau frequently thought of as an indicator of 'early' pathological changes (Ramsden et al., 2005, Adams et al., 2009), we observed diffuse staining of the cell soma and processes in both $_{LOW}$TAU and $_{HIGH}$TAU mice at the 4-months-old (Figure 4.2.C) and Figure 4.6.). This diffuse staining pattern was not observed with any other antibody used, supporting the opinion that S202 phosphorylation occurs early on in the temporal cascade of pathological tau development.

At 13-months in $_{LOW}$TAU mice, absolute NFT numbers detected with CP13 and indeed all antibodies used, were found to be sparse, affecting only a few hippocampal neurones in each section examined. This was in contrast to the extremely large numbers of inclusions present throughout the hippocampus of $_{HIGH}$TAU mice at this age. In the CA1 region, while absolute NFT numbers were found to be comparable to 24-month $_{LOW}$TAU mice, a main effect of antibody was detected, indicating significant differences in the numbers of NFTs detected with each antibody. In agreement with previous data that

MC1 and CP13 detect epitopes present in early NFT formation (Ramsden et al., 2005), these antibodies were found to identify the highest numbers of pathological inclusions in the CA1 region, possibly representing the continued initiation of NFT development at all ages. Similarly, PHF-1, a marker of late-stage pathological tau (*ibid*), detected the lowest number of NFTs of the antibodies used.

Where cell counts were available for the CA1 and CA3 regions, the ratio of NFTs to the average number of cells of the animal was calculated and compared between $_{HIGH}$TAU 13-month-old and 24-month $_{LOW}$TAU mice. With all antibodies used, a significant effect of genotype was detected in both hippocampal areas, representing significantly fewer NFTs in 24-month $_{LOW}$TAU mice compared to 13-month $_{HIGH}$TAU animals. The emergence of an effect of genotype within CA1 when comparing the calculated ratios, may be due to a small amount of loss of NFT containing neurones within CA1 in $_{HIGH}$TAU mice at 13-months, resulting in extracellular 'ghost' tangles. These ghost NFTs are the remnants of tangle-bearing neurones following their death. As they are not readily degraded, ghost tangles often present a morphology similar to the intracellular NFTs of living neurones (Kril et al., 2002). Thus while cell counts are slightly decreased, numbers of NFTs are not seen to differ, resulting in comparable absolute NFT numbers between $_{HIGH}$TAU 13-month and $_{LOW}$TAU 24-month-old mice. Indeed, double staining of phosphorylated tau (AT8) and neuronal cell bodies revealed what appeared to be a small minority of extracellular NFTs in 13-month $_{HIGH}$TAU animals within the CA1 region (Figure 4.9.); however, such staining was used for qualitative purposes only, with the calculation of the ratio of NFTs to the number of cells deemed more reliable for the present study.

Some degree of mossy fibre staining was observed in all transgenic mice at all ages. Mossy fibre staining has been documented previously (Sydow et al., 2011, Harris et al., 2012) and reflects the physiological localisation of tau in axons (Trojanowski et al., 1989, McMillan et al., 2011, Liu and Gotz, 2013), highlighted here due to the density of axons in this fibre tract. While staining was not quantified, some qualitative observations were made.

While tau is present in axons physiologically, HT7 reactivity within these fibres reveals that human tau is sorted within murine neurones, allowing it to adopt a physiological intracellular position. Reactivity with all AT8, CP13, MC1 and PHF-1 indicates a level of pathological tau modification takes place within axons prior to

mislocation to the cell soma and the development of aggregates. These observations have been made previously, with CP13, MC1 and PHF-1 reactivity being observed in the mossy fibre tract of young tau transgenic mice (Harris et al., 2012).

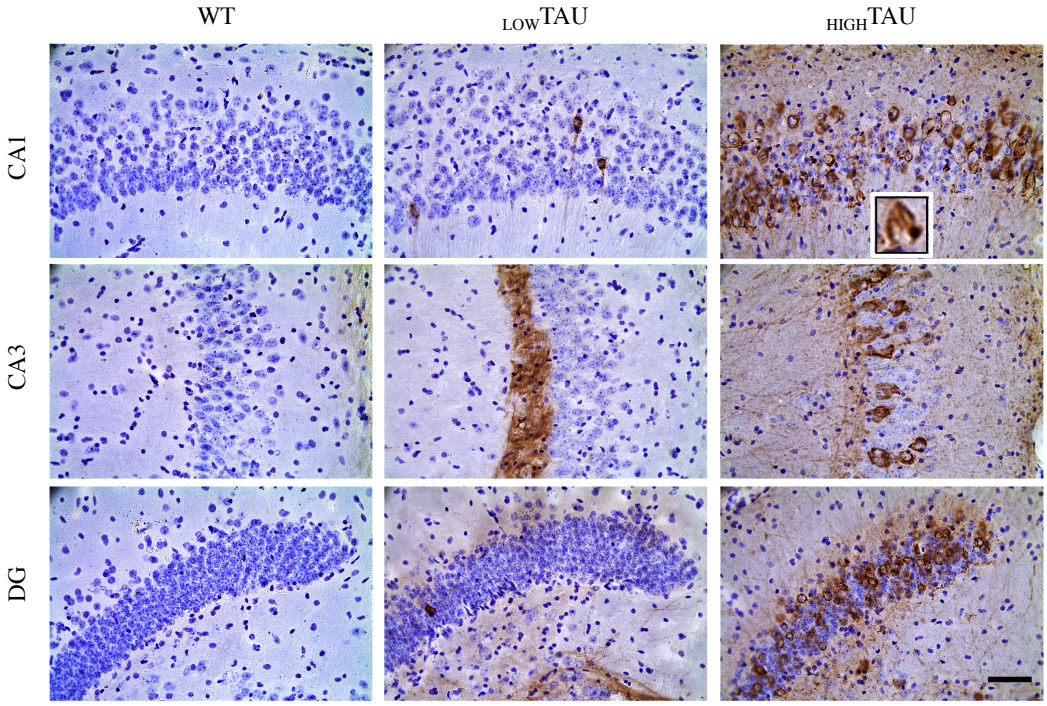

Figure 4.9. Representative images of the CA1, CA3 and DG regions of the hippocampus double stained for pathological tau and neuronal nuclei at 13 months of age reveal occasional extracellular NFTs within the CA1 region of $_{HIGH}$TAU mice. Sections were double stained using **cresyl violet** (neuronal nuclei) and **AT8** (S202/ T205) developed using DAB HRP. An extracellular NFT (NFT with no associated nucleus) is shown (*insert*) in the representative image from the CA1 region of the $_{HIGH}$TAU mouse. Extracellular NFTs were found to account for only a small minority of NFTs, and were only ever observed within CA1. Scale: 50μm.

It is suggested that a level of hyperphosphorylation/ misfolding occurs in axons before tau is mislocated to the somatodendritic compartment. This development of pathological tau, and even its mislocation, can be tolerated by the neurone for some time as is seen in hibernating animals (Arendt et al., 2003). The hibernation period in such animals is interrupted by arousal periods lasting up to one day (*ibid*), where tau is de-phosphorylated and re-sorted to the axonal compartment, meaning that the time a neurone spends harbouring large amounts of hyperphosphorylated or misfolded tau is limited. Following a prolonged period of exposure of a neurone to hyperphosphorylated or misfolded mislocated tau, a cell may loose its ability to reverse this process; and thus the tau becomes pathological, forming soluble toxic species which result in deleterious effects on the neurone, and finally aggregates, which develop into mature NFTs within the soma.

At 13-months, a lower degree of fibre reactivity was observed in $_{HIGH}$TAU mice when compared to $_{LOW}$TAU animals. It is suggested that a decrease in fibre staining is indicative of tau mislocation into the somatodendritic compartment, possibly caused by the summation of multiple modifications and overloaded axonal phosphatase activity (Bertrand et al., 2010b). The mislocated tau can be observed as NFTs, with the number of inclusions appearing to negatively correlate to the degree of mossy fibre staining. It has previously been suggested (de Calignon et al., 2012) that a loss of axonal immunoreactivity may also signify axonal degeneration prior to neurone loss; however, axonal density was not quantified in the present study.

In summary, it is shown that the mutated human tau protein produced in these models is processed correctly into the axonal compartment within hippocampal neurones in both the $_{LOW}$TAU and $_{HIGH}$TAU lines of TauD35 mice. With increasing age we see that this tau assumes common pathological conformations, as well as aggregating to form NFTs, with increasing transgene dose shown to accelerate this development. In terms of NFT development, $_{HIGH}$TAU mice of 13 months of age are found to be comparable to 4.5/5 month old rTg4510 mice (Ramsden et al., 2005). In $_{HIGH}$TAU mice of 17.5 months of age, already presenting with the moribund phenotype typical of this line, significant neuronal loss is observed within the CA1 region. Such features are characteristic of human tauopathies, making both TauD35 models valuable new tools to study tau dysfunction. In highlighting the more pathologically aggressive nature of the $_{HIGH}$TAU transgenic line, compared to the $_{LOW}$TAU model, we also provide conformation of the functionality of the extra transgene copies harboured by $_{HIGH}$TAU mice.

CHAPTER 5

Introduction: Behaviour

The degree of both NFT pathology and neuronal loss has been correlated to the cognitive decline of AD patients (Arriagada et al., 1992, Gomez-Isla et al., 1997, Giannakopoulos et al., 2003, Guillozet et al., 2003). Indeed we see that the selective spatial distribution of both of these characteristic pathologies is compatible with the temporal development of cognitive symptoms in AD, where an initial impairment of episodic memory is typical due to isolation and degeneration of medial temporal lobe structures including the hippocampus. As the transgene is expressed under the CaMKIIα promoter, and is thus strongly expressed in the hippocampus (www.mouse.brain-map.org (Lein et al., 2007)), and with the obvious vulnerability of the hippocampus to NFT development and neurone loss (as displayed in AD), one may hypothesise that hippocampal-dependent behavioural deficits would be among the first to show.

In order to determine if TauD35 mice present with hippocampal-dependent memory dysfunction, 12-month-old mice were tested using the T-maze forced alternation task. In addition to this memory dependent task, mice were also examined for changes in locomotion and anxiety using the open field and light/dark box behavioural tests.

The age of behavioural testing was chosen in order to be sufficiently prior to the presentation of the ailing phenotype developed by a proportion of TauD35 mice, later discovered to be of the $_{HIGH}$TAU line. The motor component of the pathological phenotype seen in $_{HIGH}$TAU mice between 17 and 20 months of age would preclude behavioural testing. Due to the low sample numbers of $_{HIGH}$TAU mice included, data presented herein is treated as pilot data for further testing.

At the time of behavioural testing, it was not yet known that two transgenic lines existed within the TauD35 mouse model. Following post-hoc copy number analysis of all mice, data were separated into $_{LOW}$TAU and $_{HIGH}$TAU. Unfortunately, this resulted in low sample numbers of $_{HIGH}$TAU mice being included. Behavioural data included within this chapter is therefore treated as pilot data for further testing.

T-maze forced alternation task

The present investigation has so far concentrated on the characterisation of tau pathology within the hippocampus. Therefore the behavioural task chosen for testing was one that shows high sensitivity to hippocampal dysfunction (Dudchenko, 2001, Deacon and Rawlins, 2006).

The T-maze forced alternation task tests 'spatial working memory', that is, the mouse must remember what arm of the maze it has previously visited and alter its choice on the second run in order to receive a consumable reward. This type of short-term memory is utilised within the one trial, and once used should be forgotten (Dudchenko, 2004).

The innate behaviour of rodents means that they will naturally tend to alter their choice of goal arm. This instinctive behaviour is necessary for rodents to locate food, water, shelter and mates within their natural habitat, and is a tendency encouraged during the habituation period using the food reward. This means that even prior to training, WT mice will show a ~75% correct response rate in the task, with this increasing to >90% correct following the training period (Deacon and Rawlins, 2006, Cacucci et al., 2008). Since the early use of the T-maze, it has been observed that rats with damage to the hippocampus display clear deficits in their ability to correctly perform within the maze, tending instead to perform at the level of chance (50% correct) (Aggleton et al., 1986, Dudchenko et al., 2000, discussed in O'Keefe, 1978). This finding demonstrates the high sensitivity of the T-maze alternation task to dysfunction within the hippocampus. The exact reason for this high dependency on the hippocampus has not yet been fully elucidated (Dudchenko, 2001), but is likely due to the complex role of the hippocampus in processing spatial information (O'Keefe, 1978).

Adding a short delay between the sample and choice runs can increase the cognitive demand of the T-maze; by simply increasing the amount of time the animal must remember its previous choice. This method can increase the chance of detecting more subtle cognitive deficits. In the present study, delays of 1, 3, 6 and 10 minutes were chosen. In order to prevent mice becoming demotivated to perform the task, trials using longer delays were always interspersed with trails of the shortest delay period.

The room within which the task was performed contained visible landmark cues on each of the 4 walls. Previous work using rats has noted that the presence of such cues is not

necessary to performance in the task; however, if present, rats will use the cues to aid the correct choice (although they are still not completely reliant on them) (Dudchenko, 2001).

The protocol used within the present study for testing within the T-maze was adapted from that previously published for use on mice (Cacucci et al., 2008).

Locomotor and Anxiety testing

As well as the assessment of hippocampal-dependent memory deficits using the T-maze, mice were also evaluated in terms of locomotor activity and anxiety levels. To do this, the behaviour of transgenic mice in the open field and light/dark box was compared to WT littermates. Both the open field and light/dark box are based on the approach-avoidance conflict. This conflict is established by the contradiction of the innate behaviour of a mouse, such as its natural exploratory behaviour, with the aversive properties of a large open space or brightly lit environment.

Open field

The open field test was first developed in the early 1930s by Calvin Hall, and consists simply of an inescapable open arena. Despite its development using rats, the test has also been shown to be successful for use on mice (Prut and Belzung, 2003). Its simplicity and ability to quickly measure many clearly defined behaviours led to its huge popularity. Even today, some 80 years after its first use, the open field provides one of most common tests for locomotor activity, exploration and anxiety-related behaviours (*ibid*).

For the present study, the open field has been used for testing two main parameters: time spent in centre, taken as an indicator of anxiety; and total distance travelled, as a measure of overall exploratory/locomotor activity. Both parameters are examined in 5-minute time bins, giving an idea of changes in anxiety-related behaviour and exploratory behaviour, respectively, over time.

Light/dark box

Another common test used to assess anxiety-related behaviour in mice is the light/dark box. First developed by Crawley and Goodwin (1980), the light/dark box consists of an

aversive (light) compartment and safe (dark) compartment. Mice will naturally favour the dark enclosed compartment; however, an urge to explore the enclosure will drive the mouse to enter the light compartment. Measurements for evaluating anxiety include: latency to enter the dark compartment and latency to return to the light compartment, the number of transitions between the two compartments, as well as the total time spent in either compartment.

Results: Behaviour

Hippocampal-dependent memory

No memory deficit in either $_{LOW}$TAU or $_{HIGH}$TAU mice at 12 months

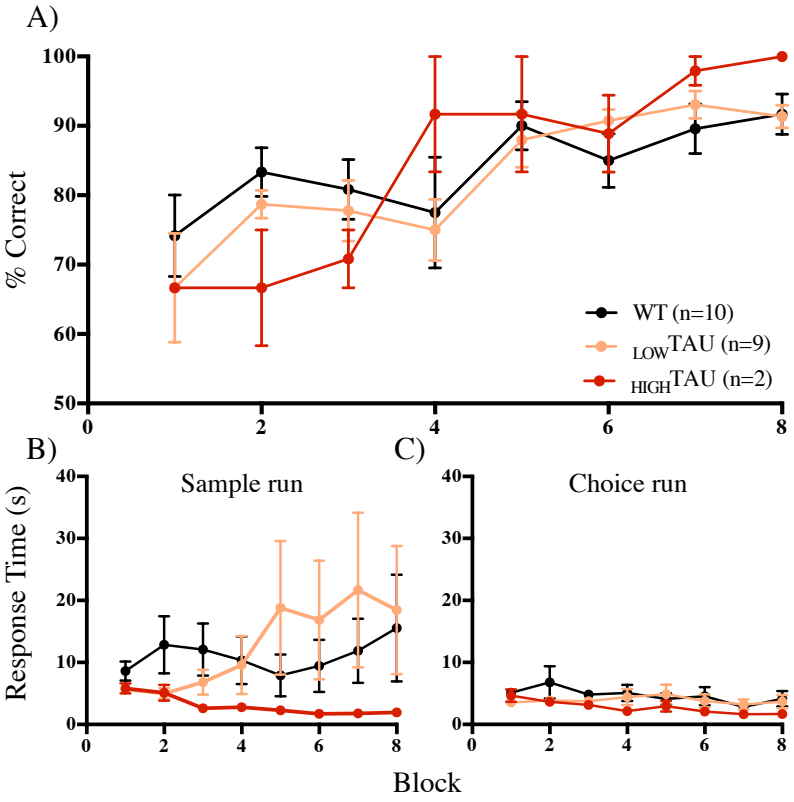

Figure 5.1. No deficit in hippocampal-dependent memory in $_{LOW}$TAU or $_{HIGH}$TAU mice compared to WT controls. A) Percent correct responses across training block (2 days). B) Response time of sample (1st) run across training block. C) Response time of choice (2nd) run across training block. Error bars indicate SEM.

Hippocampal-dependent memory was assessed using the T-maze forced alternation task in mice of 12 months of age. Correct responses were pooled into 2-day blocks for analysis. The percentage of correct trials initially following habituation for both transgenic lines were not found to differ from WT mice. Over the following 7 training blocks, both transgenic lines were seen to learn the task as well as WT littermates. With all groups reaching >90% correct by the end of training (training block: $F_{(7, 126)} = 8.348$, $p < 0.0001$) (Figure 5.1.A)).

For both sample and choice runs, each mouse was timed from the point of placement into the start arm, until all four feet were over a specified line at the entry point to each goal arm. These values were recorded as 'response times'. Prolonged response times for choice runs effectively introduce a delay to the trial, increasing the amount of time the mouse must remember its previous choice, and thus must be monitored. Mice that completed the trial with a response time of over two standard deviations from the mean response time of that genotype for two or more consecutive training blocks, for either the sample or choice run, were excluded from all analyses. One WT mouse fulfilled this criterion and was subsequently excluded from the analyses of all testing. Response times were not found to differ significantly for either the sample or choice runs for transgenic mice compared to WT, however, faster response times, particularly during the sample run, were noted for both $_{HIGH}$TAU animals tested (Figure 5.1.B)).

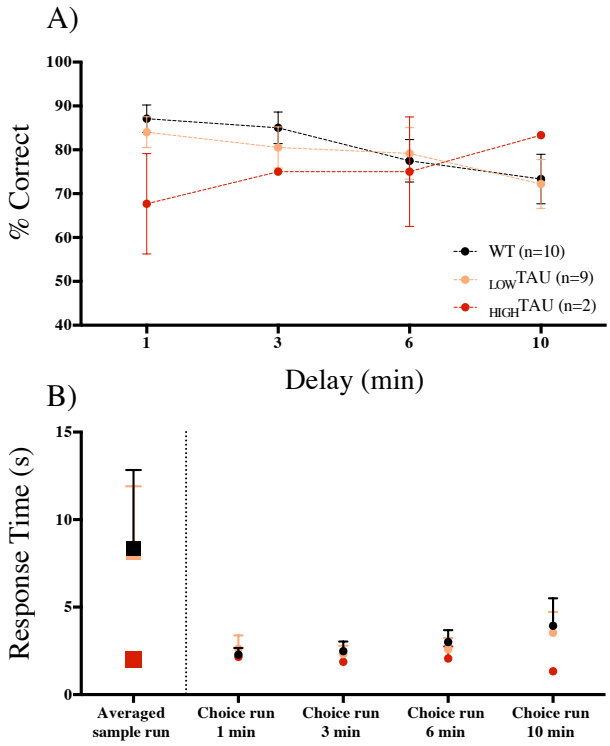

Figure 5.2. No deficit in hippocampal-dependent memory in $_{LOW}$TAU or $_{HIGH}$TAU mice compared to WT controls with increasing delay. A) Percent correct responses with increasing delays of 1, 3, 6 and 10 minutes. All 1-minute delays have been averaged. B) Response times of sample (average of all sample runs during the testing period) and choice runs with increasing delay time. Error bars indicate SEM.

Varying delays were then introduced between the sample and choice runs. Delays of 1, 3 and 6 minutes were chosen initially in the hope of detecting more subtle cognitive deficits. While the performance of WT and both transgenic lines was seen to decrease slightly with increasing delay, changes were not found to be significant. Therefore, to further increase cognitive demand, a delay time of 10 minutes was introduced. To prevent the mice becoming demotivated to perform the task, these trials were run interspersed pseudorandomly with the shortest delay time of 1 minute. All trials including a delay time of 1 minute were grouped for analysis (Figure 5.2.A)). For both

WT and $_{LOW}$TAU mice, performance in trials using a 10-minute delay were again slightly decreased, however, accuracy remained above chance (50%). The slight reduction in the percentage of correct choices made by WT mice with increasing delay time excludes the possibility of contamination of the choices made by 'intra-maze' factors such as olfactory cues. In contrast, $_{HIGH}$TAU mice did not display a consistent reduction in performance with the longest delay time. These results confirm an absence of a deficit in hippocampal-dependent memory in $_{LOW}$TAU mice at this age, while also suggesting no impairment in $_{HIGH}$TAU animals.

Response times for delay trials were again recorded, all sample run times were grouped for analysis (Figure 5.2.B)). No significant differences were detected between transgenic and WT mice for either sample or choice runs, however, as was observed during training, $_{HIGH}$TAU mice displayed extremely fast response times for sample runs.

While firm conclusions about the status of hippocampal-dependent memory in $_{HIGH}$TAU mice are prevented due to the low sample number, the similar behaviour within the T-maze of the 2 mice tested certainly suggests that $_{HIGH}$TAU mice are unimpaired in this memory task, as well as displaying a more rapid response time on the first sample run, possibly reflecting disinhibitory behaviour.

Locomotor and anxiety testing

Open field

In order to assess overall locomotor activity in the transgenic cohorts compared to WT mice, total distance travelled within the open field arena was measured. As expected, the total distance travelled over time decreased in WT mice, seeing a reduction of 37% from the first 5-minutes to the last 5 minute period, reflecting habituation to the environment. The behaviour of $_{LOW}$TAU mice was seen to follow that displayed by WTs, with the total distance travelled over the 15-minute test period decreasing by 35%. Interestingly, $_{HIGH}$TAU mice displayed a significantly different pattern of behaviour (genotype × time: $F_{(4, 38)} = 4.562$, $p = 0.0042$) (Figure 5.3.A)). The distance travelled by $_{HIGH}$TAU mice in the first 5 minutes of being placed within the arena was lower than that seen in WT and $_{LOW}$TAU animals, however, mice continued to explore at the same rate throughout the test period, displaying no habituation to the environment. In calculating the total path

length of the three genotypes, it is seen that in fact all groups travelled the same total distance during the open field test (Figure 5.3.D)); $_{HIGH}$TAU mice, however, were initially less active, suggesting increased anxiety, and then did not habituate to the environment staying moderately active throughout.

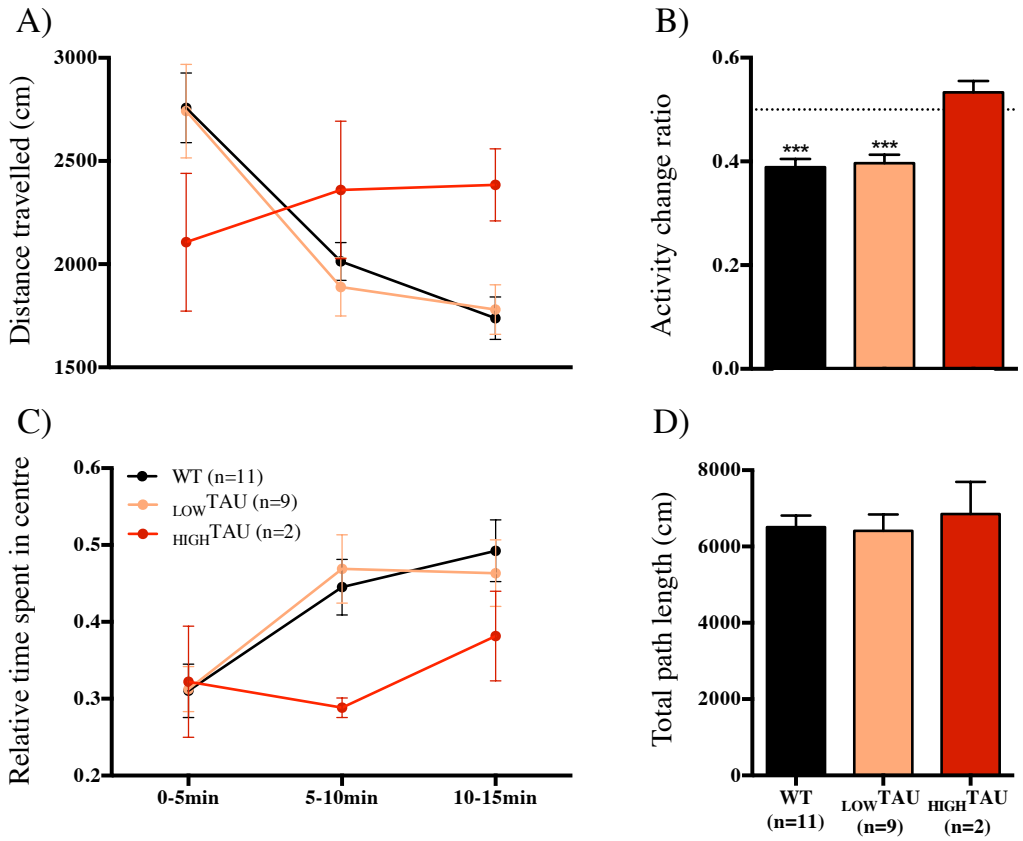

Figure 5.3. $_{HIGH}$TAU mice display a lack of habituation to a novel environment in the open field. A) Distance travelled across 15 minutes, binned in 5-minute blocks. Two-way ANOVA reveals a significant interaction between genotype and time (p=0.0042). B) Activity change ratio, representing the amount of activity in the 3rd period relative to the summed activity in the 1st and 3rd periods. One-sample *t*-test with a hypothesised mean of 0.5 (no change in activity), significance indicated by p<0.001***. C) The relative time spent within a defined central region compared to time spent in the periphery of the arena (area equal between centre and periphery), binned in 5 minute blocks. D) Total distance travelled within the 15 minute testing period. Error bars indicate SEM.

As initial levels of activity differed between genotypes, the activity change ratio was calculated to assess habituation. Using this score (outlined by Bolivar (2009), in which the distance travelled in the final 5 minute period is divided by the sum of the distance travelled in the first and final 5 minute blocks; a score of 0.5 indicates unchanged activity), we see that $_{HIGH}$TAU mice do not habituate, in comparison to significant habituation displayed by the WT and $_{LOW}$TAU groups (activity change ratio, 1-sample *t*-test against a defined value of 0.5; WT: 0.39, p=0.0001; $_{LOW}$TAU: 0.39, p=0.0002; $_{HIGH}$TAU: 0.53, p=0.365) (Figure 5.3.B)).

Time spent within a defined central region (equal area within centre and surround) relative to the periphery of the arena was taken as a general marker of anxiety-like behaviour. All mice displayed some increase in the relative time spent within the centre throughout the time of the trial (time in centre: $F_{(2, 38)} = 8.592$, $p = 0.0008$), reflecting a decrease in anxiety with habituation (Figure 5.3.C)). For WT mice, this saw relative centre-time increase from 31±3.5% in the 1st period to 49±4% in the 3rd period, a trend mirrored by $_{LOW}$TAU mice (1st period: 31±3%, 3rd period: 46±4%). $_{HIGH}$TAU mice, however, displayed a slightly different pattern of behaviour, with the amount of time they spent within the centre of the arena increasing to a lesser extent from 32±7% initially, to only 38±6% in the final 5 minutes. This final increase in $_{HIGH}$TAU centre-time also took longer to achieve, again suggesting a deficit in habituation in these mice. In spite of this, analysis of variance did not reveal significant differences between genotypes likely due to low sample numbers of $_{HIGH}$TAU mice.

Light/dark box

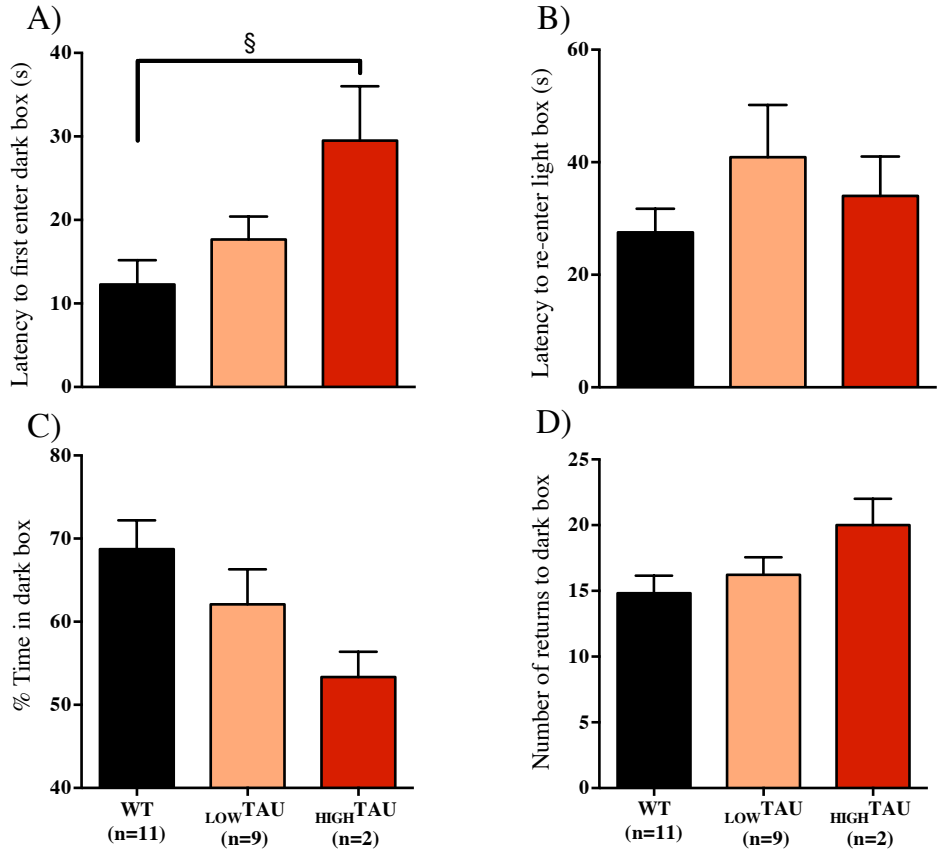

Figure 5.4. Tendency towards a reduction in anxiety-like behaviour in $_{HIGH}$TAU animals. A) Latency to first enter the dark compartment following placement within the light box. One-way ANOVA; $^{§}p=0.059$ B) Latency to re-enter the light compartment. C) Percentage time spent within the dark compartment. Axis has been cut at 40%, the percentage of time that would be predicted for a mouse to spend within the dark compartment based on the relative sizes of each box. D) The number of transitions between the light and dark compartments. Error bars indicate SEM.

In addition to the open field, mice were also tested using the light/dark box. During this 6-minute assessment, 6 parameters were measured including: latency to enter the dark compartment and latency to return to the light compartment, the number of transitions between the two compartments, as well as the total time spent in either compartment.

WT mice behaved in a manner comparable to previous work using C57Bl/6 animals in all parameters measured (Costall et al., 1989). Neither $_{LOW}$TAU nor $_{HIGH}$TAU mice displayed significantly different behaviour from WT littermates in all elements of the test (Figure 5.4.); however, analysis of variance did reveal a tendency towards a difference between WT and $_{HIGH}$TAU animals in the amount of time taken to first enter the dark compartment ($p=0.059$) (Figure 5.4.A)). Here, WT mice displayed a typical latency time to enter the dark compartment of 12.27 ± 2.93s. The longer latency of $_{HIGH}$TAU mice (29.5 ± 6.5s) to enter the safety of the dark box may be interpreted as reduced anxiety in this line leading to an increase in exploration time of the light compartment in the first instance (Costall et al., 1989). However, one may therefore anticipate an increase in the percentage of time spent in the light compartment throughout the course of the test. By predicting the amount of time a mouse would spend in each compartment based on random activity, we would expect just 40% of the 6 minutes to be spent in the dark box, a forecast based on the relative sizes of each section (3/5 light, 2/5 dark). In fact, WT mice stayed within the dark compartment for 69 ± 3.5% of their time, highlighting their natural aversion to open and bright spaces. $_{HIGH}$TAU mice, however, spent only 53 ± 3% within the dark box. Although not significantly different, one may argue that $_{HIGH}$TAU mice do show a leaning towards a reduction in time spent within the dark compartment, a measurement considered the most consistently useful in the assessment of the anxiolytic action of drugs (Bourin and Hascoet, 2003).

Original work by Crawley and Goodwin (1980) on the anxiolytic effects of benzodiazepines, described that rather than the total amount of time spent within each compartment, the essential feature of anxiolytic action was an increase in the number of transitions between compartments. The number of transitions performed by WT mice in the present study averaged a characteristic 14.8 ± 1.3, with this value rising to 20.0 ± 2.0 for $_{HIGH}$TAU animals. While not significant, again one may conclude these results indicate potentially interesting differences in the anxiety-like behaviour of $_{HIGH}$TAU mice.

Summary and Discussion: Behaviour

In order to assess possible deficits in hippocampal-dependent spatial working memory within our tauopathy model, the T-maze forced alternation task was chosen, due to its high sensitivity to dysfunction within the hippocampus (O'Keefe, 1978).

During training, both $_{LOW}$TAU and $_{HIGH}$TAU mice were seen to learn the maze as well as their WT counterparts, with all mice reaching over 90% correct by the final training block. In a bid to uncover more subtle deficits, a delay of 1, 3, 6 or 10 minutes was then introduced between the sample and choice runs, increasing the length of time during which the mouse must remember its previous choice. Again the performance of both $_{LOW}$TAU and $_{HIGH}$TAU mice did not differ from WT controls. These data show that $_{LOW}$TAU mice do not display detectable impairment of hippocampal-dependent memory at 12 months of age using the T-maze forced alternation task. While sample numbers for $_{HIGH}$TAU mice are extremely low, data collected thus far certainly does not suggest the presence of a deficit in spatial working memory in this line. Thus, it would seem that the large NFT load (Chapter 4) present within the hippocampus of $_{HIGH}$TAU mice of this age, does not affect this form of hippocampal-dependent memory.

Behavioural data collected from rTg4510 mice at 4.5 months (an age showing comparable pathology to $_{HIGH}$TAU mice of 12/13-months) revealed a deficit in the retention of spatial reference memory by way of a decrease in search bias for the target quandrant in the Morris water maze (SantaCruz et al., 2005, Hoover et al., 2010). While not a test of working memory, the hippocampal-dependency of this task does indicate deficits in hippocampal function due to tau dysfunction, a feature not detected within the present study.

For WT and $_{LOW}$TAU mice during both the training and testing (delay) phases, response times were seen to be highly variable for the sample run, with an overall mean of approximately 10 seconds recorded for both groups. During the choice run, however, response times were found to be more consistent, with the average run time for each genotype consistently recorded as less than 5 seconds. Differences in the averaged response times between the sample and choice runs are attributed to the fact that prior to each sample run, a long period has ensued in which the mouse has been away from the maze, be that either the approximate 1 hour inter-trial interval, or overnight. The sample runs therefore include a time in which the mouse is re-familiarising itself with the maze,

resulting in higher variability. Choice runs, however, occur with a maximum of 10-minutes (during delay trials) away from the maze, therefore producing more consistent response times. It is of note, however; that the two $_{HIGH}$TAU mice tested both displayed extremely fast response times on both the sample and choice runs, with response times of less than 3 seconds commonly recorded.

Despite the low sample number of $_{HIGH}$TAU animals included within this test (n=2), both mice were seen to display these extremely fast response times on the first sample run with great consistency. It is thus possible that this finding may reflect reduced anxiety or disinhibition of the $_{HIGH}$TAU line. As the mice perform well on the task, it negates the possibility that these particularly fast response times are the result of abnormal repetitive behaviour.

Patients of FTDP-17 often display a range of behavioural disturbances earlier in the disease process, including disinhibition, with memory deficits manifesting only late in the disease (Wszolek et al., 2006). Data gathered through use of the T-maze forced alternation task therefore supports use of the $_{HIGH}$TAU mouse line as a model for this neurodegenerative tauopathy.

In contrast to the T-maze forced alternation task, results gathered from open field and light/dark box testing are somewhat harder to interpret. Primarily used within the present context to provide control testing for T-maze results, the open field and light/dark box are often simply described as assessing anxiety-related behaviours, which have been attributed to alterations within the amygdala (Cook et al., 2014). Use of these tests within the present study, however, exposed interesting changes in the behaviour of $_{HIGH}$TAU mice compared to other genotypes, results that may in fact fit better with the earliest clinical symptoms of personality and behavioural changes presented by patients with FTDP-17 (Wszolek et al., 2006).

Within the open field test, differences in the behaviour of $_{HIGH}$TAU mice compared to both WT and $_{LOW}$TAU animals were evident. While the total path length of each of the three genotypes was found to be comparable, analysis of the distance travelled plotted against time exposes that $_{HIGH}$TAU mice achieve this overall distance through a different pattern of behaviour. WT and $_{LOW}$TAU animals are seen to begin their time within the open field arena with a relatively high level of ambulation, which shows a characteristic decrease over the 15-minute test period as mice become habituated with their

environment (Bolivar, 2009). $_{HIGH}$TAU mice, however, travel a shorter distance within the first 5 minutes than WT or $_{LOW}$TAU mice, but then maintain this level of ambulation for the duration of the test. As all mice travel comparable total distances within the 15-minutes, this result seems to reflect higher initial anxiety, with reduced habituation to the environment, rather than hypo- or hyperactivity. In calculating the activity change ratios outlined by Bolivar (2009), in which the initial level of activity is considered, we confirm an absence of habituation in $_{HIGH}$TAU mice. Previous work with the similar mouse model, rTg4510, also revealed reduced habituation to an open field environment at an age displaying similar pathology to that studied in the present experiments (SantaCruz et al., 2005).

All genotypes displayed an increase in the time spent within the central region of the open field during the 15-minute testing period, reflecting a decrease in anxiety due to habituation to the environment. While not significant, $_{HIGH}$TAU mice did display a tendency to spend less time within the centre compared to both WT and $_{LOW}$TAU mice. Again this result agrees with previous data from rTg4510 mice, in which a reduction in the time spent within the centre of an open field arena was seen at an age corresponding pathologically to that used presently (Cook et al., 2014). A reduction in time spent within the centre is typically taken as a marker of increased anxiety, however, results gathered through use of the light/dark box (discussed below) conflict with this conclusion. Conflicting results were also gathered by Cook et al., (2014) using separate anxiety testing, possibly leading one to conclude that rather than an increase in anxiety, a reduction in the amount of time P301L mutant tauopathy mouse models spend within the centre of an open field, may instead indicate a reduced ability to habituate to a novel environment.

Testing using the light/dark box was used to assess simple anxiety-like behaviours of transgenic mice compared to WT controls. Neither $_{LOW}$TAU nor $_{HIGH}$TAU mice displayed significantly changed behaviour compared to their WT littermates in any of the six parameters considered; however, a tendency towards an increase in the time taken for $_{HIGH}$TAU mice to first enter the dark compartment was noted. As is discussed by Bourin and Hascoet (2003), the meaning of this measure is somewhat difficult to determine and is thus rarely discussed. Potential deficits in the general locomotor activity of $_{HIGH}$TAU mice resulting in simply slower ambulation (and therefore an increased latency to enter the dark box) are disregarded, due to the observation of a high number of transitions

between the two compartments throughout the test. This is supported by the fact $_{HIGH}$TAU mice travelled an equal overall distance to WT and $_{LOW}$TAU mice within the open field test, as well as their extremely fast response times during both the sample and choice runs of the T-maze forced alternation task; thus demonstrating the ability of $_{HIGH}$TAU mice to run quickly, and to continue moving for a time period exceeding the duration of the light/dark box test (6 mintues).

It may be that a longer delay to enter the 'safety' of the dark box is a result of decreased anxiety, resulting in a longer period of exploration of the light compartment in the first instance, as is seen after administration of anxiolytic drugs such as Diazepam and GR38032F to WT C57Bl/6 mice (Costall et al., 1989). In addition, $_{HIGH}$TAU mice show a leaning towards a reduced amount of total time spent within the light compartment and an increase in the number of transitions between compartments, both also indicative of a reduction in anxiety. Similarities between these data from $_{HIGH}$TAU mice and similar rTg4510 mice in the light/dark box are again noted. Cook et al., (2014) describe an increase in the amount of time spent within the light compartment in rTg4510 mice, which agrees with the trend recorded in $_{HIGH}$TAU animals.

Overall, neither transgenic line exhibits a change in hippocampal-dependent spatial working memory compared to WT controls at 12 months of age, assessed using the T-maze forced alternation task. This finding demonstrates the resilience of hippocampal memory networks to the tau dysfunction present in these lines, in particular within $_{HIGH}$TAU animals, which already present with a high NFT load at this age (Chapter 4). Interestingly, $_{HIGH}$TAU mice were seen to display extremely fast response times during the first, sample run within the T-maze, suggestive of disinhibitory behaviour. Indeed, both the open field and light/dark box tests also revealed interesting differences in the behaviour of $_{HIGH}$TAU mice, including deficits in habituation to a novel environment and potential reductions in anxiety-like behaviour. In this respect, the pilot data presented suggests the $_{HIGH}$TAU model emulates human FTDP-17, in that behavioural and personality changes, such as disinhibition, are among the first to show, with memory only loss occurring much later in the disease process (Wszolek et al., 2006). Such results are also found to be somewhat comparable to data from tau$^{-/-}$ animals, suggesting that these behavioural changes are due to a loss of normal tau function (Ikegami et al., 2000).

CHAPTER 6

Introduction: Electrophysiology

Due to the consensus that synaptic dysfunction is likely one of the first indicators of AD (Scheff et al., 2006), it followed that an electrophysiological characterisation be undertaken in the attempt to identify the earliest synaptic changes, prior to the development of NFT pathology. Extensive electrophysiological studies were completed at 4 months of age. This age corresponds to further work within the lab (Cummings et al., 2015) on the $APP_{swe}xPS1_{M146V}$ double transgenic (TASTPM) (Howlett et al., 2004) and the single APP_{swe} transgenic (TAS10) (Richardson et al., 2003) mouse models of amyloid-β dysfunction, allowing for comparison, as well as being prior to the development of NFTs within TauD35 mice (Chapter 4). Some electrophysiological recordings were also conducted in 13- and 24-month-old mice to allow for an understanding of electrophysiological changes with age.

At the time of electrophysiological testing, there was yet no indication that two transgenic lines existed within the TauD35 mouse model. Data from transgenic animals is therefore grouped within this chapter. Tail samples were, however, kept for post hoc genotyping and following copy number determination, data were plotted as scatters with $_{LOW}$TAU and $_{HIGH}$TAU indicated as can be seen throughout. For rare cases where copy number could not be determined, data has been presented in grey. Where potential differences between transgenic lines were noted all attempts were made to increase the sample numbers for both transgenic lines if mice were available.

Within this chapter, I will discuss both whole-cell patch clamp experiments and extracellular recordings of synaptic transmission, performed using 400μm thick acute slices, cut transversely with respect to the hippocampus (Figure 6.1.A)). An introduction to the electrophysiological techniques employed is given in Appendix 1. Previous work within the lab has identified large changes in excitatory transmission within the hippocampus of the double transgenic TASTPM model of amyloid-β dysfunction (Cummings et al., 2015). In addition, the recent discovery of the postsynaptic role of tau, in the targeting of Fyn to dendritic spines and subsequent effects on NMDA-Rs (Chapter 1) also fuelled the decision to concentrate solely on excitatory synaptic transmission within the hippocampus for this initial characterisation.

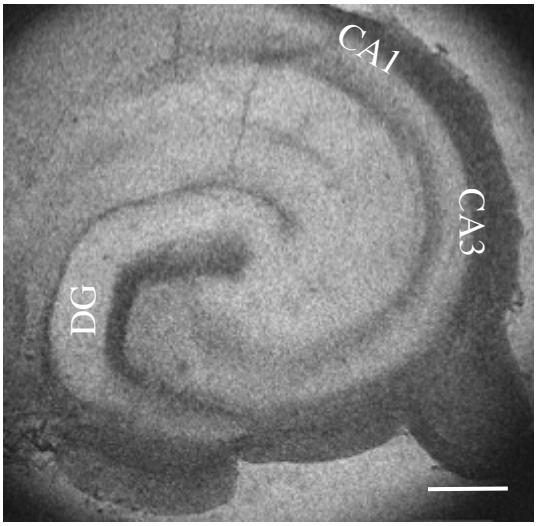

Figure 6.1. A) (*Left*) Pseudo-Normarski (or differential interference contrast (DIC)) image of an acute transverse hippocampal slice, obtained using the transmission settings on an Olympus Fluoview confocal microscope mounted on an upright Olympus BX50WI microscope and 5X water immersion objective. Scale: 400µm.

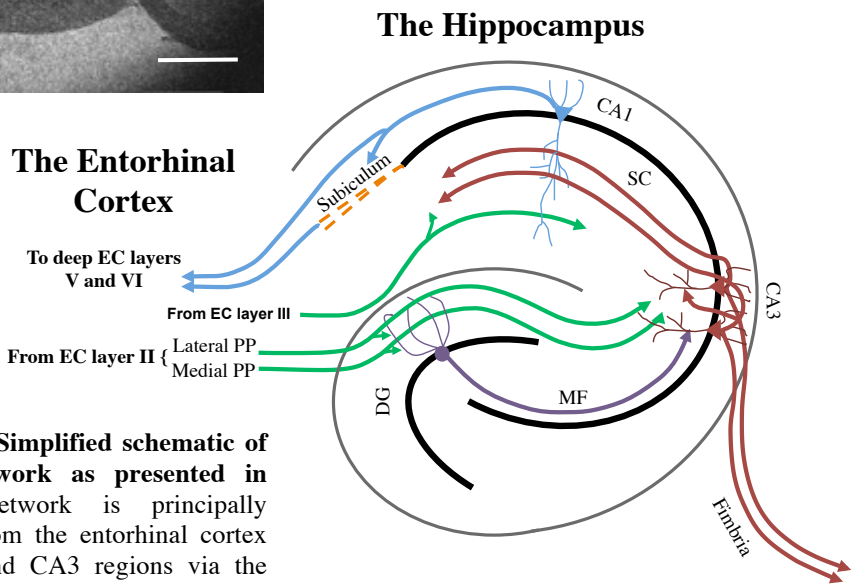

Figure 6.1. B) (*Right*) Simplified schematic of the hippocampal network as presented in Figure 1.3. The network is principally unidirectional. Input from the entorhinal cortex connects to the DG and CA3 regions via the medial and lateral perforant paths. CA3 cells receive input from the dentate gyrus via mossy fibres (MF). CA3 connects to CA1 via the Schaffer collateral (SC) pathway. CA1 also receives direct input via the perforant path. CA1 neurones provide input to the subiculum, which in turn forms the main output of the hippocampus.

The acute transverse hippocampal slice (Figure 6.1.A)) provided the optimal experimental system for electrophysiological characterisation. Developed in 1971 (Skrede and Westgaard), the acute slice typically describes a 300-500µm thick slice of hippocampus, which is kept alive *in vitro*. Acute slices made from mice, under the present conditions, can be kept healthy for up to 8 hours. The excitatory trisynaptic circuit of the hippocampus is preserved well in the transverse plane, exposing the extremely well defined and densely packed principle cell layers creating the circuit described in Chapter 1 (as can be seen as darker bands in Figure 6.1.A)). This preparation provides the stability and clarity of cell layers needed for electrophysiology, with the lamina structure of the dendritic and cell body layers ideal for extracellular recordings.

Two hippocampal regions were chosen for electrophysiological study: the CA1 and DG (Figure 6.1.B)). The CA1 region possesses some of the most vulnerable cells to the effects of tau dysfunction, as is demonstrated through their considerable NFT development and extensive loss in human AD patients as well as animal models of tauopathy (West et al., 1994, SantaCruz et al., 2005). The CA1 also provides a well-characterised and accessible area, with the SC-CA1 synapses by far the most studied with regards to LTP.

As is presented in Figure 6.1.B), in mice, the granule cells of the DG receive their principle input from layer II of the EC (ECII). This input comes in the form of two main pathways arising from the medial and lateral EC. Axons from the former, medial EC, project via the medial perforant path (mPP), which terminates in the middle third of the DG molecular layer (Hjorth-Simonsen and Jeune, 1972). The lateral EC in turn projects via the lateral perforant path (lPP), which is found to terminate on granule cell dendrites in the outer third of the molecular layer (Hjorth-Simonsen, 1972).

In AD, it is the pyramidal neurons of the EC that are first affected by tau pathology (Braak and Braak, 1991), as well as seeing substantial neurone loss even during the early stages of the disease (Gomez-Isla et al., 1996). Therefore, along with the CA1, it appears that EC pyramidal neurones (in particular the large neurones of layer II (Morrison and Hof, 1997)) show a specific vulnerability to tau dysfunction. Consequently, in order to assess possible changes in neurotransmitter release from ECII, synaptic transmission was recorded from the postsynaptic DG granule cells. Whole-cell patch clamp techniques were used to investigate both spontaneous and evoked transmission, with paired-pulse ratio (PPR) recordings made following stimulation to the mPP.

The mice presently under study express mutated tau under the CaMKIIα promoter and thus, as expression levels within these vulnerable neurones is high (www.mouse.brain-map.org (Lein et al., 2007)), one may predict degeneration of synaptic transmission within the EC and CA1 as an early event within the disease progression of this model.

Spontaneous excitatory postsynaptic currents

Excitatory currents have been isolated within the present study through use of the gamma-aminobutyric acid ($GABA_A$) receptor antagonist, SR95531 (also known as gabazine). Using whole-cell patch clamp techniques without application of exogenous stimulation, spontaneous excitatory postsynaptic currents (EPSCs) were investigated in both CA1 and the DG.

Spontaneous postsynaptic currents can result from either the stochastic fusion of a single vesicle of neurotransmitter with the presynaptic membrane, therefore representing release at a single synapse (known as miniature (m) EPSCs); or from spontaneous action potentials (APs) within a presynaptic neurone triggering the release of neurotransmitter from a single axon, therefore representing release from either a single, or multiple presynaptic sites (known as spontaneous (s) EPSCs). These mEPSCs and sEPSCs can be separated from each other pharmacologically via application of the voltage-gated sodium channel blocker, tetrodotoxin (TTX), which inhibits the generation of APs and thus isolates mEPSCs.

CA1 at 4 months of age

Electrophysiological data from the hippocampus was initially collected at 4 months of age. This age is prior to the development of NFTs within TauD35 mice (Chapter 4), and thus investigates possible functional deficits prior to the development of one of the cardinal features of neurodegenerative tauopathies.

No difference in the membrane resistance of CA1 pyramidal cells at 4 months of age

Using whole-cell patch clamp techniques allows one to document certain properties about the patched cell. The membrane resistance of individual CA1 pyramidal cells was obtained from examination of a test-pulse (+5mV, 40ms), applied immediately after achieving whole-cell configuration and stabilization of the cell. Analysis of variance revealed no difference between genotypes in the presence or absence of TTX at 4 months of age (Figure 6.2.).

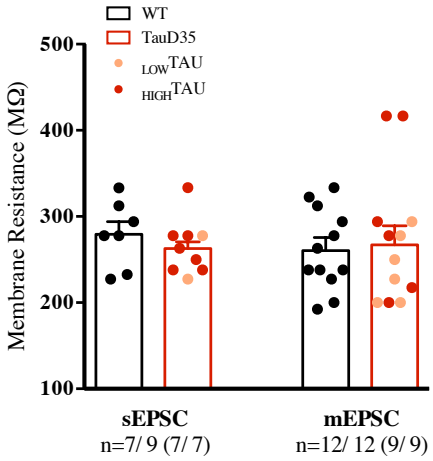

Figure 6.2. No difference in the membrane resistance of CA1 pyramidal neurones recorded in the presence (mEPSC) and absence (sEPSC) of TTX at 4 months of age. Bar graphs represent data *per animal*, with statistical analysis run on these data. Error bars indicate SEM. Scatter plots represent results *from individual cells* from WT, $_{LOW}$TAU and $_{HIGH}$TAU animals. Sample numbers are given per cell, with sample numbers per animal given in parentheses.

Basal synaptic transmission within the CA1 region: No difference between genotypes for either spontaneous or miniature EPSCs

The frequency of sEPSCs and mEPSCs within the CA1 region of the hippocampus were not found to differ significantly between genotypes, indicating that the number of release sites (n), release probability (Pr) and AP generation are not affected by the presence of the transgene at this young age (Figure 6.3.A)). A significant main effect of TTX was detected (TTX: $F_{(1, 39)} = 4.393$, $p<0.05$), signifying the contribution of spontaneous AP-driven release in the absence of TTX.

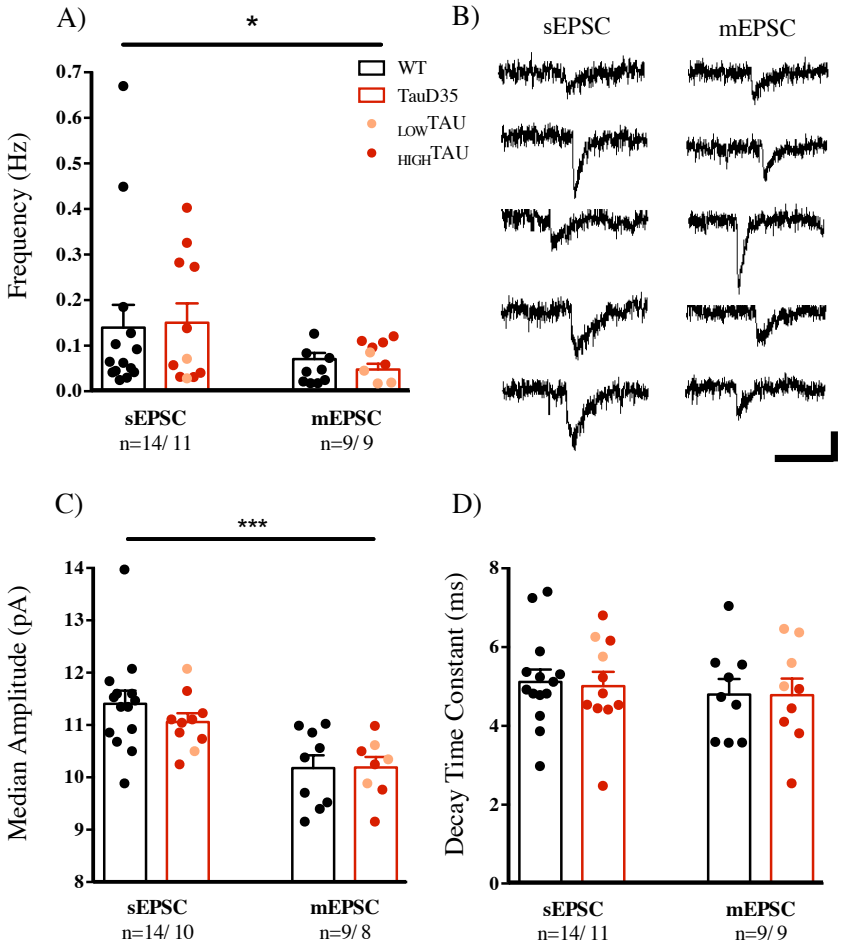

Figure 6.3. No difference between genotypes in spontaneous excitatory currents recorded in the presence (mEPSC) and absence (sEPSC) of TTX from CA1 pyramidal neurones at 4 months of age. A) Frequency of excitatory currents. A significant effect of TTX was detected using a two-way ANOVA, significance indicated by $p<0.05$*. B) Representative current traces recorded in the presence and absence of TTX. C) Mean of the median amplitude. A significant effect of TTX was detected using a two-way ANOVA, significance indicated by $p<0.001$***. D) No difference detected in the decay time of excitatory currents. Scale: 10pA, 50ms. Error bars indicate SEM. Scatter plots indicate $_{LOW}$TAU and $_{HIGH}$TAU data.

TTX treatment was seen to result in a significant reduction in the median amplitude of EPSCs recorded from both WT and TauD35 mice (TTX: $F_{(1, 37)} = 19.25$, $p<0.0001$) (Figure 6.3.C)). As sEPSCs are the result of spontaneous APs within the presynaptic neurone, it is likely this result reflects the AP-driven simultaneous release of neurotransmitter from multiple axonal boutons in the absence of TTX. The decay time of EPSCs was not seen to differ between genotypes or with TTX treatment (Figure 6.3.D)), indicating that neither the presence of the transgene nor TTX affects AMPA-R kinetics.

Dentate Gyrus at 4 months of age

No differences in the membrane resistance of DG granule cells at 4 months of age

The membrane resistance of individual DG granule cells was obtained from examination of a test-pulse (+5mV, 40ms), applied immediately after achieving whole-cell configuration and stabilization of the recording. As was observed previously in data from CA1 pyramidal neurones, at this age, no differences were observed in granule cell membrane resistance between WT and TauD35 mice (Figure 6.4.).

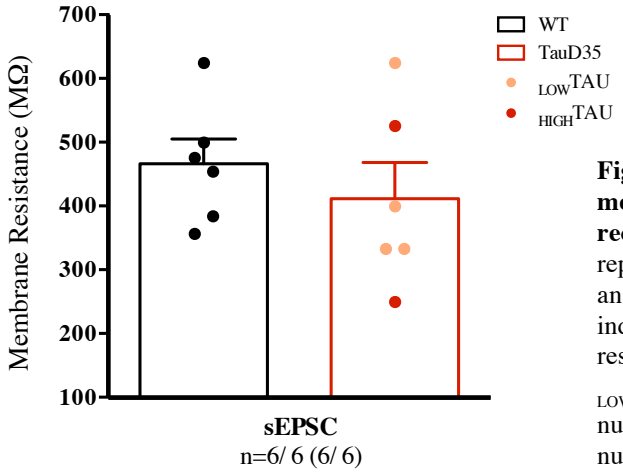

Figure 6.4. No difference in the membrane resistance of DG granule cells recorded at 4 months of age. Bar graphs represent data *per animal*, with statistical analysis run on these data. Error bars indicate SEM. Scatter plots represent results *from individual cells* from WT, $_{LOW}$TAU and $_{HIGH}$TAU animals. Sample numbers are given per cell, with sample numbers per animal given in parentheses.

No differences in basal synaptic transmission within the DG

Only sEPSCs were recorded from DG granule cells at 4-months. At this age, no differences were observed in the frequency, median amplitude or decay time constant of sEPSCs between WT and transgenic animals (Figure 6.5.).

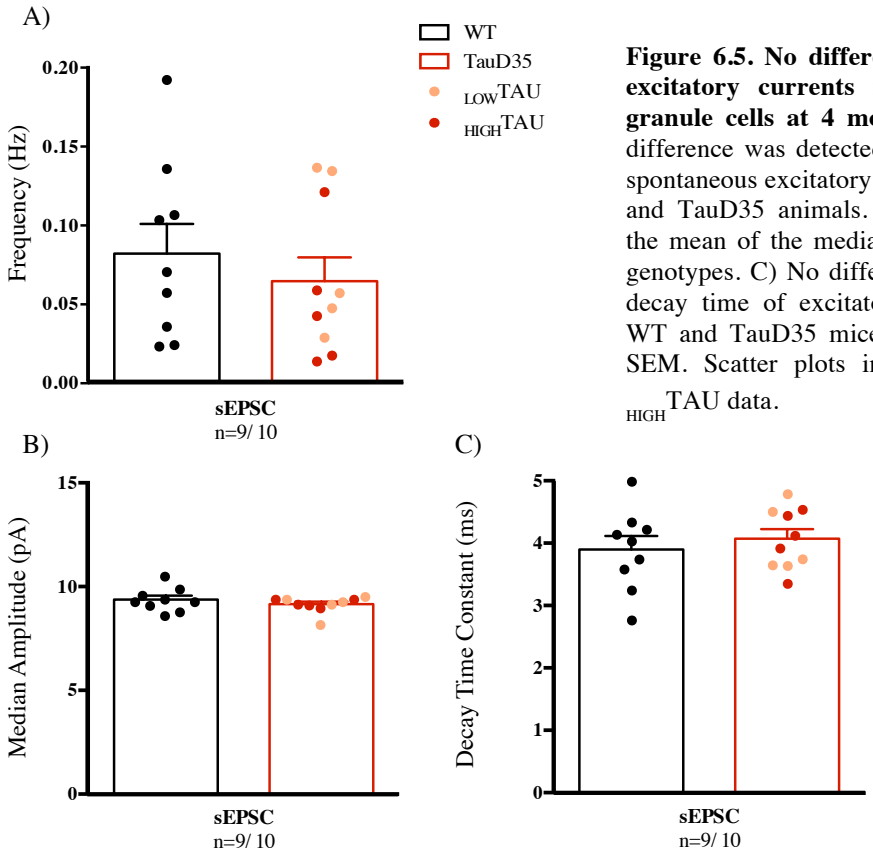

Figure 6.5. No difference in spontaneous excitatory currents recorded from DG granule cells at 4 months of age. A) No difference was detected in the frequency of spontaneous excitatory currents between WT and TauD35 animals. B) No difference in the mean of the median amplitude between genotypes. C) No difference detected in the decay time of excitatory currents between WT and TauD35 mice. Error bars indicate SEM. Scatter plots indicate $_{LOW}$TAU and $_{HIGH}$TAU data.

CA1 at 13 months of age

In order to investigate changes in spontaneous activity with increasing age and development of NFTs, sEPSCs were recorded within the CA1 region at 13 months of age. As was discovered later, this age corresponds to a time of large disparity in tau pathology between $_{LOW}$TAU and $_{HIGH}$TAU mice. Scatter plots presented throughout allow insight into potential differences in the electrophysiological properties between the two lines, with the transgenic lines discussed separately at points of interest.

A significant difference in the membrane resistance of CA1 pyramidal cells at 13 months of age

The membrane resistance of CA1 pyramidal cells were obtained as described previously, from examination of a test-pulse (+5mV, 40ms), applied immediately after achieving whole-cell configuration and stabilization of the patch. In contrast to results observed at 4-months, a significant difference (p=0.03) in the membrane resistance of these neurons was observed between WT and TauD35 mice at this older age (Figure 6.6.). An increase in the membrane resistance of layer III cortical pyramidal neurons has been noted previously in the rTg4510 mouse model at both early and advanced stages of pathology development (Crimins et al., 2012).

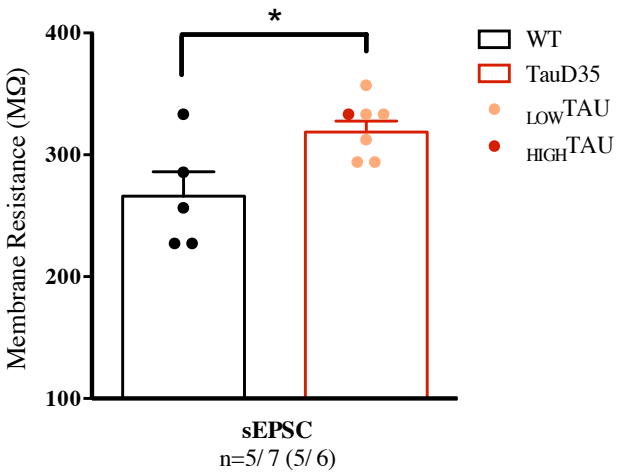

Figure 6.6. Increased membrane resistance of TauD35 CA1 pyramidal neurones recorded at 13 months of age. Bar graphs represent data *per animal*, with an unpaired Student's *t-test* analysis run on these data (p=0.03). Error bars indicate SEM. Scatter plots represent results *from individual cells* from WT, $_{LOW}$TAU and $_{HIGH}$TAU animals. Sample numbers are given per cell, with sample numbers per animal given in parentheses.

Basal synaptic transmission within the CA1 region: A trend toward an increase in median EPSC amplitude in TauD35 mice

The frequencies of sEPSCs recorded from the CA1 region of the hippocampus were not found to differ significantly between genotypes ($F_{(2, 17)} = 0.6978$, p=0.5) (Figure 6.7.A)).

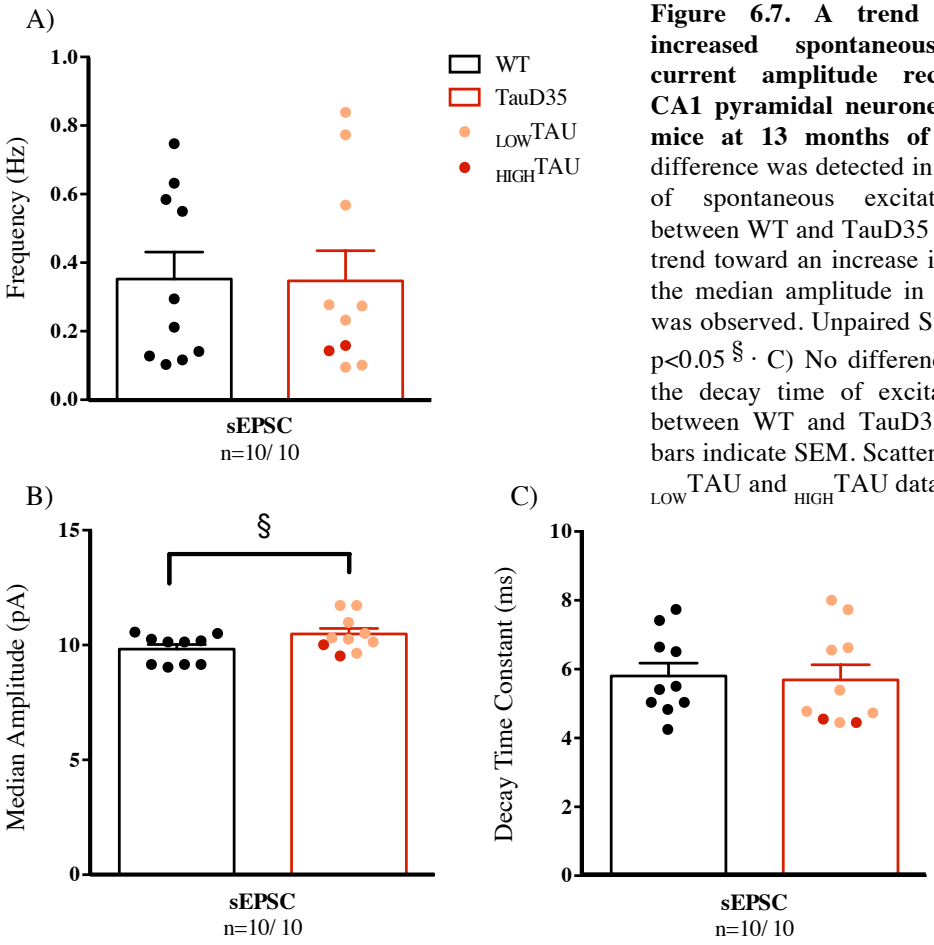

Figure 6.7. A trend towards an increased spontaneous excitatory current amplitude recorded from CA1 pyramidal neurones of TauD35 mice at 13 months of age. A) No difference was detected in the frequency of spontaneous excitatory currents between WT and TauD35 animals. B) A trend toward an increase in the mean of the median amplitude in TauD35 mice was observed. Unpaired Student's t-test, p<0.05 § · C) No difference detected in the decay time of excitatory currents between WT and TauD35 mice. Error bars indicate SEM. Scatter plots indicate $_{LOW}$TAU and $_{HIGH}$TAU data.

Comparison of the median amplitude of sEPSCs recorded at this age revealed a trend toward a significant increase in sEPSC amplitude in TauD35 animals compared to WT ($p=0.051$) (Figure 6.7.B)). No difference in the decay time of sEPSCs was detected between genotypes, indicating no change in AMPA-R receptor kinetics (Figure 6.7.C)).

It is noted, however, that the frequency, amplitude and decay time constant of sEPSCs recorded from the 2 $_{HIGH}$TAU mice included in this data set were low in comparison to data obtained from $_{LOW}$TAU animals. This suggests that excitatory synaptic transmission at the SC-CA1 synapse is altered by the development of mature tau pathology in these mice; however, due to the age of the animals, unfortunately sample numbers could not be increased for $_{HIGH}$TAU mice prior to the completion of this thesis.

Evoked excitatory activity

In addition to assessing basal excitatory synaptic transmission, more specific synaptic properties can be evaluated through evoking activity within particular axonal pathways and recording the responses of recipient neurones. Using whole-cell patch clamp techniques to record the responses of CA1 pyramidal and DG granule cells, activity was evoked within the SC and mPP pathways, respectively, using 2 closely time stimuli. The interval between the 2 stimuli can been varied, and the PPR calculated. As is discussed in Appendix 1, this allows one to infer certain information about the Pr of the synapses under study. As before, excitatory transmission has been isolated through use of the $GABA_A$ receptor antagonist, SR95531 (gabazine).

CA1 at 4 months of age

No difference in PPR at SC-CA1 synapses at 4 months of age

The responses of CA1 pyramidal neurones to stimulation of the SC pathway were recorded, and the PPR calculated with varying inter-pulse interval. Both WT and TauD35 mice were found to display characteristic facilitation of the second response (Wu and Saggau, 1994) with a loss of stimulus interaction occurring with an inter-pulse interval of ≥400ms. Analysis of variance confirmed a main effect of inter-pulse interval (interval: $F_{(6, 96)} = 17.87$, $p<0.0001$), with no differences detected between genotypes (Figure 6.8.).

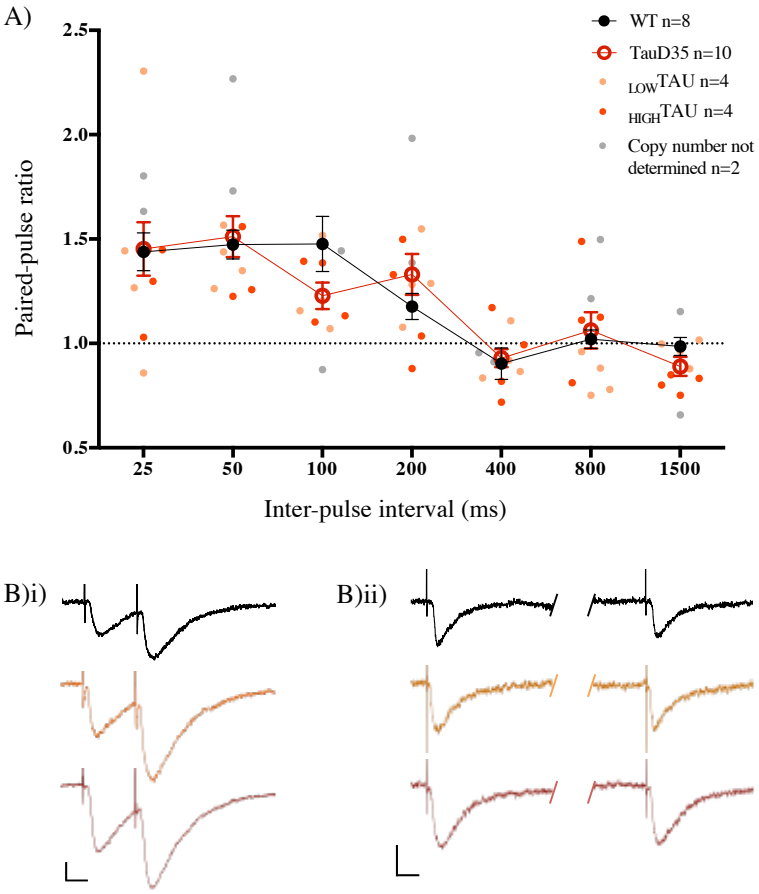

Figure 6.8. No difference in the paired-pulse ratio recorded at the SC-CA1 synapse at 4 months of age. A) PPRs obtained from CA1 pyramidal cells in response to stimulation of the Schaffer collateral pathway. No difference was detected between genotypes at inter-pulse intervals of 25-1500ms. Error bars indicate SEM. Scatter plots indicate $_{LOW}$TAU and $_{HIGH}$TAU data. B)i) Representative traces of CA1 responses to paired stimulation at an inter-pulse interval of 25ms. Scale: 10pA, 10ms B)ii) Representative traces of CA1 responses to paired stimulation at an inter-pulse interval of 400ms. Scale: 10pA, 20ms. WT (*black*), $_{LOW}$TAU (*orange*), $_{HIGH}$TAU (*red*).

Dentate Gyrus at 4 months of age

Decrease in Pr of mPP-DG synapses in TauD35 mice at 4 months of age

In order to investigate the possibility of tau dysfunction within ECII affecting the Pr of mPP synapses, we recorded responses from granule cells in response to paired-pulse stimulation of the mPP.

The mPP synapses respond to paired stimuli by displaying characteristic depression, commonly thought to be due to an inherently high Pr, as reducing external Ca^{2+} eliminates this depression (McNaughton, 1980). WT mice in the present study were observed to display this typical feature, showing paired-pulse depression (PPD) in response to paired stimuli with intervals up to 800ms (Figure 6.9.A)). Interestingly, TauD35 mice exhibited a different pattern of behaviour, with a two-way ANOVA revealing a significant interaction of genotype with increasing inter-pulse interval (interval x genotype: $F_{(6, 180)} = 2.600$, p=0.02). Sidak's *post hoc* analysis exposed a significant increase in the PPR of TauD35 mice only at an interval of 100ms (p=0.04), despite paired-pulse facilitation (PPF) occurring at intervals of 50, 100 and 200ms in this line (Figure 6.9.A)). An increase in PPR here likely represents a decrease in the Pr of these synapses in TauD35 mice of 4 months of age.

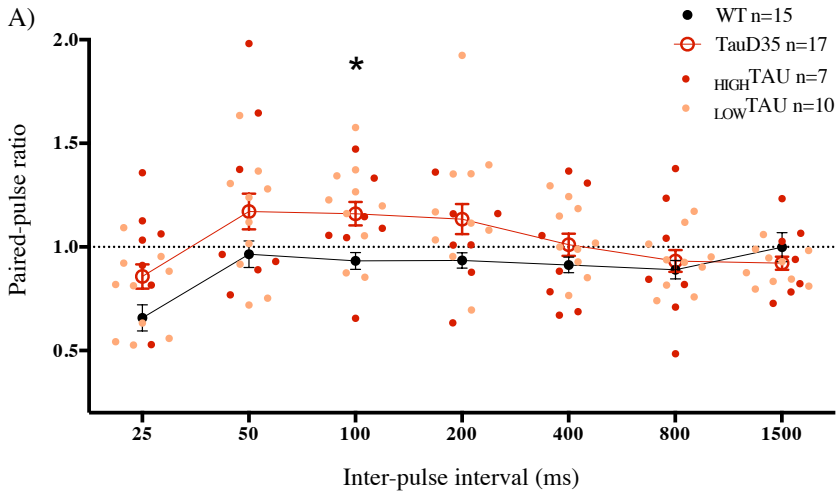

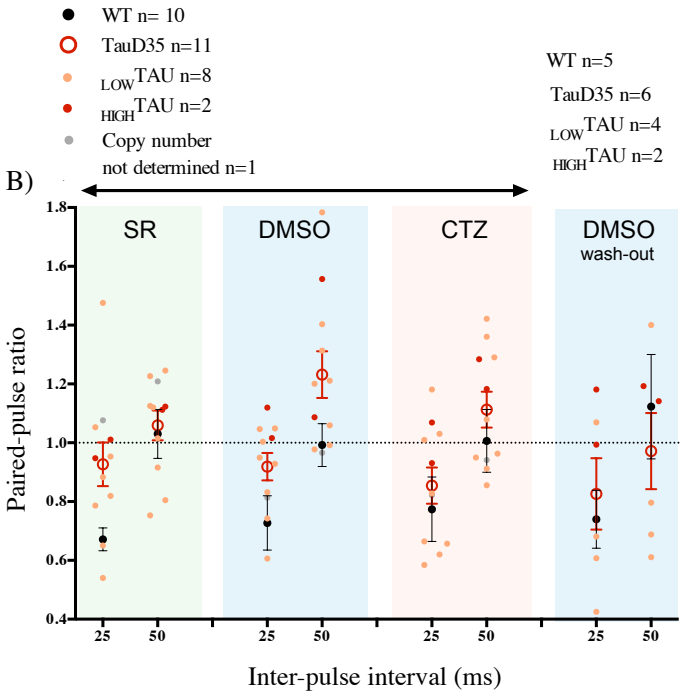

Figure 6.9. An increase in the paired-pulse ratio recorded from TauD35 DG granule cells in response to stimulation of the medial perforant pathway at 4 months of age. A) A significant increase in PPR was recorded at an inter-pulse interval of 100ms in TauD35 mice compared to WT animals. Two-way ANOVA, with Sidak's *post hoc* comparison, significance indicated by $p<0.05$* B) The shortest inter-pulse intervals of 25 and 50ms recorded in the presence of AMPA-R desensitisation inhibitor, CTZ, revealed no contribution of AMPA-R desensitisation in causing PPD at these short intervals. Error bars indicate SEM. Scatter plots indicate $_{LOW}$TAU and $_{HIGH}$TAU data.

AMPA-R desensitisation does not contribute to PPD

While the PPD of mPP synapses is generally thought to be the result of an inherently high Pr (McNaughton, 1980), desensitisation of AMPA-Rs may play a role. AMPA-Rs mediate fast excitatory synaptic transmission within the central nervous system, opening and desensitising within a few milliseconds. The role of desensitisation is essential to ensure a brief postsynaptic current even if the time course of glutamate clearance from the synapse is not optimal. Colquhoun et al., (1992) showed that paired fast application (1ms) of glutamate to outside-out patches of DG granule cells resulted in depression of the second response. The removal of the presynaptic element in these experiments demonstrates an inherent property of granule cells (as well as pyramidal cells to a

slightly lesser extent) to show depression of the second of two responses, a property likely caused by the desensitisation of AMPA-Rs. It is possible that the pre- and postsynaptic elements combine in producing the characteristic PPD of mPP synapses.

In order to examine whether AMPA-R desensitisation contributed to the PPD recorded at the shortest inter-pulse intervals tested, as well as examine any possible differences in desensitisation between genotypes, PPRs were obtained using 25 and 50ms inter-pulse intervals, in the presence of the AMPA-R desensitization inhibitor, cyclothiazide (CTZ, 100μM). Control experiments were performed using the vehicle, dimethyl sulfoxide (DMSO, 0.025%) on each slice prior to the application of CTZ. This allowed for the exclusion of possible side effects on synaptic transmission caused by presence of the solvent, as has been reported previously (McLarnon et al., 1986).

AMPA-R desensitisation was not found to contribute to the PPD depression observed in WT mice at the shortest inter-pulse intervals of 25 and 50ms. In addition, the PPRs calculated for transgenic mice at these shortest inter-pulse intervals were not affected by the inhibition of AMPA-R desensitisation (Figure 6.9.B)).

CA1 at 13 months of age

No difference in PPR at SC-CA1 synapses at 13-months

Both WT and TauD35 mice were found to display the PPF characteristic of this synapse (Wu and Saggau, 1994) at inter-pulse intervals below 400ms. A main effect of interval was detected assessed using a two-way ANOVA (interval: $F_{(6, 66)} = 46.06$, $p<0.0001$) (Figure 6.10.). *Unfortunately, it was later discovered that no $_{HIGH}$TAU mice had been included within this data set, and thus scatter plots of transgenic data are not included.*

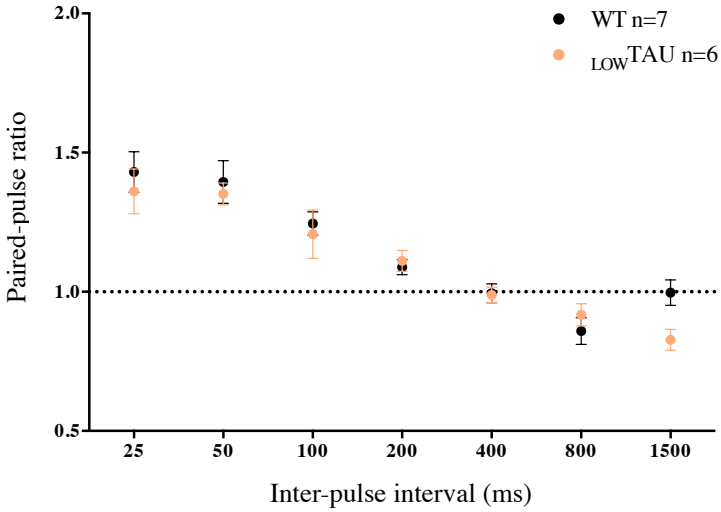

Figure 6.10. No difference in the paired-pulse ratio recorded from CA1 pyramidal cells in response to stimulation of the Schaffer collateral pathway at 13 months of age. No difference was detected between WT and $_{LOW}$TAU mice at inter-pulse intervals of 25-1500ms. Error bars indicate SEM.

Extracellular field recordings

In order to assess various properties of synaptic transmission from a population of SC-CA1 synapses, extracellular recording techniques were employed. Stimulation of CA3 axons was used to evoke dendritic responses from a population of CA1 pyramidal neurone apical dendrites, recorded using an electrode placed within the stratum radiatum of CA1. Further details of the theory and analysis of extracellular field recordings can be found in Appendix 1.

This recording technique was used to assess: 1) overall synaptic efficiency (input-output relationship), 2) release probability (PPR recordings) and 3) synaptic plasticity (long-term potentiation (LTP) experiments) from a population of SC-CA1 synapses. As is described in Appendix 1, LTP experiments have been split temporally for analysis, into post-tetanic potentiation (PTP, 1st minute post-tetanus), short-term potentiation (STP, 8-12 minutes post-tetanus) and LTP (51-60 minutes post-tetanus).

4 months of age

No difference in basal synaptic transmission of SC-CA1 synapses

Extracellular field recordings from SC-CA1 synapses at 4 months of age were contributed to by undergraduate students, Kenrick Yap and Emma Spowart under my supervision.

The input-output relationship with increasing stimulus strength was used as a measure of overall synaptic efficacy, as well as providing a measure by which to determine the stimulus strength for subsequent recording. As one would expect, the fEPSP size (determined using initial fEPSP slope) was seen to increase with increasing stimulus strength for both genotypes, with a main effect of input voltage identified (voltage: $F_{(7, 280)} = 208.7$, $p<0.0001$) (Figure 6.11.A)). No difference in input-output relationship was detected between WT and TauD35 animals. *It was noted that the fEPSP response recorded from $_{LOW}$TAU mice appeared consistently smaller compared to WT and $_{HIGH}$TAU animals. Data were therefore separated for analysis using a two-way ANOVA with Tukey's post hoc test. A significant reduction in $_{LOW}$TAU fEPSP response was seen for input voltages exceeding 60V (60V: p=0.05; 70V: p=0.032; 80V: p=0.031). A reduction in input-output relationship has been observed previously in female rTg4510 mice, at an age prior to the development of detectable tau pathology (Dalby et al., 2014).*

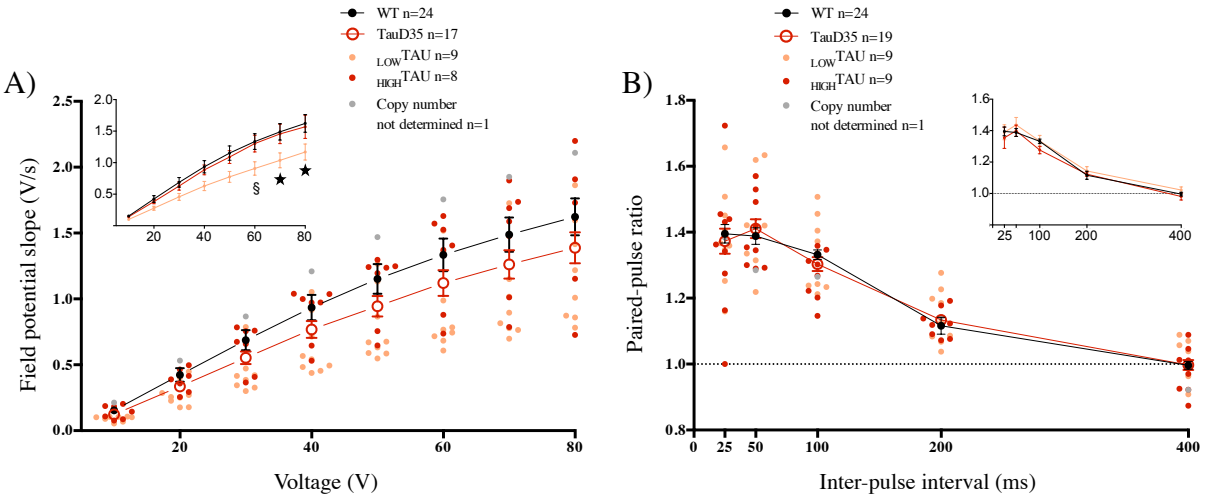

Figure 6.11. Basal synaptic transmission recorded at the SC-CA1 synapse at 4 months of age. A) Input-output relationship showed increased fEPSP amplitude in response to increasing stimulus intensity applied to SC axons for both WT and TauD35 mice. No difference was detected between genotypes. *(Insert) shows separated $_{LOW}$TAU and $_{HIGH}$TAU data (Two-way ANOVA, Tukey's post hoc comparison, p=0.05§, p<0.05 ★).* B) PPR obtained from a population of CA1 neurones in response to stimulation of SC axons. No difference was detected between genotypes at inter-pulse intervals of 25-400ms. *(Insert) shows separated $_{LOW}$TAU and $_{HIGH}$TAU data*. Error bars indicate SEM. Scatter plots indicate $_{LOW}$TAU and $_{HIGH}$TAU data.

As whole-cell patch clamp recordings of PPR at SC-CA1 synapses only examine synapses impinging on that one cell, PPR over increasing inter-pulse intervals was also examined using extracellular field recordings, allowing synapses onto numerous CA1 neurones to be investigated simultaneously. As observed using patch, the PPR calculated displayed facilitation for inter-pulse intervals <400ms (interval: $F_{(4,\ 164)} = 194.9$, $p<0.0001$), with no differences detected between WT and transgenic mice (Figure 6.11.B)).

No difference in long-term synaptic plasticity

In order to investigate long-term synaptic plasticity at SC-CA1 synapses in 4-month-old mice, an extracellular stimulating electrode was used to apply high-frequency tetanic stimulation to the SC axons. Two protocols were employed; one, referred to as 'weak' stimulation consisted of 3 trains of 20 pulses at 100Hz, repeated three times with an interval of 1.5 seconds. The other, referred to as 'strong' stimulation consisted of 5 trains of 100 pulses at 100Hz, repeated 5 times with an interval of 1.5 seconds. These two protocols aimed at overcoming any differences that may lie in the ability to induce LTP, such as changes in induction threshold (Schneider et al., 2001). fEPSP responses were monitored for 60 minutes post-tetanus.

The responses to both weak (Figure 6.13.A)i)) and strong (Figure 6.12.A)) tetanic stimulation were compared between WT and TauD35 mice. No differences were detected in PTP, STP or LTP between genotypes, using either stimulation. As one may expect, LTP induction using the strong high frequency tetanus resulted in a larger magnitude LTP (WT: 167.2 ± 12.3%) than was produced following weaker stimulation (WT: 139.5 ± 5.8%). The absence of a difference between genotypes implies that TauD35 mice at 4 months of age are capable of sustaining extremely strong tetanic stimulation at the SC-CA1 synapse and that mechanisms of LTP induction are in place.

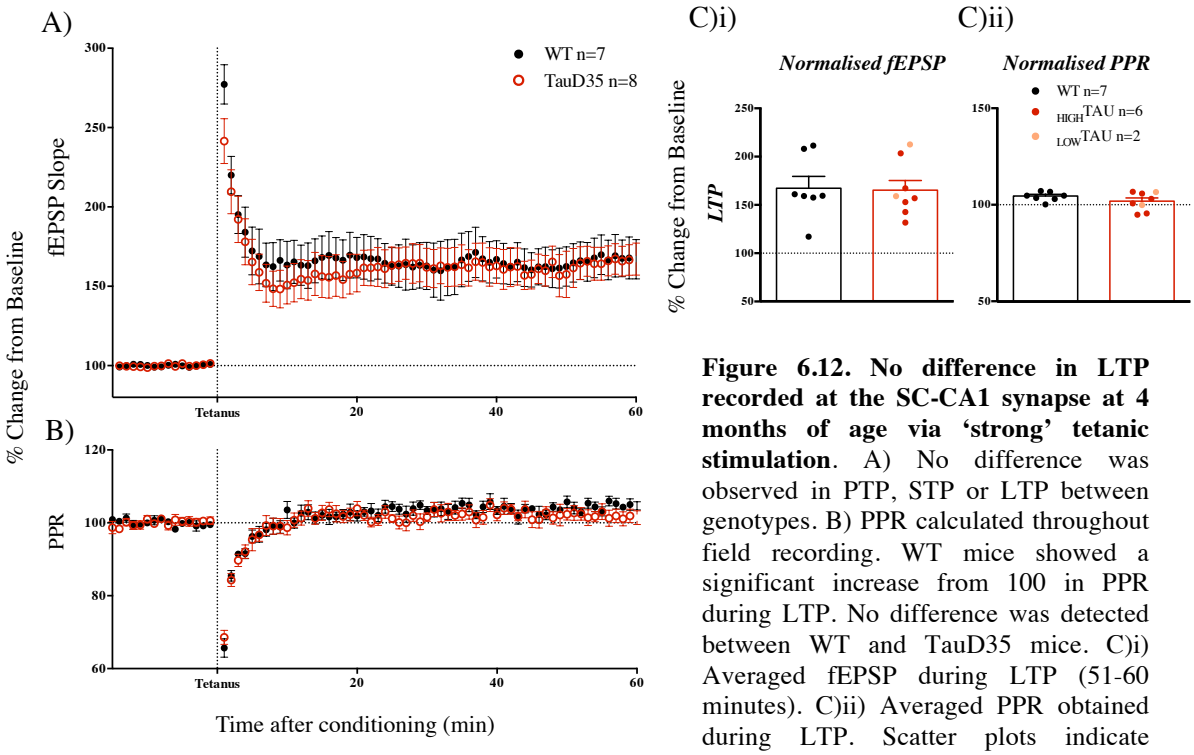

Figure 6.12. No difference in LTP recorded at the SC-CA1 synapse at 4 months of age via 'strong' tetanic stimulation. A) No difference was observed in PTP, STP or LTP between genotypes. B) PPR calculated throughout field recording. WT mice showed a significant increase from 100 in PPR during LTP. No difference was detected between WT and TauD35 mice. C)i) Averaged fEPSP during LTP (51-60 minutes). C)ii) Averaged PPR obtained during LTP. Scatter plots indicate $_{LOW}$TAU and $_{HIGH}$TAU data. Error bars indicate SEM.

All LTP experiments were monitored using paired stimuli, applied with a constant inter-pulse interval of 50ms. This allowed for PPR calculation and thus an indication of the site of LTP expression, be it pre- or postsynaptic (McNaughton, 1982). The PPR recorded from WT mice during LTP was compared to 100% using a one-sample t-test. Transgenic data was then compared to WT by was of an unpaired Student's t-test. This method of analysis provided an indication of what is typical for a WT C57Bl/6J mouse, while subsequently determining whether the presence of the transgene in TauD35 mice altered this. The PPR recorded during LTP in WT mice was not found to differ significantly from 100% following weak stimulation, with no differences detected between genotypes (Figure 6.13.A)ii). These data indicate the source of the LTP

recorded to be postsynaptic. Interestingly, strong stimulation was seen to produce a significant increase in WT PPR recorded during 51-60 minutes (p=0.002), indicating a reduction in Pr, with no difference detected between WT and TauD35 mice (p=0.2) (Figure 6.12.B)). This reduction in Pr would work to oppose potentiation, possibly acting as a compensatory mechanism to the strong high frequency stimulation, indicating that the observed potentiation has a large postsynaptic component.

WT mice exhibit NMDA-R independent synaptic plasticity at 4-months

In using the NMDA-R antagonist, AP5, we aimed to investigate whether the P301L mutation harboured by the TauD35 model affects the NMDA-R-dependence of LTP at SC-CA1 synapses. As discussed in Appendix 1, while NMDA-R-dependent LTP is believed to provide the primary mechanism of potentiation at this synapse (Collingridge et al., 1983), other forms, namely voltage-gated Ca^{2+} channel (VGCC)-dependent LTP, have been also described here (Grover and Teyler, 1990).

The more active D- isomer of AP5 was bath applied at a concentration of 25μM for 15 minutes prior to the commencement of baseline recording to allow for equilibration. Following establishment of a stable baseline and application of the tetanus, AP5 was maintained within the bath for a further 15 minutes prior to washout. Theoretically, by blocking NMDA-Rs during the high frequency tetanus, the postsynaptic influx of Ca^{2+} required for the induction of LTP (Appendix 1) is prevented, thus inhibiting synaptic potentiation. Responses were recorded for a further 60 minutes without the presence of AP5 before the application of a second tetanus to ensure the slices were viable and potentiation could be established (Figure 6.13.A)i)).

Analysis of variance revealed that AP5 caused a significant reduction of both PTP (AP5: $F_{(1, 47)} = 79.30$, $p<0.0001$) and STP (AP5: $F_{(1, 47)} = 79.34$, $p<0.0001$) (Figure 6.13.B)i) and C)i), supporting original work using the NMDA-R antagonist (Collingridge et al., 1983). However, between 5 and 25 minutes post-tetanus, a potentiation of the fEPSP was seen to develop to some degree in both genotypes (Figure 6.13.A)i). Analysis revealed that in the presence of AP5, 4-month-old WT mice do not display a significant reduction of LTP. This result is in contrast to data collected from TauD35 mice, where AP5 was seen to significantly reduce the magnitude of LTP at this age (p=0.002) (Figure 6.13.D)i).

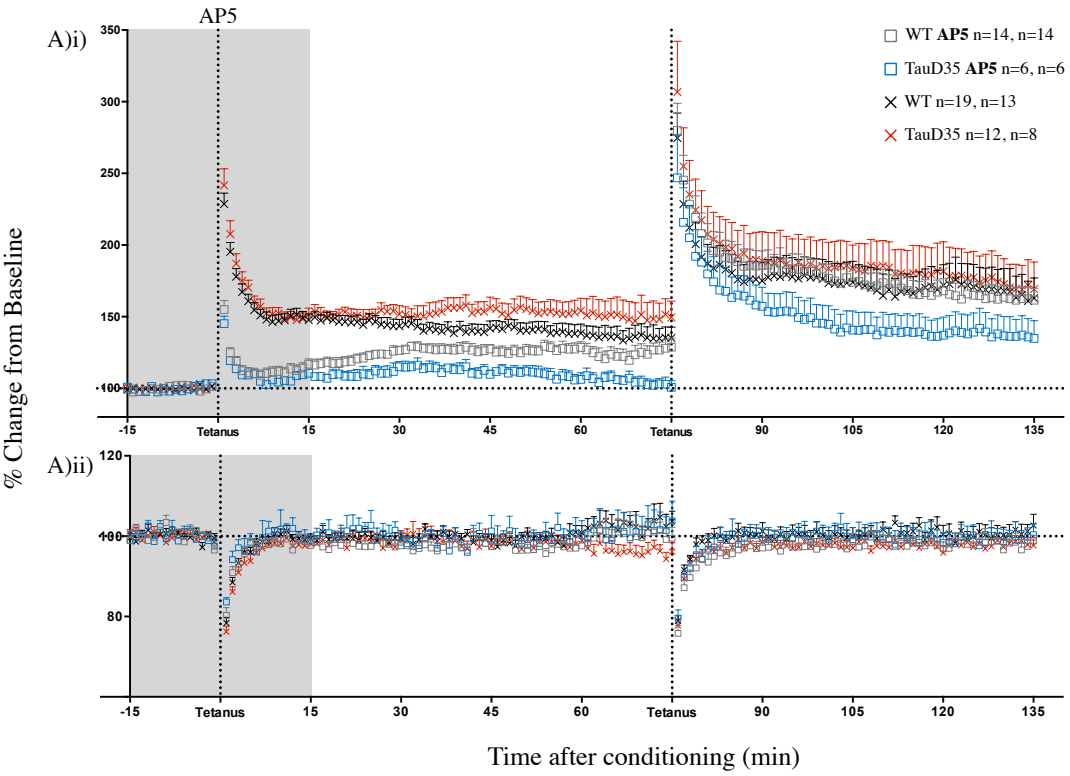

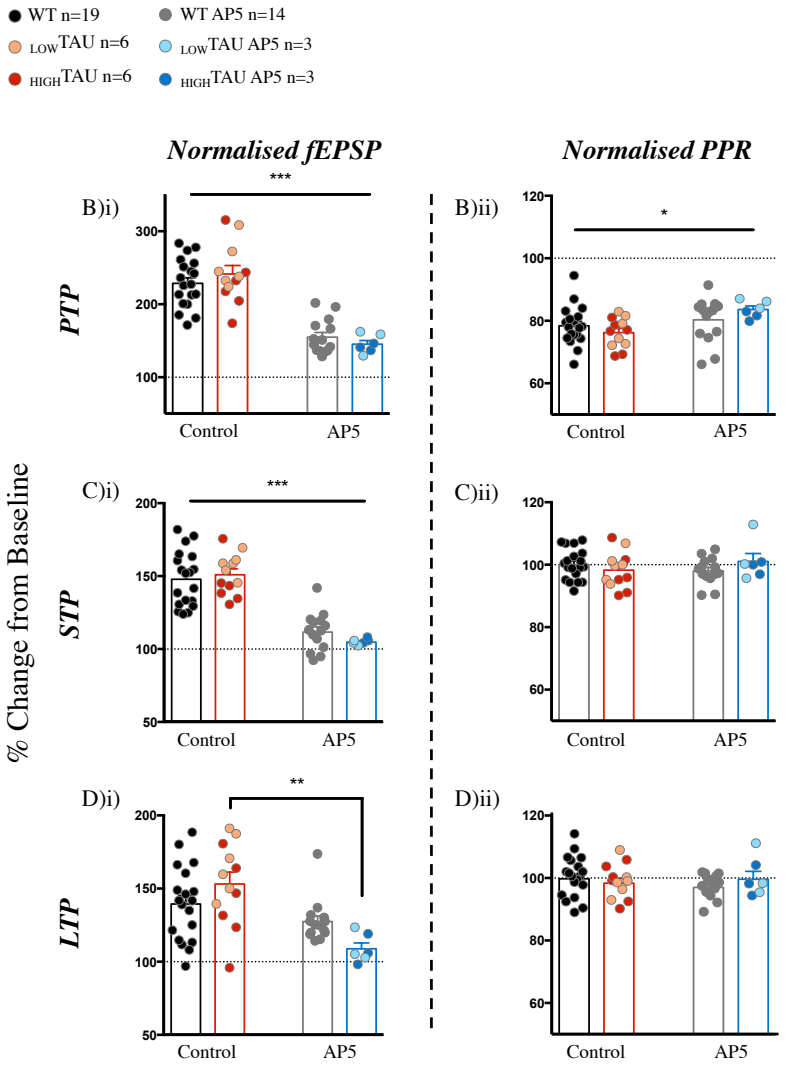

Figure 6.13. PTP, STP and LTP recorded at the SC-CA1 synapse in the absence and presence of NMDA-R antagonist, AP5 at 4 months of age via 'weak' tetanic stimulation. A)i) Field recordings form WT and TauD35 mice in the presence and absence of AP5. While not included in analysis, a second tetanus was performed to ensure viability of slices. A)ii) PPR obtained (50ms inter-pulse interval) in the presence and absence of AP5. B)i) PTP (1st minute) recorded in the presence and absence of AP5. B)ii) PPR obtained during PTP in the presence and absence of AP5. C)i) STP (8-12 minutes) recorded in the presence and absence of AP5. C)ii) PPR obtained during STP in the presence and absence of AP5. D)i) LTP (51-60 minutes) recorded in the presence and absence of AP5. D)ii) PPR obtained during LTP in the presence and absence of AP5. Two-way ANOVA with Sidak's *post hoc* comparison, significance indicated by p<0.05*, p<0.01**, p<0.001***. Error bars indicate SEM. Scatter plots indicate LOWTAU and HIGHTAU data.

The lack of NMDA-R-dependent LTP at this synapse in WT mice contradicts the previous long held opinion that the form of LTP expressed here is dependent upon the NMDA-R (Collingridge et al., 1983, Malenka, 1991). It is possible that this may represent species differences, as earlier work was completed using rats instead of mice. Present data indeed suggest, that under certain conditions, murine SC-CA1 synapses can potentiate without Ca^{2+} influx through postsynaptic NMDA-Rs at 4 months of age.

Analysis of the PPR calculated during PTP, revealed that the reduction in PTP observed in the presence of AP5, was likely due to a decrease in Pr during this first minute. Analysis of variance of PPR during this time exposed a main effect of AP5 (AP5: $F_{(1, 47)} = 6.625$, p=0.013) (Figure 6.13..B)ii). No change in PPR was detected during either STP or LTP (Figure 6.13.C)ii) and D)ii), implying that any effects of AP5 during these periods are not the result of presynaptic changes.

Due to the atypical timing of LTP onset (over 5-25 minutes post-tetanus) control experiments were performed in order to rule out any effects of AP5 washout (Figure 6.14.). During these experiments, AP5 was washed out of the bath solution immediately following tetanic stimulation. Data revealed a similar increasing synaptic potentiation over time, with a significant LTP developing by 51-60 minutes in WT slices (one-sample t-test, compared to 100%, p=0.021). This slowly developing LTP was also witnessed by Grover and Teyler (1990) following high frequency stimulation with AP5 present throughout the experiment, supporting the conclusion that the washout of AP5 does not contribute to the increasing potentiation seen in the present experiments.

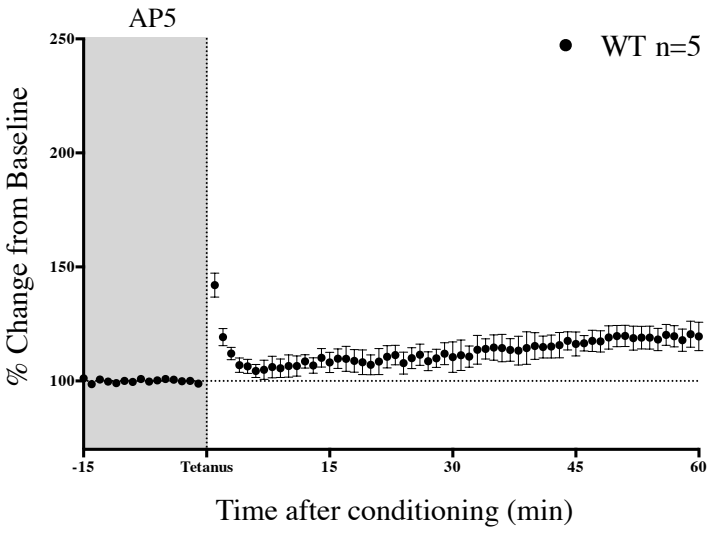

Figure 6.14. LTP recorded from the SC-CA1 synapse of WT mice at 4 months of age in the presence of AP5. AP5 was washed out immediately following tetanic stimulation in order to rule out any effect of AP5 washout in causing the slowly developing LTP witnessed in Figure 6.13.A)i)

13 months of age

Extracellular field recordings of SC-CA1 synapses at 13-months

No difference in basal synaptic transmission of SC-CA1 synapses

The input-output relationship between increasing stimulus strength and fEPSP amplitude was assessed at 13-months (Figure 6.15.A)). As expected, both genotypes displayed an increase in fEPSP size with increasing stimulus strength, with a main effect of voltage detected (voltage: $F_{(7, 112)} = 79.47$, $p<0.0001$). *In contrast to data collected at 4-months, no difference was observed in the input-output relationship between WT, $_{LOW}$TAU and $_{HIGH}$TAU animals. Only a single $_{HIGH}$TAU sample was included in this data set.*

PPR was assessed via field recordings in 13-month-old animals (Figure 6.15.B)). As we have observed previously at SC-CA1 synapses, the PPR decreased with increasing inter-pulse stimulus, with the two stimuli ceasing to interact by an inter-pulse interval of 400ms (interval: $F_{(4, 124)} = 97.44$, $p<0.0001$). No difference was observed between WT and TauD35 mice. *At the shortest interval of 25ms, it was noted that $_{HIGH}$TAU samples (n=4) appeared to display an increase in PPR, suggestive of a reduction in Pr. Upon data separation, Tukey's post hoc analysis revealed a significant difference between $_{LOW}$TAU and $_{HIGH}$TAU animals, at this 25ms interval (p=0.03).*

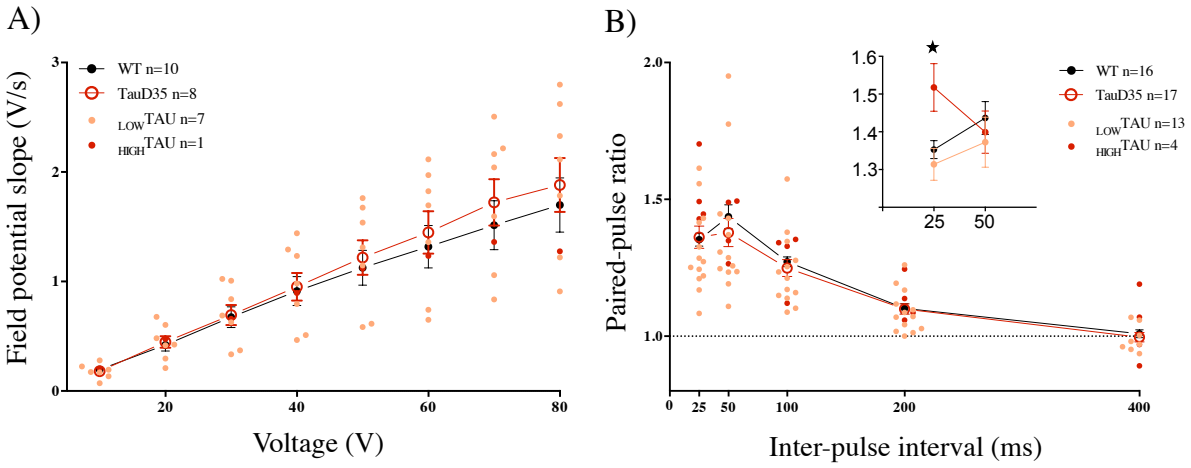

Figure 6.15. Basal synaptic transmission recorded at the SC-CA1 synapse at 13 months of age. A) Input-output relationship showed increased fEPSP amplitude in response to increasing stimulus intensity applied to SC axons for both WT and TauD35 mice. No difference was detected between genotypes. B) PPR obtained from a population of CA1 neurones in response to stimulation of SC axons. No difference was detected between genotypes at inter-pulse intervals of 25-400ms. *(Insert) shows separated $_{LOW}$TAU and $_{HIGH}$TAU data recorded using 25 and 50ms inter-pulse intervals (Two-way ANOVA, Tukey's post hoc comparison, p<0.05★).* Error bars indicate SEM. Scatter plots indicate $_{LOW}$TAU and $_{HIGH}$TAU data.

No difference in long-term synaptic plasticity

LTP was assessed at 13 months of age using the weak stimulation protocol. No difference was detected in PTP, STP or LTP between WT and TauD35 mice (Figure 6.16.A)i)). Analysis of the PPR calculated during LTP, exposed a significant decrease from 100% in WT mice (one-sample t-test, p=0.03), revealing a presynaptic contribution to LTP in the form of an increase in Pr. TauD35 data did not differ from WT, suggesting an increase in Pr during LTP in both genotypes (Figure 6.16.A)ii)).

Both WT and TauD35 mice exhibit a significant amount of NMDAR-dependent synaptic plasticity

Experiments using the NMDA-R antagonist, AP5, were conducted at 13-months to study possible changes in the NMDA-R-dependence of LTP with age, as has previously been suggested to occur at SC-CA1 synapses in rats (Shankar et al., 1998).

As was observed at 4 months of age, analysis of variance revealed a significant effect of AP5 in reducing the magnitude of PTP (AP5: $F_{(1, 55)} = 186.1$, $p<0.0001$) and STP (AP5: $F_{(1, 55)} = 122.5$, $p<0.0001$) (Figure 6.16.B)i) and C)i). However, in contrast to data collected at 4-months, at 13 months of age, AP5 was seen to cause a significant reduction of LTP in both WT and TauD35 animals (AP5: $F_{(1, 55)} = 27.01$, $p<0.0001$) (Figure 6.16.D)i)). This reduction in LTP in WT mice indicates that at this age, WT mice possess LTP induction mechanisms dependent on NMDA-Rs. It is however of note, that despite a significant overall effect of AP5, a proportion of potentiation does remain within these mice, implying induction through NMDA-R-independent processes occurs to some extent (Figure 6.16.A)i)).

Analysis of the PPR obtained during both PTP and STP revealed an effect of AP5 treatment on Pr compared to control (no AP5) (AP5: PTP: $F_{(1, 55)} = 11.82$, $p=0.001$; STP: $F_{(1, 55)} = 4.471$, $p=0.039$) (Figure 6.16.B)ii) and C)ii)). This AP5-dependent change in the PPR calculated during STP contrasts with 4-month data, where the reduction in fEPSP response size was found to be due to postsynaptic mechanisms. These data instead imply a presynaptic component, in that the decrease in STP magnitude may be in part due to a reduced Pr. The effect of AP5 on LTP, however, did not appear to be due to changes in Pr (Figure 6.16.D)ii)).

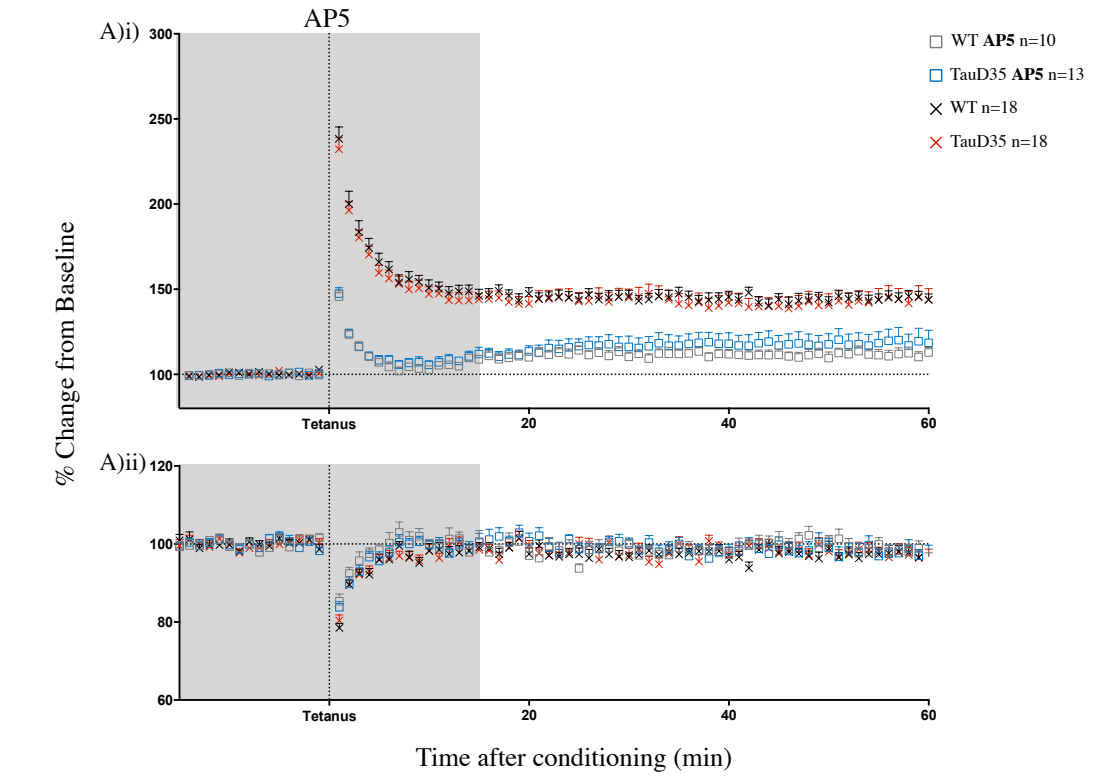

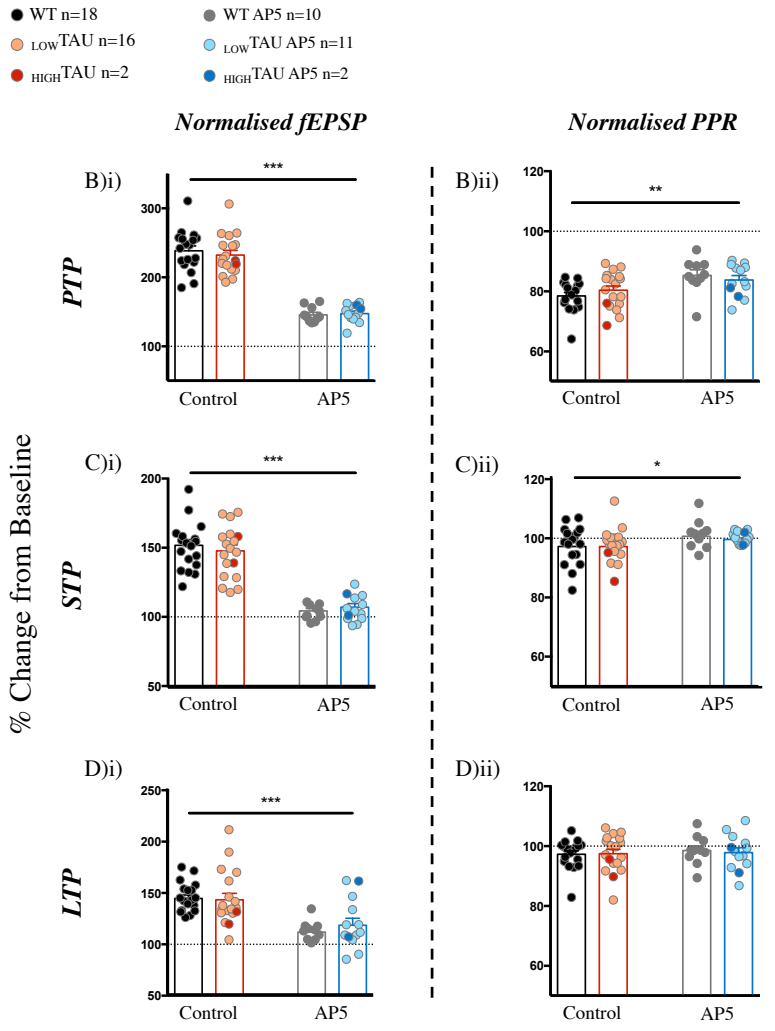

Figure 6.16. PTP, STP and LTP recorded at the SC-CA1 synapse in the absence and presence of NMDA-R antagonist, AP5 at 13 months of age via 'weak' tetanic stimulation. A)i) Field recordings form WT and TauD35 mice in the presence and absence of AP5. A)ii) PPR obtained (50ms inter-pulse interval) in the presence and absence of AP5. B)i) PTP (1st minute) recorded in the presence and absence of AP5. B)ii) PPR obtained during PTP in the presence and absence of AP5. C)i) STP (8-12 minutes) recorded in the presence and absence of AP5. C)ii) PPR obtained during STP in the presence and absence of AP5. D)i) LTP (51-60 minutes) recorded in the presence and absence of AP5. D)ii) PPR obtained during LTP in the presence and absence of AP5. Two-way ANOVA with Sidak's *post hoc* comparison, significance indicated by p<0.05*, p<0.01**, p<0.001***. Error bars indicate SEM. Scatter plots indicate LOWTAU and HIGHTAU data.

24 months of age

In addition to 4- and 13-month-old data, extracellular recordings were also completed at 24 months of age. While this old age presents some difficulty in obtaining patch clamp recordings, extracellular field recordings can be made with ease, allowing insight into the properties of synaptic transmission at this age. Unfortunately, due to the advanced age of the animals, sample numbers at 24-months were low for both WT and TauD35 groups. *Due to the development of a pathological phenotype between 17- and 20-months and consequent obligation to cull these animals, $_{HIGH}$TAU mice were not available for experimentation at 24 months of age.*

Extracellular field recordings at 24-months

No difference in basal synaptic transmission

An increase in the fEPSP amplitude with increasing stimulus intensity was observed in both WT and TauD35 mice at 24 months of age (voltage: $F_{(7, 98)} = 155.5$, $p<0.0001$). As was seen at 13-months, no differences were detected in the input-output relationship between WT and transgenic animals (Figure 6.17.A)).

Both WT and TauD35 mice displayed similar PPR across all inter-pulse intervals. As was observed at younger ages, a decline toward a ratio of 1 was seen with increasing inter-pulse interval (interval: $F_{(4, 56)} = 81.34$, $p<0.0001$) (Figure 6.17.B)).

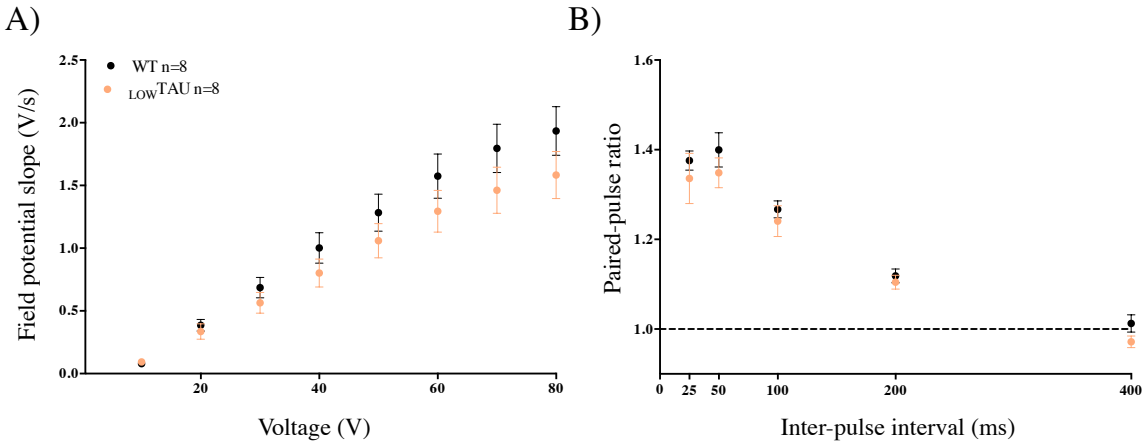

Figure 6.17. Basal synaptic transmission recorded at the SC-CA1 synapse at 24 months of age. A) Input-output relationship showed increased fEPSP amplitude in response to increasing stimulus intensity applied to SC axons for both WT and TauD35 mice. No difference was detected between genotypes. B) PPR obtained from a population of CA1 neurones in response to stimulation of SC axons. No difference was detected between genotypes at inter-pulse intervals of 25-400ms. Error bars indicate SEM.

No difference in long-term synaptic plasticity

The weak tetantic stimulation protocol produced consistent potentiation within both WT and TauD35 mice at 24 months of age. No differences were detected in the levels of PTP, STP or LTP between the genotypes (Figure 6.18.A)i)), with analysis of PPR during LTP revealing the postsynaptic locus of LTP expression (Figure 6.18.A)ii)).

Both WT and TauD35 mice display NMDAR-independent synaptic plasticity

The addition of AP5 at 24-months led to the now characteristic reduction of PTP and inhibition of STP, seen at previous ages, in both WT and TauD35 animals (AP5: PTP: $F_{(1, 20)} = 75.51$, $p<0.0001$; STP: $F_{(1, 20)} = 38.40$, $p<0.0001$) (Figure 6.18.B)i) and C)i)). No effect of AP5 was detected during LTP (Figure 6.18.D)i)), indicating the development of an NMDA-R-independent form of potentiation over the 60-minute recording time (Figure 6.18.A)i)).

As recognized previously, AP5 had a significant effect on the PPR calculated during PTP (AP5: $F_{(1, 20)} = 6.430$, $p=0.02$) (Figure 6.18.B)ii)), suggesting a reduced Pr compared to control (no AP5) as the cause of the reduction in fEPSP response size during the first minute post-tetanus in the presence of the antagonist. PPR during both STP and LTP did not display an effect of AP5 (Figure 6.18.C)ii) and D)ii)), suggesting postsynaptic mechanisms are responsible for the inhibition of STP and development of LTP.

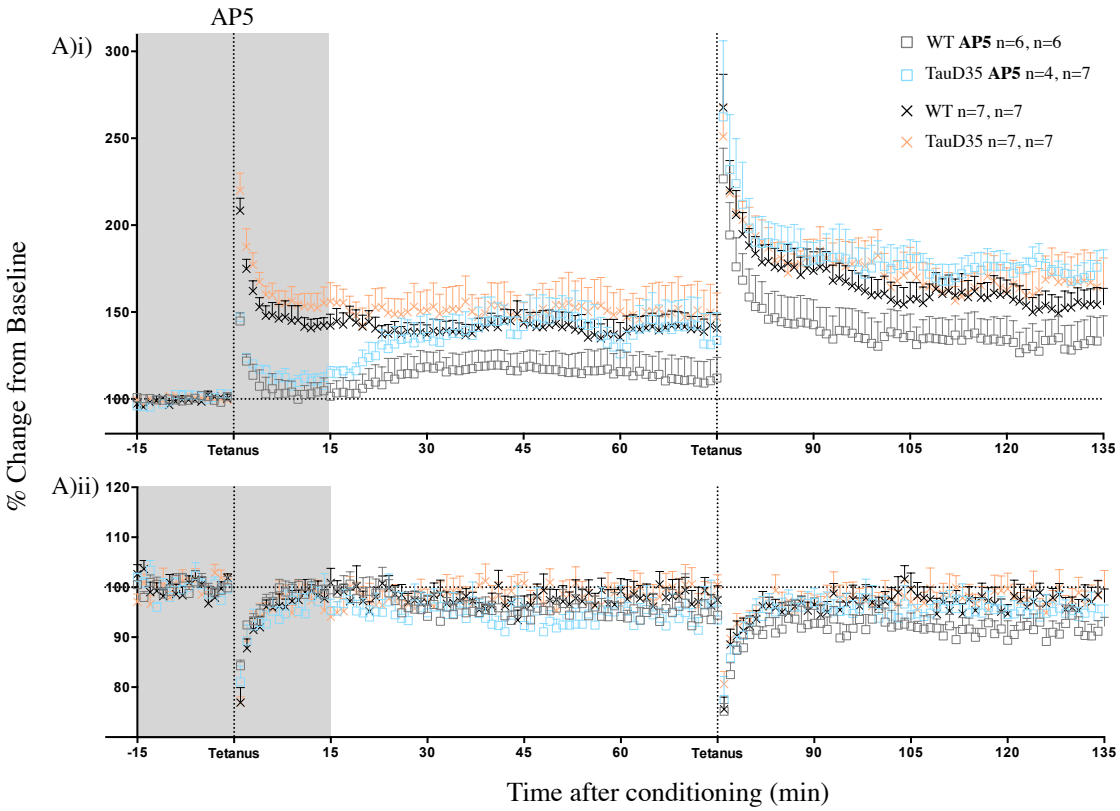

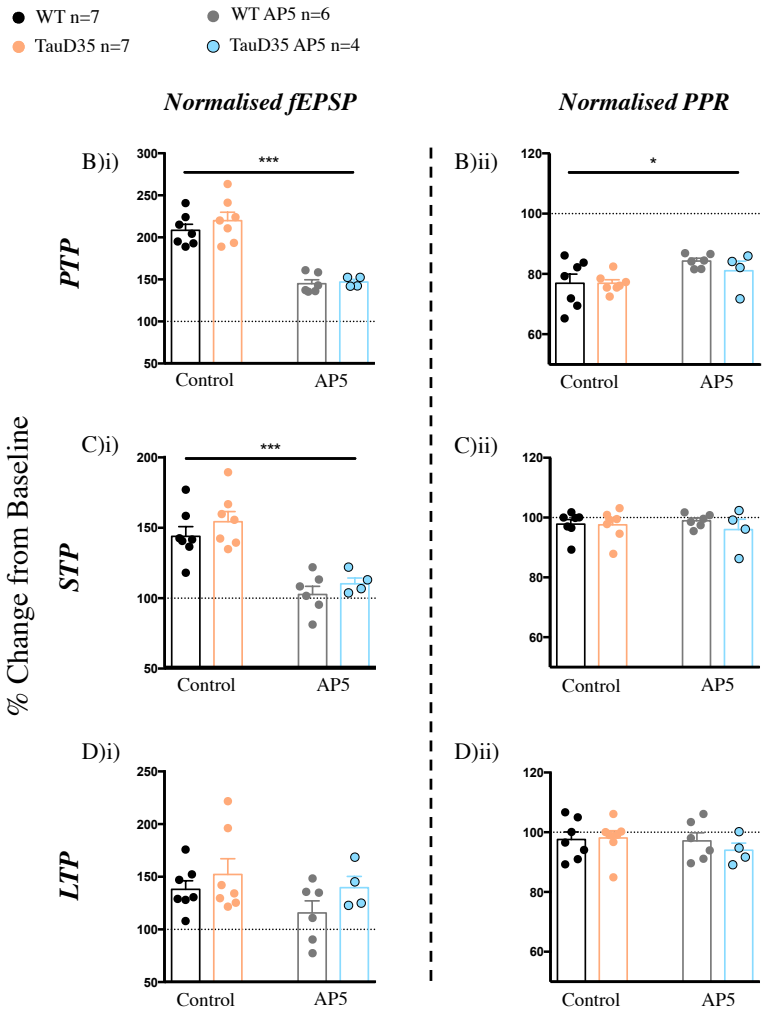

Figure 6.18. PTP, STP and LTP recorded at the SC-CA1 synapse in the absence and presence of NMDA-R antagonist, AP5 at 24 months of age via 'weak' tetanic stimulation. A)i) Field recordings form WT and TauD35 mice in the presence and absence of AP5. While not included in analysis, a second tetanus was performed to ensure viability of slices. A)ii) PPR obtained (50ms inter-pulse interval) in the presence and absence of AP5. B)i) PTP (1st minute) recorded in the presence and absence of AP5. B)ii) PPR obtained during PTP in the presence and absence of AP5. C)i) STP (8-12 minutes) recorded in the presence and absence of AP5. C)ii) PPR obtained during STP in the presence and absence of AP5. D)i) LTP (51-60 minutes) recorded in the presence and absence of AP5. D)ii) PPR obtained during LTP in the presence and absence of AP5. Two-way ANOVA with Sidak's *post hoc* comparison, significance indicated by p<0.05*, p<0.001***. Error bars indicate SEM. Scatter plots indicate $_{LOW}$TAU and $_{HIGH}$TAU data.

No change in WT SC-CA1 properties with ageing

Interestingly, extracellular field recordings revealed remarkable consistency at SC-CA1 synapses in WT mice with ageing. In comparing select elements such as half-maximal fEPSP response size (Figure 6.19.A), PPRs obtained using 25ms inter-pulse interval (Figure 6.19.B), LTP (Figure 6.19.C) and PPR calculated during LTP (Figure 6.19.D), we expose how CA3-CA1 connectivity, CA3 Pr, as well as the SC-CA1 long-term plasticity together with the postsynaptic locus of its expression, remain consistent (one-way ANOVA) in WT animals between 4 and 24 months of age.

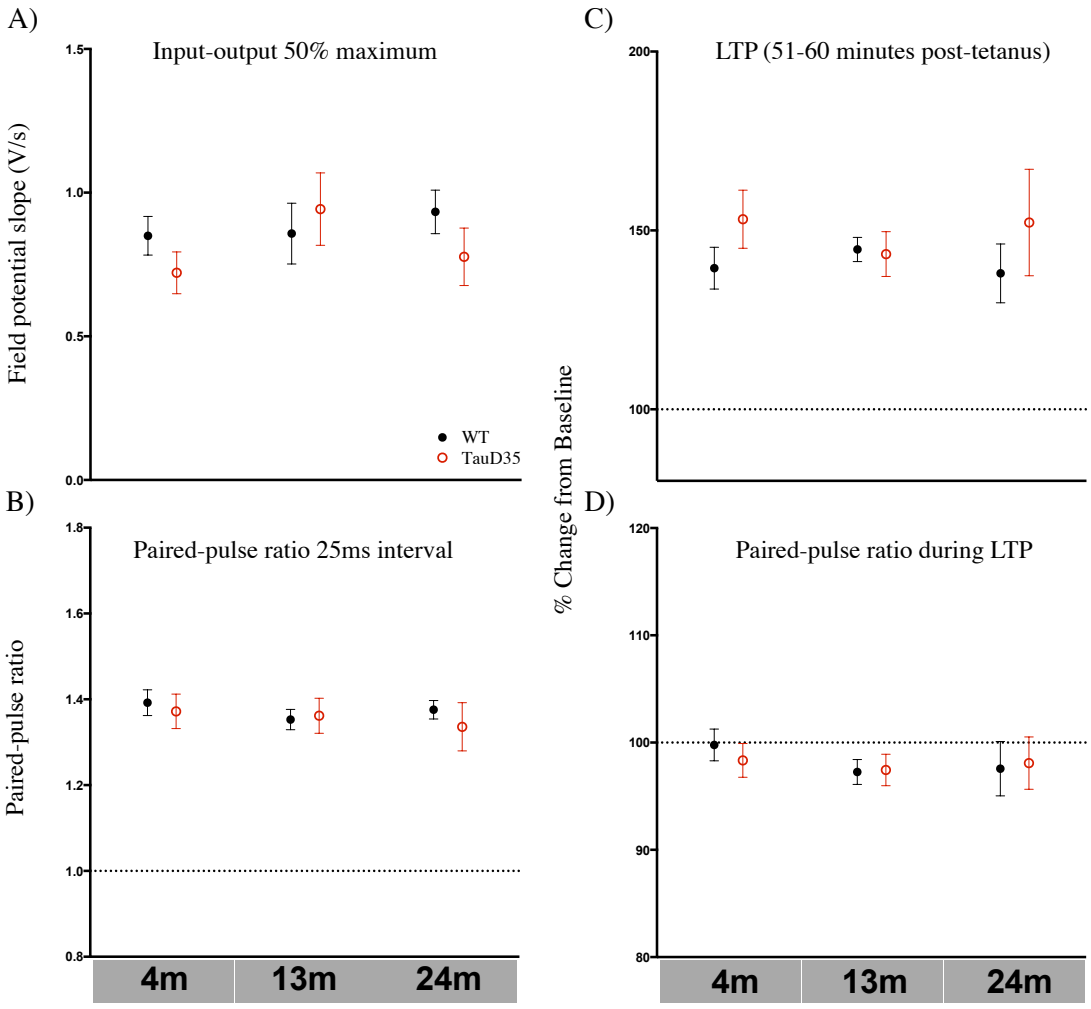

Figure 6.19. Extracellular field data collected from SC-CA1 synapses, compared across 4-, 13- and 24-months. A) Half maximal response to increasing stimulus voltage collected using an input-output protocol. B) 25ms inter-pulse interval data collected during PPR experiments. C) Average LTP (51-60 minutes post-tetanus). D) PPR obtained during LTP. Error bars indicate SEM.

Summary and Discussion: Electrophysiology

Unfortunately, at the time of electrophysiological testing it was not yet known that two transgenic groups existed within the TauD35 line. Thus, electrophysiological experiments were not designed to accommodate this fact, resulting in inconsistent sample sizes frequently too small for the analysis of $_{LOW}$TAU and $_{HIGH}$TAU data separately. Data from transgenic animals has therefore been grouped within this chapter. Following post-hoc copy number analysis of all mice, data from $_{LOW}$TAU and $_{HIGH}$TAU mice were separated and represented as scatter plots. For many experiments, electrophysiological data gathered from both transgenic lines were comparable. For those data where possible differences were observed, data were separated and all effort made to increase sample numbers for the individual transgenic lines. Where mice of the correct age/genotype were not available and thus sample numbers could not be increased, results are treated as pilot data for further experimentation, with caution exercised in the interpretation of such results.

A summary of the central data recorded has been tabulated within the following discussion according to the type of experiment. Data is then discussed only where significant differences are observed between WT and TauD35 animals.

Spontaneous Excitatory activity

Spontaneous Excitatory Activity											
		Membrane resistance		***Frequency***		***Amplitude***		***Decay***	
4m	CA1	mEPSC	sEPSC	mEPSC	sEPSC	mEPSC	sEPSC	mEPSC	sEPSC
		--	--	--	--	--	--	--	--
	DG	sEPSC		sEPSC		sEPSC		sEPSC	
		--		--		--		--	
13m	CA1	sEPSC		sEPSC		sEPSC		sEPSC	
		↑ TauD35*		--		↑ TauD35§		--	

Table 6.1. Summary table of spontaneous excitatory activity recorded from the CA1 and DG at 4- and 13 months of age. Differences indicated are between WT and TauD35 mice. (**--**) indicates no significant difference observed between genotypes. Arrows indicate direction of the change. Significance of difference given by *p<0.05, §p=0.051.

Embedded within the lipid bilayer are ion channels, which provide a route for ions to cross the membrane. The fewer ion channels that are open, the higher the membrane resistance. Membrane resistance is therefore a measure of membrane permeability, or how many ion channels are open; as well as being related to cell surface area, as (assuming constant channel density) smaller cells express fewer ion channels.

At 13 months of age, a significant increase in membrane resistance is observed in the CA1 pyramidal neurons of TauD35 mice. At this age, transgenic animals (*both $_{LOW}$TAU and $_{HIGH}$TAU*) exhibit NFT pathology. It is therefore hypothesised that intracellular tau mislocation/aggregation may affect ion channel trafficking at this age. It is also possible that the detachment of tau from MTs and relocation to the somatodendritic compartment within these neurons could possibly result in MT severing and disassembly (discussed in Jean and Baas, 2013), leading to a reduction in MT scaffold support of the neurone and thus axonal or dendritic retraction.

In addition to this increase in membrane resistance, 13-month-old TauD35 mice display a trend towards an increase in the amplitude of sEPSCs compared to WT. An increase in sEPSC amplitude may suggest the possibility of alterations to postsynaptic glutamate (AMPA-Rs) receptors in TauD35 animals, such as the insertion of new receptors or alterations in the conductance of existing receptors; however, the difference here is small, and may possibly be influenced by an increase in membrane resistance improving the clamp of the cell.

Inspection of the scatter of 13-month transgenic sEPSC data (Figure 6.7.A),B) and C)) revealed that despite very low sample numbers, currents recorded from $_{HIGH}$TAU mice consistently displayed a lower frequency and decay time compared to data collected from WT and $_{LOW}$TAU animals.

A reduction in sEPSC frequency suggests either a reduction in n, Pr or a decrease in AP-driven spontaneous release of glutamate from SC afferent terminals in $_{HIGH}$TAU animals at this age. The extracellular PPR recordings at 13-months did not reveal a significant interaction between genotypes; however, a reduction in Pr was seen at the shortest inter-pulse interval of 25ms (Figure 6.15.B)). This observation suggests a possible contribution of reduced Pr to the lower sEPSC frequencies recorded at this age in $_{HIGH}$TAU mice. The seemingly lower decay time constants of the $_{HIGH}$TAU sEPSC currents suggest possible changes in AMPA-R kinetics.

Paired-pulse ratio

Evoked Excitatory Activity		
		Paired-pulse ratio (PPR)
4m	CA1	**--**
	DG	⬆ TauD35* (100ms interval)
13m	CA1	**--** (*NOTE: No $_{HIGH}$TAU incl.*)

Table 6.2. Summary table of evoked excitatory activity recorded from the CA1 and DG at 4- and 13 months of age. Differences indicated are between WT and TauD35 mice. (**--**) indicates no significant difference observed between genotypes. Arrows indicate direction of the change. Significance of difference given by *p<0.05.

The responses of WT CA1 pyramidal cells to paired-pulse stimulation of the SC axons displayed characteristic facilitation of the second response at inter-pulse intervals <400ms. This characteristic PPF is explained through the residual Ca^{2+} hypothesis (discussed in Appendix 1), as has been demonstrated previously by the work of Wu and Saggau (1994). As one may expect, the PPRs obtained from a single CA1 neurone mirrored those from a population of CA1 cells, at both 4 and 13 months of age.

PPR data obtained though extracellular field recordings at 13 months of age, show a significant difference between $_{LOW}$TAU and $_{HIGH}$TAU animals at the shortest inter-pulse interval of 25ms. As we have seen, this age corresponds to a time of large disparity in the severity of tau pathology (Chapter 4). While sample numbers for $_{HIGH}$TAU mice are low in this case (n=4), compared to data from WT and $_{LOW}$TAU animals, this result implies a reduction in the Pr of glutamate from CA3 neurones at an age corresponding to high NFT load. This would be consistent with a hypothesis that the development of pathological tau, and its mislocation from the axon to somatodendritic compartment, results in the disruption of axonal transport of vital components necessary for neurotransmitter release. This may lead to a lower release probability in $_{HIGH}$TAU mice at the shortest interval of 25ms.

The PPR of the mPP-DG synapses was recorded only at 4 months of age using whole-cell patch clamp techniques. Unfortunately, older animals were not available to follow-up this line of experiments prior to completion of this thesis. Analysis revealed a

significant increase in the PPR of TauD35 animals compared to WTs at an inter-pulse interval of 100ms. At all other inter-pulse intervals <400ms, TauD35 animals displayed a higher PPR, seeing PPF at intervals between 50 and 200ms, compared to the PPD witnessed in WT mice. This finding indicates a decrease in the Pr of these mPP boutons even at this young age.

Despite the opinion that the characteristic mPP PPD is the result of an inherently high Pr (McNaughton, 1980), studies by von Engelhardt et al., (2010) suggest a possible role for postsynaptic AMPA-R function in creating this depression in response to paired stimuli. More specifically, they suggest that the strong interaction between synaptic AMPA-Rs and a novel auxiliary protein, CKAMP44, within granule cells of the DG increases the desensitisation of AMPA-Rs. CKAMP44 knock-out mice display a switch from PPD to PPF in the mPP compared to control animals, in a manner comparable to results gathered from PPR experiments from TauD35 mice. Due to the possibility that decreased AMPA-R desensitisation may contribute to the increase in PPR in transgenic animals, its occurrence was investigated in all genotypes. Studies concluded that AMPA-R desensitisation does not contribute to the PPD seen at mPP-DG synapses with the shortest inter-pulse intervals of 25 and 50ms, leading us to conclude that the characteristic mPP PPD is due to the high Pr of mPP synapses, and that transgenic mice display a reduction of this Pr at a relatively young age.

Extracellular Field recordings

Extracellular Field Recordings					
		Input-output	***PPR***	***LTP***	***LTP in presence of AP5 (NMDAR-LTP)*** 'Weak' TET
4m	SC-CA1	-- ($_{LOW}TAU$* ↓)	--	'Strong' TET -- / 'Weak' TET --	↓ TauD35**
13m	SC-CA1	--	-- ($_{HIGH}TAU$* ↑ 25ms interval)	'Weak' TET --	Main effect of AP5, ↓ WT + ↓ TauD35***
24m *(ONLY $_{LOW}$TAU TRANSGENICS)*	SC-CA1	--	--	'Weak' TET --	--

Table 6.3. Summary table of extracellular field recordings, obtained from the SC-CA1 synapse at 4-, 13- and 24 months of age. Differences indicated are between WT and TauD35 mice, with the exception of LTP recorded in the presence of AP5, in which data is compared to that obtained in the absence of the drug. (**--**) indicates no significant difference observed between genotypes. Arrows indicate direction of the change. Significance of difference given by *p<0.05, ***p<0.001. WT (*black arrow*), TauD35 grouped (*dark red arrow*), $_{LOW}$TAU (*orange arrow*), $_{HIGH}$TAU (*bright red arrow*).

Input-output relationship

At the youngest age of 4-months, $_{LOW}$TAU mice displayed a significantly reduced fEPSP slope at the highest stimulation intensities of 60-80V, compared to WT and $_{HIGH}$TAU animals. A similar result has been observed previously in female rTg4510 mice, at an age prior to detectable tau pathology (Dalby et al., 2014). Interestingly, this deficit was not observed in data collected from $_{HIGH}$TAU animals, and was no longer observed at the older ages of 13- and 24-months, suggesting this reduction in input-output to be an early occurrence in the progression of tauopathy that has already been compensated in $_{HIGH}$TAU mice at 4-months of age.

A reduced input-output relationship is indicative of reduced connectivity between CA3 and CA1 neurones. This may be caused by fewer SC axons/fewer synapses, a decrease in Pr, fewer postsynaptic receptors or a reduction in either afferent or postsynaptic excitability. By measuring slope of the EPSP response, however, we can disregard alterations in postsynaptic excitability. The PPR obtained at 4-months at the same synapse, also did not reveal any changes in $_{LOW}$TAU animals, suggesting that a reduction in Pr is not the cause of the decrease in input-output relationship. Looking to mEPSCs recorded from CA1 neurones at 4-months, we see that the frequency of mEPSCs is not changed in $_{LOW}$TAU animals compared to WT, which along with PPR data, implies that a reduction in synapse number is not the cause for the decrease in input-output relationship. Likewise, the amplitudes of mEPSCs were not seen to differ between genotypes, suggesting this difference is also not the result of changes in postsynaptic receptors. One must, however, bear in mind, that SC synapses do not account for all synaptic connections onto CA1 neurones. Nonetheless, in order to mask changes present in SC terminals, synapses originating in alternative areas (such as the EC) would have to display a change in the opposite direction. We thus conclude that this deficit of $_{LOW}$TAU mice at 4 months of age is likely the result of changes in CA3 axonal excitability.

This deficit is also not observed in older animals, suggesting (as was proposed for $_{HIGH}$TAU animals) that any deficits are compensated for by this time. No change in PPR at 13- and 24-months, however, suggests any compensation is not accomplished via changes in Pr, and thus changes in postsynaptic receptors, or the excitability of axons may be implemented at a pivotal point in tau-induced dysfunction. Recording mEPSCs at these advanced ages would provide an indication of whether an increase in the number of postsynaptic AMPA-Rs contributes to compensating for this deficit. The difficulties of performing patch clamp recordings in older animals, however, may lead to a decrease in resolution, limiting the recording of small amplitude currents such as miniatures.

Potentiation of the SC-CA1 synapse and its dependence on NMDA-Rs

It has previously been suggested that despite a lack of change in overall LTP with ageing (Figure 6.19.C)), age-related differences may occur in separate elements composing the total magnitude of potentiation (Shankar et al., 1998). These ideas prompted us to examine the NMDA-R-dependency of LTP across age.

NMDA-R-dependence of short-term potentiation: PTP and STP

While no differences were detected between genotypes, the reduction in PTP amplitude in the presence of AP5 is intriguing. This reduction has been seen previously in the presence of AP5 (Grover and Teyler, 1990, 1992, Stevens et al., 1994, Grover and Teyler, 1995) however, the reasons behind such an observation have not been speculated upon.

During the present experiments, PPR was calculated throughout the entire recording period, allowing insight into whether changes in Pr contributed to LTP. These data recorded during PTP were separated, and plotted in the presence and absence of AP5 for each genotype. As predicted, the PPR recorded during the first minute was greatly reduced in all recordings, indicating an increase in Pr as responsible for PTP (McNaughton, 1982), and thus exposing its presynaptic locus. However, results showed that in the presence of AP5, PPR was decreased to a lesser extent for all genotypes at all ages. This suggests that NMDA-Rs contribute to the increase in Pr following tetanic stimulation at the SC-CA1 synapse.

Although classically thought of as postsynaptic receptors, the role of presynaptic NMDA-Rs, in particular their role in regulating the release of neurotransmitter, is gaining acceptance (Duguid and Smart, 2009). In 2010, McGuinness et al., elegantly showed the presence of NMDA-Rs on CA3 axonal boutons of rat organotypic cell cultures. Using a range of techniques, they exposed that the activation of these NMDA-Rs was dependent on AP-evoked release of glutamate, and that once activated, these receptors contributed to the Ca^{2+} influx into the bouton along with voltage-gated Ca^{2+} channels (VGCCs), increasing Pr. While these presynaptic receptors may not contribute significantly to the rise in intracellular Ca^{2+} concentration *during* the 100Hz induction protocol (McGuinness et al., 2010), they may play a specific role in aiding intracellular Ca^{2+} concentration to remain elevated over the first minute post-tetanus, perhaps through promoting the loading of mitochondria with Ca^{2+} during tetanic stimulation (Lee et al., 2007), or by further increasing the activation of PKC (Brager et al., 2003).

Despite this speculation, it is proposed that the reduction in both WT and TauD35 fEPSP amplitude immediately following tetanus (PTP) in the presence of AP5, is due to the inhibition of presynaptic NMDA-Rs, removing their contribution to the increase in Pr.

The inhibition of STP by AP5 observed across all genotypes and ages was perhaps more striking. These data indicated a component of STP that displayed an unwavering dependence upon NMDA-Rs. This component could be separated from the rapidly decaying early STP that was seen to lead on from PTP, and the later developing LTP. This pattern of inhibition mirrors experiments conducted by Gover and Teyler throughout the 1990s (Grover and Teyler, 1990, 1992, 1995), in which STP was blocked following high frequency stimulation in the presence of AP5 (these experiments are discussed further below).

In 2014, Park et al., reviewed data from their lab in which they describe two separate components of STP. Termed STP1 and STP2, they propose that these components contribute the rapidly decaying and slower decaying elements of STP, respectively; with different combinations of NMDA-Rs contributing these two separate components. The present study supports the idea that STP is formed from two separate elements. It appears that under our conditions, the existence of the slower STP2 is wholly dependent upon NMDA-R activation during induction, whereas the earlier, rapidly decaying STP1 can be produced to some extent by other factors, possibly VGCCs.

NMDA-R-dependence of long-term potentiation

The induction of LTP at the SC-CA1 synapse has long been thought to be dependent on the activation of postsynaptic NMDA-Rs (Collingridge et al., 1983, Malenka, 1991, Bliss and Collingridge, 1993). For this reason, the existence of a level of potentiation within WT animals of all ages in the presence of the competitive NMDA-R antagonist, AP5, was unexpected. To understand these data, we looked to experiments conducted during the 1990s in which an NMDA-R-independent form of LTP was demonstrated at SC-CA1 synapses by Grover and Teyler (Grover and Teyler, 1990, 1992, 1995). Grover and Teyler demonstrated that application of an extremely high frequency tetanus (4 trains of 100 pulses at 200Hz, 5s interval) in the presence of 50μM D, L-AP5 produced a slowly developing LTP, resembling that observed during present experiments. Their studies concluded that this potentiation was the result of frequency-dependent activation of postsynaptic VGCCs, as application of the L-type VGCC blocker, nifedipine, abolished the LTP. Using the same protocol used by Grover and Teyler, Onuma et al., (1998) later demonstrated that this VGCC-dependent LTP (VGCC-LTP) could occur at the SC-CA1 synapse within young male C57Bl/6 mice.

The stimulus protocol used in our experiments was weaker than that originally deemed necessary by Grover and Teyler to establish VGCC-LTP. However, in 1996, Cavus and Teyler demonstrated that LTP induced using a 100Hz frequency tetanus (2 trains of 100 pulses at 100Hz, 20s interval) produced a compound LTP, composed of both VGCC-LTP and NMDA-R-dependent LTP (NMDAR-LTP). This, along with the comparable characteristics of the EPSPs post-tetanus, including a reduced maximum PTP amplitude, inhibited STP and the gradual development of LTP over 5-25 minutes all indicate that similar mechanisms involving VGCCs are operating during the current experiments; although investigations using nifedipine or a similar VGCC antagonist are essential for confirmation. Also the lack of change in PPR during LTP suggests that presynaptic mechanisms are not involved in generating the potentiation observed, further pointing toward postsynaptic VGCCs being accountable for the LTP we observed.

If LTP induced at the SC-CA1 synapse using a 100Hz stimulation protocol is in fact the compound product of both NMDAR-LTP and VGCC-LTP (Cavus and Teyler, 1996), it would appear that despite possible variations in the contributions of each component, these mechanisms work to keep the level of overall potentiation constant from 4-24 months of age. Interestingly, previous studies using WT rats have suggested that the contribution of NMDAR-LTP and NMDAR-independent LTP do differ with ageing. Shankar et al., (1998) proposed that the contribution of NMDAR-independent LTP to the overall compound potentiation increased as the rats aged from 2 to 24-months. Results from WT mice within the present study appear to contradict this finding, instead displaying a trend towards a decrease in NMDAR-independent LTP contribution across age, with the highest involvement of NMDAR-independent LTP at the youngest age of 4 months. This contribution is then seen to decrease slightly by 24 months of age (Figure 6.20.A) grey squares) (one-way ANOVA, $p=0.08$). It is, however, of note that due to low sample numbers of 24-month-old recordings it is not possible to draw firm conclusions from these data; although species differences between mice and rats may result in variation.

The pattern of NMDAR-independent LTP contribution across age in TauD35 mice significantly contrasts that of WT mice (interaction: ($F_{(2, 47)} = 4.337$, $p=0.019$). Transgenic data tend in the other direction, increasing slightly from 4- to 24 months of age, although no significant change in the contribution of NMDAR-LTP is recorded over this time (one-way ANOVA, $p=0.1$) (Figure 6.20.A) blue squares).

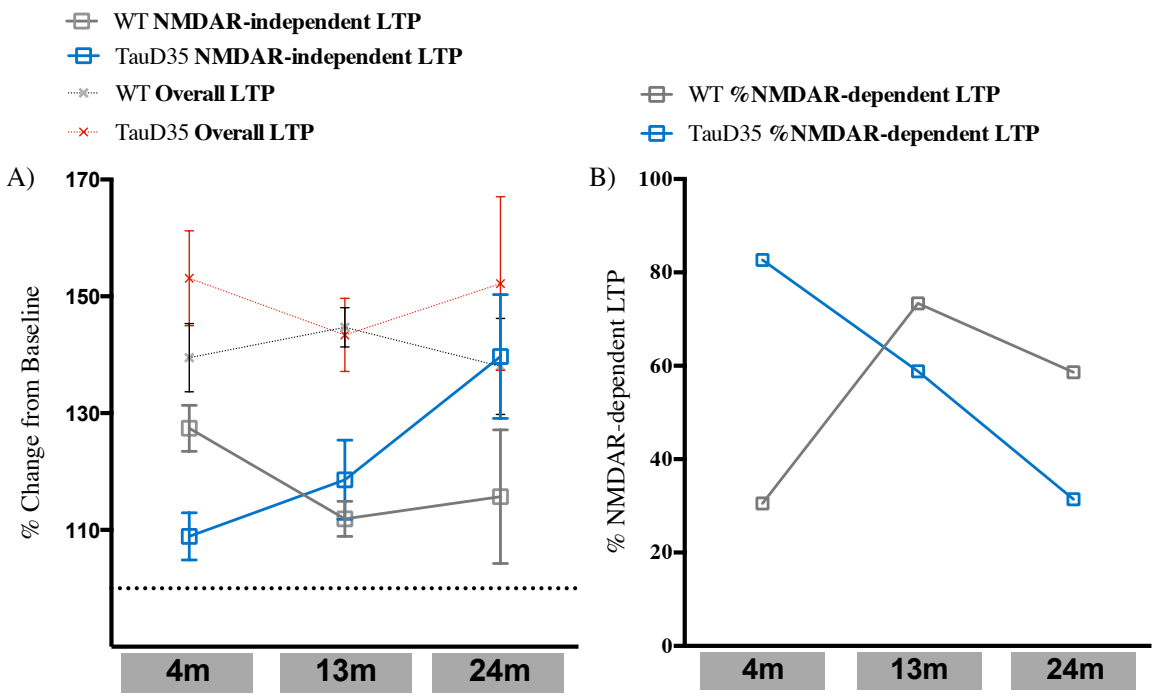

Figure 6.20. Age-dependent changes in the contribution of different components of LTP at 4-, 13- and 24-months. A) The level of NMDA-R-independent LTP in WT mice tends toward a decrease with increasing age, one-way ANOVA p=0.08. NMDA-R-independent LTP recorded from TauD35 mice appears to rise with increasing age, however, analysis reveals no significant change from 4- to 24 months of age (p=0.1). Analysis using a two-way ANOVA reveals a significant interaction between WT and TauD35 NMDAR-independent LTP (p=0.019). Overall LTP levels have been included for reference. Error bars indicate SEM. B) Percent of LTP dependent on NMDA-Rs in WT and TauD35 animals of increasing age.

Despite the low number of $_{HIGH}$TAU animals tested for NMDA-R-dependency, separation of transgenic data revealed that $_{LOW}$TAU and $_{HIGH}$TAU mice displayed a similar increase in NMDA-R-independent LTP with age ($_{LOW}$TAU % LTP in AP5 4m: 110.3 ± 6.5%; 13m: 116 ± 6.9%; 24m: 139.7 ± 10.6%; $_{HIGH}$TAU % LTP in AP5 4m: 107.5 ± 6 %; 13m: 133 ± 27 %). The increase in NMDA-independent LTP appeared to occur somewhat faster in $_{HIGH}$TAU animals, possibly reflecting dose-dependent effects. Collectively these data prompt further work in aged animals, as well as work to increase the number of $_{HIGH}$TAU samples. $_{HIGH}$TAU animals are now being bred for this purpose, and will be at the correct age in early 2016.

Conclusion

In conclusion, TauD35 mice are not seen to differ considerably from WT mice in terms of the electrophysiological parameters tested within the hippocampus in the present study, including no differences in LTP even up to very advanced ages. The use of AP5 has, however, revealed possibly very interesting results regarding the NMDAR-dependency of LTP at the SC-CA1 synapse in WT mice, suggesting other mechanisms may indeed be capable of inducing potentiation at this synapse, in particular at younger adult ages. This work highlights the potential for species differences between rats and mice, and raises important considerations with regard to the increased use of mice in LTP experiments in recent years. The age-dependent contribution of NMDAR-LTP to overall potentiation was significantly different in WT and TauD35 mice, suggesting that the role of NMDA-Rs in inducing LTP may be altered by the development of tau pathology. It is feasible that increased tau dysfunction and mislocation with ageing within the neurone results in disruption of NMDA-R trafficking or anchoring within the synapse, as has been suggested previously (Hoover et al., 2010), leading to an upregulation of NMDA-R-independent mechanisms to compensate.

Apart from these interesting differences in the NMDA-R-dependency of LTP, very few changes were observed in the synaptic transmission of TauD35 mice compared to controls. Of note, were significant changes within the mPP-DG synapses at 4 months of age, prior to NFT development within the hippocampus, suggesting the possible dysfunction of the pyramidal cells of the medial EC as one of the earliest alterations in TauD35 mice. Unfortunately, due to the timing of electrophysiological experimentation within the DG, older mice were not available to follow-up this finding prior to completion of this thesis.

CHAPTER 7

Discussion

Within this thesis I present a novel transgenic mouse model of tauopathy known as TauD35, developed to further aid understanding of the aetiology of neurodegenerative tauopathies and provide an additional system with which to test novel therapeutics. This mouse line expresses human tau, carrying the familial FTDP-17 mutation, P301L. Following initial functional investigations, the TauD35 model was in fact found to exist as two separate lines, termed $_{LOW}$TAU and $_{HIGH}$TAU, differing genetically by transgene copy number and thus protein expression level. The $_{HIGH}$TAU line harbour approximately double the number of tau transgene copies and ~1.6 times the level of human tau protein when compared to $_{LOW}$TAU animals. Together, the $_{LOW}$TAU and $_{HIGH}$TAU models provide an opportunity to study dose-dependent effects of tau dysfunction, as well as allowing the dissociation of tau pathology and ageing.

The detection of these two lines late in the course of this PhD resulted in low sample numbers for many functional experiments, particularly for the $_{HIGH}$TAU model, which was seen to decline in numbers due to a lack of selective breeding. ***For the purpose of the following discussion, however, results will be reviewed and hypotheses postulated based on the data available.***

The hippocampus was chosen for this initial characterisation due to its particular vulnerability to pathology and neurone loss in AD (the most prevalent tauopathy) (Braak and Braak, 1991, Scahill et al., 2002), as well as tau aggregate formation in cases of FTDP-17 carrying the P301L mutation (Spillantini et al., 1998, Mirra et al., 1999). It is of course of note, that the specific neuronal vulnerability deduced from human patients may be modified through the use of non-physiological promoters to drive transgene expression in animal models. Interestingly, however, CaMKIIα and endogenous tau display relatively similar spatial expression throughout the brain, as is seen in Figure 7.1., making use of the CaMKIIα promoter a reasonable choice for models transgenic for tau. This was supported by the fact that TauD35 mice, in particular the $_{HIGH}$TAU line, exhibited a high vulnerability of CA1 pyramidal neurones to the development of tau pathology and neuronal loss, mirroring the cellular vulnerability observed in AD patients (West et al., 1994).

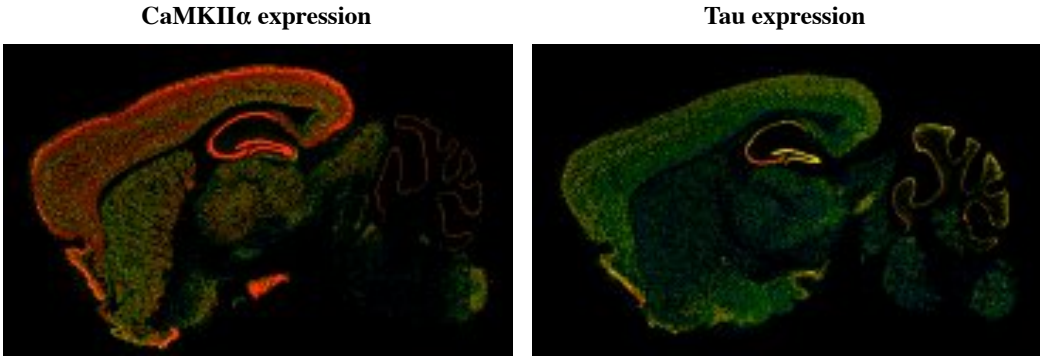

Figure 7.1. Gene expression of CaMKIIα and tau within the mouse brain. Sagittal sections from 1.8-month-old C57Bl6/J mice showing the similar regional expression of CaMKIIα and tau within the brain, including high cortical and hippocampal expression. Note the forebrain neurone specific expression of CaMKIIα.
Images taken from the Allen Brain Atlas (www.mouse.brain-map.org (Lein et al., 2007))

Molecular and histological characterisation: validation of $_{LOW}$TAU and $_{HIGH}$TAU lines

The relatively small (~1.6 times) increase in mutated human tau protein expressed by $_{HIGH}$TAU mice compared to their $_{LOW}$TAU counterparts was seen to result in substantial differences in the timing and extent of tau pathology development. This was particularly evident at 13 months of age, when $_{LOW}$TAU mice were seen to display only occasional NFTs within the hippocampus, compared to the extensive NFT load observed in $_{HIGH}$TAU animals. At this age, the ratio of NFTs (detected using a human tau-specific antibody, HT7) to number of cells, within the CA1 area of the hippocampus in $_{HIGH}$TAU mice was 63 times the ratio of NFTs calculated in $_{LOW}$TAU animals in the same hippocampal region. This non-linear relationship between protein expression level and NFT development has been observed previously (SantaCruz et al., 2005), suggesting a dependence on protein concentration for aggregation initiation, as well as a role for seeding in pathology progression.

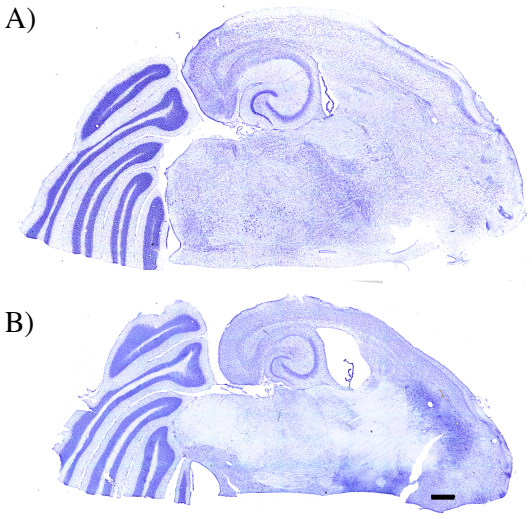

Figure 7.2. Representative whole transverse sections from 17.5-month-old WT (A) and $_{HIGH}$TAU (B) animals, stained with cresyl violet. A) WT control section. B) $_{HIGH}$TAU animals show significant neuronal loss within the hippocampus, along with cortical thinning and enlargement of the lateral ventricle. Note the comparable size of the cerebellum between WT and $_{HIGH}$TAU animals, compared to the overall shrinkage of the forebrain. Scale bar: 500µm.

It is likely that this considerably elevated pathology development in $_{HIGH}$TAU mice is a contributing factor on the path to the severe pathological phenotype displayed by these animals in later life. Analysis of neuronal loss in those mice already displaying these pathological symptoms showed extensive neurodegeneration, particularly within the CA1 region of the hippocampus (>50% loss of neurones), with additional examination of overall transverse sections exposing substantial cortical thinning and ventricle enlargement (Figure 7.2.). It is thus presumed, that within $_{HIGH}$TAU mice, the increase in mutated human tau protein expression leads to elevated toxic species of tau evidenced by an increase in pathology. This increased toxicity causes widespread neuronal loss, eventually leading to sickness and death of the animal. The observation that the timing of the final neurodegenerative phenotype of the $_{HIGH}$TAU mice occurs within a relatively short time window (17-20 months) will be a useful feature of this model allowing detailed analysis of the factors leading to this phenotype in the preceding months. The $_{HIGH}$TAU mice are now being bred for this purpose for future studies.

Molecular and histological characterisation: development of pathological tau

The pathological species of tau developed by $_{LOW}$TAU and $_{HIGH}$TAU animals were investigated by both molecular and histological techniques, using antibodies including the phosphorylation dependent CP13 (S202) and PHF-1 (S396/S404). Data obtained using Western blotting techniques revealed physiological levels of S202 and S396/S404 phosphorylated tau in WT mice of 4- and 13 months of age. Using immunohistochemistry, however, phosphorylated tau was not detected in WT mice at any age. This difference is likely due to the fact that the protein of interest is denatured and concentrated into a thin band for Western blotting, making this technique more sensitive to low concentrations of protein. The low concentration of phosphorylated tau is likely too diffuse throughout the cellular compartment to be observed using immunohistochemistry.

Similarly, at 4 months of age, prior to the development of NFTs detected by immunohistochemistry in either the $_{LOW}$TAU or $_{HIGH}$TAU transgenic lines, a significant degree of phosphorylated tau was identified using both CP13 (Figure 7.3.) and PHF-1 through use of Western blotting. At this relatively young age, all transgenic mice did exhibit a degree of axonal mossy fibre staining, detected with all antibodies used. The presence of S396/S404 phosphorylated tau in Western blot data therefore likely reflects the existence of phosphorylated tau within the axonal compartment, while the diffuse

staining of S202 phosphorylated tau within the somatodendritic compartment of both transgenic lines would have contributed to the level of protein detected by Western blot.

With age, both transgenic lines were seen to develop a high quantity of twisted intracellular NFTs, an observation that correlated to the appearance of a sarkosyl-insoluble 64kDa tau band in Western blots. It is established that this band is created from the hyperphosphorylation of the 0N4R isoform of tau (Goedert et al., 1992), however, due to the protocol employed to prepare samples for Western blot, it is not aggregated into mature NFTs (Greenberg and Davies, 1990). This band thus represents a hyperphosphorylated, insoluble species, assumed to be aggregated to some extent.

In addition to the presence of sarkosyl-insoluble tau migrating at 64kDa in older animals, insoluble tau was also observed at 4 months of age and at 13-months in $_{LOW}$TAU animals, migrating with a lower molecular weight of ~54kDa. The dephosphorylated 0N4R isoform of tau migrates with an approximate weight of 50kDa (Buee et al., 2000), thus suggesting that the sarkosyl-insoluble tau observed at these younger ages displays a low level of phosphorylation. Sahara et al., (2002) studied this lower weight insoluble fraction from younger mice using electron microscopy, and determined that this tau does indeed have a fibrous appearance, but is shorter in length than those fibres observed from older animals. It therefore seems that the insoluble tau migrating at ~54kDa contains a low level of phosphorylation and is aggregated into short low order filaments, possibly representing the early stages of further, more mature aggregate formation.

In summary, phosphorylated tau is detected in both $_{LOW}$TAU and $_{HIGH}$TAU animals at 4 months of age. While some of this protein is insoluble in sarkosyl, it is not seen to form aggregates detectable by immunohistochemistry. At 13-months, $_{LOW}$TAU animals display a very low number of NFTs, along with a small decrease in the amount of phosphorylated protein detected by Western blot. $_{HIGH}$TAU animals, however, display a heavy NFT load at 13-months, corresponding to the appearance of insoluble tau migrating at 64kDa, despite an overall decrease in phosphorylated tau species detected by Western blot, owing to the loss of NFTs during homogenate sample preparation. This situation is mirrored in $_{LOW}$TAU animals of 24 months of age (Figure 7.3.).

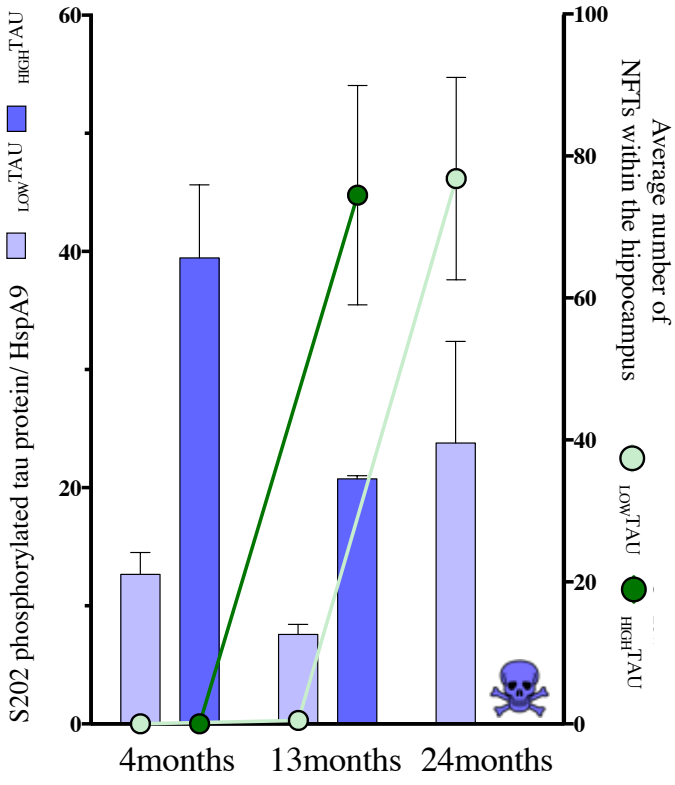

Figure 7.3. Visual comparison of the absolute number of NFTs detected using CP13 (S202) via immunohistochemistry to the amount of S202 phosphorylated tau protein detected within the whole hippocampus by Western blotting at 4-, 13- and 24 months of age in $_{LOW}$TAU and $_{HIGH}$TAU mice. NFT data were obtained by averaging the absolute number of NFTs counted within a defined area (240x400µm) within the CA1, CA3 and DG regions. At 4-months, no NFTs had developed, despite a large amount of S202 phosphorylated tau protein being present within the hippocampus of both transgenic lines. Following the development of a significant NFT load in $_{HIGH}$TAU mice of 13-months, the amount of S202 protein appears decreased, owing to the loss of NFTs during homogenate preparation. 13-month $_{HIGH}$TAU and 24-month $_{LOW}$TAU mice display similar absolute numbers of NFTs and S202 protein within the hippocampus. No $_{HIGH}$TAU animals survive until 24 months of age. Error bars indicate SEM.

Functional characterisation: consequences of pathological tau

Behaviour

For investigations into behavioural changes at 12 months of age, data from the $_{HIGH}$TAU mice available displayed a high level of consistency. Within the T-maze forced alternation task, $_{HIGH}$TAU mice performed extremely well, finishing the testing phase with a correct response rate of 100%. This finding indicates that in spite of the high NFT load present within the hippocampus of these mice at this age, hippocampal-dependent spatial working memory was not affected. This supports observations from AD patients, in which substantial hippocampal degeneration is observed prior to the onset of the first clinical symptoms including deficits in declarative memory (Lehericy et al., 1994, Jack et al., 1997), indicating that severe cell loss is required to produce detectable symptoms. $_{HIGH}$TAU animals displaying the characteristic pathological phenotype developed by these mice between the ages of 17- and 20-months develop a significant level of neurodegeneration, including >50% cell loss within the CA1 region of the hippocampus. It would, however, be unfeasible to complete behavioural testing during this time due to

the significant reductions in movement initiation and ambulation displayed by these animals. On the other hand, it is hoped that with the continued breeding of this line and the predictability of pathological phenotype onset, it will be possible to assess behavioural alterations immediately preceding the development of moribund symptoms.

Assessment of changes in anxiety and locomotion using the open field and light/dark box revealed interesting differences in the behaviour of $_{HIGH}$TAU animals. Despite their unaffected spatial memory, $_{HIGH}$TAU mice were seen to show a deficit in habituation to a novel environment, as well as displaying a potential reduction in anxiety-like behaviour. The nature of these tests, however, does not provide sufficient specificity to attribute these changes to dysfunction within a particular brain region. Interestingly, during T-maze testing $_{HIGH}$TAU mice also exhibited extremely fast response times on the first, sample run, suggestive of disinhibition. Together, these changes to the behaviour of $_{HIGH}$TAU animals more closely mimics the initial symptoms of FTDP-17, in which patients exhibit complex and heterogenous personality and behavioural changes, including disinhibition (Wszolek et al., 2006).

Synaptic transmission

The majority of electrophysiological testing concentrated on the young age of 4 months. At this time, NFTs were not observed in either $_{LOW}$TAU or $_{HIGH}$TAU animals, although diffuse staining was observed throughout the intracellular compartments of all hippocampal neurones using the 'early' CP13 antibody, which recognises tau phosphorylated at S202. Concentrating electrophysiological analysis at this young age aimed to detect the very earliest changes in the functioning of neurones resulting from tau dysfunction. Neither the membrane resistance nor basal synaptic transmission of CA1 pyramidal neurones or DG granules cells in either $_{LOW}$TAU or $_{HIGH}$TAU animals was altered at 4-months, indicating that the phosphorylation of tau at S202 and mislocation into the somatodendritic compartment does not change these parameters.

Examination of PPRs at this age did, however, expose a reduction in the Pr of mPP synapses (originating in the medial EC) onto DG granules cells in both transgenic lines. The neurones of the EC were not analysed histologically or using molecular biology within the present study, and thus detailed conclusions regarding pathological tau species harboured by these cells are not known. It is of note, however, that the formation of NFTs was not noted in any brain region at this age (*data not shown*), implying that this change in Pr is the result of soluble pathological tau species. This

result is interesting as the EC is an area known to show particular vulnerability to tau dysfunction in AD (Braak and Braak, 1991, Gomez-Isla et al., 1996), supporting the use of both the $_{LOW}$TAU and $_{HIGH}$TAU lines as models of tauopathy.

By 13 months of age, the two transgenic lines had developed a significantly different NFT burden within the hippocampus, with mice of the $_{HIGH}$TAU line exhibiting an extremely high NFT load compared to their $_{LOW}$TAU counterparts. This divergence in pathology corresponds to an apparent separation of basal synaptic transmission and PPR data obtained from both transgenic lines. At this age, $_{HIGH}$TAU animals display changes indicative of a reduction in Pr, as well as possible changes to AMPA-R density/kinetics compared to WT and $_{LOW}$TAU animals, suggesting that a more mature development of tau pathology is required to disrupt these parameters.

At this age, the CA3 neurones of $_{HIGH}$TAU animals contain significant numbers of NFTs, although no cell loss is observed. In terms of the reduction in Pr, it is proposed that NFTs inflict a detrimental effect on Pr. It is possible that disruptions in axonal transport created through a loss of physiological tau function, as well as the physical barrier created by the large intracellular aggregate, may impede the passage of the materials needed for neurotransmitter release from these neurones, such as mitochondria (Eckert et al., 2014). Indeed, alterations in MT-dependent transport have been recently observed to occur *in vivo*, correlating to the development of pathological tau species in two separate mouse models of tauopathy (rTg4510, Majid et al., 2014; JNPL3, Bertrand et al., 2013).

However, not all alterations in synaptic transmission occurred following an increase in tau pathology, as was demonstrated by the reduction in input-output only in $_{LOW}$TAU animals of 4-months of age. The input-output relationship recorded extracellularly measures the postsynaptic potential in response to increasing stimulus strength applied to the presynaptic axons. At 4-months, when both $_{LOW}$TAU and $_{HIGH}$TAU mice display only diffuse staining of S202 phosphorylated tau, the input-output relationship of $_{LOW}$TAU mice at the SC-CA1 synapse is significantly reduced at the highest stimulation intensities of 60, 70 and 80V. As is discussed within Chapter 6, a reduction in input-output at this synapse is indicative of reduced connectivity between the CA3 and CA1 neurones, possibly caused by a variety of factors. Examination of other electrophysiological features including PPR and mEPSCs led to the conclusion that such a decrease in input-output is the result of a reduction in CA3 axonal excitability. A

similar reduction in input-output at this synapse has been reported previously in the rTg4510 tauopathy model at an age showing comparable pathology, i.e. very limited phosphorylated tau staining, detected using an antibody recognising tau phosphorylated at S202/T205, described as a model of a pretangle stage (Dalby et al., 2014). The authors go on to show that this deficit is also present in mice at an age displaying considerable tau pathology but still in the absence of neurodegeneration. This was not the case within the present study, however, with no deficit observed in either transgenic line at 13-months or in $_{LOW}$TAU animals of 24-months. Thus, results gathered from $_{LOW}$TAU and $_{HIGH}$TAU mice, appear to show a reduction in SC-CA1 connectivity at only the very earliest stages of tau dysfunction, with no difference detected at a higher dose of pathological tau or with increasing age. It is proposed that the reduced excitability of CA3 neurones is compensated in those mice experiencing an increased level of tau dysfunction. At the youngest age of 4-months, it may be that the increased overexpression of tau in the $_{HIGH}$TAU line compensates for the loss of tau function experienced by both transgenic animals. By 13 and 24 months of age, the longer exposure to tau dysfunction endured by those animals initiates compensatory mechanism resulting in an increase in excitability of CA3 neurones. An alternative hypothesis is that TauD35 mice exhibit a delayed maturation of the SC-CA1 pathway, which is masked in $_{HIGH}$TAU animals at 4 months of age by the increased overexpression of human tau. By 13-months, the pathway has matured, and thus displays similar excitability to that of WT mice.

Synaptic plasticity

One intriguing finding of the present study revealed that in both WT and transgenic lines, at all ages studied, the LTP expressed at the SC-CA1 synapse was not wholly NMDA-R-dependent, as is often assumed from previous work using rats (Collingridge et al., 1983). Instead, all mice showed some level of potentiation 60 minutes following tetanus application, presumed to be dependent on voltage-gated calcium channels. Interestingly, however, the contribution of these two forms of LTP was seen to alter with age. Moreover, this age-dependent adjustment in NMDA-R-dependency was different in WT and transgenic mice. Due to the advanced age, small numbers of both WT and $_{LOW}$TAU mice were included at 24-months, leading to a larger error at this age and possibly preventing detection of a significant change in NMDA-R-dependency across age for both WT and transgenic animals. Even so, we observe an overall trend towards an increase in the NMDA-R-dependency of LTP in WT mice with increasing age

(Figure 7.4.). This increase contrasts data collected from WT rats, in which the NMDA-R-dependent component of LTP was decreased in mice of 24-months compared to young animals of 2 months of age (Shankar et al., 1998), possibly representing important species differences between rats and mice.

Data obtained from transgenic mice revealed that at 4-months, when $_{LOW}$TAU and $_{HIGH}$TAU animals displayed a similar level of diffuse S202 phosphorylated tau within CA1 neurones, both lines exhibited similar levels of NMDA-R-dependency at the SC-CA1 synapse (Figure 7.4.). The contrast to data from WT counterparts indicates that the rise in tau S202 phosphorylation, and its relocation into the somatodendritic compartment results in an increase in the contribution of NMDA-R-dependent LTP. This may be due to an increase in postsynaptic Fyn localisation and the resultant phosphorylation of NMDA-Rs anchoring them to PSD-95 (Ittner et al., 2010). With the added contribution of NMDA-Rs, NMDA-R-independent LTP may be down regulated to compensate, keeping the overall LTP magnitude constant.

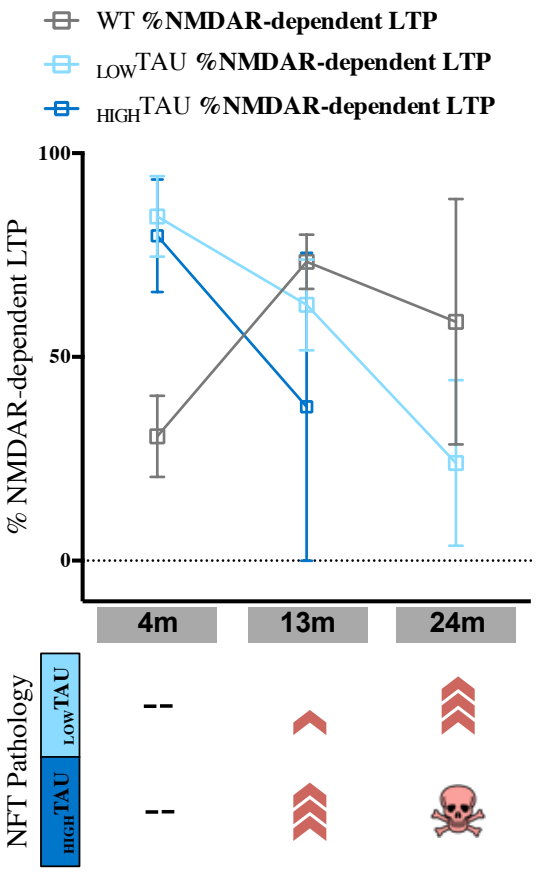

Figure 7.4. The dependence of LTP on NMDA-Rs at the SC-CA1 synapse in $_{LOW}$TAU, $_{HIGH}$TAU and WT animals across 4-, 13- and 24-months of age. The degree of NFT load within the hippocampus in both transgenic lines is represented below (number of arrows represents the severity of pathology). Error bars indicate SEM.

At 13 months of age, both transgenic lines then displayed a tendency towards a decrease in the percentage of NMDA-R-dependency, with this decrease possibly more exaggerated in data from $_{HIGH}$TAU mice (Figure 7.4.). With further ageing (and progression of tau pathology), the dependency of LTP on NMDA-Rs continued to decline in $_{LOW}$TAU animals (Figure 7.4.). From these data it is hypothesised that as tau pathology matures, there is a reduction in the number of postsynaptic NMDA-Rs, lowering the NMDAR-dependent component of LTP and thus causing independent mechanisms to be up regulated in response, maintaining the overall level of LTP. A decrease in postsynaptic AMPA- and NMDA-R numbers has previously been linked to the accumulation of pathological tau within the insula cortex and ventral

striatum of a mouse model of tauopathy, which harbours all isoforms of human tau carrying the V337M mutation (Warmus et al., 2014). Notably, the pathology described by Warmus et al., was at a pretangle stage rather than a point of mature NFT accumulation, although differences in the tau mutation and brain area studied could affect the point at which tau pathology decreases NMDA-R function. The authors attribute the observed decrease in synaptic glutamate receptors to a tau-dependent depletion of the receptor scaffolding protein, PSD-95, which was found to occur in the absence of any neurodegeneration or even synapses loss. A reduction in synaptic glutamate receptors has also been reported in hippocampal neurones cultured from rTg4510 mice (Hoover et al., 2010), indicating a similar phosphorylated tau-dependent reduction in the synaptic localisation of both AMPA- and NMDA-Rs in the absence of synapse loss.

Taken altogether, the evidence suggests that tau phosphorylation and mislocation to the somatodendritic compartment (and possibly into dendritic spines (Hoover et al., 2010)) in both $_{LOW}$TAU and $_{HIGH}$TAU animals affects the function of NMDA-Rs. Initially, the effects manifest as an increase in NMDA-R function, possibly through increased anchoring of the NMDA-R to the scaffolding protein, PSD-95 (Ittner et al., 2010). Following further phosphorylation and the initiation of aggregation, this mislocated tau begins to disrupt the insertion and/or anchoring of NMDA-Rs to the PSD (Hoover et al., 2010), potentially through contributing to the depletion of PSD-95 (Warmus et al., 2014). Interestingly, gene-expression analysis of TauD35 mice (discussed further below, data adapted from Matarin et al., 2015), reveals a significant reduction in the expression of GluN1, an obligatory subunit of the NMDA-R, in both $_{LOW}$TAU and $_{HIGH}$TAU animals by 18 months of age (Figure 7.5). It may therefore be suggested that the development of pathological tau species brings about a reduction in NMDA-Rs through altering the expression of genes encoding the receptor.

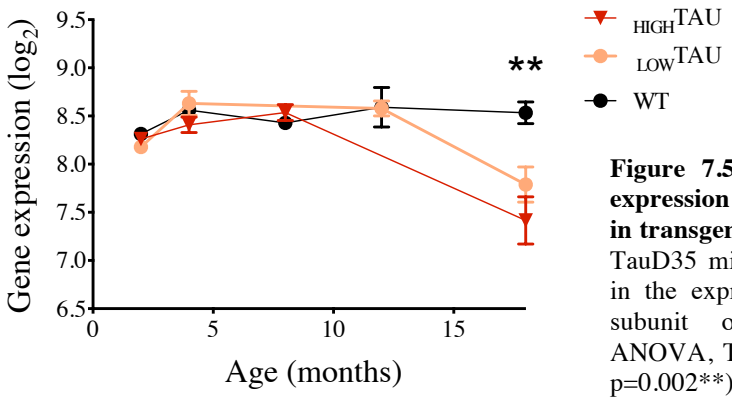

Figure 7.5. Significant reduction in the expression of Grin1 (GluN1) at 18-months in transgenic animals. At 18-months of age, TauD35 mice display a significant decrease in the expression of GluN1, an obligatory subunit of the NMDA-R. (One-way ANOVA, Tukey's multiple comparison test, p=0.002**) compared to WT controls.

Gene expression increases in $_{LOW}$TAU and $_{HIGH}$TAU animals at 18-months

Analysis of separated transgenic data at 18 months of age was completed by Dr Dervis Salih. Immunohistochemistry completed for publication (Matarin et al., 2015) was performed by Dr Marina Yasvoina. Consequently these data have been included here for discussion, rather than within the results chapters.

A recent collaborative project including members of my current laboratory produced genome-wide gene-expression data from TauD35 mice at 2-, 4-, 8- and 18 months of age (Matarin et al., 2015). At the time of this study by Matarin et al., it was not yet confirmed that the TauD35 mouse model existed as two separate lines, however, as data was analysed correlating individual mouse pathology to gene-expression, these data stand. In fact, post hoc copy number analysis revealed that the majority of animals included in Matarin et al., were of the $_{HIGH}$TAU line. Additional microarray analysis has been completed since publication, increasing the numbers of $_{LOW}$TAU animals included. Here I present further analysis of all data obtained from 18-month animals, with $_{LOW}$TAU and $_{HIGH}$TAU animals of this age separated. These gene expression changes were only completed within the hippocampus in keeping with the hippocampal characterisation presented within this thesis.

As is described in Matarin et al., TauD35 mice did not display substantial changes in gene expression until relatively late in the disease process, lagging months behind the appearance of NFTs, with the majority of significant changes not detected until 18 months of age (see www.mouseac.org for changes in individual gene expression). It therefore followed that the additional analysis presented here be completed at 18-months. At this age, 85% of genes that showed differential expression in the TauD35 animals were increased, with only 15% being significantly decreased (Matarin et al., 2015), fuelling our decision to concentrate only on those genes displaying an increase in expression for the current analysis. Of those genes showing a significant reduction in expression at 18-months many fell into categories relating to synapses and neurotransmission, likely reflecting the loss of synapses and cells (*ibid*).

At this advanced age, both $_{LOW}$TAU and $_{HIGH}$TAU mice display NFT pathology within the hippocampus, although substantial differences in pathology load between the two lines exist, as was presented at other ages in Chapter 4. In separating the NFT counts completed for publication (Matarin et al., 2015) into $_{LOW}$TAU and $_{HIGH}$TAU animals, it is established that within the hippocampus $_{HIGH}$TAU mice exhibit approximately 14 times

the NFT number detected with the tau phosphorylation-dependent antibody, AT8 (S202/T205), when compared to $_{LOW}$TAU animals. Cell counts were not completed on animals used for publication. Despite this, it is predicted that the $_{HIGH}$TAU mice used for gene-expression analysis displayed substantial neurodegeneration as all were noted as presenting with the pathological phenotype characteristic of this line at this age. As is presented in Chapter 4, mice displaying this moribund phenotype exhibit >50% loss of CA1 pyramidal cells, with substantial degeneration also observed within the DG.

A)

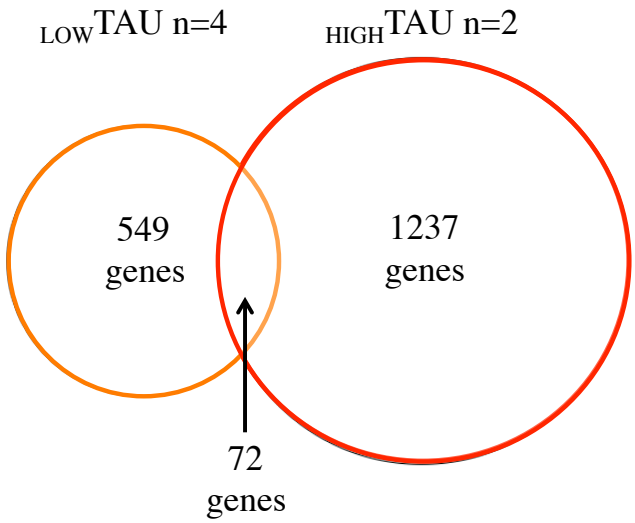

Figure 7.6. Genes increased >20% in $_{LOW}$TAU and $_{HIGH}$TAU mice compared to WT at 18-months. A) Venn diagram depicting the overlap between genes increased >20% (ANOVA, p<0.01) within the hippocampus of $_{LOW}$TAU and $_{HIGH}$TAU animals of 18 months of age. B) Table of representative gene ontology (GO) categories identified using WebGestalt displaying a significant increase in either $_{LOW}$TAU or $_{HIGH}$TAU mice. Representative categories are similar to those identified using Ingenuity. Significant increases (p-values) are highlighted in red.

B)

	GO No.	**$_{LOW}$TAU**	**$_{HIGH}$TAU**	**Exclusive to $_{HIGH}$TAU**
Immune system process	*0002376*	>0.05	$1.04x10^{-49}$	$1.22x10^{-44}$
Intracellular protein kinase cascade	*0007243*	>0.05	$7.69x10^{-18}$	$2.89x10^{-17}$
Programmed cell death	*0012501*	>0.05	$6.05x10^{-9}$	$4.19x10^{-8}$
Mitochondrion	*0005739*	$2.28x10^{-13}$	>0.05	>0.05
Ribosome	*0005840*	$1.45x10^{-10}$	>0.05	>0.05

Genes that displayed >20% (P<0.01) increase compared to WT within the hippocampus were extracted for both $_{LOW}$TAU and $_{HIGH}$TAU animals. Any genes that were increased in both transgenic lines were subtracted from $_{HIGH}$TAU data to give those genes 'exclusive

to $_{HIGH}$TAU' (Figure 7.6.B)). Detected genes for each genotype were examined using WebGestalt and Ingenuity, with representative gene ontology (GO) categories presented for each genotype (Figure 7.6.B)). For $_{LOW}$TAU animals, the majority of genes exhibiting significant increases in expression were categorised into relatively unspecific GO categories, including 'intracellular', 'cytoplasm' and 'cell'. Of more interest, were the high number of genes detected showing increased expression relating to mitochondria and ribosomes. Such genes were not common to $_{HIGH}$TAU mice of the same age (Figure 7.6.B)), indicating that mitochondrial and ribosomal dysfunction occurs prior to the development of a severe NFT load and onset of neurodegeneration. It is possible, that this genetic overexpression pattern is present within only a subset of neurones, and is a prerequisite for subsequent NFT development, or even cell death.

In contrast, $_{HIGH}$TAU animals exhibited a rise in the expression of genes involved in the immune system and inflammation, apoptosis, as well as more general categories revolving around protein binding.

The increase in the expression of genes relating to apoptosis corresponds to the neurodegeneration present within the hippocampus of $_{HIGH}$TAU animals at this age, implying a role for apoptosis in producing the cell loss associated with neurodegenerative tauopathies. More specifically, a rise in the expression of genes such as the initiator and executioner caspases 8 ($p=0.0006$) and 6 ($p=0.02$) (McIlwain et al., 2013) is observed only within this transgenic line compared to WT animals (Figure 7.7.A) and B)). Both caspase 6 (Guo et al., 2004, Albrecht et al., 2007) and caspase 8 (Rohn et al., 2001) have been shown to be increased in an active form within the brains of AD patients, as well as both being increased in primary hippocampal cultured neurones following transfection with a truncated form of tau (Chung et al., 2003). Caspase 8 mRNA is also increased in the hippocampus and cortex of rTg4510 mice from 5.5months (Spires-Jones et al., 2008), an age corresponding to significant cell loss in this mouse line (Spires et al., 2006).

There is, however, a growing body of evidence that dissociates caspase activation and cell death. In particular, the executioner caspase 6 has also been linked to the formation of NFTs in AD, rather than acute apoptosis. Guo et al., (2004) demonstrated that active caspase 6 is associated with pretangles, implying it is associated with the initial stages of NFT formation. This is in line with later work by de Calignon et al., (2010), who revealed caspase activation prior to NFT formation, suggesting that caspases may have a role in initiating NFT formation rather then the other way around.

Interestingly, caspase 6 activation has also been observed in the brains of some non-cognitively impaired individuals, at which time it was mostly confined to the EC and CA1 (Albrecht et al., 2007), two areas which, as has been discussed, show particular vulnerability to the development of tau pathology and cell loss in AD. In 2008, Spires-Jones et al., demonstrated that the caspase activation associated with NFT pathology in tauopathy disorders does not cause acute cell death, suggesting that activation of caspases is not the cause of neurodegeneration. They propose that NFT formation is protective, sequestering caspases and thus limiting proteolytic damage. This idea was supported by their later work (de Calignon et al., 2010), with others (Wang et al., 2014) suggesting that the initiation of tau hyperphosphorylation is employed by cells to aid them in escaping from acute apoptosis, however, this later leads to the accumulation of hyperphosphorylated tau, which is not reversed, leading to chronic neurodegeneration.

Despite this previous evidence for caspase involvement in NFT formation, we did not observe an increase in the gene expression of caspases in $_{LOW}$TAU animals, which at this age continue to develop NFTs but do not display neurone loss. Thus, from the results presented here, it is suggested that instead the upregulation of caspase 6 and 8 expression may be associated with neuronal death.

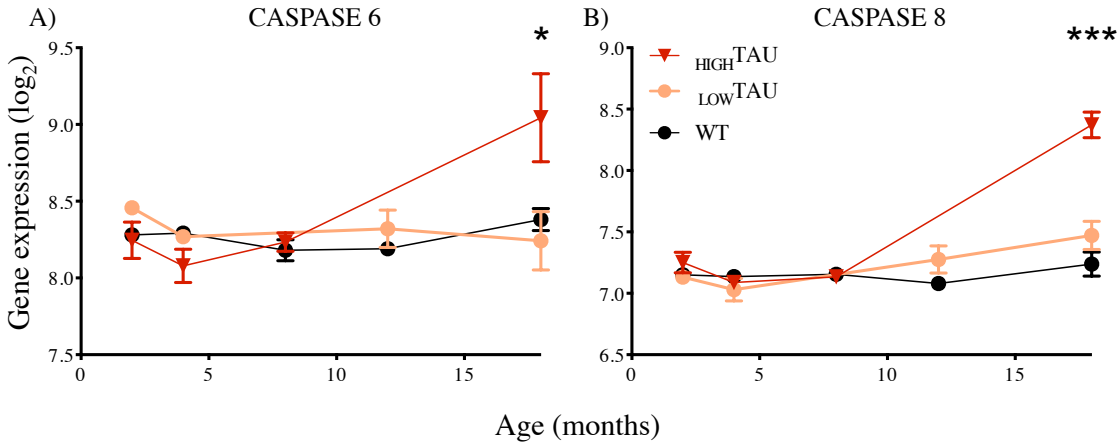

Figure 7.7. $_{HIGH}$TAU animals show a significant increase in the gene expression of caspase 6 (A) and 8 (B) at 18-months of age. At 18-months of age, $_{HIGH}$TAU mice display a significant increase in the expression of caspase 6 (A) (One-way ANOVA, Tukey's multiple comparison test, p=0.02*), and caspase 8 (B)) (One-way ANOVA, Tukey's multiple comparison test, p=0.0006***) compared to WT controls.

It was reported previously, that TauD35 mice of 18 months of age displayed elevated expression of immune-related genes (Matarin et al., 2015). We now reveal that this previous observation was true only of $_{HIGH}$TAU mice, with significant changes not apparent in $_{LOW}$TAU animals.

In 2014, Wes et al., completed gene-expression analysis on 4 and 6 month old rTg4510 mice. The results from this experiment were very interesting in terms of the data presented here. They revealed that rTg4510 mice at 6 months displayed a significant increase in the expression of genes relating to the immune system. At this age, rTg4510 mice show a significant NFT load within the hippocampus, as well as significant neurodegeneration (Spires et al., 2006), comparable to the situation at 18-months in $_{HIGH}$TAU animals. However, this is a different mouse model, expressing a different level of the transgene, different integration site, on a different background strain. Moreover, the mice used for the study by Wes et al., were female. The fact that the results in these mouse lines are so similar, despite these differences support that the upregulation of genes involved in the immune system and inflammatory response within the hippocampus is a common consequence of tau dysfunction. More specifically, Wes et al., reveal a substantial increase in the expression of genes involved in the complement cascade, a finding mirrored in $_{HIGH}$TAU animals (Figure 7.8.A), B) and C)).

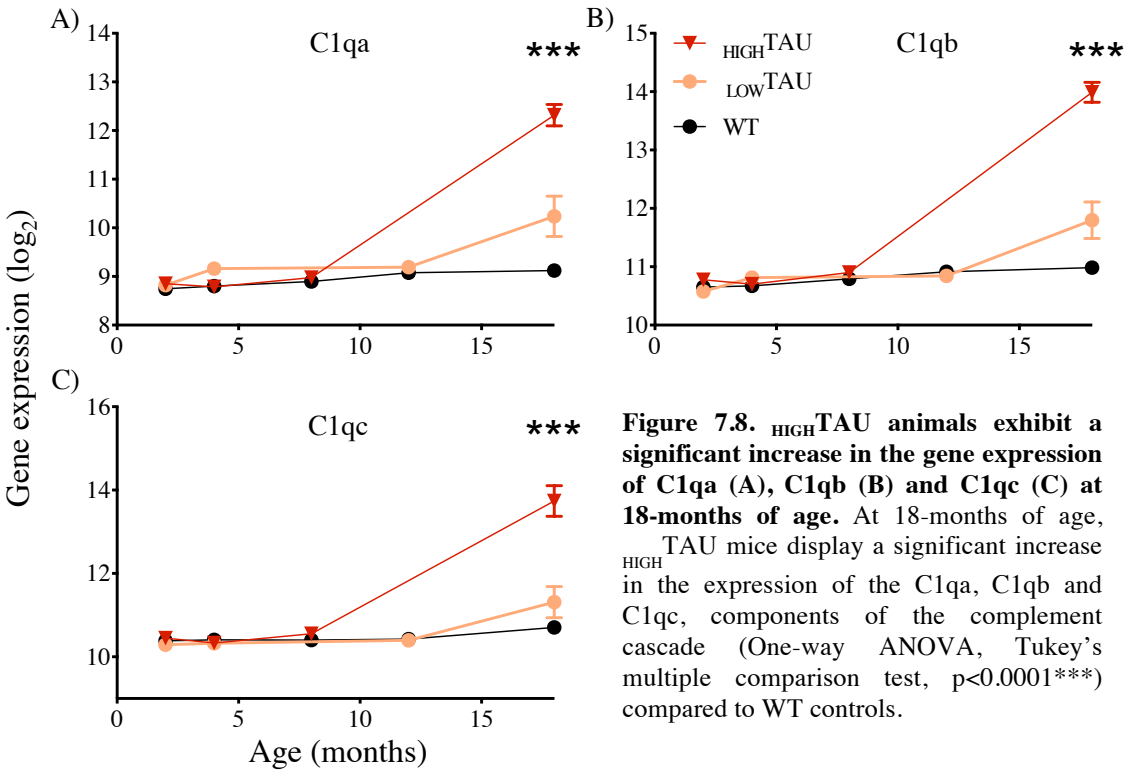

Figure 7.8. $_{HIGH}$TAU animals exhibit a significant increase in the gene expression of C1qa (A), C1qb (B) and C1qc (C) at 18-months of age. At 18-months of age, $_{HIGH}$TAU mice display a significant increase in the expression of the C1qa, C1qb and C1qc, components of the complement cascade (One-way ANOVA, Tukey's multiple comparison test, p<0.0001***) compared to WT controls.

Remarkably, this finding is not solely common to tauopathy models. As was reported in Matarin et al., a significant rise in immune gene expression has also been observed in a model of amyloid-β dysfunction (TASTPM). Again, the expression of genes involved in the complement cascade were found to be increased significantly within the hippocampus of these animals. This model of amyloid-β dysfunction does not

show neurodegeneration, demonstrating that the rise in immune genes is independent of cell death; instead seeming to correlate significantly with the development of pathology in the form of amyloid-β plaques. We therefore looked to 13-month-old $_{HIGH}$TAU mice, to see if there was evidence for a change in microglial status prior to neurodegeneration, as it is these cells that constitute the principle cellular component of the immune system within the brain (Heneka et al., 2014).

We see from Figure 7.9. that $_{HIGH}$TAU animals display a clear rise in the number of microglia within all subregions of the hippocampus. In $_{HIGH}$TAU mice displaying a heavy NFT load, microglia are seen to infiltrate the cell layers in high numbers, an event not observed in $_{LOW}$TAU animals at a stage of early NFT formation. This finding indicates that the inflammatory response may be upregulated prior to degeneration, rather than in response to cell death.

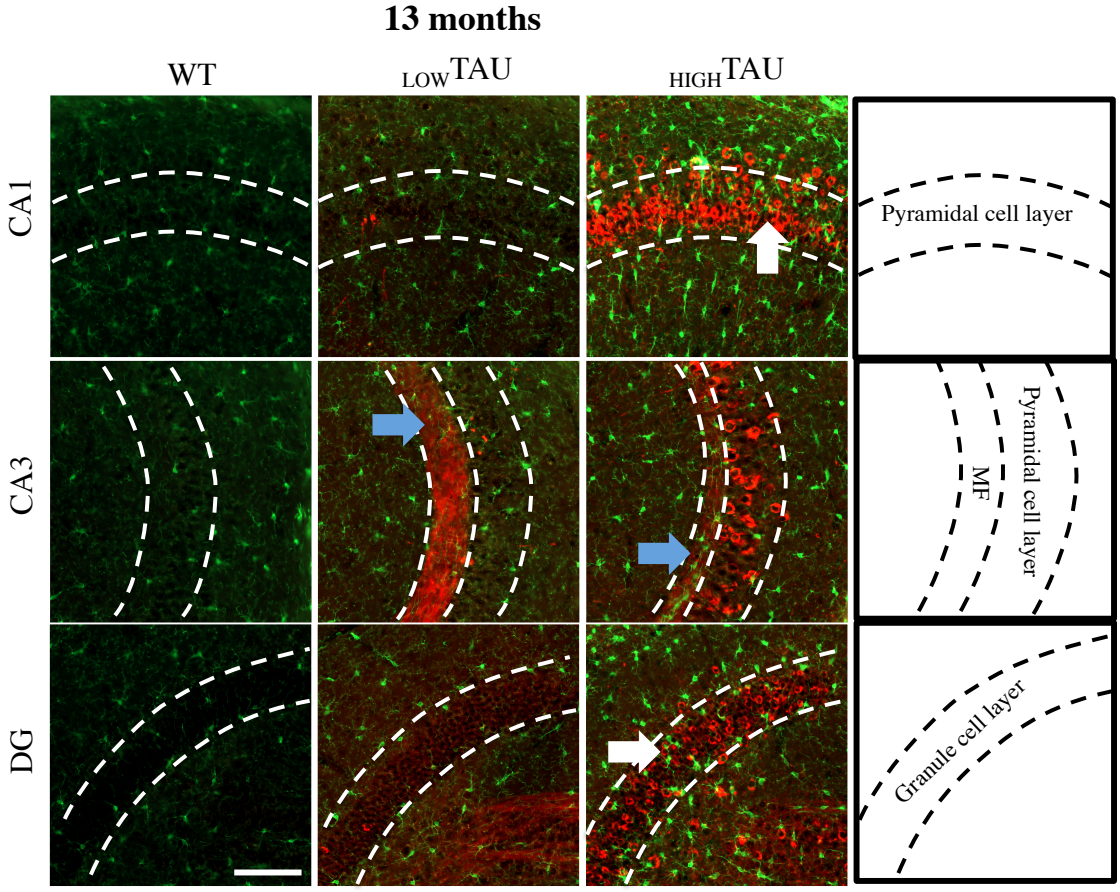

Figure 7.9. Microglia appear increased within the hippocampus of $_{HIGH}$TAU animals at 13 months. Double immunostaining with CP13 (S202 phosphorylated tau, ***red***) and Iba1 (microglia, ***green***). Dashed white lines indicate the cell body layers of each subregion of the hippocampus. The mossy fibre pathway is also outlined in $_{LOW}$TAU and $_{HIGH}$TAU animals. White arrows indicate the infiltration of the CA1 and DG cell body layers by microglia in $_{HIGH}$TAU animals. Blue arrows indicate the infiltration of microglia into the mossy fibre pathway in both $_{LOW}$TAU and $_{HIGH}$TAU mice. *MF*: Mossy fibre pathway. Scale bar: 100μm.
Double CP13 and Iba1 staining was completed by Wenfei Lui.

As tau aggregate formation has begun in $_{LOW}$TAU animals of 13-months, but microglia have not yet been upregulated, it is suggested that it is the development of tau pathology that initiates the rise in microglia. Indeed, misfolded protein aggregates, including tau (Morales et al., 2013), have been shown to activate microglia (Heneka et al., 2014). In terms of tau, this activation may only occur following the neuronal release of tau, an event on the pathway to tau pathology propagation (discussed in Chapter 1).

In addition to analysing gene-expression changes within the whole hippocampus, Wes et al., also examined gene changes in the cellular layers of subregions of the hippocampus, using microdissected samples. This work revealed that the majority of gene changes at 6-months in rTg4510 mice occurred within the CA1 region, including an increase in immune genes. This is an interesting finding considering the apparent vulnerability of this region to tau pathology development and neurone loss in both rTg4510 (SantaCruz et al., 2005) and $_{HIGH}$TAU animals, as well as AD patients (West et al., 1994). Very few gene-expression changes, however, were observed within this region at the earlier age of 4-months in rTg4510 mice. The authors attribute this relative lack of gene-expression changes at this younger age to the enrichment of neurones and low numbers of glial cells contained within these samples. Yet as we see in Figure 7.9., microglia do infiltrate the cell body layers of the hippocampus following the development of substantial tau pathology, prior to neurodegeneration.

Overall summary of the $_{LOW}$TAU and $_{HIGH}$TAU transgenic lines

Table 7.1. summarises existing transgenic models of tauopathy harbouring a single isoform of human tau carrying the P301L mutation. Included are the novel $_{LOW}$TAU and $_{HIGH}$TAU lines presented within this thesis, allowing for easy comparison of background strain, promoter and transgenic tau level. Below, the positive and negative aspects of both these transgenic lines are reviewed.

Line	Background Strain	Tau Isoform/ Mutation	Promoter	Transgenic Tau Level	Ref
JNPL3	C57Bl/DBA2/SW	4R0N/ P301L	mPrP	1x	(Lewis et al., 2000)
pR5	C57Bl/6	4R2N/ P301L	mThy-1.2	0.7x	(Gotz et al., 2001a)
Tau-4R/2N-P301L	FVB/N	4R2N/ P301L	mThy-1.2	4x	(Terwel et al., 2005)
rTg4510	FVB/N	4R0N/ P301L	CaMKIIα-Tet-Off	13x	(SantaCruz et al., 2005)
$_{LOW}$TAU	C56Bl/6J	4R0N/ P301L	CaMKIIα	4x	Unpublished
$_{HIGH}$TAU	C56Bl/6J	4R0N/ P301L	CaMKIIα	6.5x	Unpublished

Table 7.1. Comparison of $_{LOW}$TAU and $_{HIGH}$TAU animal models with common transgenic mouse models harbouring a single isoform of human tau carrying the P301L mutation. Transgenic tau levels are given as the level of transgenic human tau compared to endogenous murine tau. References are given for publications in which the line is first described. *mPrP* (murine prion protein).

Positive aspects of the $_{HIGH}$TAU and $_{LOW}$TAU lines:

- Molecular and histological characterisation confirmed that the human tau transgenes harboured by $_{LOW}$TAU and $_{HIGH}$TAU mice are functional, resulting in an ~1.6 times increase in human tau protein expression in $_{HIGH}$TAU animals, compared to the $_{LOW}$TAU line.

- Use of the CaMKIIα promoter removes complications caused by tau pathology within the spinal cord, as has been seen in other tauopathy models (Lewis et al., 2000), as well as producing a relatively similar spatial expression pattern as endogenous tau, with high expression in the cortex and hippocampus.
- The transgenic tau expressed in both lines is seen to form pathological species observed in human tauopathies, including conformationally altered (Weaver et al., 2000) and specifically phosphorylated species (Su et al., 1994) [http://cnr.iop.kcl.ac.uk/hangerlab/tautable (Hanger et al., 2009)].
- Both lines see the mislocation of pathological tau into the somatodendritic compartment in an age-dependent manner, going on to develop mature intracellular NFTs, which display a twisted, filamentous appearance.
- The pattern of pathology development and neurodegeneration within the hippocampus of $_{LOW}$TAU and $_{HIGH}$TAU animals is what may be predicted considering the overlapping spatial expression pattern of CaMKIIα and endogenous tau within the brain, and the specific neuronal vulnerability observed in tauopathies such as AD. In particular, the vulnerability of CA1 pyramidal neurones is modelled well in the $_{HIGH}$TAU line.
- Use of both $_{LOW}$TAU and $_{HIGH}$TAU animals concurrently provides an opportunity to study the dose-dependent effects of pathological tau development independent of age.
- While both the $_{LOW}$TAU and $_{HIGH}$TAU lines exhibit a less aggressive development of pathology and neurodegeneration compared to the rTg4510 model of tauopathy (for example, *rTg4510*: tau pathology 4.5/5m, neurodegeneration in CA1 (60%) 5.5m. *$_{HIGH}$TAU*: similar level of pathology within the hippocampus 13m, similar level of degeneration in CA1 (50%) 17.5m), this provides a longer time window in which to study the very earliest changes associated with tau dysfunction.
- Lastly, the $_{LOW}$TAU and $_{HIGH}$TAU models provide an alternative in a research area dominated by the use of the rTg4510 mouse model. There are of course disadvantages to the use of mouse models of disease, including: the use of non-physiological promoters to drive expression, uncertainty of the transgene integration site and often the high overexpression of the protein of interest. The existence of these disadvantages, however, means that the power of animal models lies in the use of multiple different lines and the identification of common dysfunctions.

Negative aspects of the $_{HIGH}$TAU and $_{LOW}$TAU lines:

- The development of pathology and neurodegeneration occur relatively slowly, even within the $_{HIGH}$TAU line. Due to the expense and time investment needed to age mice to the required level of pathological tau development, a more aggressive model may be preferred.
- The $_{LOW}$TAU and $_{HIGH}$TAU lines do not harbour the Tet-Off sequence required for the control of transgene expression, as is the case in other models of tauopathy (SantaCruz et al., 2005). Transgenic tau is thus continually expressed throughout development in these lines preventing experiments investigating the reversal of deficits following transgene suppression.

Conclusion

Within tauopathy research, and indeed dementia research in general, the common use of mouse models has been undeniably vital in extending our understanding of the aetiology of disease. The existence of a variety of models is however essential, particularly with regards to the development and testing of new treatments due to the heterogeneity of the human population and the limitations of individual models. Here I present two novel and complimentary transgenic mouse models of tauopathy. Both the $_{LOW}$TAU and $_{HIGH}$TAU transgenic lines are functional, producing dose- and age-dependent development of common pathological species of tau. The $_{LOW}$TAU line exhibits an extensive NFT burden within the hippocampus by 24 months of age, with no neurodegeneration observed up until this age. The $_{HIGH}$TAU line presents an extensive NFT load by 13 months of age, at which point the very first indications of cell loss within the CA1 region are noted. During the following 4 to 7 months $_{HIGH}$TAU animal pathology advances rapidly, culminating in the presentation of a moribund phenotype common to transgenic tauopathy models carrying the P301L mutation (Lewis et al., 2000, Ramsden et al., 2005, Terwel et al., 2005). At this point these mice exhibit significant neurodegeneration within the hippocampus, with >50% loss of CA1 pyramidal neurones. This cell loss is likely the consequence of a rise in programmed cell death, as indicated by the increase in expression of genes relating to apoptosis.

It is unfortunate that the $_{HIGH}$TAU line was found to represent only a small proportion of the total TauD35 transgenic animals, and that without prior knowledge of two separate transgenic lines and thus selective breeding, $_{HIGH}$TAU numbers continued to decline. This resulted in a disappointingly low sample number of $_{HIGH}$TAU mice for

many experiments, complicating the ability to draw definitive conclusions. Despite this, particular experiments did indicate functional changes in $_{HIGH}$TAU mice compared to WT and $_{LOW}$TAU animals particularly at 13 months of age, when a large difference in NFT pathology existed between the two transgenic lines. This included a likely reduction in Pr at SC-CA1 synapses, changes in AMPA-R kinetics, as well as an inability to habituate, apparent reduction in anxiety-like behaviour and presentation of disinhibition. $_{HIGH}$TAU animals of 13-months also presented with a decrease in the contribution of NMDA-Rs to the induction of LTP, possibly via disruption to the insertion and/or anchoring of NMDA-Rs to the PSD, depletion of the scaffold protein, PSD-95, or through influencing gene-expression. As is suggested by Warmus et al., (2014), boosting NMDA-R function via use of the Food and Drug Administration–approved NMDA-R co-agonist cycloserine for example, may prove a beneficial treatment for neurodegenerative tauopathy disorders. The efficacy of the compensation of the reduction in NMDA-R-dependent LTP may, however, underlie the resistance of transgenic mice (and by inference, people with AD) to cognitive dysfunction until late in disease progression.

Despite the fact that the majority of functional changes within the hippocampus corresponded to the manifestation of significant numbers of NFTs, it is not suggested that the presence of NFTs results in these changes. Taking the reduction in Pr at the SC-CA1 synapse seen in $_{HIGH}$TAU mice at 13–months compared to $_{LOW}$TAU mice of the same age, one may reason that this reduction is due to the substantial increase in NFTs displayed by the $_{HIGH}$TAU line. Yet, in studying PPR in $_{LOW}$TAU mice at 24-months we observe no indication of a deficit in Pr, despite the extensive NFT load present. It is therefore possible that the increased overexpression of mutated human tau in $_{HIGH}$TAU mice brings about a rise in soluble pathological tau that may cause any toxicity seen. Indeed, one of the earliest functional changes, a reduction in the Pr of mPP synapses, was found to occur prior to NFT development in either transgenic line at 4 months of age. This result indicates that changes in synaptic transmission can occur prior to the development of aggregates in cell groups vulnerable to tau dysfunction.

There is also a significant rise in the expression of immune genes at an age displaying substantial neurodegeneration in the $_{HIGH}$TAU line, with a particular emphasis on components of the complement cascade, paralleling data from a separate, similar model of tauopathy (Wes et al., 2014). However, it is also apparent that an upregulation of microglia is present prior to cell loss in $_{HIGH}$TAU animals, suggesting that the increase in

the immune system may not simply be a consequence of cell death. It is therefore proposed that microglial activation in tauopathy disorders occurs prior to neurodegeneration, but only after pathology has matured to a point at which pathological tau is released from neurones, or neurones begin expressing a pathological signal. At this point, microglia begin to infiltrate the cell layer where they may influence cell survival.

In contrast to $_{HIGH}$TAU mice, a significant rise in immune gene-expression and substantial upregulation of microglia was also observed in the TASTPM mouse model of amyloid-β dysfunction at an early stage, in a manner directly relating to plaque load (Matarin et al., 2015). TASTPM mice do not, however, go on to display neurodegeneration. These data may suggest as an extracellular protein, amyloid-β is able to trigger an early increase in the immune response in TASTPM mice. Interestingly, in this model, microglia are not seen to infiltrate the cell body layers of the hippocampus, tending instead to associate with plaques. It is possible that this disparity in the location of increased microglia between models of tau and amyloid-β dysfunction alters their effect on neuronal survival. Potential differences in the consequential actions of microglia between activation by pathological tau or amyloid-β may also alter their contribution to neurodegeneration.

In addition to the increased expression of elements of the complement cascade, other key genes associated with the immune response were found to be increased in both $_{HIGH}$TAU animals and the TASTPM model of rising amyloid-β (Matarin et al., 2015), including certain genes highlighted as risk factors for the development of AD through genome-wide association studies in humans. These included: *Trem2* (Guerreiro et al., 2013, Jonsson et al., 2013), *Cd33* (Naj et al., 2011) and *Inpp5d* (Lambert et al., 2013), which all play a role in the regulation or coordination of microglial activation. Together, these data highlight that the upregulation of the immune system provides a common event in animals modelling aspects of neurodegenerative disease, as well as lending support to the idea that modulating microglial activation may provide a potential therapeutic target for this class of disease (McGeer and McGeer, 2015). Microglia are indeed known to modulate synaptic function (Heneka et al., 2014), suggesting that changes in synaptic transmission resulting in the behavioural alterations such as disinhibition or a reduction in habituation may be the consequence of the upregulation of microglia in $_{HIGH}$TAU mice of 13-months preceding cell loss. In contrast, deficits in overall cognitive function may be resistant to these changes, and are thus not observed prior to substantial neurodegeneration.

APPENDIX 1

An introduction to the theory of electrophysiology

Whole-cell patch clamp recordings

Original work published by Neher and Sakmann (1976) paved the way for modern electrophysiology. Here, they described a technique that allowed them to resolve single channel currents across a patch of membrane of frog skeletal muscle. In the following years the technique was refined, creating improved resolution (produced via generation of a 'gigaohm (GΩ) seal' between the glass pipette tip and the cell membrane) as well as various different cell-free and cell-attached recording configurations (Hamill et al., 1981).

The present study used the whole-cell voltage clamp configuration. In order to obtain this configuration; following the generation of a GΩ seal, the patch of membrane below the patch pipette is ruptured. This creates continuity between the cell and recording electrode located within the patch pipette. A ground electrode located within the extracellular solution is used to set the potential difference between the intracellular and bath solutions. The cell is 'clamped' to a defined voltage using a differential amplifier connected to the recording electrode. The membrane potential is continuously compared to the command voltage, and upon alterations in membrane potential (caused by the opening of ion channels), the differential amplifier passes an equal compensatory current. This compensatory current is recorded as representative of membrane conductance.

Use of the acute hippocampal slice for patch clamp recordings, (without the need for enzyme treatment) was first described by Edwards et al., (1989). In contrast to the isolated cell preparations used prior to this, the acute slice allowed recordings to be made in the context of their endogenous surroundings, preserving network connections. Use of the acute preparation therefore allows for a more 'true' measurement of spontaneous activity received by the target cell (that is the spontaneous activity of the neuronal network generated by either spontaneous action potential firing or spontaneous quantal release). *It is of course noted that acute slices do not fully represent physiological activity, however, they do provide improvements on isolated cell recordings and indeed*

aim to detect any changes that may be relevant physiologically. In addition all genotypes are investigated under the same conditions, allowing for reliable comparisons. In using whole-cell voltage clamp techniques to record spontaneous activity, we are able to infer certain information about the presynaptic network within which this cell lies; such as, the frequency of action potential (AP) driven neurotransmitter release, number of release sites (n) and the neurotransmitter release probability of individual synapses (Pr). Certain postsynaptic conclusions may also be deduced, including basic cell properties and changes in neurotransmitter receptor density and conductance (based on quantal size (q) determined by miniature amplitude).

Conclusions involving the n, Pr and q are made based on the quantal theory of neurotransmitter release developed during the 1950s (Del Castillo and Katz, 1954). While the theory was developed using the neuromuscular junction, its central ideas hold true for the fast central synapses under investigation in the present study. The theory is based on the idea that a single vesicle of neurotransmitter is the minimum amount available for release at a synapse, with all vesicles containing approximately the same amount of a specific neurotransmitter.

By inhibiting AP firing using a sodium channel blocker, one can record the postsynaptic currents resulting from the spontaneous release of single quantum, known as miniature excitatory postsynaptic currents (mEPSCs). In contrast to the neuromuscular junction, one vesicle of neurotransmitter at fast central synapses is enough to cause near saturation of the relatively small number of postsynaptic receptors available (Edwards, 1995). It therefore follows that the amplitude of miniature currents (or quantal size, q) is determined by the density and conductance of these postsynaptic receptors, as an increase in release would bear little effect on the size of the response. The frequency at which these events occur infers information about the n and Pr of the afferents contacting the target cell.

Evoked currents using whole-cell patch clamp recordings

In addition to recording spontaneous activity, one can also record a response in the target cell by stimulating afferent fibres impinging on it. By applying two stimuli in close succession, and varying the time between the two pulses, one can calculate the paired-pulse ratio (PPR) of the synapse under study, as well as determining the interval time at which the stimuli cease interacting. This ratio is calculated using the amplitude of the

two evoked postsynaptic current responses, and provides insight into the Pr of the presynaptic site.

The ratio calculated can reveal both a facilitation of the second response (termed paired-pulse facilitation (PPF)), or a reduction (termed paired-pulse depression (PPD)). The basic theory behind what causes either PPF or PPD is based on the residual calcium (Ca^{2+}) and neurotransmitter vesicle availability resulting from the original Pr of that synapse (reviewed in: (Zucker, 1989, Zucker and Regehr, 2002)).

For a group of synapses with an inherently low Pr (such as SC-CA1 synapses), the first pulse causes neurotransmitter release from only a small number of synapses. If the second pulse is delivered within a very short time frame (i.e. within 400ms), residual Ca^{2+} from the first stimulation remains within the presynaptic terminals. This is additive to the Ca^{2+} influx for the second pulse, resulting in neurotransmitter release from a greater number of synapses, and thus a larger postsynaptic current is recorded. The synapse has seen an increase in the reliability of release. For synapses with a high Pr, the first pulse will cause a depletion of the synaptic vesicles. While residual Ca^{2+} from the first response remains, the exhaustion of vesicles from the readily releasable pool of neurotransmitter results in a reduction in the size of the second response.

This residual Ca^{2+} hypothesis, while most popular, provides a simplistic view of the cause of PPF and PPD, and in fact, the grounds for short-term plasticity (in particular for PPD) are likely exceedingly more complicated. Zucker and Regehr (2002) provide a detailed discussion of further contributing factors to PPD, including the role of metabotropic receptors, retrograde messengers, postsynaptic receptor desensitization and glial cell contributions.

Extracellular field recordings

Using the acute slice preparation, electrodes are placed extracellularly within the stratum radiatum of the CA1 area. Here, the stimulating electrode is able to elicit an AP in the SC axons of CA3 neurones, which can be recorded as a postsynaptic potential response from CA1 apical dendrites. Extracellular recording allows one to record the responses of a population of neurones, creating a 'field' potential. As the synapses under study use glutamate as the principle neurotransmitter, the responses recorded are known as field excitatory postsynaptic potentials or fEPSPs. Here, the postsynaptic responses are recorded as negative voltage deflections due to the current 'sink' of positive ions

(namely sodium ions, Na^{2+}) created by the opening of glutamate receptor ion channels. By using a linear slope fit to the initial portion (10-50%) of the slope as a measure proportional to the response amplitude, we exclude possible interference from slower polysynaptic potentials, and thus this measure primarily reflects activation of the postsynaptic fast ionotropic AMPA-Rs. This method of analysis also excludes contamination caused by the firing of the target cells, known as a population spike. This population spike can be seen as an upward voltage deflection in the postsynaptic response, resulting from the current sink created near the cell body region and consequential passive current source in the dendritic (recording) region.

I have exploited extracellular field recordings within this project to gain some understanding of synaptic plasticity within TauD35 mice at various ages. For studies into the long-term potentiation of synapses (discussed below), the ability to record extracellulary from a population of neurones provides benefits over single cell patch recordings. One large advantage lies in removing the consequence of intracellular washout produced by the use of whole-cell patch clamp techniques. Following the rupture of the area of membrane underneath the patch pipette, cell dialysis commences. Due to the large volume of intracellular pipette solution in comparison to the volume of intracellular cytosol, over time (<10 minutes) the cytosol is completely replaced with the pipette solution. This washout has large consequences on the maintenance (and possibly even induction, depending on the timing of stimulation) of long-term changes in synaptic transmission, due to the loss of essential kinases and other components of intracellular signaling cascades (discussed below). Alternatives to this problem lie in other forms of patch clamp recordings, such as perforated patch or intracellular recordings; however, these techniques allow only synaptic changes in a single cell to be recorded. Extracellular field recordings allow for changes in a population of neurones, in response to a given stimulus, to be recorded as a whole.

Following the establishment of a stable baseline response and application of a high-frequency tetanus, fEPSPs were recorded within the present study for 1 hour. The responses recorded post-tetanus can be divided temporally as: post-tetanic potentiation (PTP), defined as the 1st minute; short-term potentiation (STP), defined as 8-12 minutes; and LTP, defined as 51-60 minutes after induction (Figure A.1.).

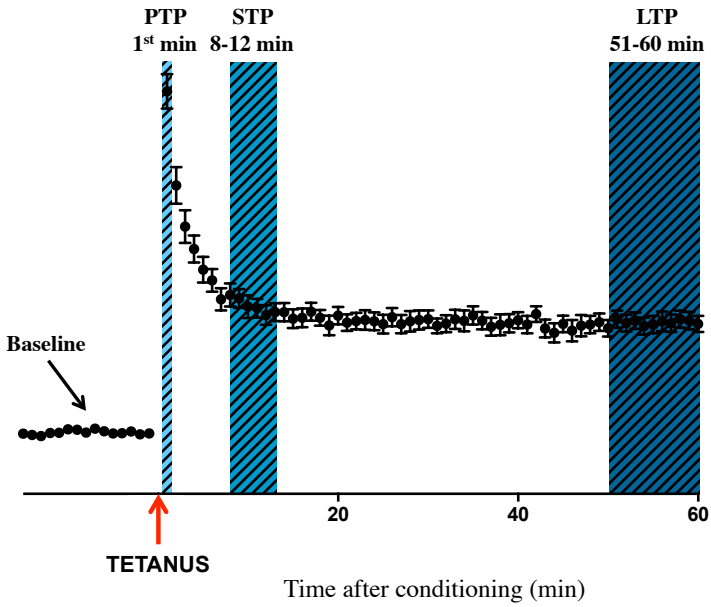

Figure A.1. Representative figure of a typical extracellular LTP recording from the SC-CA1 synapse. A stable baseline is established for 15 minutes prior to application of high-frequency tetanic stimulation. Responses post-tetanus are divided temporally as PTP (1st minute), STP (8-12 minutes) and LTP (51-60 minutes). Error bars indicate SEM.

PTP is observed as a large, and quickly decaying (<60s (Malenka, 1991)), increase in synaptic transmission occurring immediately post-tetanus. Previous experiments have established the resistance of PTP to NMDA-R antagonists (Malenka, 1991), and along with the observed decrease in PPR during PTP, it is agreed that this potentiation is result of residual Ca^{2+} within the presynaptic terminal.

The story is, however, a little more complicated when looking at STP, with no consensus about what constitutes STP yet established. Recent attempts at clarifying this issue have split STP into two parts, distinguished pharmacologically, named STP1 and STP2 (Park et al., 2014). They conclude that STP1 may represent an early decremental form of LTP in that it requires NMDA-Rs composed of the same subunits (GluN2A and GluN2B) as those involved in LTP. This opinion, that STP represents an unstable part of LTP was often argued previously, however, Park et al., (2014) extend this, claiming a second component (STP2) dependent on NMDA-Rs formed from a different composition of subunits, namely GluN2B and GluN2D, also contributes to STP. The subunit combinations of NMDA-Rs contributing STP2 are not expressed within the synapse; this, along with observed changes in PPR during STP, complements the theory that this component of STP may be expressed presynaptically. Both forms of STP are highly dependent on induction protocol and the frequency of stimuli post-tetanus used to monitor synaptic transmission, with the number of monitoring (test) stimuli leading to the decay of STP. Park et al., (2014) used a theta-burst stimulation protocol to induce potentiation, followed by test stimulation at a frequency of 0.067Hz, concluding that STP1 decayed with a time constant of 7 minutes (~28 stimuli), whereas STP2 decayed more slowly, with a time constant of 16 minutes (~64 stimuli). The high frequency

tetanus used in the present study is perhaps more conducive of STP than the theta-burst protocol utilised by Park et al., (2014); however, following LTP induction, transmission is monitored using a stimulation frequency (paired stimuli 50ms apart) of 0.1Hz. This test frequency would predict a more rapid decay time constant of STP than reported by Park et al., (2014), of approximately 5 minutes for STP1 and 11 minutes for STP2, with the paired stimuli likely altering these estimates. It is also possible the slightly lower recording temperature used in the present study (32.5 vs. 30±1°C) may also affect these decay times. Indeed a decremental potentiation is observed in the present LTP studies <15 minutes. STP is thus defined within the present experiments as the potentiation observed between 8 and 12 minutes post-tetanus. In addition to analysis of PTP (the first minute), this allows an overview of short-term forms of plasticity, prior to stabilization. The final 10 minutes of recording (51-60 minutes) was taken as a measure of LTP (discussed below).

Long-term potentiation

Long-term potentiation (LTP) describes one of the most important forms of experimental synaptic plasticity, providing one of the best ways in which to study the neuronal capability of long-lasting alterations likely used in learning and memory.

Bliss and Lømo first discovered LTP in 1973 (Bliss and Lømo, 1973). Using both anaesthetized (Bliss and Lømo, 1973) or awake (Bliss and Gardner-Medwin, 1973) rabbits, Bliss, Lømo and Gardner-Medwin showed that extracellular application of high-frequency electrical stimulation to the perforant path enhanced synaptic transmission, for hours and days respectively, between the stimulated axons and DG granule cells. The presynaptic stimulation applied caused persistent postsynaptic activity, sufficient to cause long-lasting changes to the postsynaptic response. Thus, these experiments supported the theory postulated in 1949 by Donald Hebb, that:

> '*When an axon of cell A is near enough to excite a cell B and repeatedly or persistently takes part in firing it, some growth process or metabolic change takes place in one or both cells such that A's efficiency, as one of the cells firing B, is increased*' (Hebb, 1949).

Properties of LTP

Since its discovery, it has become clear that the cellular mechanisms leading to the phenomenon of LTP can vary hugely; depending on the neuronal circuit, or indeed

synapse within which it is operating, the age or time point being studied and possibly even the induction protocol used. Still today, controversy also surrounds whether LTP is expressed via pre- or postsynaptic mechanisms (discussed in Bliss and Collingridge, 2013). It has been suggested that both LTP and its opposing partner long-term depression (LTD), may be better thought of as general classes of synaptic phenomena, varying widely in the specific forms expressed (Malenka and Bear, 2004); and dependent on experimental situations, LTP can be expressed by both pre- or postsynaptic mechanisms.

Below I review the widely accepted theory of NMDA-R-dependent LTP. This type of LTP is generally understood to underlie potentiation between CA1 and CA3 neurones at the SC-CA1 synapse (Collingridge et al., 1983, Malenka, 1991) and is by far the most extensively studied with regard to this diverse phenomenon. Other forms of LTP, which do not rely on the activation of NMDA-Rs (NMDA-R-independent forms), are discussed briefly.

Properties of NMDA-R-dependent LTP

LTP has, over the years, been so often described in terms of three basic properties: input specificity, cooperativity and associativity (Bliss and Collingridge, 1993). Input specificity describes that only synapses active at the time of stimulation are potentiated, LTP is not shown by neighbouring synapses that were not activated by the stimulation. In fact, the two terms cooperativity and associativity describe the same phenomenon, mistakenly interpreted (McNaughton, 2003) from the 1978 publication by McNaughton and Douglas. Indeed both describe the necessity of the induction stimulus of LTP to be supra-threshold. Be this via the ability of a 'strong' stimulus at a single site to induce the 'cooperation' of many afferents, or the application of a 'weak' and 'strong' stimulation to separate but convergent inputs 'associating' to result in LTP. We find that this cooperative/ associative property of LTP was alluded to in Hebb's postulate. The phrases, '*...takes part in firing it'* and '*...as one of the cells firing B'* suggests the idea that an input may be strengthened by way of other inputs.

During the 1980s Hebb's postulate received further support with a major discovery that gave the theory a molecular basis. Using a newly developed antagonist, specific for NMDA-Rs (2-amino-5-phosphonopentanoate, AP5) Collingridge et al., (1983) showed that, while blocking NMDA-Rs had no effect on basal synaptic transmission, or the

maintenance of already established LTP, it reversibly blocked the induction of LTP. This finding fuelled much research into NMDA-Rs and, by the end of the decade, much had been learnt about how this receptor worked. Crucial was the discovery that Mg^{2+} ions work to block the ion channel pore of the NMDA-R during basal synaptic transmission (Coan and Collingridge, 1985) and that this block is voltage-dependent (Nowak et al., 1984). This allows the NMDA-R to act as a coincidence detector, requiring presynaptic activity for glutamate release, along with sufficient postsynaptic depolarization to release the Mg^{2+} block. This 'sufficient postsynaptic depolarization' is described by the properties of cooperativity/ associativity and captured by the common reduction of Hebb's postulate: '*cells that fire together, wire together*'. Input specificity is also given a mechanistic explanation, with the fact that depolarization is not enough to activate the NMDA-R; rather, it also requires the binding of glutamate, a process that provides synapse specificity.

Induction and expression mechanisms of postsynaptic NMDA-R-dependent LTP

As we have seen, the opening of the NMDA-R is reliant on sufficient depolarization of the postsynaptic membrane (by way of other glutamate receptors), allowing the release of Mg^{2+} from the ion pore at the centre of the receptor, along with the binding of glutamate (and glycine, usually ignored due to its high abundance) to the extracellular portion. Once open, the receptor permits the flow of Ca^{2+} (as well as Na^{+} and K^{+}) into the cell. This rise in intracellular Ca^{2+} is known to be essential in the initiation of LTP; however, from this point, definitive answers on the required intracellular signalling components become a little hazier.

It is however agreed, that the Ca2+/calmodulin-dependent protein kinase (CaMKII) plays a key role in the production of postsynaptic NMDA-R-dependent LTP. The influx of Ca^{2+} through the NMDA-R results in Ca^{2+} binding to calmodulin. This complex then binds CaMKII, leading to a conformational change in the kinase allowing for its auto-phosphorylation. The resultant activated form of CaMKII is then able to instigate various downstream effects, within its activation period of approximately 1 minute (Lisman et al., 2012). One consequence of CaMKII activation is its binding to the GluN2B subunit of the NMDA-R (Strack and Colbran, 1998). This interaction anchors active CaMKII at the synapse, where it is therefore available to cause the phosphorylation of the GluA1 subunit of the AMPA-R (Mammen et al., 1997), increasing conductance through the receptor. Active CaMKII can also lead to an increase in the numbers of synaptic AMPA-

Rs, possibly via the phosphorylation of stargazin (an AMPA-R auxiliary protein), which allows the AMPA-Rs to bind to PSD-95, and thus captures extrasynaptic AMPA-Rs that have diffused into the synapse (Opazo et al., 2010). It is thus either the phosphorylation of existing AMPA-Rs or an increase in the number of synaptic AMPA-Rs (through insertion or capturing of extracellular receptors) that CaMKII is proposed to potentiate the postsynaptic response.

In addition to the enhancement of AMPA-R conductance at active synapses after potentiation, previously inactive 'silent' synapses can also be uncovered. This collection of synapses are described as silent due to an absence of excitatory postsynaptic currents (EPSCs), which has been argued to be caused by both pre- and postsynaptic factors depending on the synapse under study (reviewed by (Kerchner and Nicoll, 2008)). At hippocampal SC-CA1 synapses, evidence suggests the cause of the silence is due to a lack of postsynaptic AMPA-Rs (Isaac et al., 1995, Liao et al., 1995). Upon sub-threshold stimulation paired with postsynaptic depolarization, a slow, AP5-sensitive EPSC could be detected, indicating the lone expression of NMDA-Rs. During the high-intensity stimulation needed for LTP induction, the mechanisms described above come into play, with postsynaptic depolarization releasing the Mg^{2+} block from the NMDARs allowing Ca^{2+} influx. The subsequent activation of CaMKII results in the insertion of AMPA-Rs into the postsynaptic density (PSD), leading to the appearance of AMPA-R mediated EPSCs at this synapse.

The roles of other kinases implicated in the induction of LTP are less well established, and it is unknown whether their presence is required, or if they only act to modify LTP. Protein kinase A (PKA or cAMP-dependent protein kinase) is believed to enhance CaMKII auto-phosphorylation through the inhibition of protein phosphatase 1. Protein kinase C (PKC), in particular in its constitutively active form PKMξ, has also been proposed as essential for LTP. While Ca^{2+} influx also activates Ras, a small G-protein, which works to trigger the mitogen-activated protein kinase (MAPK) cascade, thought to be important in LTP (Malenka and Bear, 2004).

The mechanisms described so far explain a brief and simplified view on the procedures involved in the induction of LTP. These mechanisms are responsible for the increase in synaptic strength lasting up to 1 hour, and hence cover the period of time looked at within the present study.

The mechanisms allowing LTP to last for days require gene transcription and the synthesis of new protein. Various kinases are thought to link activity (and the subsequent Ca^{2+} rise) to the nucleus. Here they activate CREB, a key transcription factor in the maintenance of LTP. From this point, many morphological changes have been reported, including the growth of new dendritic spines as well as the enlargement of existing spines (discussed in (Malenka and Bear, 2004).

NMDA-R-independent LTP: induction and expression

Although the majority of studies have concentrated on investigating NMDA-R-dependent forms of LTP, due to the wide variation in experimental preparation and protocol used, it is perhaps not surprising that some studies have reported forms of LTP independent of the NMDA-R.

Using AP5, the same NMDA antagonist used by Collingridge et al., (1983) to demonstrate the NMDA-R-dependency of LTP, Grover and Teyler (1990) uncovered another component of LTP at SC-CA1 synapses, seemingly NMDA-R independent. This LTP component was reliant on increases in intracellular Ca^{2+}, was dependent on stimulation frequency and only partially blocked by AP5. To test their theory that another channel could be responsible for the necessary rise in intracellular Ca^{2+} they applied the L-type voltage-gated calcium channel (VGCC) antagonist, nifedipine. Indeed, this fully ablated the remaining LTP seen after AP5 application. Due to the necessity of increased intracellular Ca^{2+}, it was proposed that this form of LTP is maintained through the Ca^{2+}-dependent mechanisms required for NMDA-R-dependent LTP. Later studies, however, discounted the possibility that both forms of LTP are maintained by exactly the same mechanisms, although some interaction between signalling pathways may occur (Grover and Teyler, 1995, Cavus and Teyler, 1996). Indeed, both NMDA-R-dependent and VGCC-dependent LTP have since been demonstrated *in vivo,* where they have shown to result in additive potentiation at SC-CA1 synapses (Morgan and Teyler, 1999). The contribution of VGCCs on the induction of LTP at the SC-CA1 synapse is reliant on the intensity of stimulation protocol (Grover and Teyler, 1990) and may also alter with age (Shankar et al., 1998), providing some explanation for contradictory results when investigating LTP induction even at one synapse.

Variations in the synapse studied can also result in differences in the forms of LTP induction. The mossy fibre synapses onto CA3 pyramidal cells are one such example of this (Harris and Cotman, 1986). The mechanisms that have been proposed to explain the induction of LTP at these synapses revolve around an NMDAR-independent method, possibly involving a requirement for presynaptic metabotropic glutamate receptors as well as kainate receptors (reviewed by Bortolotto et al., 2005 and Nicoll and Schmitz, 2005).

While some controversy still surrounds the induction of LTP at the mossy fibre-CA3 synapse, it is widely agreed that LTP is expressed presynaptically, via an increase in Pr resulting from the likely involvement of an increase in cyclic adenosine monophosphate (Nicoll and Schmitz, 2005). These examples show us that the induction and expression of LTP are not as straight forward as just postsynaptic NMDAR-dependent LTP.

Paired-pulse ratio as an indicator of the site of LTP expression

As we have seen, the application of two stimuli in close succession allows one to calculate the PPR, with this ratio granting insight into the Pr of the synapse under study. For the PPR experiments discussed so far, the interval between the two stimuli is altered, allowing insight into the temporal properties of the resultant facilitation or depression. For the LTP recordings performed for this thesis, however, two stimuli were applied to the pathway at a constant interval of 50ms throughout the duration of the recording, both prior to and post tetanic stimulation. Analyzing the PPR in this way provides some indication as to whether short- and long-term changes in synaptic transmission are the result of a change in presynaptic Pr (McNaughton, 1982). A lack of change in PPR would therefore indicate that any alteration in synaptic transmission is due to postsynaptic modifications.

Immediately following the application of the high frequency tetanus, it is characteristic to observe a reduction in PPR (Park et al., 2014). In the present study, this reduction in ratio returns to baseline over approximately 15-20 minutes, corresponding to a decrease in synaptic potentiation described as PTP and STP. The change in PPR during this time reveals the presynaptic nature of PTP (as well as possibly STP (*ibid*)), in that the synaptic potentiation witnessed is a result of increased glutamate release.

References

Abramov E, Dolev I, Fogel H, Ciccotosto GD, Ruff E, Slutsky I (2009) Amyloid-beta as a positive endogenous regulator of release probability at hippocampal synapses. Nat Neurosci 12:1567-1576.

Adams SJ, Crook RJ, Deture M, Randle SJ, Innes AE, Yu XZ, Lin WL, Dugger BN, McBride M, Hutton M, Dickson DW, McGowan E (2009) Overexpression of wild-type murine tau results in progressive tauopathy and neurodegeneration. Am J Pathol 175:1598-1609.

Aggleton JP, Hunt PR, Rawlins JN (1986) The effects of hippocampal lesions upon spatial and non-spatial tests of working memory. Behavioural brain research 19:133-146.

Aguzzi A, Rajendran L (2009) The transcellular spread of cytosolic amyloids, prions, and prionoids. Neuron 64:783-790.

Albrecht S, Bourdeau M, Bennett D, Mufson EJ, Bhattacharjee M, LeBlanc AC (2007) Activation of caspase-6 in aging and mild cognitive impairment. Am J Pathol 170:1200-1209.

Alonso Adel C, Li B, Grundke-Iqbal I, Iqbal K (2006) Polymerization of hyperphosphorylated tau into filaments eliminates its inhibitory activity. Proc Natl Acad Sci U S A 103:8864-8869.

Alonso Adel C, Mederlyova A, Novak M, Grundke-Iqbal I, Iqbal K (2004) Promotion of hyperphosphorylation by frontotemporal dementia tau mutations. J Biol Chem 279:34873-34881.

Ando K, Leroy K, Heraud C, Yilmaz Z, Authelet M, Suain V, De Decker R, Brion JP (2011) Accelerated human mutant tau aggregation by knocking out murine tau in a transgenic mouse model. Am J Pathol 178:803-816.

Andorfer C, Kress Y, Espinoza M, de Silva R, Tucker KL, Barde YA, Duff K, Davies P (2003) Hyperphosphorylation and aggregation of tau in mice expressing normal human tau isoforms. J Neurochem 86:582-590.

Arendt T, Bullmann T (2013) Neuronal plasticity in hibernation and the proposed role of the microtubule-associated protein tau as a "master switch" regulating synaptic gain in neuronal networks. Am J Physiol Regul Integr Comp Physiol 305:R478-489.

Arendt T, Stieler J, Strijkstra AM, Hut RA, Rudiger J, Van der Zee EA, Harkany T, Holzer M, Hartig W (2003) Reversible paired helical filament-like phosphorylation of tau is an adaptive process associated with neuronal plasticity in hibernating animals. J Neurosci 23:6972-6981.

Arrasate M, Mitra S, Schweitzer ES, Segal MR, Finkbeiner S (2004) Inclusion body formation reduces levels of mutant huntingtin and the risk of neuronal death. Nature 431:805-810.

Arriagada PV, Growdon JH, Hedley-Whyte ET, Hyman BT (1992) Neurofibrillary tangles but not senile plaques parallel duration and severity of Alzheimer's disease. Neurology 42:631-639.

Augustinack JC, Schneider A, Mandelkow EM, Hyman BT (2002) Specific tau phosphorylation sites correlate with severity of neuronal cytopathology in Alzheimer's disease. Acta Neuropathol 103:26-35.

Avila J, Lucas JJ, Perez M, Hernandez F (2004) Role of tau protein in both physiological and pathological conditions. Physiol Rev 84:361-384.

Ballatore C, Lee VM, Trojanowski JQ (2007) Tau-mediated neurodegeneration in Alzheimer's disease and related disorders. Nat Rev Neurosci 8:663-672.

Bancher C, Brunner C, Lassmann H, Budka H, Jellinger K, Wiche G, Seitelberger F, Grundkeiqbal I, Iqbal K, Wisniewski HM (1989) Accumulation of Abnormally Phosphorylated-Tau Precedes the Formation of Neurofibrillary Tangles in Alzheimers-Disease. Brain Res 477:90-99.

Berger Z, Roder H, Hanna A, Carlson A, Rangachari V, Yue M, Wszolek Z, Ashe K, Knight J, Dickson D, Andorfer C, Rosenberry TL, Lewis J, Hutton M, Janus C (2007) Accumulation of pathological tau species and memory loss in a conditional model of tauopathy. J Neurosci 27:3650-3662.

Berriman J, Serpell LC, Oberg KA, Fink AL, Goedert M, Crowther RA (2003) Tau filaments from human brain and from in vitro assembly of recombinant protein show cross-beta structure. Proc Natl Acad Sci U S A 100:9034-9038.

Bertrand A, Khan U, Hoang DM, Novikov DS, Krishnamurthy P, Rajamohamed Sait HB, Little BW, Sigurdsson EM, Wadghiri YZ (2013) Non-invasive, in vivo monitoring of neuronal transport impairment in a mouse model of tauopathy using MEMRI. NeuroImage 64:693-702.

Bertrand J, Plouffe V, Senechal P, Leclerc N (2010a) The pattern of human tau phosphorylation is the result of priming and feedback events in primary hippocampal neurons. Neuroscience 168:323-334.

Bertrand J, Senechal P, Zummo-Soucy M, Plouffe V, Leclerc N (2010b) The formation of tau pathological phospho-epitopes in the axon is prevented by the dephosphorylation of selective sites in primary hippocampal neurons over-expressing human tau. J Neurochem 114:1353-1367.

Bhaskar K, Yen SH, Lee G (2005) Disease-related modifications in tau affect the interaction between Fyn and Tau. J Biol Chem 280:35119-35125.

Binder LI, Frankfurter A, Rebhun LI (1985) The distribution of tau in the mammalian central nervous system. J Cell Biol 101:1371-1378.

Bird TD, Nochlin D, Poorkaj P, Cherrier M, Kaye J, Payami H, Peskind E, Lampe TH, Nemens E, Boyer PJ, Schellenberg GD (1999) A clinical pathological comparison of three families with frontotemporal dementia and identical mutations in the tau gene (P301L). Brain 122 (Pt 4):741-756.

Blennow K, de Leon MJ, Zetterberg H (2006) Alzheimer's disease. Lancet 368:387-403.

Bliss TV, Collingridge GL (1993) A synaptic model of memory: long-term potentiation in the hippocampus. Nature 361:31-39.

Bliss TV, Collingridge GL (2013) Expression of NMDA receptor-dependent LTP in the hippocampus: bridging the divide. Mol Brain 6:5.

Bliss TV, Gardner-Medwin AR (1973) Long-lasting potentiation of synaptic transmission in the dentate area of the unanaestetized rabbit following stimulation of the perforant path. J Physiol 232:357-374.

Bliss TV, Lømo T (1973) Long-lasting potentiation of synaptic transmission in the dentate area of the anaesthetized rabbit following stimulation of the perforant path. J Physiol 232:331-356.

Boccara CN, Sargolini F, Thoresen VH, Solstad T, Witter MP, Moser EI, Moser MB (2010) Grid cells in pre- and parasubiculum. Nat Neurosci 13:987-994.

Boehm J (2013) A 'danse macabre': tau and Fyn in STEP with amyloid beta to facilitate induction of synaptic depression and excitotoxicity. Eur J Neurosci 37:1925-1930.

Bolivar VJ (2009) Intrasession and intersession habituation in mice: from inbred strain variability to linkage analysis. Neurobiology of learning and memory 92:206-214.

Bolmont T, Clavaguera F, Meyer-Luehmann M, Herzig MC, Radde R, Staufenbiel M, Lewis J, Hutton M, Tolnay M, Jucker M (2007) Induction of tau pathology by intracerebral infusion of amyloid-beta -containing brain extract and by amyloid-beta deposition in APP x Tau transgenic mice. Am J Pathol 171:2012-2020.

Bortolotto ZA, Nistico R, More JC, Jane DE, Collingridge GL (2005) Kainate receptors and mossy fiber LTP. Neurotoxicology 26:769-777.

Bourin M, Hascoet M (2003) The mouse light/dark box test. European journal of pharmacology 463:55-65.

Braak H, Braak E (1991) Neuropathological stageing of Alzheimer-related changes. Acta Neuropathol 82:239-259.

Braak H, Braak E (1997) Frequency of stages of Alzheimer-related lesions in different age categories. Neurobiol Aging 18:351-357.

Braak H, Del Tredici K (2011a) Alzheimer's pathogenesis: is there neuron-to-neuron propagation? Acta Neuropathol 121:589-595.

Braak H, Del Tredici K (2011b) The pathological process underlying Alzheimer's disease in individuals under thirty. Acta Neuropathol 121:171-181.

Braak H, Thal DR, Ghebremedhin E, Del Tredici K (2011) Stages of the pathologic process in Alzheimer disease: age categories from 1 to 100 years. J Neuropathol Exp Neurol 70:960-969.

Brager DH, Cai X, Thompson SM (2003) Activity-dependent activation of presynaptic protein kinase C mediates post-tetanic potentiation. Nat Neurosci 6:551-552.

Brandt R, Leger J, Lee G (1995) Interaction of tau with the neural plasma membrane mediated by tau's amino-terminal projection domain. J Cell Biol 131:1327-1340.

Brion JP, Smith C, Couck AM, Gallo JM, Anderton BH (1993) Developmental changes in tau phosphorylation: fetal tau is transiently phosphorylated in a manner similar to paired helical filament-tau characteristic of Alzheimer's disease. J Neurochem 61:2071-2080.

Buee L, Bussiere T, Buee-Scherrer V, Delacourte A, Hof PR (2000) Tau protein isoforms, phosphorylation and role in neurodegenerative disorders. Brain research Brain research reviews 33:95-130.

Buzsaki G, Moser EI (2013) Memory, navigation and theta rhythm in the hippocampal-entorhinal system. Nat Neurosci 16:130-138.

Cacucci F, Yi M, Wills TJ, Chapman P, O'Keefe J (2008) Place cell firing correlates with memory deficits and amyloid plaque burden in Tg2576 Alzheimer mouse model. Proc Natl Acad Sci U S A 105:7863-7868.

Cairns NJ, Bigio EH, Mackenzie IR, Neumann M, Lee VM, Hatanpaa KJ, White CL, 3rd, Schneider JA, Grinberg LT, Halliday G, Duyckaerts C, Lowe JS, Holm IE, Tolnay M, Okamoto K, Yokoo H, Murayama S, Woulfe J, Munoz DG, Dickson DW, Ince PG, Trojanowski JQ, Mann DM, Consortium for Frontotemporal Lobar D (2007) Neuropathologic diagnostic and nosologic criteria for frontotemporal lobar degeneration: consensus of the Consortium for Frontotemporal Lobar Degeneration. Acta Neuropathol 114:5-22.

Calhoun ME, Kurth D, Phinney AL, Long JM, Hengemihle J, Mouton PR, Ingram DK, Jucker M (1998) Hippocampal neuron and synaptophysin-positive bouton number in aging C57BL/6 mice. Neurobiol Aging 19:599-606.

Cavus I, Teyler T (1996) Two forms of long-term potentiation in area CA1 activate different signal transduction cascades. Journal of neurophysiology 76:3038-3047.

Chan DC (2006) Mitochondrial fusion and fission in mammals. Annual review of cell and developmental biology 22:79-99.

Chirita CN, Necula M, Kuret J (2003) Anionic micelles and vesicles induce tau fibrillization in vitro. J Biol Chem 278:25644-25650.

Chung CW, Hong YM, Song S, Woo HN, Choi YH, Rohn T, Jung YK (2003) Atypical role of proximal caspase-8 in truncated Tau-induced neurite regression and neuronal cell death. Neurobiol Dis 14:557-566.

Cisse M, Halabisky B, Harris J, Devidze N, Dubal DB, Sun B, Orr A, Lotz G, Kim DH, Hamto P, Ho K, Yu GQ, Mucke L (2011) Reversing EphB2 depletion rescues cognitive functions in Alzheimer model. Nature 469:47-52.

Clavaguera F, Bolmont T, Crowther RA, Abramowski D, Frank S, Probst A, Fraser G, Stalder AK, Beibel M, Staufenbiel M, Jucker M, Goedert M, Tolnay M (2009) Transmission and spreading of tauopathy in transgenic mouse brain. Nat Cell Biol 11:909-913.

Cleveland DW, Hwo SY, Kirschner MW (1977) Physical and chemical properties of purified tau factor and the role of tau in microtubule assembly. J Mol Biol 116:227-247.

Coan EJ, Collingridge GL (1985) Magnesium ions block an N-methyl-D-aspartate receptor-mediated component of synaptic transmission in rat hippocampus. Neuroscience letters 53:21-26.

Collingridge GL, Kehl SJ, McLennan H (1983) Excitatory amino acids in synaptic transmission in the Schaffer collateral-commissural pathway of the rat hippocampus. J Physiol 334:33-46.

Colquhoun D, Jonas P, Sakmann B (1992) Action of brief pulses of glutamate on AMPA/kainate receptors in patches from different neurones of rat hippocampal slices. J Physiol 458:261-287.

Cook C, Dunmore JH, Murray ME, Scheffel K, Shukoor N, Tong J, Castanedes-Casey M, Phillips V, Rousseau L, Penuliar MS, Kurti A, Dickson DW, Petrucelli L, Fryer JD (2014) Severe amygdala dysfunction in a MAPT transgenic mouse model of frontotemporal dementia. Neurobiol Aging 35:1769-1777.

Costall B, Jones BJ, Kelly ME, Naylor RJ, Tomkins DM (1989) Exploration of mice in a black and white test box: validation as a model of anxiety. Pharmacology, biochemistry, and behavior 32:777-785.

Crawley J, Goodwin FK (1980) Preliminary report of a simple animal behavior model for the anxiolytic effects of benzodiazepines. Pharmacology, biochemistry, and behavior 13:167-170.

Crimins JL, Rocher AB, Luebke JI (2012) Electrophysiological changes precede morphological changes to frontal cortical pyramidal neurons in the rTg4510 mouse model of progressive tauopathy. Acta Neuropathol 124:777-795.

Cummings DM, Liu W, Portelius E, Bayram S, Yasvoina M, Ho SH, Smits H, Ali SS, Steinberg R, Pegasiou CM, James OT, Matarin M, Richardson JC, Zetterberg H, Blennow K, Hardy JA, Salih DA, Edwards FA (2015) First effects of rising amyloid-beta in transgenic mouse brain: synaptic transmission and gene expression. Brain.

Dalby NO, Volbracht C, Helboe L, Larsen PH, Jensen HS, Egebjerg J, Elvang AB (2014) Altered function of hippocampal CA1 pyramidal neurons in the rTg4510 mouse model of tauopathy. J Alzheimers Dis 40:429-442.

David DC, Hauptmann S, Scherping I, Schuessel K, Keil U, Rizzu P, Ravid R, Drose S, Brandt U, Muller WE, Eckert A, Gotz J (2005) Proteomic and functional analyses reveal a mitochondrial dysfunction in P301L tau transgenic mice. J Biol Chem 280:23802-23814.

Dawson HN, Ferreira A, Eyster MV, Ghoshal N, Binder LI, Vitek MP (2001) Inhibition of neuronal maturation in primary hippocampal neurons from tau deficient mice. J Cell Sci 114:1179-1187.

de Calignon A, Fox LM, Pitstick R, Carlson GA, Bacskai BJ, Spires-Jones TL, Hyman BT (2010) Caspase activation precedes and leads to tangles. Nature 464:1201-1204.

de Calignon A, Polydoro M, Suarez-Calvet M, William C, Adamowicz DH, Kopeikina KJ, Pitstick R, Sahara N, Ashe KH, Carlson GA, Spires-Jones TL, Hyman BT (2012) Propagation of tau pathology in a model of early Alzheimer's disease. Neuron 73:685-697.

De Felice FG, Velasco PT, Lambert MP, Viola K, Fernandez SJ, Ferreira ST, Klein WL (2007) Abeta oligomers induce neuronal oxidative stress through an N-methyl-D-aspartate receptor-dependent mechanism that is blocked by the Alzheimer drug memantine. J Biol Chem 282:11590-11601.

Deacon RM, Rawlins JN (2006) T-maze alternation in the rodent. Nature protocols 1:7-12.

Decker H, Jurgensen S, Adrover MF, Brito-Moreira J, Bomfim TR, Klein WL, Epstein AL, De Felice FG, Jerusalinsky D, Ferreira ST (2010) N-methyl-D-aspartate receptors are required for synaptic targeting of Alzheimer's toxic amyloid-beta peptide oligomers. J Neurochem 115:1520-1529.

DeKosky ST, Scheff SW (1990) Synapse loss in frontal cortex biopsies in Alzheimer's disease: correlation with cognitive severity. Ann Neurol 27:457-464.

Del Castillo J, Katz B (1954) Quantal components of the end-plate potential. J Physiol 124:560-573.

Dixit R, Ross JL, Goldman YE, Holzbaur EL (2008) Differential regulation of dynein and kinesin motor proteins by tau. Science 319:1086-1089.

Dubey M, Chaudhury P, Kabiru H, Shea TB (2008) Tau inhibits anterograde axonal transport and perturbs stability in growing axonal neurites in part by displacing kinesin cargo:

neurofilaments attenuate tau-mediated neurite instability. Cell motility and the cytoskeleton 65:89-99.

DuBoff B, Gotz J, Feany MB (2012) Tau promotes neurodegeneration via DRP1 mislocalization in vivo. Neuron 75:618-632.

Dudchenko PA (2001) How do animals actually solve the T maze? Behavioral neuroscience 115:850-860.

Dudchenko PA (2004) An overview of the tasks used to test working memory in rodents. Neuroscience and biobehavioral reviews 28:699-709.

Dudchenko PA, Wood ER, Eichenbaum H (2000) Neurotoxic hippocampal lesions have no effect on odor span and little effect on odor recognition memory but produce significant impairments on spatial span, recognition, and alternation. J Neurosci 20:2964-2977.

Duguid IC, Smart TG (2009) Chapter 14: Presynaptic NMDA Receptors. In: Biology of the NMDA Receptor (Van Dongen, A. M., ed) Boca Raton (FL), USA: CRC Press.

Duyckaerts C, Potier MC, Delatour B (2008) Alzheimer disease models and human neuropathology: similarities and differences. Acta Neuropathol 115:5-38.

Duyckaerts C, Uchihara T, Seilhean D, He Y, Hauw JJ (1997) Dissociation of Alzheimer type pathology in a disconnected piece of cortex. Acta Neuropathol 93:501-507.

Eckert A, Nisbet R, Grimm A, Gotz J (2014) March separate, strike together--role of phosphorylated TAU in mitochondrial dysfunction in Alzheimer's disease. Biochim Biophys Acta 1842:1258-1266.

Edwards FA (1995) Anatomy and electrophysiology of fast central synapses lead to a structural model for long-term potentiation. Physiol Rev 75:759-787.

Edwards FA, Konnerth A, Sakmann B, Takahashi T (1989) A thin slice preparation for patch clamp recordings from neurones of the mammalian central nervous system. Pflugers Archiv : European journal of physiology 414:600-612.

Eisenberg D, Jucker M (2012) The amyloid state of proteins in human diseases. Cell 148:1188-1203.

Emmer KL, Waxman EA, Covy JP, Giasson BI (2011) E46K human alpha-synuclein transgenic mice develop Lewy-like and tau pathology associated with age-dependent, detrimental motor impairment. J Biol Chem 286:35104-35118.

Farid M, Corbo CP, Alonso AD (2013) Tau binds ATP and induces its aggregation. Microsc Res Tech.

Feuillette S, Miguel L, Frebourg T, Campion D, Lecourtois M (2010) Drosophila models of human tauopathies indicate that Tau protein toxicity in vivo is mediated by soluble cytosolic phosphorylated forms of the protein. J Neurochem 113:895-903.

Fox LM, William CM, Adamowicz DH, Pitstick R, Carlson GA, Spires-Jones TL, Hyman BT (2011) Soluble tau species, not neurofibrillary aggregates, disrupt neural system integration in a tau transgenic model. J Neuropathol Exp Neurol 70:588-595.

Frost B, Jacks RL, Diamond MI (2009a) Propagation of tau misfolding from the outside to the inside of a cell. J Biol Chem 284:12845-12852.

Frost B, Ollesch J, Wille H, Diamond MI (2009b) Conformational diversity of wild-type Tau fibrils specified by templated conformation change. J Biol Chem 284:3546-3551.

Galpern WR, Lang AE (2006) Interface between tauopathies and synucleinopathies: a tale of two proteins. Ann Neurol 59:449-458.

Gamblin TC, Chen F, Zambrano A, Abraha A, Lagalwar S, Guillozet AL, Lu M, Fu Y, Garcia-Sierra F, LaPointe N, Miller R, Berry RW, Binder LI, Cryns VL (2003) Caspase cleavage of tau: linking amyloid and neurofibrillary tangles in Alzheimer's disease. Proc Natl Acad Sci U S A 100:10032-10037.

Gerson JE, Kayed R (2013) Formation and propagation of tau oligomeric seeds. Frontiers in neurology 4:93.

Giannakopoulos P, Herrmann FR, Bussiere T, Bouras C, Kovari E, Perl DP, Morrison JH, Gold G, Hof PR (2003) Tangle and neuron numbers, but not amyloid load, predict cognitive status in Alzheimer's disease. Neurology 60:1495-1500.

Giasson BI, Forman MS, Higuchi M, Golbe LI, Graves CL, Kotzbauer PT, Trojanowski JQ, Lee VM (2003) Initiation and synergistic fibrillization of tau and alpha-synuclein. Science 300:636-640.

Glenner GG, Wong CW (1984) Alzheimer's disease and Down's syndrome: sharing of a unique cerebrovascular amyloid fibril protein. Biochemical and biophysical research communications 122:1131-1135.

Goate A, Chartier-Harlin MC, Mullan M, Brown J, Crawford F, Fidani L, Giuffra L, Haynes A, Irving N, James L, et al. (1991) Segregation of a missense mutation in the amyloid precursor protein gene with familial Alzheimer's disease. Nature 349:704-706.

Goedert M, Clavaguera F, Tolnay M (2010) The propagation of prion-like protein inclusions in neurodegenerative diseases. Trends Neurosci 33:317-325.

Goedert M, Jakes R (1990) Expression of separate isoforms of human tau protein: correlation with the tau pattern in brain and effects on tubulin polymerization. Embo J 9:4225-4230.

Goedert M, Jakes R (2005) Mutations causing neurodegenerative tauopathies. Biochim Biophys Acta 1739:240-250.

Goedert M, Spillantini MG, Cairns NJ, Crowther RA (1992) Tau proteins of Alzheimer paired helical filaments: abnormal phosphorylation of all six brain isoforms. Neuron 8:159-168.

Goedert M, Spillantini MG, Jakes R, Rutherford D, Crowther RA (1989a) Multiple isoforms of human microtubule-associated protein tau: sequences and localization in neurofibrillary tangles of Alzheimer's disease. Neuron 3:519-526.

Goedert M, Spillantini MG, Potier MC, Ulrich J, Crowther RA (1989b) Cloning and sequencing of the cDNA encoding an isoform of microtubule-associated protein tau containing four tandem repeats: differential expression of tau protein mRNAs in human brain. Embo J 8:393-399.

Gomez-Isla T, Hollister R, West H, Mui S, Growdon JH, Petersen RC, Parisi JE, Hyman BT (1997) Neuronal loss correlates with but exceeds neurofibrillary tangles in Alzheimer's disease. Ann Neurol 41:17-24.

Gomez-Isla T, Price JL, McKeel DW, Jr., Morris JC, Growdon JH, Hyman BT (1996) Profound loss of layer II entorhinal cortex neurons occurs in very mild Alzheimer's disease. J Neurosci 16:4491-4500.

Gotz J, Chen F, Barmettler R, Nitsch RM (2001a) Tau filament formation in transgenic mice expressing P301L tau. J Biol Chem 276:529-534.

Gotz J, Chen F, van Dorpe J, Nitsch RM (2001b) Formation of neurofibrillary tangles in P301l tau transgenic mice induced by Abeta 42 fibrils. Science 293:1491-1495.

Gotz J, Ittner LM (2008) Animal models of Alzheimer's disease and frontotemporal dementia. Nat Rev Neurosci 9:532-544.

Gotz J, Ittner LM, Fandrich M, Schonrock N (2008) Is tau aggregation toxic or protective: a sensible question in the absence of sensitive methods? J Alzheimers Dis 14:423-429.

Gotz J, Probst A, Spillantini MG, Schafer T, Jakes R, Burki K, Goedert M (1995) Somatodendritic localization and hyperphosphorylation of tau protein in transgenic mice expressing the longest human brain tau isoform. Embo J 14:1304-1313.

Greenberg SG, Davies P (1990) A preparation of Alzheimer paired helical filaments that displays distinct tau proteins by polyacrylamide gel electrophoresis. Proc Natl Acad Sci U S A 87:5827-5831.

Grimwood S, Gilbert E, Ragan CI, Hutson PH (1996) Modulation of 45Ca2+ influx into cells stably expressing recombinant human NMDA receptors by ligands acting at distinct recognition sites. J Neurochem 66:2589-2595.

Grover LM, Teyler TJ (1990) Two components of long-term potentiation induced by different patterns of afferent activation. Nature 347:477-479.

Grover LM, Teyler TJ (1992) N-methyl-D-aspartate receptor-independent long-term potentiation in area CA1 of rat hippocampus: input-specific induction and preclusion in a non-tetanized pathway. Neuroscience 49:7-11.

Grover LM, Teyler TJ (1995) Different mechanisms may be required for maintenance of NMDA receptor-dependent and independent forms of long-term potentiation. Synapse 19:121-133.

Grundke-Iqbal I, Iqbal K, Quinlan M, Tung YC, Zaidi MS, Wisniewski HM (1986a) Microtubule-associated protein tau. A component of Alzheimer paired helical filaments. J Biol Chem 261:6084-6089.

Grundke-Iqbal I, Iqbal K, Tung YC, Quinlan M, Wisniewski HM, Binder LI (1986b) Abnormal phosphorylation of the microtubule-associated protein tau (tau) in Alzheimer cytoskeletal pathology. Proc Natl Acad Sci U S A 83:4913-4917.

Guerreiro R, Wojtas A, Bras J, Carrasquillo M, Rogaeva E, Majounie E, Cruchaga C, Sassi C, Kauwe JS, Younkin S, Hazrati L, Collinge J, Pocock J, Lashley T, Williams J, Lambert JC, Amouyel P, Goate A, Rademakers R, Morgan K, Powell J, St George-Hyslop P, Singleton A, Hardy J, Alzheimer Genetic Analysis G (2013) TREM2 variants in Alzheimer's disease. The New England journal of medicine 368:117-127.

Guillozet AL, Weintraub S, Mash DC, Mesulam MM (2003) Neurofibrillary tangles, amyloid, and memory in aging and mild cognitive impairment. Archives of neurology 60:729-736.

Guo H, Albrecht S, Bourdeau M, Petzke T, Bergeron C, LeBlanc AC (2004) Active caspase-6 and caspase-6-cleaved tau in neuropil threads, neuritic plaques, and neurofibrillary tangles of Alzheimer's disease. Am J Pathol 165:523-531.

Guo JL, Covell DJ, Daniels JP, Iba M, Stieber A, Zhang B, Riddle DM, Kwong LK, Xu Y, Trojanowski JQ, Lee VM (2013a) Distinct alpha-synuclein strains differentially promote tau inclusions in neurons. Cell 154:103-117.

Guo JL, Lee VM (2011) Seeding of Normal Tau by Pathological Tau Conformers Drives Pathogenesis of Alzheimer-like Tangles. J Biol Chem 286:15317-15331.

Guo Q, Li H, Cole AL, Hur JY, Li Y, Zheng H (2013b) Modeling Alzheimer's disease in mouse without mutant protein overexpression: cooperative and independent effects of Abeta and tau. PLoS One 8:e80706.

Haass C, Selkoe DJ (2007) Soluble protein oligomers in neurodegeneration: lessons from the Alzheimer's amyloid beta-peptide. Nat Rev Mol Cell Biol 8:101-112.

Hafting T, Fyhn M, Molden S, Moser MB, Moser EI (2005) Microstructure of a spatial map in the entorhinal cortex. Nature 436:801-806.

Hamill OP, Marty A, Neher E, Sakmann B, Sigworth FJ (1981) Improved patch-clamp techniques for high-resolution current recording from cells and cell-free membrane patches. Pflugers Archiv : European journal of physiology 391:85-100.

Hanger DP, Anderton BH, Noble W (2009) Tau phosphorylation: the therapeutic challenge for neurodegenerative disease. Trends Mol Med 15:112-119.

Hanger DP, Gibb GM, de Silva R, Boutajangout A, Brion JP, Revesz T, Lees AJ, Anderton BH (2002) The complex relationship between soluble and insoluble tau in tauopathies revealed by efficient dephosphorylation and specific antibodies. FEBS letters 531:538-542.

Harada A, Oguchi K, Okabe S, Kuno J, Terada S, Ohshima T, Sato-Yoshitake R, Takei Y, Noda T, Hirokawa N (1994) Altered microtubule organization in small-calibre axons of mice lacking tau protein. Nature 369:488-491.

Hardy JA, Higgins GA (1992) Alzheimer's disease: the amyloid cascade hypothesis. Science 256:184-185.

Harris EW, Cotman CW (1986) Long-term potentiation of guinea pig mossy fiber responses is not blocked by N-methyl D-aspartate antagonists. Neuroscience letters 70:132-137.

Harris JA, Koyama A, Maeda S, Ho K, Devidze N, Dubal DB, Yu GQ, Masliah E, Mucke L (2012) Human P301L-mutant tau expression in mouse entorhinal-hippocampal network causes tau aggregation and presynaptic pathology but no cognitive deficits. PLoS One 7:e45881.

Hebb DO (1949) The Organization of behaviour. New York: Wiley & Sons.

Heneka MT, Kummer MP, Latz E (2014) Innate immune activation in neurodegenerative disease. Nature reviews Immunology 14:463-477.

Hjorth-Simonsen A (1972) Projection of the lateral part of the entorhinal area to the hippocampus and fascia dentata. The Journal of comparative neurology 146:219-232.

Hjorth-Simonsen A, Jeune B (1972) Origin and termination of the hippocampal perforant path in the rat studied by silver impregnation. The Journal of comparative neurology 144:215-232.

Hoover BR, Reed MN, Su J, Penrod RD, Kotilinek LA, Grant MK, Pitstick R, Carlson GA, Lanier LM, Yuan LL, Ashe KH, Liao D (2010) Tau mislocalization to dendritic spines mediates synaptic dysfunction independently of neurodegeneration. Neuron 68:1067-1081.

Howlett DR, Richardson JC, Austin A, Parsons AA, Bate ST, Davies DC, Gonzalez MI (2004) Cognitive correlates of Abeta deposition in male and female mice bearing amyloid precursor protein and presenilin-1 mutant transgenes. Brain Res 1017:130-136.

Hurtado DE, Molina-Porcel L, Iba M, Aboagye AK, Paul SM, Trojanowski JQ, Lee VM (2010) A{beta} accelerates the spatiotemporal progression of tau pathology and augments tau amyloidosis in an Alzheimer mouse model. Am J Pathol 177:1977-1988.

Hutton M, Lendon CL, Rizzu P, Baker M, Froelich S, Houlden H, Pickering-Brown S, Chakraverty S, Isaacs A, Grover A, Hackett J, Adamson J, Lincoln S, Dickson D, Davies P, Petersen RC, Stevens M, de Graaff E, Wauters E, van Baren J, Hillebrand M, Joosse M, Kwon JM, Nowotny P, Che LK, Norton J, Morris JC, Reed LA, Trojanowski J, Basun H, Lannfelt L, Neystat M, Fahn S, Dark F, Tannenberg T, Dodd PR, Hayward N, Kwok JB, Schofield PR, Andreadis A, Snowden J, Craufurd D, Neary D, Owen F, Oostra BA, Hardy J, Goate A, van Swieten J, Mann D, Lynch T, Heutink P (1998) Association of missense and 5'-splice-site mutations in tau with the inherited dementia FTDP-17. Nature 393:702-705.

Iba M, Guo JL, McBride JD, Zhang B, Trojanowski JQ, Lee VM (2013) Synthetic tau fibrils mediate transmission of neurofibrillary tangles in a transgenic mouse model of Alzheimer's-like tauopathy. J Neurosci 33:1024-1037.

Ihara Y, Nukina N, Miura R, Ogawara M (1986) Phosphorylated tau protein is integrated into paired helical filaments in Alzheimer's disease. J Biochem 99:1807-1810.

Ikegami S, Harada A, Hirokawa N (2000) Muscle weakness, hyperactivity, and impairment in fear conditioning in tau-deficient mice. Neuroscience letters 279:129-132.

Imai Y, Ibata I, Ito D, Ohsawa K, Kohsaka S (1996) A novel gene iba1 in the major histocompatibility complex class III region encoding an EF hand protein expressed in a monocytic lineage. Biochemical and biophysical research communications 224:855-862.

Iqbal K, Gong CX, Liu F (2014) Microtubule-associated protein tau as a therapeutic target in Alzheimer's disease. Expert opinion on therapeutic targets 18:307-318.

Iqbal K, Liu F, Gong CX, Alonso Adel C, Grundke-Iqbal I (2009) Mechanisms of tau-induced neurodegeneration. Acta Neuropathol 118:53-69.

Irwin DJ, Lee VM, Trojanowski JQ (2013) Parkinson's disease dementia: convergence of alpha-synuclein, tau and amyloid-beta pathologies. Nat Rev Neurosci 14:626-636.

Isaac JT, Nicoll RA, Malenka RC (1995) Evidence for silent synapses: implications for the expression of LTP. Neuron 15:427-434.

Ittner LM, Gotz J (2007) Pronuclear injection for the production of transgenic mice. Nature protocols 2:1206-1215.

Ittner LM, Gotz J (2011) Amyloid-beta and tau--a toxic pas de deux in Alzheimer's disease. Nat Rev Neurosci 12:65-72.

Ittner LM, Ke YD, Delerue F, Bi M, Gladbach A, van Eersel J, Wolfing H, Chieng BC, Christie MJ, Napier IA, Eckert A, Staufenbiel M, Hardeman E, Gotz J (2010) Dendritic function of tau mediates amyloid-beta toxicity in Alzheimer's disease mouse models. Cell 142:387-397.

Ittner LM, Ke YD, Gotz J (2009) Phosphorylated Tau interacts with c-Jun N-terminal kinase-interacting protein 1 (JIP1) in Alzheimer disease. J Biol Chem 284:20909-20916.

Jack CR, Jr., Petersen RC, Xu YC, Waring SC, O'Brien PC, Tangalos EG, Smith GE, Ivnik RJ, Kokmen E (1997) Medial temporal atrophy on MRI in normal aging and very mild Alzheimer's disease. Neurology 49:786-794.

Jarrard LE (1993) On the role of the hippocampus in learning and memory in the rat. Behavioral and neural biology 60:9-26.

Jaworski T, Dewachter I, Lechat B, Croes S, Termont A, Demedts D, Borghgraef P, Devijver H, Filipkowski RK, Kaczmarek L, Kugler S, Van Leuven F (2009) AAV-tau mediates pyramidal neurodegeneration by cell-cycle re-entry without neurofibrillary tangle formation in wild-type mice. PLoS One 4:e7280.

Jean DC, Baas PW (2013) It cuts two ways: microtubule loss during Alzheimer disease. Embo J 32:2900-2902.

Jeganathan S, Hascher A, Chinnathambi S, Biernat J, Mandelkow EM, Mandelkow E (2008) Proline-directed pseudo-phosphorylation at AT8 and PHF1 epitopes induces a compaction of the paperclip folding of Tau and generates a pathological (MC-1) conformation. J Biol Chem 283:32066-32076.

Jeganathan S, von Bergen M, Brutlach H, Steinhoff HJ, Mandelkow E (2006) Global hairpin folding of tau in solution. Biochemistry 45:2283-2293.

Jicha GA, Bowser R, Kazam IG, Davies P (1997) Alz-50 and MC-1, a new monoclonal antibody raised to paired helical filaments, recognize conformational epitopes on recombinant tau. Journal of neuroscience research 48:128-132.

Jin M, Shepardson N, Yang T, Chen G, Walsh D, Selkoe DJ (2011) Soluble amyloid beta-protein dimers isolated from Alzheimer cortex directly induce Tau hyperphosphorylation and neuritic degeneration. Proc Natl Acad Sci U S A 108:5819-5824.

Jonsson T, Stefansson H, Steinberg S, Jonsdottir I, Jonsson PV, Snaedal J, Bjornsson S, Huttenlocher J, Levey AI, Lah JJ, Rujescu D, Hampel H, Giegling I, Andreassen OA, Engedal K, Ulstein I, Djurovic S, Ibrahim-Verbaas C, Hofman A, Ikram MA, van Duijn CM, Thorsteinsdottir U, Kong A, Stefansson K (2013) Variant of TREM2 associated with the risk of Alzheimer's disease. The New England journal of medicine 368:107-116.

Kanaan NM, Morfini GA, LaPointe NE, Pigino GF, Patterson KR, Song Y, Andreadis A, Fu Y, Brady ST, Binder LI (2011) Pathogenic forms of tau inhibit kinesin-dependent axonal transport through a mechanism involving activation of axonal phosphotransferases. J Neurosci 31:9858-9868.

Kerchner GA, Nicoll RA (2008) Silent synapses and the emergence of a postsynaptic mechanism for LTP. Nat Rev Neurosci 9:813-825.

Kfoury N, Holmes BB, Jiang H, Holtzman DM, Diamond MI (2012) Trans-cellular propagation of Tau aggregation by fibrillar species. J Biol Chem 287:19440-19451.

Khatoon S, Grundke-Iqbal I, Iqbal K (1992) Brain levels of microtubule-associated protein tau are elevated in Alzheimer's disease: a radioimmuno-slot-blot assay for nanograms of the protein. J Neurochem 59:750-753.

Kimura T, Ono T, Takamatsu J, Yamamoto H, Ikegami K, Kondo A, Hasegawa M, Ihara Y, Miyamoto E, Miyakawa T (1996) Sequential changes of tau-site-specific phosphorylation during development of paired helical filaments. Dementia 7:177-181.

Klein WL (2013) Synaptotoxic amyloid-beta oligomers: a molecular basis for the cause, diagnosis, and treatment of Alzheimer's disease? J Alzheimers Dis 33 Suppl 1:S49-65.

Klein WL, Krafft GA, Finch CE (2001) Targeting small Abeta oligomers: the solution to an Alzheimer's disease conundrum? Trends Neurosci 24:219-224.

Koffie RM, Hyman BT, Spires-Jones TL (2011) Alzheimer's disease: synapses gone cold. Molecular neurodegeneration 6:63.

Kopeikina KJ, Hyman BT, Spires-Jones TL (2012) Soluble forms of tau are toxic in Alzheimer's disease. Transl Neurosci 3:223-233.

Kopeikina KJ, Polydoro M, Tai HC, Yaeger E, Carlson GA, Pitstick R, Hyman BT, Spires-Jones TL (2013) Synaptic alterations in the rTg4510 mouse model of tauopathy. The Journal of comparative neurology 521:1334-1353.

Kosik KS, Joachim CL, Selkoe DJ (1986) Microtubule-associated protein tau (tau) is a major antigenic component of paired helical filaments in Alzheimer disease. Proc Natl Acad Sci U S A 83:4044-4048.

Kril JJ, Patel S, Harding AJ, Halliday GM (2002) Neuron loss from the hippocampus of Alzheimer's disease exceeds extracellular neurofibrillary tangle formation. Acta Neuropathol 103:370-376.

Lambert JC, Ibrahim-Verbaas CA, Harold D, Naj AC, Sims R, Bellenguez C, DeStafano AL, Bis JC, Beecham GW, Grenier-Boley B, Russo G, Thorton-Wells TA, Jones N, Smith AV, Chouraki V, Thomas C, Ikram MA, Zelenika D, Vardarajan BN, Kamatani Y, Lin CF, Gerrish A, Schmidt H, Kunkle B, Dunstan ML, Ruiz A, Bihoreau MT, Choi SH, Reitz C, Pasquier F, Cruchaga C, Craig D, Amin N, Berr C, Lopez OL, De Jager PL, Deramecourt V, Johnston JA, Evans D, Lovestone S, Letenneur L, Moron FJ, Rubinsztein DC, Eiriksdottir G, Sleegers K, Goate AM, Fievet N, Huentelman MW, Gill M, Brown K, Kamboh MI, Keller L, Barberger-Gateau P, McGuiness B, Larson EB, Green R, Myers AJ, Dufouil C, Todd S, Wallon D, Love S, Rogaeva E, Gallacher J, St George-Hyslop P, Clarimon J, Lleo A, Bayer A, Tsuang DW, Yu L, Tsolaki M, Bossu P, Spalletta G, Proitsi P, Collinge J, Sorbi S, Sanchez-Garcia F, Fox NC, Hardy J, Deniz Naranjo MC, Bosco P, Clarke R, Brayne C, Galimberti D, Mancuso M, Matthews F, European Alzheimer's Disease I, Genetic, Environmental Risk in Alzheimer's D, Alzheimer's Disease Genetic C, Cohorts for H, Aging Research in Genomic E, Moebus S, Mecocci P, Del Zompo M, Maier W, Hampel H, Pilotto A, Bullido M, Panza F, Caffarra P, Nacmias B, Gilbert JR, Mayhaus M, Lannefelt L, Hakonarson H, Pichler S, Carrasquillo MM, Ingelsson M, Beekly D, Alvarez V, Zou F, Valladares O, Younkin SG, Coto E, Hamilton-Nelson KL, Gu W, Razquin C, Pastor P, Mateo I, Owen MJ, Faber KM, Jonsson PV, Combarros O, O'Donovan MC, Cantwell LB, Soininen H, Blacker D, Mead S, Mosley TH, Jr., Bennett DA, Harris TB, Fratiglioni L, Holmes C, de Bruijn RF, Passmore P, Montine TJ, Bettens K, Rotter JI, Brice A, Morgan K, Foroud TM, Kukull WA, Hannequin D, Powell JF, Nalls MA, Ritchie K, Lunetta KL, Kauwe

JS, Boerwinkle E, Riemenschneider M, Boada M, Hiltuenen M, Martin ER, Schmidt R, Rujescu D, Wang LS, Dartigues JF, Mayeux R, Tzourio C, Hofman A, Nothen MM, Graff C, Psaty BM, Jones L, Haines JL, Holmans PA, Lathrop M, Pericak-Vance MA, Launer LJ, Farrer LA, van Duijn CM, Van Broeckhoven C, Moskvina V, Seshadri S, Williams J, Schellenberg GD, Amouyel P (2013) Meta-analysis of 74,046 individuals identifies 11 new susceptibility loci for Alzheimer's disease. Nature genetics 45:1452-1458.

Larson M, Sherman MA, Amar F, Nuvolone M, Schneider JA, Bennett DA, Aguzzi A, Lesne SE (2012) The complex PrP(c)-Fyn couples human oligomeric Abeta with pathological tau changes in Alzheimer's disease. J Neurosci 32:16857-16871a.

Lasagna-Reeves CA, Castillo-Carranza DL, Sengupta U, Clos AL, Jackson GR, Kayed R (2011) Tau oligomers impair memory and induce synaptic and mitochondrial dysfunction in wild-type mice. Molecular neurodegeneration 6:39.

Lauren J, Gimbel DA, Nygaard HB, Gilbert JW, Strittmatter SM (2009) Cellular prion protein mediates impairment of synaptic plasticity by amyloid-beta oligomers. Nature 457:1128-1132.

Lee D, Lee KH, Ho WK, Lee SH (2007) Target cell-specific involvement of presynaptic mitochondria in post-tetanic potentiation at hippocampal mossy fiber synapses. J Neurosci 27:13603-13613.

Lee G, Newman ST, Gard DL, Band H, Panchamoorthy G (1998) Tau interacts with src-family non-receptor tyrosine kinases. J Cell Sci 111 (Pt 21):3167-3177.

Lehericy S, Baulac M, Chiras J, Pierot L, Martin N, Pillon B, Deweer B, Dubois B, Marsault C (1994) Amygdalohippocampal MR volume measurements in the early stages of Alzheimer disease. AJNR American journal of neuroradiology 15:929-937.

Lein ES, Hawrylycz MJ, Ao N, Ayres M, Bensinger A, Bernard A, Boe AF, Boguski MS, Brockway KS, Byrnes EJ, Chen L, Chen L, Chen TM, Chin MC, Chong J, Crook BE, Czaplinska A, Dang CN, Datta S, Dee NR, Desaki AL, Desta T, Diep E, Dolbeare TA, Donelan MJ, Dong HW, Dougherty JG, Duncan BJ, Ebbert AJ, Eichele G, Estin LK, Faber C, Facer BA, Fields R, Fischer SR, Fliss TP, Frensley C, Gates SN, Glattfelder KJ, Halverson KR, Hart MR, Hohmann JG, Howell MP, Jeung DP, Johnson RA, Karr PT, Kawal R, Kidney JM, Knapik RH, Kuan CL, Lake JH, Laramee AR, Larsen KD, Lau C, Lemon TA, Liang AJ, Liu Y, Luong LT, Michaels J, Morgan JJ, Morgan RJ, Mortrud MT, Mosqueda NF, Ng LL, Ng R, Orta GJ, Overly CC, Pak TH, Parry SE, Pathak SD, Pearson OC, Puchalski RB, Riley ZL, Rockett HR, Rowland SA, Royall JJ, Ruiz MJ, Sarno NR, Schaffnit K, Shapovalova NV, Sivisay T, Slaughterbeck CR, Smith SC, Smith KA, Smith BI, Sodt AJ, Stewart NN, Stumpf KR, Sunkin SM, Sutram M, Tam A, Teemer CD, Thaller C, Thompson CL, Varnam LR, Visel A, Whitlock RM, Wohnoutka PE, Wolkey CK, Wong VY, Wood M, Yaylaoglu MB, Young RC, Youngstrom BL, Yuan XF, Zhang B, Zwingman TA, Jones AR (2007) Genome-wide atlas of gene expression in the adult mouse brain. Nature 445:168-176.

Lesne SE (2013) Breaking the Code of Amyloid- Oligomers. Int J Cell Biol 2013:950783.

LeVine H, 3rd (1999) Quantification of beta-sheet amyloid fibril structures with thioflavin T. Methods in enzymology 309:274-284.

Levy-Lahad E, Wijsman EM, Nemens E, Anderson L, Goddard KA, Weber JL, Bird TD, Schellenberg GD (1995) A familial Alzheimer's disease locus on chromosome 1. Science 269:970-973.

Lewis J, Dickson DW, Lin WL, Chisholm L, Corral A, Jones G, Yen SH, Sahara N, Skipper L, Yager D, Eckman C, Hardy J, Hutton M, McGowan E (2001) Enhanced neurofibrillary degeneration in transgenic mice expressing mutant tau and APP. Science 293:1487-1491.

Lewis J, McGowan E, Rockwood J, Melrose H, Nacharaju P, Van Slegtenhorst M, Gwinn-Hardy K, Paul Murphy M, Baker M, Yu X, Duff K, Hardy J, Corral A, Lin WL, Yen SH, Dickson DW, Davies P, Hutton M (2000) Neurofibrillary tangles, amyotrophy and progressive motor disturbance in mice expressing mutant (P301L) tau protein. Nature genetics 25:402-405.

Li X, Kumar Y, Zempel H, Mandelkow EM, Biernat J, Mandelkow E (2011) Novel diffusion barrier for axonal retention of Tau in neurons and its failure in neurodegeneration. Embo J 30:4825-4837.

Liao D, Hessler NA, Malinow R (1995) Activation of postsynaptically silent synapses during pairing-induced LTP in CA1 region of hippocampal slice. Nature 375:400-404.

Lim YA, Rhein V, Baysang G, Meier F, Poljak A, Raftery MJ, Guilhaus M, Ittner LM, Eckert A, Gotz J (2010) Abeta and human amylin share a common toxicity pathway via mitochondrial dysfunction. Proteomics 10:1621-1633.

Lindwall G, Cole RD (1984) Phosphorylation affects the ability of tau protein to promote microtubule assembly. J Biol Chem 259:5301-5305.

Ling H, Hardy J, Zetterberg H (2015) Neurological consequences of traumatic brain injuries in sports. Molecular and cellular neurosciences.

Lisman J, Yasuda R, Raghavachari S (2012) Mechanisms of CaMKII action in long-term potentiation. Nat Rev Neurosci 13:169-182.

Liu C, Gotz J (2013) Profiling murine tau with 0N, 1N and 2N isoform-specific antibodies in brain and peripheral organs reveals distinct subcellular localization, with the 1N isoform being enriched in the nucleus. PLoS One 8:e84849.

Liu L, Drouet V, Wu JW, Witter MP, Small SA, Clelland C, Duff K (2012) Trans-synaptic spread of tau pathology in vivo. PLoS One 7:e31302.

Majid T, Ali YO, Venkitaramani DV, Jang MK, Lu HC, Pautler RG (2014) In vivo axonal transport deficits in a mouse model of fronto-temporal dementia. NeuroImage Clinical 4:711-717.

Malenka RC (1991) Postsynaptic factors control the duration of synaptic enhancement in area CA1 of the hippocampus. Neuron 6:53-60.

Malenka RC, Bear MF (2004) LTP and LTD: an embarrassment of riches. Neuron 44:5-21.

Mammen AL, Kameyama K, Roche KW, Huganir RL (1997) Phosphorylation of the alpha-amino-3-hydroxy-5-methylisoxazole4-propionic acid receptor GluR1 subunit by calcium/calmodulin-dependent kinase II. J Biol Chem 272:32528-32533.

Mandelkow EM, Mandelkow E (2012) Biochemistry and cell biology of tau protein in neurofibrillary degeneration. Cold Spring Harbor perspectives in medicine 2:a006247.

Matarin M, Salih DA, Yasvoina M, Cummings DM, Guelfi S, Liu W, Nahaboo Solim MA, Moens TG, Paublete RM, Ali SS, Perona M, Desai R, Smith KJ, Latcham J, Fulleylove M,

Richardson JC, Hardy J, Edwards FA (2015) A genome-wide gene-expression analysis and database in transgenic mice during development of amyloid or tau pathology. Cell reports 10:633-644.

Matthews-Roberson TA, Quintanilla RA, Ding H, Johnson GV (2008) Immortalized cortical neurons expressing caspase-cleaved tau are sensitized to endoplasmic reticulum stress induced cell death. Brain Res 1234:206-212.

Mattson MP, Magnus T (2006) Ageing and neuronal vulnerability. Nat Rev Neurosci 7:278-294.

McGeer PL, McGeer EG (2015) Targeting microglia for the treatment of Alzheimer's disease. Expert opinion on therapeutic targets 19:497-506.

McGuinness L, Taylor C, Taylor RD, Yau C, Langenhan T, Hart ML, Christian H, Tynan PW, Donnelly P, Emptage NJ (2010) Presynaptic NMDARs in the hippocampus facilitate transmitter release at theta frequency. Neuron 68:1109-1127.

McIlwain DR, Berger T, Mak TW (2013) Caspase functions in cell death and disease. Cold Spring Harbor perspectives in biology 5:a008656.

McLarnon JG, Saint DA, Quastel DM (1986) The actions of dimethyl sulfoxide on neuromuscular transmission. Mol Pharmacol 30:631-638.

McMillan PJ, Kraemer BC, Robinson L, Leverenz JB, Raskind M, Schellenberg G (2011) Truncation of tau at E391 promotes early pathologic changes in transgenic mice. J Neuropathol Exp Neurol 70:1006-1019.

McNaughton BL (1980) Evidence for two physiologically distinct perforant pathways to the fascia dentata. Brain Res 199:1-19.

McNaughton BL (1982) Long-term synaptic enhancement and short-term potentiation in rat fascia dentata act through different mechanisms. J Physiol 324:249-262.

McNaughton BL (2003) Long-term potentiation, cooperativity and Hebb's cell assemblies: a personal history. Philosophical transactions of the Royal Society of London Series B, Biological sciences 358:629-634.

Millecamps S, Julien JP (2013) Axonal transport deficits and neurodegenerative diseases. Nat Rev Neurosci 14:161-176.

Mirra SS, Murrell JR, Gearing M, Spillantini MG, Goedert M, Crowther RA, Levey AI, Jones R, Green J, Shoffner JM, Wainer BH, Schmidt ML, Trojanowski JQ, Ghetti B (1999) Tau pathology in a family with dementia and a P301L mutation in tau. J Neuropathol Exp Neurol 58:335-345.

Mocanu MM, Nissen A, Eckermann K, Khlistunova I, Biernat J, Drexler D, Petrova O, Schonig K, Bujard H, Mandelkow E, Zhou L, Rune G, Mandelkow EM (2008) The potential for beta-structure in the repeat domain of tau protein determines aggregation, synaptic decay, neuronal loss, and coassembly with endogenous Tau in inducible mouse models of tauopathy. J Neurosci 28:737-748.

Mondragon-Rodriguez S, Trillaud-Doppia E, Dudilot A, Bourgeois C, Lauzon M, Leclerc N, Boehm J (2012) Interaction of endogenous tau with synaptic proteins is regulated by NMDA-receptor dependent tau phosphorylation. J Biol Chem.

Morales I, Jimenez JM, Mancilla M, Maccioni RB (2013) Tau oligomers and fibrils induce activation of microglial cells. J Alzheimers Dis 37:849-856.

Morgan SL, Teyler TJ (1999) VDCCs and NMDARs underlie two forms of LTP in CA1 hippocampus in vivo. Journal of neurophysiology 82:736-740.

Morris RGM (1981) Spatial Localization Does Not Require the Presence of Local Cues. Learning and Motivation 12:239-260.

Morrison BM, Hof PR, Morrison JH (1998) Determinants of neuronal vulnerability in neurodegenerative diseases. Ann Neurol 44:S32-44.

Morrison JH, Hof PR (1997) Life and death of neurons in the aging brain. Science 278:412-419.

Mukrasch MD, von Bergen M, Biernat J, Fischer D, Griesinger C, Mandelkow E, Zweckstetter M (2007) The "jaws" of the tau-microtubule interaction. J Biol Chem 282:12230-12239.

Myers AJ, Pittman AM, Zhao AS, Rohrer K, Kaleem M, Marlowe L, Lees A, Leung D, McKeith IG, Perry RH, Morris CM, Trojanowski JQ, Clark C, Karlawish J, Arnold S, Forman MS, Van Deerlin V, de Silva R, Hardy J (2007) The MAPT H1c risk haplotype is associated with increased expression of tau and especially of 4 repeat containing transcripts. Neurobiol Dis 25:561-570.

Naj AC, Jun G, Beecham GW, Wang LS, Vardarajan BN, Buros J, Gallins PJ, Buxbaum JD, Jarvik GP, Crane PK, Larson EB, Bird TD, Boeve BF, Graff-Radford NR, De Jager PL, Evans D, Schneider JA, Carrasquillo MM, Ertekin-Taner N, Younkin SG, Cruchaga C, Kauwe JS, Nowotny P, Kramer P, Hardy J, Huentelman MJ, Myers AJ, Barmada MM, Demirci FY, Baldwin CT, Green RC, Rogaeva E, St George-Hyslop P, Arnold SE, Barber R, Beach T, Bigio EH, Bowen JD, Boxer A, Burke JR, Cairns NJ, Carlson CS, Carney RM, Carroll SL, Chui HC, Clark DG, Corneveaux J, Cotman CW, Cummings JL, DeCarli C, DeKosky ST, Diaz-Arrastia R, Dick M, Dickson DW, Ellis WG, Faber KM, Fallon KB, Farlow MR, Ferris S, Frosch MP, Galasko DR, Ganguli M, Gearing M, Geschwind DH, Ghetti B, Gilbert JR, Gilman S, Giordani B, Glass JD, Growdon JH, Hamilton RL, Harrell LE, Head E, Honig LS, Hulette CM, Hyman BT, Jicha GA, Jin LW, Johnson N, Karlawish J, Karydas A, Kaye JA, Kim R, Koo EH, Kowall NW, Lah JJ, Levey AI, Lieberman AP, Lopez OL, Mack WJ, Marson DC, Martiniuk F, Mash DC, Masliah E, McCormick WC, McCurry SM, McDavid AN, McKee AC, Mesulam M, Miller BL, Miller CA, Miller JW, Parisi JE, Perl DP, Peskind E, Petersen RC, Poon WW, Quinn JF, Rajbhandary RA, Raskind M, Reisberg B, Ringman JM, Roberson ED, Rosenberg RN, Sano M, Schneider LS, Seeley W, Shelanski ML, Slifer MA, Smith CD, Sonnen JA, Spina S, Stern RA, Tanzi RE, Trojanowski JQ, Troncoso JC, Van Deerlin VM, Vinters HV, Vonsattel JP, Weintraub S, Welsh-Bohmer KA, Williamson J, Woltjer RL, Cantwell LB, Dombroski BA, Beekly D, Lunetta KL, Martin ER, Kamboh MI, Saykin AJ, Reiman EM, Bennett DA, Morris JC, Montine TJ, Goate AM, Blacker D, Tsuang DW, Hakonarson H, Kukull WA, Foroud TM, Haines JL, Mayeux R, Pericak-Vance MA, Farrer LA, Schellenberg GD (2011) Common variants at MS4A4/MS4A6E, CD2AP, CD33 and EPHA1 are associated with late-onset Alzheimer's disease. Nature genetics 43:436-441.

Nave KA (2010) Myelination and the trophic support of long axons. Nat Rev Neurosci 11:275-283.

Neher E, Sakmann B (1976) Single-channel currents recorded from membrane of denervated frog muscle fibres. Nature 260:799-802.

Nicoll RA, Schmitz D (2005) Synaptic plasticity at hippocampal mossy fibre synapses. Nat Rev Neurosci 6:863-876.

Nowak L, Bregestovski P, Ascher P, Herbet A, Prochiantz A (1984) Magnesium gates glutamate-activated channels in mouse central neurones. Nature 307:462-465.

O'Keefe J (1979) A review of the hippocampal place cells. Progress in neurobiology 13:419-439.

O'Keefe J, Dostrovsky J (1971) The hippocampus as a spatial map. Preliminary evidence from unit activity in the freely-moving rat. Brain Res 34:171-175.

O'Keefe JaN, L. (1978) The Hippocampus as a Cognitve Map. Oxford University Press, Walton Street, Oxford: Oxford University Press.

Oddo S, Caccamo A, Kitazawa M, Tseng BP, LaFerla FM (2003a) Amyloid deposition precedes tangle formation in a triple transgenic model of Alzheimer's disease. Neurobiol Aging 24:1063-1070.

Oddo S, Caccamo A, Shepherd JD, Murphy MP, Golde TE, Kayed R, Metherate R, Mattson MP, Akbari Y, LaFerla FM (2003b) Triple-transgenic model of Alzheimer's disease with plaques and tangles: intracellular Abeta and synaptic dysfunction. Neuron 39:409-421.

Okawa Y, Ishiguro K, Fujita SC (2003) Stress-induced hyperphosphorylation of tau in the mouse brain. FEBS letters 535:183-189.

Onuma H, Lu YF, Tomizawa K, Moriwaki A, Tokuda M, Hatase O, Matsui H (1998) A calcineurin inhibitor, FK506, blocks voltage-gated calcium channel-dependent LTP in the hippocampus. Neuroscience research 30:313-319.

Opazo P, Labrecque S, Tigaret CM, Frouin A, Wiseman PW, De Koninck P, Choquet D (2010) CaMKII triggers the diffusional trapping of surface AMPARs through phosphorylation of stargazin. Neuron 67:239-252.

Pagani L, Eckert A (2011) Amyloid-Beta interaction with mitochondria. Int J Alzheimers Dis 2011:925050.

Park P, Volianskis A, Sanderson TM, Bortolotto ZA, Jane DE, Zhuo M, Kaang BK, Collingridge GL (2014) NMDA receptor-dependent long-term potentiation comprises a family of temporally overlapping forms of synaptic plasticity that are induced by different patterns of stimulation. Philosophical transactions of the Royal Society of London Series B, Biological sciences 369:20130131.

Parsley SL, Pilgram SM, Soto F, Giese KP, Edwards FA (2007) Enriching the environment of alphaCaMKIIT286A mutant mice reveals that LTD occurs in memory processing but must be subsequently reversed by LTP. Learning & memory 14:75-83.

Patterson KR, Remmers C, Fu Y, Brooker S, Kanaan NM, Vana L, Ward S, Reyes JF, Philibert K, Glucksman MJ, Binder LI (2011) Characterization of prefibrillar Tau oligomers in vitro and in Alzheimer disease. J Biol Chem 286:23063-23076.

Peeraer E, Bottelbergs A, Van Kolen K, Stancu IC, Vasconcelos B, Mahieu M, Duytschaever H, Ver Donck L, Torremans A, Sluydts E, Van Acker N, Kemp JA, Mercken M, Brunden KR, Trojanowski JQ, Dewachter I, Lee VM, Moechars D (2015) Intracerebral injection of

preformed synthetic tau fibrils initiates widespread tauopathy and neuronal loss in the brains of tau transgenic mice. Neurobiol Dis 73:83-95.

Petry FR, Pelletier J, Bretteville A, Morin F, Calon F, Hebert SS, Whittington RA, Planel E (2014) Specificity of anti-tau antibodies when analyzing mice models of Alzheimer's disease: problems and solutions. PLoS One 9:e94251.

Pevalova M, Filipcik P, Novak M, Avila J, Iqbal K (2006) Post-translational modifications of tau protein. Bratisl Lek Listy 107:346-353.

Pittman AM, Fung HC, de Silva R (2006) Untangling the tau gene association with neurodegenerative disorders. Hum Mol Genet 15 Spec No 2:R188-195.

Planel E, Richter KE, Nolan CE, Finley JE, Liu L, Wen Y, Krishnamurthy P, Herman M, Wang L, Schachter JB, Nelson RB, Lau LF, Duff KE (2007) Anesthesia leads to tau hyperphosphorylation through inhibition of phosphatase activity by hypothermia. J Neurosci 27:3090-3097.

Polydoro M, Acker CM, Duff K, Castillo PE, Davies P (2009) Age-dependent impairment of cognitive and synaptic function in the htau mouse model of tau pathology. J Neurosci 29:10741-10749.

Prut L, Belzung C (2003) The open field as a paradigm to measure the effects of drugs on anxiety-like behaviors: a review. European journal of pharmacology 463:3-33.

Puzzo D, Privitera L, Fa M, Staniszewski A, Hashimoto G, Aziz F, Sakurai M, Ribe EM, Troy CM, Mercken M, Jung SS, Palmeri A, Arancio O (2011) Endogenous amyloid-beta is necessary for hippocampal synaptic plasticity and memory. Ann Neurol 69:819-830.

Ramsden M, Kotilinek L, Forster C, Paulson J, McGowan E, SantaCruz K, Guimaraes A, Yue M, Lewis J, Carlson G, Hutton M, Ashe KH (2005) Age-dependent neurofibrillary tangle formation, neuron loss, and memory impairment in a mouse model of human tauopathy (P301L). J Neurosci 25:10637-10647.

Rapoport M, Dawson HN, Binder LI, Vitek MP, Ferreira A (2002) Tau is essential to beta -amyloid-induced neurotoxicity. Proc Natl Acad Sci U S A 99:6364-6369.

Renner M, Lacor PN, Velasco PT, Xu J, Contractor A, Klein WL, Triller A (2010) Deleterious effects of amyloid beta oligomers acting as an extracellular scaffold for mGluR5. Neuron 66:739-754.

Rhein V, Song X, Wiesner A, Ittner LM, Baysang G, Meier F, Ozmen L, Bluethmann H, Drose S, Brandt U, Savaskan E, Czech C, Gotz J, Eckert A (2009) Amyloid-beta and tau synergistically impair the oxidative phosphorylation system in triple transgenic Alzheimer's disease mice. Proc Natl Acad Sci U S A 106:20057-20062.

Richardson JC, Kendal CE, Anderson R, Priest F, Gower E, Soden P, Gray R, Topps S, Howlett DR, Lavender D, Clarke NJ, Barnes JC, Haworth R, Stewart MG, Rupniak HT (2003) Ultrastructural and behavioural changes precede amyloid deposition in a transgenic model of Alzheimer's disease. Neuroscience 122:213-228.

Roberson ED, Halabisky B, Yoo JW, Yao J, Chin J, Yan F, Wu T, Hamto P, Devidze N, Yu GQ, Palop JJ, Noebels JL, Mucke L (2011) Amyloid-beta/Fyn-induced synaptic, network, and

cognitive impairments depend on tau levels in multiple mouse models of Alzheimer's disease. J Neurosci 31:700-711.

Roberson ED, Scearce-Levie K, Palop JJ, Yan F, Cheng IH, Wu T, Gerstein H, Yu GQ, Mucke L (2007) Reducing endogenous tau ameliorates amyloid beta-induced deficits in an Alzheimer's disease mouse model. Science 316:750-754.

Rocher AB, Crimins JL, Amatrudo JM, Kinson MS, Todd-Brown MA, Lewis J, Luebke JI (2010) Structural and functional changes in tau mutant mice neurons are not linked to the presence of NFTs. Exp Neurol 223:385-393.

Rohn TT, Head E, Nesse WH, Cotman CW, Cribbs DH (2001) Activation of caspase-8 in the Alzheimer's disease brain. Neurobiol Dis 8:1006-1016.

Sahara N, DeTure M, Ren Y, Ebrahim AS, Kang D, Knight J, Volbracht C, Pedersen JT, Dickson DW, Yen SH, Lewis J (2013) Characteristics of TBS-extractable hyperphosphorylated tau species: aggregation intermediates in rTg4510 mouse brain. J Alzheimers Dis 33:249-263.

Sahara N, Lewis J, DeTure M, McGowan E, Dickson DW, Hutton M, Yen SH (2002) Assembly of tau in transgenic animals expressing P301L tau: alteration of phosphorylation and solubility. J Neurochem 83:1498-1508.

Sanders DW, Kaufman SK, DeVos SL, Sharma AM, Mirbaha H, Li A, Barker SJ, Foley AC, Thorpe JR, Serpell LC, Miller TM, Grinberg LT, Seeley WW, Diamond MI (2014) Distinct tau prion strains propagate in cells and mice and define different tauopathies. Neuron 82:1271-1288.

SantaCruz K, Lewis J, Spires T, Paulson J, Kotilinek L, Ingelsson M, Guimaraes A, DeTure M, Ramsden M, McGowan E, Forster C, Yue M, Orne J, Janus C, Mariash A, Kuskowski M, Hyman B, Hutton M, Ashe KH (2005) Tau suppression in a neurodegenerative mouse model improves memory function. Science 309:476-481.

Scahill RI, Schott JM, Stevens JM, Rossor MN, Fox NC (2002) Mapping the evolution of regional atrophy in Alzheimer's disease: unbiased analysis of fluid-registered serial MRI. Proc Natl Acad Sci U S A 99:4703-4707.

Scheff SW, Price DA, Schmitt FA, Mufson EJ (2006) Hippocampal synaptic loss in early Alzheimer's disease and mild cognitive impairment. Neurobiol Aging 27:1372-1384.

Schellenberg GD, Bird TD, Wijsman EM, Orr HT, Anderson L, Nemens E, White JA, Bonnycastle L, Weber JL, Alonso ME, et al. (1992) Genetic linkage evidence for a familial Alzheimer's disease locus on chromosome 14. Science 258:668-671.

Scheuner D, Eckman C, Jensen M, Song X, Citron M, Suzuki N, Bird TD, Hardy J, Hutton M, Kukull W, Larson E, Levy-Lahad E, Viitanen M, Peskind E, Poorkaj P, Schellenberg G, Tanzi R, Wasco W, Lannfelt L, Selkoe D, Younkin S (1996) Secreted amyloid beta-protein similar to that in the senile plaques of Alzheimer's disease is increased in vivo by the presenilin 1 and 2 and APP mutations linked to familial Alzheimer's disease. Nat Med 2:864-870.

Schneider I, Reverse D, Dewachter I, Ris L, Caluwaerts N, Kuiperi C, Gilis M, Geerts H, Kretzschmar H, Godaux E, Moechars D, Van Leuven F, Herms J (2001) Mutant presenilins disturb neuronal calcium homeostasis in the brain of transgenic mice, decreasing the threshold for excitotoxicity and facilitating long-term potentiation. J Biol Chem 276:11539-11544.

Schonheit B, Zarski R, Ohm TG (2004) Spatial and temporal relationships between plaques and tangles in Alzheimer-pathology. Neurobiol Aging 25:697-711.

Schulz KL, Eckert A, Rhein V, Mai S, Haase W, Reichert AS, Jendrach M, Muller WE, Leuner K (2012) A new link to mitochondrial impairment in tauopathies. Mol Neurobiol 46:205-216.

Scoville WB, Milner B (1957) Loss of recent memory after bilateral hippocampal lesions. Journal of neurology, neurosurgery, and psychiatry 20:11-21.

Selkoe DJ, Podlisny MB (2002) Deciphering the genetic basis of Alzheimer's disease. Annu Rev Genomics Hum Genet 3:67-99.

Shankar S, Teyler TJ, Robbins N (1998) Aging differentially alters forms of long-term potentiation in rat hippocampal area CA1. Journal of neurophysiology 79:334-341.

Shipton OA, Leitz JR, Dworzak J, Acton CE, Tunbridge EM, Denk F, Dawson HN, Vitek MP, Wade-Martins R, Paulsen O, Vargas-Caballero M (2011) Tau protein is required for amyloid {beta}-induced impairment of hippocampal long-term potentiation. J Neurosci 31:1688-1692.

Simon D, Garcia-Garcia E, Royo F, Falcon-Perez JM, Avila J (2012) Proteostasis of tau. Tau overexpression results in its secretion via membrane vesicles. FEBS letters 586:47-54.

Simon-Sanchez J, Schulte C, Bras JM, Sharma M, Gibbs JR, Berg D, Paisan-Ruiz C, Lichtner P, Scholz SW, Hernandez DG, Kruger R, Federoff M, Klein C, Goate A, Perlmutter J, Bonin M, Nalls MA, Illig T, Gieger C, Houlden H, Steffens M, Okun MS, Racette BA, Cookson MR, Foote KD, Fernandez HH, Traynor BJ, Schreiber S, Arepalli S, Zonozi R, Gwinn K, van der Brug M, Lopez G, Chanock SJ, Schatzkin A, Park Y, Hollenbeck A, Gao J, Huang X, Wood NW, Lorenz D, Deuschl G, Chen H, Riess O, Hardy JA, Singleton AB, Gasser T (2009) Genome-wide association study reveals genetic risk underlying Parkinson's disease. Nature genetics 41:1308-1312.

Skrede KK, Westgaard RH (1971) The transverse hippocampal slice: a well-defined cortical structure maintained in vitro. Brain Res 35:589-593.

Snyder EM, Nong Y, Almeida CG, Paul S, Moran T, Choi EY, Nairn AC, Salter MW, Lombroso PJ, Gouras GK, Greengard P (2005) Regulation of NMDA receptor trafficking by amyloid-beta. Nat Neurosci 8:1051-1058.

Solstad T, Boccara CN, Kropff E, Moser MB, Moser EI (2008) Representation of geometric borders in the entorhinal cortex. Science 322:1865-1868.

Soto C (2003) Unfolding the role of protein misfolding in neurodegenerative diseases. Nat Rev Neurosci 4:49-60.

Spillantini MG, Crowther RA, Kamphorst W, Heutink P, van Swieten JC (1998) Tau pathology in two Dutch families with mutations in the microtubule-binding region of tau. Am J Pathol 153:1359-1363.

Spires TL, Orne JD, SantaCruz K, Pitstick R, Carlson GA, Ashe KH, Hyman BT (2006) Region-specific dissociation of neuronal loss and neurofibrillary pathology in a mouse model of tauopathy. Am J Pathol 168:1598-1607.

Spires-Jones TL, de Calignon A, Matsui T, Zehr C, Pitstick R, Wu HY, Osetek JD, Jones PB, Bacskai BJ, Feany MB, Carlson GA, Ashe KH, Lewis J, Hyman BT (2008) In vivo imaging reveals

dissociation between caspase activation and acute neuronal death in tangle-bearing neurons. J Neurosci 28:862-867.

Spires-Jones TL, Hyman BT (2014) The intersection of amyloid beta and tau at synapses in Alzheimer's disease. Neuron 82:756-771.

Spires-Jones TL, Kopeikina KJ, Koffie RM, de Calignon A, Hyman BT (2011) Are Tangles as Toxic as They Look? J Mol Neurosci.

Stefansson H, Helgason A, Thorleifsson G, Steinthorsdottir V, Masson G, Barnard J, Baker A, Jonasdottir A, Ingason A, Gudnadottir VG, Desnica N, Hicks A, Gylfason A, Gudbjartsson DF, Jonsdottir GM, Sainz J, Agnarsson K, Birgisdottir B, Ghosh S, Olafsdottir A, Cazier JB, Kristjansson K, Frigge ML, Thorgeirsson TE, Gulcher JR, Kong A, Stefansson K (2005) A common inversion under selection in Europeans. Nature genetics 37:129-137.

Stevens CF, Tonegawa S, Wang Y (1994) The role of calcium-calmodulin kinase II in three forms of synaptic plasticity. Current biology : CB 4:687-693.

Stewart S, Cacucci F, Lever C (2011) Which memory task for my mouse? A systematic review of spatial memory performance in the Tg2576 Alzheimer's mouse model. J Alzheimers Dis 26:105-126.

Strack S, Colbran RJ (1998) Autophosphorylation-dependent targeting of calcium/ calmodulin-dependent protein kinase II by the NR2B subunit of the N-methyl- D-aspartate receptor. J Biol Chem 273:20689-20692.

Su JH, Cummings BJ, Cotman CW (1994) Early phosphorylation of tau in Alzheimer's disease occurs at Ser-202 and is preferentially located within neurites. Neuroreport 5:2358-2362.

Sydow A, Van der Jeugd A, Zheng F, Ahmed T, Balschun D, Petrova O, Drexler D, Zhou L, Rune G, Mandelkow E, D'Hooge R, Alzheimer C, Mandelkow EM (2011) Tau-induced defects in synaptic plasticity, learning, and memory are reversible in transgenic mice after switching off the toxic Tau mutant. J Neurosci 31:2511-2525.

Tai HC, Serrano-Pozo A, Hashimoto T, Frosch MP, Spires-Jones TL, Hyman BT (2012) The synaptic accumulation of hyperphosphorylated tau oligomers in Alzheimer disease is associated with dysfunction of the ubiquitin-proteasome system. Am J Pathol 181:1426-1435.

Takashima A, Murayama M, Murayama O, Kohno T, Honda T, Yasutake K, Nihonmatsu N, Mercken M, Yamaguchi H, Sugihara S, Wolozin B (1998) Presenilin 1 associates with glycogen synthase kinase-3beta and its substrate tau. Proc Natl Acad Sci U S A 95:9637-9641.

Taube JS (2007) The head direction signal: origins and sensory-motor integration. Annu Rev Neurosci 30:181-207.

Taube JS, Muller RU, Ranck JB, Jr. (1990) Head-direction cells recorded from the postsubiculum in freely moving rats. I. Description and quantitative analysis. J Neurosci 10:420-435.

Taylor SC, Berkelman T, Yadav G, Hammond M (2013) A defined methodology for reliable quantification of Western blot data. Molecular biotechnology 55:217-226.

Terry RD, Masliah E, Salmon DP, Butters N, DeTeresa R, Hill R, Hansen LA, Katzman R (1991) Physical basis of cognitive alterations in Alzheimer's disease: synapse loss is the major correlate of cognitive impairment. Ann Neurol 30:572-580.

Terwel D, Lasrado R, Snauwaert J, Vandeweert E, Van Haesendonck C, Borghgraef P, Van Leuven F (2005) Changed conformation of mutant Tau-P301L underlies the moribund tauopathy, absent in progressive, nonlethal axonopathy of Tau-4R/2N transgenic mice. J Biol Chem 280:3963-3973.

Terwel D, Muyllaert D, Dewachter I, Borghgraef P, Croes S, Devijver H, Van Leuven F (2008) Amyloid activates GSK-3beta to aggravate neuronal tauopathy in bigenic mice. Am J Pathol 172:786-798.

Towbin H, Staehelin T, Gordon J (1979) Electrophoretic transfer of proteins from polyacrylamide gels to nitrocellulose sheets: procedure and some applications. Proc Natl Acad Sci U S A 76:4350-4354.

Treusch S, Cyr DM, Lindquist S (2009) Amyloid deposits: protection against toxic protein species? Cell Cycle 8:1668-1674.

Trojanowski JQ, Schuck T, Schmidt ML, Lee VM (1989) Distribution of tau proteins in the normal human central and peripheral nervous system. The journal of histochemistry and cytochemistry : official journal of the Histochemistry Society 37:209-215.

Tucker KL, Meyer M, Barde YA (2001) Neurotrophins are required for nerve growth during development. Nat Neurosci 4:29-37.

Uchihara T (2007) Silver diagnosis in neuropathology: principles, practice and revised interpretation. Acta Neuropathol 113:483-499.

Um JW, Nygaard HB, Heiss JK, Kostylev MA, Stagi M, Vortmeyer A, Wisniewski T, Gunther EC, Strittmatter SM (2012) Alzheimer amyloid-beta oligomer bound to postsynaptic prion protein activates Fyn to impair neurons. Nat Neurosci 15:1227-1235.

Um JW, Strittmatter SM (2013) Amyloid-beta induced signaling by cellular prion protein and Fyn kinase in Alzheimer disease. Prion 7:37-41.

Umeda T, Maekawa S, Kimura T, Takashima A, Tomiyama T, Mori H (2014) Neurofibrillary tangle formation by introducing wild-type human tau into APP transgenic mice. Acta Neuropathol 127:685-698.

van Groen T, Miettinen P, Kadish I (2003) The entorhinal cortex of the mouse: organization of the projection to the hippocampal formation. Hippocampus 13:133-149.

von Bergen M, Barghorn S, Li L, Marx A, Biernat J, Mandelkow EM, Mandelkow E (2001) Mutations of tau protein in frontotemporal dementia promote aggregation of paired helical filaments by enhancing local beta-structure. J Biol Chem 276:48165-48174.

von Engelhardt J, Mack V, Sprengel R, Kavenstock N, Li KW, Stern-Bach Y, Smit AB, Seeburg PH, Monyer H (2010) CKAMP44: a brain-specific protein attenuating short-term synaptic plasticity in the dentate gyrus. Science 327:1518-1522.

Vos M, Lauwers E, Verstreken P (2010) Synaptic mitochondria in synaptic transmission and organization of vesicle pools in health and disease. Frontiers in synaptic neuroscience 2:139.

Vossel KA, Zhang K, Brodbeck J, Daub AC, Sharma P, Finkbeiner S, Cui B, Mucke L (2010) Tau reduction prevents Abeta-induced defects in axonal transport. Science 330:198.

Walsh DM, Selkoe DJ (2007) A beta oligomers - a decade of discovery. J Neurochem 101:1172-1184.

Wang JZ, Wang ZH, Tian Q (2014) Tau hyperphosphorylation induces apoptotic escape and triggers neurodegeneration in Alzheimer's disease. Neuroscience bulletin 30:359-366.

Wang X, Su B, Lee HG, Li X, Perry G, Smith MA, Zhu X (2009) Impaired balance of mitochondrial fission and fusion in Alzheimer's disease. J Neurosci 29:9090-9103.

Warmus BA, Sekar DR, McCutchen E, Schellenberg GD, Roberts RC, McMahon LL, Roberson ED (2014) Tau-mediated NMDA receptor impairment underlies dysfunction of a selectively vulnerable network in a mouse model of frontotemporal dementia. J Neurosci 34:16482-16495.

Waxman EA, Giasson BI (2011) Induction of intracellular tau aggregation is promoted by alpha-synuclein seeds and provides novel insights into the hyperphosphorylation of tau. J Neurosci 31:7604-7618.

Weaver CL, Espinoza M, Kress Y, Davies P (2000) Conformational change as one of the earliest alterations of tau in Alzheimer's disease. Neurobiol Aging 21:719-727.

Weingarten MD, Lockwood AH, Hwo SY, Kirschner MW (1975) A protein factor essential for microtubule assembly. Proc Natl Acad Sci U S A 72:1858-1862.

Wes PD, Easton A, Corradi J, Barten DM, Devidze N, DeCarr LB, Truong A, He A, Barrezueta NX, Polson C, Bourin C, Flynn ME, Keenan S, Lidge R, Meredith J, Natale J, Sankaranarayanan S, Cadelina GW, Albright CF, Cacace AM (2014) Tau overexpression impacts a neuroinflammation gene expression network perturbed in Alzheimer's disease. PLoS One 9:e106050.

West MJ, Coleman PD, Flood DG, Troncoso JC (1994) Differences in the pattern of hippocampal neuronal loss in normal ageing and Alzheimer's disease. Lancet 344:769-772.

Wilhelmsen KC, Lynch T, Pavlou E, Higgins M, Nygaard TG (1994) Localization of disinhibition-dementia-parkinsonism-amyotrophy complex to 17q21-22. Am J Hum Genet 55:1159-1165.

Wille H, Drewes G, Biernat J, Mandelkow EM, Mandelkow E (1992) Alzheimer-like paired helical filaments and antiparallel dimers formed from microtubule-associated protein tau in vitro. J Cell Biol 118:573-584.

Wray S, Lewis PA (2010) A tangled web - tau and sporadic Parkinson's disease. Front Psychiatry 1:150.

Wszolek ZK, Tsuboi Y, Ghetti B, Pickering-Brown S, Baba Y, Cheshire WP (2006) Frontotemporal dementia and parkinsonism linked to chromosome 17 (FTDP-17). Orphanet J Rare Dis 1:30.

Wu JW, Herman M, Liu L, Simoes S, Acker CM, Figueroa H, Steinberg JI, Margittai M, Kayed R, Zurzolo C, Di Paolo G, Duff KE (2013) Small misfolded Tau species are internalized via bulk endocytosis and anterogradely and retrogradely transported in neurons. J Biol Chem 288:1856-1870.

Wu LG, Saggau P (1994) Presynaptic calcium is increased during normal synaptic transmission and paired-pulse facilitation, but not in long-term potentiation in area CA1 of hippocampus. J Neurosci 14:645-654.

Xu H, Rosler TW, Carlsson T, de Andrade A, Bruch J, Hollerhage M, Oertel WH, Hoglinger GU (2014) Memory deficits correlate with tau and spine pathology in P301S MAPT transgenic mice. Neuropathology and applied neurobiology 40:833-843.

Yanagisawa M, Planel E, Ishiguro K, Fujita SC (1999) Starvation induces tau hyperphosphorylation in mouse brain: implications for Alzheimer's disease. FEBS letters 461:329-333.

Yoshiyama Y, Higuchi M, Zhang B, Huang SM, Iwata N, Saido TC, Maeda J, Suhara T, Trojanowski JQ, Lee VM (2007) Synapse loss and microglial activation precede tangles in a P301S tauopathy mouse model. Neuron 53:337-351.

Zadori D, Veres G, Szalardy L, Klivenyi P, Toldi J, Vecsei L (2014) Glutamatergic dysfunctioning in Alzheimer's disease and related therapeutic targets. J Alzheimers Dis 42 Suppl 3:S177-187.

Zempel H, Thies E, Mandelkow E, Mandelkow EM (2010) Abeta oligomers cause localized Ca(2+) elevation, missorting of endogenous Tau into dendrites, Tau phosphorylation, and destruction of microtubules and spines. J Neurosci 30:11938-11950.

Zucker RS (1989) Short-term synaptic plasticity. Annu Rev Neurosci 12:13-31.

Zucker RS, Regehr WG (2002) Short-term synaptic plasticity. Annual review of physiology 64:355-405.